Adsorptive Removal of Refractory Sulphur and Nitrogen Compounds from Transportation Fuels

by

Amir Iravani

A thesis
presented to the University of Waterloo
in fulfilment of the
thesis requirement for the degree of
Doctor of Philosophy
in
Chemical Engineering

Waterloo, Ontario, Canada, 2011

AUTHOR'S DECLARATION

I hereby declare that I am the sole author of this thesis. This is a true copy of the thesis, including any required final revisions, as accepted by my examiners.

I understand that my thesis may be made electronically available to the public.

ABSTRACT

The reduction of sulphur in transportation fuel has gained significant importance as the regulatory agencies worldwide react to air quality concerns and the impact of sulphur oxides on the environment. The overall objective of this research was to identify, develop and characterize, based on underlying scientific principles, sorbents that are effective in removal of refractory sulphur compounds from fuel through the process of selective adsorption. It was determined that impregnation of powdered activated carbon with a transition metal (TM) significantly boosted the adsorption performance of the activated carbon. It is hypothesized that the impregnation resulted in the formation of new adsorptive sites that strongly interacted with the lone pairs of electrons on sulphur and nitrogen while having minor impact on the existing oxygen functional groups on the surface of the activated carbon. The percent loading of the TM was determined through wet adsorption study. The best performing sorbent was shown to have maximum adsorption capacities of approximately 1.77 and 0.76 mmol-S/g-sorbent for DBT and 4,6 DMDBT, respectively, with approximately 100% regenerability through solvent wash and thermal treatment. On average, the PTM impregnation showed approximately 137% increase in adsorption capacity of the activated carbon. The sorbent also has good adsorption capacities for organo-nitrogen compounds (i.e., quinoline and carbazole) and a low selectivity towards aromatics, which is desired in adsorptive desulphurization. The surface morphology of the activated carbon, the oxygen functional groups on the surface of the activated carbon, as well as strong (chemisorption) interaction between the TM's partly vacant and far reaching 'd' orbital and lone pair electrons on sulphur and nitrogen are considered to be the main contributing factors to the observed enhancement. It was established in this study that the adsorption isotherms of the impregnated activated carbons best fit Sips isotherm equation, which is a combination of the Langmuir and Freundlich equations. This finding fits well with our initial hypothesis regarding the introduction of new adsorptive sites as a result of TM impregnation and that the sites did not fit well with Langmuir's monolayer and uniform adsorption mechanism.

A kinetic study of the sulphur adsorption using a flow reactor showed a good fit with pseudo second order kinetic model, indicative of an adsorption that is highly dependent on the concentration of available sites on the surface of the sorbent. On average, as expected, the TM impregnated ACC exhibited a higher initial rate of adsorption. The adsorption onto TM sites tends to be more exothermic than adsorption (mainly physisorption) on activated carbon. Therefore, more thermodynamically favoured chemisorption is expected to occur more rapidly than physisorption. It was determined that on average, the initial adsorption rate does not change significantly with temperature while the sulphur adsorption capacity decreases with increase in temperature. It is postulated that the increase in temperature increases surface diffusivity but impedes diffusion flux. The impediment of the diffusion flux will result in reduction in adsorbed quantity.

It was also shown that the intra-particle diffusion exists in the adsorption of DBT on TM impregnated activated carbon, however, it is not likely that the overall adsorption is controlled or noticeable impacted by it. As the temperature of the reactor increases the Weber-Morris intra-particle diffusion plot moves away from the origin, and thus intra-particle diffusion becomes less of a controlling mechanism. This further confirms the fact that the boundary layer (i.e., surface diffusion) and potentially adsorptive interactions at the surface are the dominating mechanisms in the sulphur adsorption onto TM impregnated activated carbon.

It was determined that the distribution of TM species on the surface of the activated carbon is relatively inhomogeneous, with some areas showing well dispersed TM species while other areas showing large clusters. Different impregnation method that can improve dispersion on the surface may significantly enhance adsorption performance of the sorbent.

Furthermore, in this study impregnation of activated carbon using several other transition metals were examined. It was determined that other less expensive transition metals can also improve the adsorption performance of the activated carbon. Further study on less expensive options for impregnating the activated carbon may be beneficial.

Acknowledgment

I would like to take this opportunity to first and foremost thank Professor F.T.T. Ng for providing this exceptional research opportunity and for her continued support during the last nine years that I have carried out part-time research work under her supervision. In addition, I would like to thank Dr. Kamalakar Gunda, former post doctoral fellow in our research group, for his immense contributions along the way. I have benefitted from his knowledge and the time that he has spent on the sulphur adsorption research.

I would also like to thank Dillon Consulting Limited, company that I am currently employed at and my previous employer, SENES Consultants Limited for their support and encouragement for higher education and training.

In addition, I would like to thank other members of our research group and support staff in the department as well as in Chemistry department, both past and present, including, Jennifer Moll, Prof. Leung, Liyan Zhoa, Ming Jiang, Siva Ganeshalingam, Justin Jia, Nagaraju Pasupulety, Kun (Tina) Liu, William O'Keefe, Riku Sudo, Daniel Kim, and Kier Thomas.

Last but certainly not least, I like to thank my parents, Shapour and Touran for their unequivocal sacrifices and supports, continuous encouragements and emphasis on education. Also, many thanks to my lovely wife, Mojdeh and my beloved son Daniel Ethan, for always being an inspiration during this long journey.

TABLE OF CONTENTS

Page No.

LIST OF FIGURES VIII

LIST OF TABLES X

LIST OF ACRONYMS AND ABBREVIATIONS XII

1.0 INTRODUCTION 1
- **1.1** Research Objective 2

2.0 BACKGROUND OF SULPHUR REMOVAL 4
- **2.1** Sources of Sulphur in Fuel 4
- **2.2** Environmental Implications & Regulations 6

3.0 CURRENT METHODS OF DESULPHURIZATION 8
- **3.1** Commercially Available Desulphurization Processes 9
- **3.2** Current Desulphurization Research 13
- **3.3** Adsorption 35
- **3.4** Sorbent Selection for Sulphur Adsorption 38
  - **3.4.1.** Activated Carbon - Background 38
  - **3.4.2.** This Research Work 43

4.0 EXPERIMENTAL METHODS 45
- **4.1** Sorbent Selection and Preparation 46
  - **4.1.1.** Activated Carbon 46
  - **4.1.2.** Preliminary Sorbent Characterization 50
- **4.2** Liquid Phase Adsorption Study 54
- **4.3** Heat of Adsorption Study 59
- **4.4** Best performing sorbent and additional analysis 61

5.0 RESULTS & DISCUSSION 69
- **5.1** Adsorption Isotherms – A background Review 69
- **5.2** Sorbent Selection & Preparation 75
- **5.3** BET – Surface Area 79
- **5.4** Effect of Impregnation on Sulphur Adsorption 80
- **5.5** Flow microcalorimetry 91

6.0 STUDY OF TANTALUM IMPREGNATED ACTIVATED CARBON 98
- **6.1** Tantalum Chemistry and Impregnation 101
- **6.2** Adsorption Performance as a Function of Tantalum Loading 104
- **6.3** Impact of Tantalum Loading on Surface Area and Pore Volume 112
- **6.4** Impact of Acid Treatment on Adsorption Performance 113
- **6.5** Competitive Adsorption 115
  - **6.5.1.** Adsorption of Organo-Nitrogen Compounds 115

6.5.2. Adsorption of Aromatic Compounds....118
6.5.3. Competitive Adsorption – Sulphur / Nitrogen / Aromatics....120
6.6 Sorbent Regenerability....121
6.7 Heat of Adsorption Analysis – Ta-5/ACC....124
6.8 Sorbent Characterization....126
6.8.1. FTIR – Surface Functional Groups....126
6.8.2. Temperature-Programmed Desorption – Ammonia....128
6.8.3. HRTEM Analysis....132
6.8.4. XPS Analysis....138

7.0 FLOW REACTOR EXPERIMENT....153
7.1 Background....153
7.2 Experimental....153
7.3 Adsorption Kinetics....158
7.4 Adsorption Kinetic Model....161
7.5 Tantalum Impregnation and Adsorption Kinetics....163
7.6 Adsorption Temperature and Adsorption Kinetics....166
7.7 Intra-particle Diffusion and Adsorption....172

8.0 CONCLUSIONS AND RECOMMENDATIONS....174
8.1 Conclusions....174
8.2 Recommendations....179

REFERENCES....180

APPENDICES

Appendix A – Table A-1 – Summary of Current Sulphur Removal Techniques

Appendix B – Molecular Structures of Model Organo-Sulphur Compounds

Appendix C – Supplementary Data

Appendix C1 – Isotherms and Linearization
Appendix C2 – Calorimetry and Breakthrough
Appendix C3 – XPS Analysis – Full Survey
Appendix C4 – GC/FID Analytical Method & Calibration
Appendix C5 – Flow Reactor Experiments

LIST OF FIGURES

FIGURE 4.1 - SETARAM C80 FLOW CALORIMETRY – A SCHEMATIC DIAGRAM 60

FIGURE 4.2 - INFRARED ABSORBANCE FOR COMMON FUNCTIONAL GROUPS 68

FIGURE 5.1 - ADSORPTION ISOTHERMS FOR ACC AND IMPREGNATED ACC 82

FIGURE 5.2 - CALORIMETRY HEAT FLOW AND BREAKTHROUGH CURVES FOR DBT IN HEXADECANE ON ACC (<125 μ) AT 30 °C 92

FIGURE 5.3 - CALORIMETRY HEAT FLOW AND BREAKTHROUGH CURVES FOR DBT IN HEXADECANE ON Sr-ACC (<125 μ) AT 30 °C 93

FIGURE 5.4 - CALORIMETRY HEAT FLOW AND BREAKTHROUGH CURVES FOR DBT IN HEXADECANE ON ACC500 (250μ << 500μ) AT 30 °C 96

FIGURE 5.5 - CALORIMETRY HEAT FLOW AND BREAKTHROUGH CURVES FOR DBT IN HEXADECANE ON ACC-125μ (125μ<<250μ) AT 30 °C 97

FIGURE 6.1 - DBT ADSORPTION ISOTHERMS FOR Ta-IMPREGNATED ACC AT DIFFERENT TANTALUM LOADINGS 105

FIGURE 6.2 - 4,6 DMDBT ADSORPTION ISOTHERMS FOR Ta-IMPREGNATED ACC AT DIFFERENT TANTALUM LOADINGS 109

FIGURE 6.3 - DBT ADSORPTION ISOTHERM FOR ACID TREATED ACC 114

FIGURE 6.4 - QUINOLINE ADSORPTION ISOTHERMS FOR TA-IMPREGNATED ACC AND VIRGIN ACC 116

FIGURE 6.5 - NAPHTHALENE ADSORPTION ISOTHERMS FOR Ta-IMPREGNATED ACC AND VIRGIN ACC (BINARY SOLUTION OF NAPHTHALENE IN HEXADECANE AT 50 °C) 119

FIGURE 6.6 - THERMOGRAVIMETRIC ANALYSIS OF USED Ta-5/ACC 122

FIGURE 6.7 - HEAT FLOW CURVES FOR ACC, 5%TAACC ADSORBENTS 125

FIGURE 6.8 - FTIR ANALYSIS OF SORBENTS 127

FIGURE 6.9 - A SCHEMATIC DIAGRAM OF TPD FLOWS AND CONTROL SYSTEM 129

FIGURE 6.10 - TPD-AMMONIA FOR Ta-IMPREGNATED AND NON-IMPREGNATED ACTIVATED CARBON (ACC) 131

FIGURE 6.11 - HRTEM FOR VIRGIN ACC AND Ta-5/ACC 133

FIGURE 6.12 – HRTEM-EDX ANALYSIS FOR (a)VIRGIN ACC AND (b)Ta-5/ACC 134

FIGURE 6.13 - TEM OF Ta-5/ACC AND EDX ANALYSIS FOR THE DISPERSED Ta 136

FIGURE 6.14 - TEM OF Ta-5/ACCAND EDX ANALYSIS FOR THE CLUSTERED Ta 137

FIGURE 6.15 - DECONVOLUTED XPS SPECTRUM FOR USED (DBT) TA-5/ACC 142

FIGURE 6.16 - DECONVOLUTED XPS SPECTRUM FOR USED (CBZL+DBT) TA-5/ACC 143

FIGURE 6.17 - FITTED XPS SPECTRUM FOR UNUSED VIRGIN ACC 144

FIGURE 6.18 - FITTED XPS SPECTRUM FOR UNUSED TA-5/ACC 145

FIGURE 6.19 - FITTED XPS SPECTRUM FOR USED (DBT) TA-5/ACC 145

FIGURE 6.20 - FITTED XPS SPECTRUM FOR USED (CBZL+DBT) TA-5/ACC 146

FIGURE 6.21 - DECONVOLUTED XPS SPECTRUM FOR USED (CBZL+DBT) TA-5/ACC 146

FIGURE 6.22 - DECONVOLUTED XPS SPECTRUM FOR USED (DBT) TA-5/ACC 147

FIGURE 6.23 - DECONVOLUTED XPS SPECTRUM FOR USED (CBZL+DBT) TA-5/ACC 148

FIGURE 6.24 - DECONVOLUTED XPS SPECTRUM FOR UNUSED TA-5/ACC 150

FIGURE 6.25 - DECONVOLUTED XPS SPECTRUM FOR USED (DBT) TA-5/ACC 150

FIGURE 6.26 - DECONVOLUTED XPS SPECTRUM FOR USED (CBZL+DBT) TA-5/ACC 151

FIGURE 6.27 -FITTED XPS SPECTRUM FOR USED (CBZL+DBT) TA-5/ACC 152

FIGURE 7.1 – SORBENT ENTRAPPED IN GLASS MICROFIRER IN THE 155

FIGURE 7.2 - A SCHEMATIC DIAGRAM OF THE FLOW REACTOR EXPERIMENT 157

FIGURE 7.3 – FLOW REACTOR APPARATUS 158

LIST OF TABLES

TABLE 2.1 AN EXAMPLE OF THE AVERAGE CONTENT OF SULPHUR COMPOUNDS IN FCC 5

TABLE 3.1 - COMPARISON OF CURRENTLY AVAILABLE SULPHUR TREATMENT/REMOVAL TECHNOLOGIES 11

TABLE 3.2 – ADSORBENTS INVESTIGATED FOR ADSORPTIVE REMOVAL OF SULPHUR FROM FUEL – RESEARCH STAGE 28

TABLE 4.1 – SELECTED ACTIVATED CARBONS 47

TABLE 4.2 - METALS USED FOR AC IMPREGNATION 49

TABLE 4.3 - HEXADECANE/DBT SOLUTIONS PREPARED FOR ISOTHERMAL ADSORPTION 56

TABLE 4.4 - HEXADECANE/4,6 DMDBT SOLUTIONS PREPARED FOR ISOTHERMAL ADSORPTION 56

TABLE 4.5 - CHARACTERISTIC INFRARED ABSORPTION FREQUENCIES 67

TABLE 5.1 - ADSORPTION ISOTHERM DATA FOR DBT ON SELECTED ACTIVATED CARBON SORBENTS AT 50 °C 76

TABLE 5.2 - ADSORPTION ISOTHERM DATA FOR DBT ON ACC OF VARIOUS PARTICLE SIZES AT 50 °C 78

TABLE 5.3 - BET SURFACE AREA MEASUREMENT 79

TABLE 5.4 - COMPARISON OF ADSORPTION ISOTHERM DATA FOR DBT ON ACTIVATED CARBON BASED SORBENTS AT 50 °C 83

TABLE 5.5 - COMPARISON OF ADSORPTION ISOTHERM DATA FOR DBT ON ACTIVATED CARBON BASED SORBENTS AT 50 °C 86

TABLE 5.6 - ADSORPTION ISOTHERM DATA FOR 4,6 DMDBT ON ACTIVATED CARBON BASED SORBENTS AT 50 °C 89

TABLE 5.7 - HEAT OF ADSORPTION VALUES FOR ACTIVATED CARBON AND IMPREGNATED ACTIVATED CARBONS 95

TABLE 6.1 - ADSORPTION ISOTHERM DATA FOR DBT ON ACTIVATED CARBON BASED SORBENTS AT DIFFERENT TANTALUM LOADINGS, AT 50 °C 106

TABLE 6.2 - ADSORPTION ISOTHERM DATA FOR 4,6 DMDBT ON ACTIVATED CARBON BASED SORBENTS AT DIFFERENT TANTALUM LOADINGS, AT 50 °C 110

TABLE 6.3 - BET SURFACE AREA AND PORE VOLUME ANALYSIS 112

TABLE 6.4 - DBT ADSORPTION RESULTS FOR ACID TREATED ACC 114

TABLE 6.5 - QUINOLINE ADSORPTION ON TA-IMPREGNATED ACC AND VIRGIN ACC 116

TABLE 6.6 - CARBAZOLE ADSORPTION CAPACITY ANALYSIS FOR ACC AND TA/ACC..... 117

TABLE 6.7 - NAPHTHALENE ADSORPTION ON TA-IMPREGNATED ACC AND VIRGIN ACC (BINARY SOLUTION OF NAPHTHALENE IN HEXADECANE AT 50 °C) 119

TABLE 6.8 - COMPETITIVE ADSORPTION – DBT, QUINOLINE..... 120

TABLE 6.9 - SORBENT REGENERABILITY ANALYSIS – TA-5/ACC 123

TABLE 6.10 - COMPARISON OF HEAT OF ADSORPTION TA-5/ACC VERSUS ACC 125

TABLE 6.11 - TOTAL ANGULAR MOMENTUM VALUES FOR ORBITS IN XPS 139

TABLE 7.1 - KINETICS RESULTS – FLOW REACTOR EXPERIMENTS FOR VIRGIN ACC AND TA-5/ACC AT REACTOR TEMPERATURE OF 25 °C 166

TABLE 7.2 - KINETICS RESULTS – FLOW REACTOR EXPERIMENTS FOR TA-5/ACC AT VARIOUS REACTOR TEMPERATURES..... 171

TABLE 7.3- WEBER-MORRIS MODEL RESULTS FOR INTRA-PARTICLE DIFFUSION..... 173

LIST OF ACRONYMS AND ABBREVIATIONS

Acronym	Description
AAC	Acid-washed activated carbon
AC	Activated carbon
ACC125	Activated carbon with particle size of less 125μ << 250 μ
ACC500	Activated carbon with particle size of less 250μ << 500 μ
ACN	Activated carbon Norit
BET	Brunauer-Emmett-Teller
BT	Benzothiophene
CBZL	Carbazole
DBT	Dibenzothiophene
Dia	Aerodynamic diameter
DMDBT	Dimethyldibenzothiophene
EDX	Energy dispersive x-ray
FCC	Fluid catalytic cracking
FTIR	Fourier transform infrared spectroscopy
FID	flame ionization detector
GC	Gas chromatography
HRTEM	High resolution transmission electron microscopy
ICP	Inductively Coupled Plasma
LFO	Light fuel oil
LCO	Light cycle oil
mmol	Milli-mole
mmol-S	Milli-mole of sulphur
mmol-S/g-sorbent	Milli-mole of sulphur per gram of sorbent
μ	Micron, micrometer (10^{-6} m)
nm	Nanometer (10^{-9} m)
NO_x	Nitrogen oxides (NO + NO_2)
ppmw	Part per million – weight
Ppmw-S	Parts per million - weight – sulphur based
PEMFC	Proton exchange membrane fuel cell
QIN	Quinoline
R^2	Linear regression
SOFC	Solid oxide fuel cell
SO_2	Sulphur dioxide
STEM	Scanning Transmission Electron Microscopy
T	Thiophene
Ta	Tantalum
Ta-2/ACC	2 Wt% tantalum impregnated onto activated carbon centaur
Ta-5/ACC	5 Wt% tantalum impregnated onto activated carbon centaur
Ta-10/ACC	10 Wt% tantalum impregnated onto activated carbon centaur

Acronym	Description
Ta/ACC	Tantalum impregnated onto activated carbon (at 2% by Wt.)
TEM	Transmission Electron Microscopy
TGA	Thermogravimetric analysis
TPD	Temperature Programmed Desorption
Wt%	Percent by weight
XPS	X-ray photoelectron spectroscopy

1.0 Introduction

The increasing concern about air quality and the impact of air pollution on human health and the ecosystem has lead regulatory agencies to impose tighter regulations on key sources of pollution. With the transportation sector being a major contributor to air pollution, one of the main areas of focus for the regulators and the scientific community has been the improvement of fuel quality. One of the outcomes of this has been more stringent limits on sulphur content in fuels. In the United States, the maximum sulphur content (limit) in highway diesel fuel was reduced from 500 ppmw (based on a 1993 regulation) to 15 ppmw in 2006 and further reduced to 10 ppmw in 2010 (15 ppmw for non-road vehicles, locomotives and marine engines). Within the European Union, the sulphur content in diesel was reduced to 50 ppmw in 2005 and a further reduction to 10 ppmw in 2010 (Wen *et al.* 2010). Future regulations to further reduce the sulphur content in the fuel are expected.

Furthermore, hydrocarbon fuels can be used in proton-exchange membrane fuel cells (PEMFCs) and solid oxide fuel cells (SOFCs). For these applications the sulphur content in the hydrocarbon fuel has to be less than 1 ppmw for PEMFCs and less than 3 – 30 ppmw for SOFCs (Zhou, 2006). To ensure that fuel cell technology will be a viable replacement for current energy systems it is important to ensure fuel requirements are met using feasible methods of desulphurization.

All of these have resulted in the desulphurization process becoming an important part of fuel production. The petroleum refiners are faced with an ever so challenging task of meeting the regulatory requirements for sulphur content in fuel while maintaining product quality and economical feasibility. Commercially available methods of desulphurization are either incapable of reducing the sulphur content to such low levels (15 ppm), are extremely energy intensive or due to severe process conditions (i.e., high pressure and high temperature) result in saturation of the olefins and reduction in fuel octane number. The mandate to reduce sulphur content in fuel and the limitation with existing desulphurization methods has resulted in a surge in research and innovation to develop new methods for deep and ultra-

deep desulphurization, including adsorptive desulphurization. The focus of this research work has been on adsorptive desulphurization with a focus on developing a sorbent that has good adsorption capacity, regenerability and selectivity towards subject sulphur compounds.

Section 2.0 of this report provides a background on sulphur removal from fuel, Section 3.0 includes a literature review in this research area as well as a discussion on currently available desulphurization methodologies, both those commercially available and those in the research stage. The fundamentals of selective adsorption are also discussed in this section. The experimental work completed including, theoretical background and methodologies are presented in Section 4. The background on adsorption isotherm models used in this study and the results of the experimental work are discussed in Section 5. Section 6 discusses experimental results and characterization specific to tantalum impregnated activated carbon sorbent. Section 7 discusses adsorption kinetics and the results of the flow reactor experiments. The concluding remarks and recommendations for future research work are presented in Section 8.

1.1 Research Objective

The research work undertaken was adsorptive desulphurization for the production of low sulphur fuel. As mentioned above, existing desulphurization processes bear many deficiencies including, high energy usage, reduced fuel quality (i.e., lower octane number), solid waste generation and limited sulphur reduction capabilities. Therefore, research in the area of adsorptive desulphurization, to expand on our understanding of the sulphur adsorption process and ultimately develop a sorbent that can effectively and efficiently remove refractory sulphur compound, will benefit both the petroleum refinery industry as well as the environment.

The overall objective of this research was to identify, develop and characterize, based on sorbent characterization and underlying scientific principles, sorbents that are effective in

removing refractory sulphur compounds from fuel through the process of selective adsorption. Positive results would be beneficial for the oil refinery sector as the sector is currently struggling with the technological and cost feasibilities of meeting some of the existing and future low sulphur fuel needs. This will subsequently pave the way for use of transportation fuel in fuel cell applications, which requires ultra-low sulphur content (e.g., less than 0.1 ppmw). The specific objectives of this research were as follows:

(1) Investigate sorbent characteristics that effect sulphur adsorption capacity of activated carbons and metal-impregnated activated carbons in the adsorptive desulphurization process. The focus on activated carbon is due to numerous reasons including, relatively cheap and abundant supply, very large surface area per unit mass, surface functional groups that can interact (physisorption) with target sulphur and/or nitrogen compounds, easy to manufacture, and if not reusable after numerous regenerations, it can be combusted under controlled conditions to generate energy. The impregnation of activated carbons with metals is to develop a sorbent with enhanced adsorption capacity. This topic is further discussed in subsequent sections.

(2) Investigate key physical (e.g., pore size, pore volume, sorbent surface morphology) and/or chemical (e.g., surface functional groups) parameters that may affect the sulphur adsorption capacity of the sorbent. The focus again was on activated carbons and metal-impregnated activated carbons as per (1) above.

(3) Based on underlying scientific principles and sorbent characterization determine potential rationale for the effects of the physical and/or chemical parameters (above 2) on the adsorption performance of the selected sorbents.

(4) Identify key parameters that should be considered in developing effective desulphurization sorbents, including those that pertain to the kinetics of adsorption.

2.0 Background of Sulphur Removal

2.1 Sources of Sulphur in Fuel

Sulphur compounds are naturally present in crude oil both in the form of organic and inorganic compounds. The total sulphur content, the percent organic sulphur and the percent inorganic sulphur vary depending on the location of the extraction. The inorganic forms of sulphur include hydrogen sulfide (H_2S) and carbonyl sulphide (CS). The organic forms of sulphur include thiols (mercaptans) (e.g. methyl mercaptan, ethyl mercaptan, propyl mercaptan), thiophenes, benzothiophenes, dibenzothiophenes, benzonaphthothiophenes, benzo (d,e,f) dibenzothiophenes and their alkylated derivatives. Organic sulphur compounds with higher molecular weight are less reactive and are mostly found in diesel fuel. Conversely, those with lower molecular weight are more reactive and are mostly found in gasoline.

After hydrodesulphurization the remaining sulphur compounds in the fuel are mainly thiophene (T), benzothiophene (BT), dibenzothiophene (DBT) and their alkylated derivatives, which vary depending on the type of fuel. For gasoline the dominant sulphur containing compounds include, methylthiophenes, benzothiophene, thiophene and dimethylthiophenes. For diesel, the dominant sulphur containing compounds are methyl, dimethyl and trimethyl benzothiophenes and dibenzothiophenes (e.g. 4-MDBT, 4,6-DMDBT, 2,4,6-TMDBT, 3,6-DMDBT, DBT). For jet fuel, the dominating organo-sulphur compounds are mainly trimethyl benzothiophenes, such as 2,3,7-TMBT, 2,3,5-TMBT and 2,3,6-TMBT. Molecular structures of some of the key organo-sulphur compounds are presented in Appendix B.

In the case of diesel fuel, the majority of the refractory sulphur compounds (especially 4,6-dimethyldibenzothiophene, 4-methyldibenzothiophene and dibenzothiophene) are found in the light cycle oil (LCO). With these relatively un-reactive sulphur compounds being the

most difficult to remove with the currently available sulphur removal methods, it is sensible to focus on developing methods that can successfully remove these sulphur compounds from the LCO fraction. An example of the average content of sulphur containing compounds in the FCC for a North American refinery is presented in Table 2.1.

Table 2.1 - An Example of the Average Content of Sulphur COMPOUNDS IN FCC

Sulphur Containing Compounds	Content (ppmw)
Mercaptan Sulphur	24.2
Sulfide sulphur	7.3
Thiophene sulphur	61.9
C1 Thiophene sulphur	115
C2 Thiophene sulphur	130.6
C3 Thiophene sulphur	90.9
C4 Thiophene sulphur	88
Benzothiophene & Dibenzothiophene	238.1

Source: Irvine 1998.

2.2 Environmental Implications & Regulations

When combusting fossil fuel (gasoline, diesel, fuel oils, jet fuel, etc.) sulphur dioxide (SO_2) is emitted into the atmosphere. Emissions of SO_2, along with emissions of nitrogen oxides, are the primary cause of acidic deposition which has a significant effect on the environment, particularly in developed and developing nations. Also, sulphur containing compounds are known for their interaction with precious metals commonly used in engine exhaust catalytic converters. Sulphur originating from gasoline, diesel or lubricant oils reacts with active metals and poisons the catalyst in the catalytic converter and thus reduces its conversion capacity for other contaminants such as carbon monoxide and unburned hydrocarbons (Karjalainen *et al.* 2004).

The more stringent guidelines set by the United States Environmental Protection Agency (U.S. EPA), known as Tier II, came into effect in June 2006, which obligated the refinery sector to reduce the sulphur content of diesel fuel to 15 ppmw (from 500 ppmw) and gasoline fuel to 30 ppmw (from 350 ppmw). As mentioned above, the European Union (EU) has further reduced the allowable sulphur content of fuel from 50 ppmw (since 2005) to 10 ppmw in 2010. In the United States, fuel types such as diesel used in non-road vehicles, locomotives and marine engines are required to meet the 15 ppmw sulphur limit (as of 2010). These stringent regulatory requirements have proven to be challenging for the refineries especially with the continuous increase in the sulphur content of crude oil as well as the ever increasing cost of the refining operation and crude oil. According to Torrisi *et al.* the average sulphur content of crude oil processed in the United States has increased from 0.89 wt% in 1981 to about 1.25 wt% in 1997 (Torrisi *et al.* 2002).

The Ontario Ministry of Environment requires the petroleum refineries to report their sulphur-in-gas on a quarterly basis. Ontario's regulation was replaced by a federally regulated 30 ppm sulphur limit in gasoline since January 1, 2005.

In the Notice of Intent on Cleaner Vehicles, Engines and Fuels, published in the Canada Gazette I in February 2001, Environment Canada committed to developing measures to reduce the level of sulphur in both light and heavy fuel oils used in stationary facilities. There is currently no regulated national standard for sulphur in either Heavy Fuel Oil (HFO) or Light Fuel Oil (LFO). British Columbia, Ontario, Quebec, New Brunswick and the Montreal Urban Community regulate the sulphur content in HFO at various levels ranging from 1.1 % wt. up to 3.0 % wt. Several provinces including New Brunswick, Ontario and Quebec regulate the sulphur content of LFO at 0.5% wt. The commercial standard set by the Canadian General Standards Board (CGSB) specifies limits of 0.3% wt. sulphur content for type 0 LFO and 0.5% wt. for types 1 and 2 LFO. The CGSB does not specify any limit for sulphur in HFO.

3.0 Current Methods of Desulphurization

Currently hydrodesulphurization (HDS) uses a Co-Mo / Al_2O_3 catalyst at high pressure and high temperature. The mechanism of HDS for dibenzothiophene is known to occur through hydrogenation and hydrogenolysis. Hydrogenation refers to the formation of S-H bond whereas hydrogenolysis is the cleavage of C-S bond. Each of these two desulphurization reaction pathways occurs at different catalytic sites of the commercially used cobalt-molybdenum on alumina (Co-Mo/Al_2O_3) catalyst. The rate constants for hydrogenation of DBT and 4,6-DMDBT are 0.015 and 0.010 L/min, while the rate constants for th hydrogenolysis pathway for DBT and 4,6-DMDBT are 0.048 and 0.004 L/min, respectively. It has been proposed that during hydrogenation, the steric hindrance of methyl groups is reduced and the electron density on sulphur is increased. Therefore, hydrogenation is the preferred pathway in the desulphurization process of substituted dibenzothiophene (Ma *et al.* 2003).

Over 90% of sulphur and olefin in gasoline is in the naphtha from FCC. It is well know that sulphur removal from naphtha can be achieved by catalytic hydrodesulphurization. However, one of the most important drawbacks of this method is the hydro-saturation of olefins and thus octane loss of about 10 numbers (Cullen & Avidan, 2001).

3.1 Commercially Available Desulphurization Processes

Current commercially available deep and ultra-deep desulphurization methods for diesel fuel face a major hurdle due to the low reactivity of di-substituted benzothiophenes, such as 4,6-dimethyldibenzothiophene. The methyl groups at C4 and C6 cause steric problems for the sulphur to interact with active sites of the sorbent/catalyst. This problem is magnified due to two additional factors:

(1) Presence of nitrogen compounds and polyaromatics in diesel fuel.

(2) Presence of H_2S in the reaction system during hydrodesulphurization.

Both polyaromatics and nitrogen compounds can compete with sulphur compounds for active sites on the sorbent/catalyst surface during chemisorption, which would hinder the hydrogenation and subsequent hydrodesulphurization of sulphur compounds. On the other hand the H_2S directly competes with organic sulphur compounds and thus the hydrogenolysis of C-S. Having said that, removal of aromatics from the diesel fuel is desirable as it improves combustion characteristics and also reduces formation of harmful emissions (Song *et al.* 2003).

One of the commercially available methods of catalytic hydrodesulphurization is the S-Zorb developed by *Phillips Petroleum Company*. The company claims that the proprietary sorbent is capable of removing refractory sulphur compounds from the stream through adsorption in a fluidized bed reactor and that the sorbent can be regenerated using air (forming SO_2) and further reduced using H_2. It is also claimed that the process removes refractory species such as 4,6-dimethyldibenzothiophene. The reaction reported for benzothiophene is:

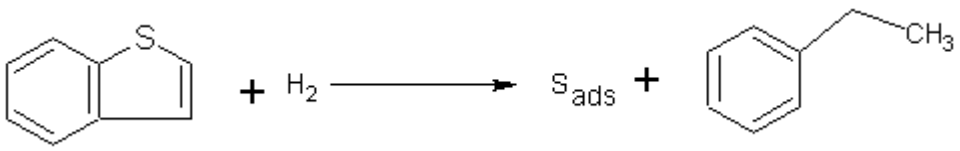

Benzothiophene + H_2 → S (ads) + ethyl benzene

One of the drawbacks of this process is that it is carried out under high temperatures (340 – 430 °C) and relatively high pressures (100 – 500 psig) (Phillips Petroleum, 2001).

Another innovative approach to sulphur removal is the ultrasound technology developed by *SulphCo Company*. This process consists of two steps:

1. Oxidation of thiophenic compounds in an ultrasound reactor forming sulfoxides and sulfones.
2. Sulfoxides and sulfones are removed by solvent extraction.

The ultrasound is used to create gas bubble cavities used for oxidation of thiophenes. This process is done under high temperature and high pressure conditions and currently there are no commercial installations. Also, the effectiveness of this process in removal of 4,6-DMDBT is unknown (Yang, 2003).

Currently available sulphur removal technologies and their pros and cons are summarized in TABLE 3.1.

TABLE 3.1 - COMPARISON OF CURRENTLY AVAILABLE SULPHUR TREATMENT/REMOVAL TECHNOLOGIES

TECHNOLOGY	OCTANE LOSS	VOLUME LOSS	SULPHUR REDUCTION CAPABILITY	HYDROGEN CONSUMPTION	COMMERCIAL INSTALLATIONS	ADDITIONAL PROS	ADDITIONAL CONS
Feed HDS	No	n/a	may not meet 30 wt ppm	High	Many	1-Improved liquid yield 2-Reduced SOx emissions	Highest initial capital cost
Catalytic Distillation hydro-treating	Yes	No	10 - 30 wt ppm	Yes	1st started up in May 2000	n/a	1-Catalyst cost 2- May produce recombined RSH 3-High capital cost
Conventional Hydrofining with octane recovery	No	up to 5%	10 wt ppm	Yes	Operating since 1991	n/a	1- Catalyst Cost 2- Total olefin saturation and Rvp increase
Selective cat naphtha Hydrofining	Yes	No	10 wt ppm	Yes	Yes	n/a	1- Catalyst cost 2-May produce recombined RSH
Dual-catalyst reactor	Yes	No	10 - 30 wt ppm	Limited	Several in Operation	No need for additional product sweetening	1- Catalyst cost 2- Includes diolefin saturation and interstage strip 3- May produced recombined RSH
Low pressure fixed-bed hydroprocessing	Yes	0.3 - 2%	10 wt ppm	Yes	Yes	n/a	1- Requires MTBE (or equivalent) addition for max yield case to recover octane. 2- Total olefin saturation and Rvp increase
Olefinic alkylation	Yes	Yes	10 wt ppm	No	One	n/a	Catalyst Cost
Sorbent	No	Yield is almost 100% of original stream	10 wt ppm	Low	Small-scale start-up in 2001	No recombined RSH formed	1- High initial capital cost 2- Sulphur yielding as SO_2
Extractive mass transfer	No	No	10 wt ppm	No	No	1- Cost savings compared to HDS as final polishing step 2- Preserves octane	1- Chemical costs 2- RSH removal only

Source: Hydrocarbon Processing: February 2002 issue, pp 45-50 (with permission)

In some of the industrial installations, or those developed methodologies ready for commercialization, the hydrodesulphurized product is blended with the hydrocarbon fraction from the adsorber. The sulphur contents of the ultra-clean fuels produced from such an integrated process may be in the range of 1 to 5 ppmw. This is achieved by integrating two desulphurization processes of Selective Adsorption of Removing Sulphur (SARS) and Hydrodesulphurization of Concentrated Fraction (HDSCS) (Ma *et al.* 2002). The inventors of the SARS claim that the process has several potential advantages over other commercialized processes, including:

(1) The SARS process is effective for ultra-deep desulphurization of liquid hydrocarbon fuels including gasoline, diesel fuel and jet fuel at room temperature.

(2) The SARS adsorption process is operated at ambient temperature and ambient pressure, without using any H_2, which leads to low energy consumption, low investment and low operating cost.

(3) For a refinery operation, the hydrodesulphurization following the SARS only deals with the sulphur fraction (HDSCS), which leads to low hydrogen consumption and low energy consumption, as well as low investment and low operating cost.

(4) Little or no octane penalty is expected for gasoline, because in the adsorption desulphurization process most of the olefins with high octane number are kept in the gasoline without suffering hydrogenation (Ma *et al.* 2002).

3.2 Current Desulphurization Research

In order to achieve ultra-deep desulphurization through formulating catalysts with improved hydrogenation activity (i.e., hydrodesulphurization), several approaches have been undertaken, including:

(1) improving hydrogenation ability of the sorbent/catalyst for enhanced hydrogenation of aromatic rings in 4,6-dimethyldibenzothiophene;

(2) integrating acidic property in the sorbent/catalyst to include isomerization of methyl groups away from C4 and C6 positions; and

(3) removing inhibiting compounds such as H_2S and tailoring reaction conditions for adsorption of sulphur compounds.

More recent developments in deep desulphurization include removal via selective adsorption of sulphur containing compounds at ambient conditions and without the use of H_2. The bench-scale experiments for this type of selective adsorption use heterogeneous sorbents (usually impregnated with metal species such as Cu and Pd) to selectively adsorb (chemisorption or physisorption, depending on the compound being adsorbed) sulphur-containing compounds (Ma *et al.* 2003). Summaries of abstracts of recent publications in the field of adsorptive sulphur removal mainly dealing with activated carbon and modified activated carbon are provided below. Also provided at the end of this section is a brief description of the adsorption mechanism in general.

Both thiophenic compounds and non-sulphur aromatic compounds can interact with metal species of the sorbent through π-electrons. π-electrons are those electrons that participate in π complexation (Ma *et al.* 2003). The same study proposes the use of this selective

adsorption method for hydrodesulphurization for a more economical desulphurization process. The proposed integrated process consists of an initial selective adsorption process for removal of sulphur containing compounds followed by hydrodesulphurization of concentrated sulphur compounds using high activity catalysts such as Co-Mo on MCM-41. The subsequent desulphurization of the concentrated sulphur compounds allows for more efficient utilization of a reactor due to the higher concentrations, faster hydrodesulphurization rate due to absence (or lesser concentration) of inhibiting aromatics (normally interfere with sulphur removal by adsorbing onto hydrogenation sites) and smaller reactor volume (volume reduction by > 94%) due to lesser quantity of materials to be processed (Ma *et al.* 2002).

Kabe *et al.* compared the reactivities of dibenzothiophene (DBT), 4-methyldibenzothiophene (4-MDBT) and 4,6-dimethyldibenzonthiophene (4,6-DMDBT) using a Co-Mo/Al_2O_3 catalyst under deep desulphurization conditions to obtain a sulphur concentration of less than 0.05 wt%. The results indicated that while conversions of all three sulphur-containing compounds to cyclohexylbenzenes were the same, the conversion into biphenyls decreased with increasing degree of alkylation (Kabe *et al.* 1993). Based on the results it was concluded that the three compounds were adsorbed to the catalyst surface via π-electrons in the aromatic rings but the alkylated species were more strongly adsorbed and the C-S bond cleavage of alkylated species was disturbed by steric hindrance of the methyl groups. This steric hindrance is expected to increase with the size of the alkyl group, i.e. from methyl to ethyl to propyl (Kabe *et al.* 1993 and Ma *et al.* 2003).

Studies incorporating mesoporous MCM-41 as a support for conventional Co-Mo catalysts have shown improved sulphur removal. The design approach makes use of high surface area of MCM-41 for higher activity per unit weight, uniform mesopores to facilitate diffusion of sulphur compounds, and mild acidity of the aluminum containing support (MCM-41) to facilitate dispersion of Co-Mo and promote isomerization (Song *et al.* 2003).

Babich and Moulijin conducted research on activated alumina in the form of fine-sized slurry in a countercurrent moving bed in a commercial process called the *IRVAD* Process (combination of inventor name "IRVine" and "ADsorption") for desulphurization. Gasoline products with sulphur as low as 0.5 ppmw were claimed. Desorption is performed with hydrogen at various temperatures up to 270°C. Ag-exchanged Y-zeolite and Cu(II)-Y were also used in temperatures as high as 200-350°C and 200-550°C, respectively, however, both showed low thiophene capacities. A transition metal compound supported on silica gel was also used intending for the metal to form a bond with the sulphur atom of the thiophenic compound. However, the sulphur adsorption capacity was low (Babich & Moulijn, 2003).

In his 2002 research, Song conducted research on reduction or elimination of sulphur poisoning of noble metals, which are used as catalyst in hydrodesulphurization. In order to reduce or eliminate the poisoning of noble metals, recently developed processes use multi-staged catalytic beds to achieve deep desulphurization. In the first stage a Co-Mo or Ni-Mo catalyst supported on alumina was used for deep hydrogenation and desulphurization. In the second step the gaseous by-products are removed and in the third step noble metals are used for further hydrogenation and desulphurization of already low sulphur content feed solution. Results showed reduction in sulphur poisoning (Song, 2002).

A systematic approach, taken by Yang *et al.* in the search of a thiophene-selective sorbent was completed in 2004. The study concluded that through π–complexation the selectivity for sulphur adsorption is improved. The calculation for the bonding between benzene and thiophene with Cu^+ and Ag^+ exchanged on Y-zeolites showed that the π–complexation bond for thiophene is stronger than that with benzene. Furthermore, the calculated bond strengths are in the proximity of 20 kcal/mol, indicating a weak chemical bond that is reasonable for the purpose of removing thiophenic compounds. The author claims that the weak chemical bonds such as π-complexation are considered to be the preferred means for selective removal of thiophene. Based on the research work completed by Yang *et al.*

effective π–complexation sorbents for sulphur removal include Cu(I)Y, CuCl/γ -Al_2O_3 and $AgNO_3/SiO_2$ (Yang *et al.* 2004).

Vapour phase adsorption isotherms of thiophene on various sorbents were measured in order to assess their suitability for sulphur removal. Direct correlation between adsorption in vapour phase and liquid phase has not been established yet, however a potential theoretical approach has been used by replacing the "saturated pressure" term with the "saturated concentration in solution" term, in order to use the results from vapour phase experiments for the liquid phase. It is assumed that a sorbent capable of adsorbing thiophene at very low partial pressures in the gas phase should also be able to do so in the liquid phase (Yang *et al.* 2004).

Another study by Yang *et al.* looks at Cu^+ and Ag^+ on Y-zeolite as an adsorbent for sulphur compounds. In this study deep desulphurization is achieved at ambient conditions using commercial diesel with sulphur content of approximately 430 ppmw. The authors claim that the chosen adsorbent supported on Y-zeolite is highly selective for sulphur compounds (evident from adsorption bond energy differentials between thiophene and benzene) and also has a relatively high sulphur-capacity. According to the study, the bonding is a π-complexation where electrons are donated from the "π*" orbital of thiophene to the vacant "s" orbital of metals (sigma donation), while the electrons from the "d" orbital of the metals are back donated to the "π*" orbital of thiophene. The results of this research work indicate significant reduction in sulphur (to levels suitable for use in PEM fuel cells) as well as promising re-generability via thermal desorption (at 350°C) or by solvent extraction (using dimethylformamide or carbon tetrachloride). An activated carbon (AC) layer to increase the capacity of the sorbent, by targeting larger sulphur compounds, was also used (Yang *et al.* 2003). The authors claim that the removal of larger sizes of thiophenic compounds using AC seems to have contributed to the reduction of the overall sulphur compounds, as it is believed that the Y-zeolite may have experienced some

steric problem with adsorption of larger sulphur compounds such as 4,6-dimethyldibenzothiophene (Yang *et al.* 2003).

Liquid phase breakthrough experiments were performed on a fixed-bed adsorber of CuY, AgY and NaY using solutions of thiophene in *n*-octane as the feed. The zeolites were activated in-situ prior to cooling and breakthrough experiments. As concluded from vapour phase isotherms, the three zeolites have similar total capacities for thiophene and benzene. It is claimed that the NaY lacks selectivity for thiophene since it does not form π – complexation. With AgY and CuY and feeds containing 2000 and 500 ppmw thiophene, the sulphur content of the effluent remained below the detection limit (~0.28 ppmw) for an extended period of time. The thiophene capacity for AgY was 7.5 wt% for a feed concentration of 2000 ppmw. The result for CuY was 21.42 wt% for the same feed. Therefore, CuY was a better sorbent in both sulphur selectivity and capacity for thiophene sulphur removal from gasoline and diesel fuels. The authors also claim that "Sulphur-free" fuel was also produced using commercial gasoline and diesel on Cu(I)Y as well as on Cu(I)Y with a layer of 15% guard-bed of activated carbon. A total of 34.3 cm^3 of diesel and 19.6 cm^3 of gasoline were purified per gram of total sorbent (Yang *et al.* 2003).

A study by Zhang *et al.* (2005) on deep desulphurization of gasoline for use in fuel cell applications looked at the performance of a cerium on Zn-Fe-O on Al_2O_3 sorbent for removal of organic sulphur compounds from gasoline, via adsorption. Based on the findings of the study, a composition consisting of 4.54 wt.% ZnO, 2.25 wt. % Fe_2O_3 and 2.5 wt.% CeO_2 illustrated best sulphur removal results. The study also claims that the regeneration of the sorbent was also successful, using a gas mixture containing 6 vol.% steam and air, and a gas space velocity of 2,400 mL/h/mL. The actual adsorption process was found to be optimal at 60 ^oC, resulting in final sulphur concentrations of less than 10ppm. The characterization of the sorbent and the adsorption was carried out using BET, XRD and SEM apparatus (Zhang *et al.* 2005).

An alternative method for reducing the sulphur content of fuel and specifically diesel is oxidative desulphurization (OD) process, in which the refractory sulphur compounds are oxidized to their corresponding sulfones and are then removed using adsorption, extraction, distillation or decomposition. Hydrogen peroxide (H_2O_2) is a commonly used oxidizing agent; however, in the absence of catalyst the oxidation process is relatively slow. A study by Garcia-Gutierrez *et al.* looked at the utilization of molybdenum supported on alumina (Mo/Al_2O_3) as a catalyst in the oxidation of organic sulphur compounds and subsequent removal of the sulfones via adsorption. The study claimed a sulphur removal of 99.7% by weight (final sulphur concentrations are not specified) (Garcia-Gutierrez *et al.* 2006).

A study by Sakanishi *et al.* on adsorptive removal of sulphur compounds (BT, 2-MBT) from naphtha fractions (model compounds: toluene, naphthalene and 1-methylnaphthalene) via carbon adsorption indicated that mesoporous activated carbon with a fine particle size was more effective in selective adsorption of 2-ring sulphur compounds from naphtha fractions (Sakanishi *et al.* 2003).

A recent study by Song *et al.* on activated carbon examined the effects of surface properties and structure of activated carbons on adsorption of BT, DBT, 4-MDBT and 4,6-DMDBT in the presence of aromatics in a model diesel compound (hexadecane). The study has looked at activated carbons and carbon blacks from different sources, including, coconut, various types of coal, wood, as well as petroleum coke. The sorbents varied in surface area (range from 254 m^2/g to 2,201 m^2/g), particle size (range from ultra fine to pellets of ~ 1.6 mm in dia.) and surface functional groups. They have characterized these activated carbons by nitrogen adsorption, X-ray diffraction and X-ray photoelectron spectroscopy (XPS) techniques. The surface functional groups were analyzed using XPS. The chemical states of C, N and O species were determined from charge-corrected high-resolution scans. Results indicated that in addition to the structural aspect of activated carbons (e.g. pore size, surface area), surface functional groups play a key role in

adsorption capacity and selectivity towards sulphur compounds. The equilibrium adsorption capacities for various carbon materials (both activated carbon and carbon black) indicated a range of 1.7 to 7.0 mg-Sulphur / g-Adsorbent (0.05 – 0.22 mmol-sulphur / g-sorbent). The results also indicated that regardless of the type of carbon material, the adsorption selectivity for sulphur compounds increased in the order of BT < DBT < 4-MDBT < 4,6-DMDBT. The paper also concluded that the increase in concentration of oxygen containing functional groups on the surface resulted in improvement in sulphur adsorption capacity. It is claimed that the regeneration of activated carbon sorbents through solvent washing was shown to be effective. A follow-up study by the same group claimed that the acidic oxygen functional groups, such as carboxyl and hydroxyl on the surface were determined to be the active sites for refractory sulphur compounds, including 4,6-DMDBT. Based on the results, the authors claim that an increase in acidic oxygen functional groups on the surface of the activated carbon can significantly improve adsorption of sulphur compounds (Song *et al.* 2006).

In a research study by Yu et al. the effect of metal ions (Ag^{+}, Ni^{2+}, Cu^{2+} and Zn^{2+}) loaded on activated carbon was studied in terms of the activation energy of desorbing the adsorbed dibenzothiophene. The metal ion was loaded on activated carbon through impregnation process. A series of temperature-programmed desorption (TPD) experiments were carried out in order to determine the activation energy of desorption. Two distinct desorption peaks were detected for all the metal impregnated activated carbons, which the authors claim is due to corresponding interaction of the sulphur compound (DBT) with the activated carbon surface (functional groups) and with the metal ions impregnated on the surface of activated carbon. The study claims that this is an indication of forming new adsorptive sites for the sulphur compounds. The desorption activation energies were measured as follows (all units in kJ/mol): Ag(I)/AC = 92.96, Zn(II)/AC = 88.64, Ni(II)/AC = 74.91, Cu(II)/AC = 69.32, AC = 54.65 and Fe(III)/AC = 47.39. The study also claims that the enhancement of interaction with sulphur compounds due to silver loading is due to the fact that Ag^{+} is a soft acid and DBT is a soft base, while

the reduction in activation energy of desorption for iron impregnated activated carbon is due to the fact that Fe^{3+} is a hard acid, while DBT was soft base. The authors claim that the loading of copper, nickel and zinc on the surfaces of the activated carbon could weaken the local hard acids of the surface of the activated carbon therefore, the DBT adsorption was somewhat enhanced (Yu et al. 2007).

The adsorption performance of seven activated carbons and three activated alumina were evaluated in a batch adsorption system and a fixed-bed flow adsorption system for removing quinoline and indole from a model diesel fuel in the coexistence of sulphur compounds and aromatics. The authors showed that different adsorbents show significantly different selectivity toward basic and non-basic nitrogen compounds (quinoline and indole) and sulphur compounds (dibenzothiophene and 4,6-dimethyldibenzothiophene). Generally, the activated carbons show higher capacity than activated alumina for removing the nitrogen compounds. The selectivity as well as adsorption capacity of the activated carbon sorbents for nitrogen compounds were correlated with their textural properties and oxygen content. The authors claim that the microporous surface area and micropore volume are not key factors in the removal of nitrogen compounds in the tested activated carbons. Also, the oxygen functionality of the activated carbons may play a more important role in determining the adsorption capacity for the nitrogen compounds since the adsorption capacity for nitrogen compounds increases with increased oxygen concentration of the activated carbons. The type of the oxygen-functional groups may be crucial in determining their selectivity for various nitrogen or sulphur compounds. Regeneration of the saturated adsorbents was conducted by toluene washing followed by heating to remove the remained toluene. The paper claims that the spent activated carbons can be regenerated to fully recover the adsorption capacity (100% regenerability) (Song et. al. 2009).

A study by Selvavathi *et al.* consisted of adsorptive desulphurization of refractory sulphur compounds including, dibenzothiophene (DBT), 4-methylbenzothiophene (4MDBT) and 4,6-dimethyl-dibenzothiophene (4,6-DMDBT). Two commercially available activated

carbons and modified forms of the same activated carbons, acid treated using HNO_3, and Ni supported systems were studied for sulphur adsorption. The modified activated carbons showed better adsorption capacity in comparison to the original activated carbons (as received) (Selvavathi *et al.* 2009).

A study was carried out by He *et al.* on adsorption desulphurization of fluid catalytic cracking (FCC) gasoline using oxidized activated carbon (via ozone) as an adsorbent. The study claims that under optimum adsorption conditions, including: activated carbon particles 80 - 100 mesh, adsorption temperature of 80°C and liquid hourly space velocity of 1.70 h^{-1}, sulphur content in initial FCC gasoline effluent after adsorption was reduced from 796 μg/g to 18 **μ**g/g, with an initial desulphurization efficiency of 97.7%. The authors also claim that the activated carbon can be regenerated after reaching saturation. The regeneration conditions were optimized as follows: ethanol as desorption agent, desorption temperature of 60°C and liquid hourly space velocity of 11.70 h^{-1} for ethanol. After reusing the activated carbon 3 times, the adsorption capacity drops to 45 **μ**g/g and the initial desulphurization efficiency drops to 94.3% (He *et al.* 2008).

A study on adsorptive desulphurization of diesel fuel was carried out using CuO supported on activated carbon and modified with acid (i.e., HNO_3) in a fixed bed reactor experiment. The factors affecting desulphurization capacity decreased in the order: mass fraction of HNO_3, calcination temperature, activation temperature, mass loading content of CuO and lastly, the temperature of the fixed bed. The author claims to have established optimum conditions for adsorptive desulphurization as follows: the mass fraction of HNO_3 at 65%, calcination temperature at 450°C, activation temperature at 80°C, CuO content of 3% (by weight), and the temperature of the fixed bed at 120°C. Under these conditions, the sorbent was regenerated three times by thermal cycling. The rate of desulphurization declined slowly (Yang *et al.* 2007).

In a study by Yu *et al.* (2007) the removal of sulphur-containing species in oil using activated carbon was explored. A batch type adsorptive apparatus was used to evaluate the desulphurization performance of activated carbons pre-treated under different conditions. The evaluation was based on adsorption isotherms. The initial sulphur content in the model oil compound used was at 440 ppmw. The study claims that the adsorption capacity towards thiophene improved for the activated carbon that was treated with acid (i.e., HNO_3) at 120°C in comparison to the untreated activated carbons. It is also claimed that the optimum adsorption performance is achievable at 20°C, an adsorption time of three hours, and an adsorbent/oil ratio of 0.09 g/g. It was determined that the adsorption isotherm for thiophene on the activated carbons satisfactorily fit the Freundlich model and equation. Thiophene adsorption on the activated carbon was determined to be spontaneous (Yu *et al.* 2007).

Kim *et al.* (2007) conducted a study on adsorptive desulphurization and denitrogenation of a model fuel containing aromatic, sulphur and nitrogen compounds. The study was done on activated carbon-based adsorbents. The results provided new insight into the adsorption properties (selectivity and capacity) of several metal-loaded carbon adsorbents for different compounds. The authors claim that in most cases, the loading of the activated carbon with metals improved the adsorption capacity towards DBT and quinoline while no change was observed for 4,6-DMDBT and indole. The authors showed that Ag loaded activated carbon improved the adsorption capacity of DBT the most, however, the reverse was observed for nitrogen compounds. In case of Ce improved the adsorption capacity for both quinoline and DBT in this study (Kim *et al.* 2007).

In a study conducted by Yao (2006) the surface of adsorptive sorbent made up of activated carbon (AC) was improved through acid treatment (HNO_3) and loading with metallic ions. It was determined that the surface acidity groups of activated carbon increased considerably because of acid treatment. The BET surface area of the activated carbon however, decreases from 667.6 m^2/g to 372 m^2/g. The surface area of the activated carbon

also decreased as a result of metal loading. The study claimed that the adsorption capacity of the sorbent improved as a result of metal ion loading. It was claimed that AC loading with Fe^{3+} exhibits good adsorption performance, with removal ratio of 85.1%, to sulphur complexes of thiophene that are difficult to be removed from gasoline (Yao, 2006).

In a study by Zhou *et al.* (2006) the adsorptive performance of modified activated carbons were evaluated for adsorptive removal of sulphur compounds from a liquid hydrocarbon fuel. In preparing an ultra-high-surface-area activated carbon from Shenfu coal through chemical activation, strong bases NaOH and KOH were used. The study claims that the preparation of sorbent through chemical treatment was optimized based on examining variables such as impregnation time, activating-agent/coal ratio, base (KOH/NaOH) ratio, and activating temperature. The claim indicates that the experimental results support the key impacts that variables such as activating-agent/coal ratio, KOH/NaOH ratio, activating temperature and activating time have on improving the performance of the activated carbon in adsorptive desulphurization. The study also claims that chemical activation with two activating agents of NaOH and KOH may be a more efficient method in developing sorbents with high desulphurization capacity (activated carbon based) in comparison with chemical activation with KOH or NaOH alone. It was determined in their study that the surface area of the activated carbon prepared with mixture of NaOH and KOH was up to 3000 m/g^2 (Zhou *et al.* 2006).

In a study by Ma *et al.* (2006), a series of semi-empirical quantum chemical calculations was performed for the fundamental understanding of the adsorptive mechanism of sulphur compounds over activated carbon. It was determined that acidic oxygen functional groups, carboxyl or hydroxyl, which exist on the surface of activated carbon are adsorption sites for sulphur compounds. The study claims an excellent linear correlation between the estimated heat of adsorption and the experimentally measured selectivity factors. The results indicated that the removal of sulphur compounds from liquid hydrocarbon fuels

could be improved by increasing the acidic oxygen functional groups on the surface of the activated carbon (Ma *et al.* 2006).

In a study by Bandosz and Conchi (2006), a series of sulphur adsorption experiments on impregnated activated carbon was completed. The activated carbon was loaded with sodium, cobalt, copper, and silver. The adsorption of dibenzothiophene was conducted at ambient temperature. The authors claimed a highly dispersed metal loading on activated carbon, with the loading controlled by selective washing. The modified activated carbon adsorbents showed good adsorption capacities and selectivity for DBT. The authors claim that the incorporated metals have three functions; (1) form new active sites for selective adsorption of sulphur compounds; (2) form structural stabilizers for the carbon substrate; and, (3) act as catalyst initiators in reactive adsorption. From the list of metals used for impregnation, cobalt and copper loaded activated carbons showed the highest adsorption capacity. The study claims that this is due to not-well defined catalytic synergetic effects. The study also claims that the presence of sulphur compounds in the structure of the activated carbon (sulfonic functional groups) results in sulphur-sulphur interactions, which improve the adsorption capacity of the sorbent towards DBT (Bandosz & Conchi, 2006).

Zhou et al (2009) conducted a study on adsorption of dibenzothiophene (DBT) from n-octane solution using activated carbon from bamboo charcoal. The equilibrium and kinetics of DBT adsorption on the sorbent as well as the adsorption isotherm of the sulphur adsorption were correlated with Langmuir and Freundlich isotherms. The authors claim that the experimental data well fitted the Freundlich adsorption mechanism. Two simplified kinetic models including pseudo first-order and pseudo second-order equations were selected to follow the adsorption processes. The study claims that the DBT adsorption is best described using the pseudo second-order kinetic equation (Zhou *et al.* 2009).

A comprehensive study on adsorption of organo-sulphur (dibenzothiophene and 4,6-dimethyldibenzothiophene) and organo-nitrogen (quinoline, indole and carbazole)

compounds on activated carbon was carried out by Wen et al (2010). The study was completed on model diesel fuel, light cycle oils and shale oil. The study claims that the activated carbon sorbent was more selective towards the cyclic nitrogen compounds in comparison to the organo-sulphur compounds examined in the study. Amongst the nitrogen compounds the greatest removal rate was achieved by quinoline, in comparison to indole and carbazole. The adsorption kinetics for nitrogen and sulphur compounds were found to follow pseudo second-order kinetics. The authors claim that the external diffusion is not a controlling step in the adsorption process. The study claims that the activated carbon has a highly heterogeneous surface in the adsorption of the said sulphur and nitrogen compounds, with the exception of carbazole, for which a homogeneous surface is claimed. The adsorption process is claimed to be spontaneous and favourable due to a negative free energy for adsorption (Wen *et al.* 2010).

A competitive adsorption study, comparing the adsorption of polycyclic aromatic sulphur heterocycles (dibenzothiophene and 4,6 dimethyldibenzothiophene) and polycyclic aromatic hydrocarbons (naphthalene, anthracene and phenanthrene) on activated carbon was studied by Bu et al (2011). The study focused on determining the impact of non-sulphur polycyclic compounds on the adsorption of sulphur compounds. The study claims that the adsorptive affinities of molecules with polycyclic aromatic skeleton structure are mainly due to the π–π dispersive interaction between the aromatic rings and the surface of the activated carbon. It is also claimed that the electron donor–acceptor mechanism plays a key role in the adsorption of sulphur compounds. The study also looked at the pore sizes of the activated carbon and claims that the adsorption of large molecules in an effective manner would require the pore size to be larger than the critical diameter of the adsorbate. Larger pore size means reduction in diffusion resistance. The study claims that the adsorption selectivity increased in the following order: naphthalene<fluorine <dibenzothiophene<4,6-dimethyldibenzothiophene<anthracene<phenanthrene. The authors also concluded that the adsorption capacity of sulphur compounds decreases significantly in the presence of polycyclic aromatic hydrocarbons. The observed competition is said to

be due to similarity in structure, molecular diameter and adsorption mechanisms between the sulphur compounds and those of polycyclic aromatic hydrocarbons (Bu, Loh *et al.* 2011).

A sulphur adsorption study was carried out by Tang et al (2011) using ion-exchanged (Ag) mesoporous aluminosilicate as the sorbent. The adsorbate was dibenzothiophene in a binary solution with n-octane. The equilibrium adsorption data for dibenzothiophene was fitted to Langmuir and Freundlich isotherm models. The study claims that the data fit well with the Langmuir isotherm model and that the temperature and the active sites on the surface of the aluminosilicate play a key role in adsorption capacity of dibenzothiophene. The authors also claim that π-complexation plays a role in sulphur adsorption and is more effective at higher temperature and that the saturated adsorption capacity had a linear correlation with the silver ions loaded on the adsorbents (i.e., higher metal contents means improved adsorption capacity). The study indicates that for more effective adsorption of sulphur species through π-complexation the process can be operated at higher temperature. The authors suggest that since adsorptive desulphurization will occur after hydrodesulphurization process, where the temperature of the reactor / content is high, having the adsorptive desulphurization occur at higher temperature would not only have a higher adsorption capacity, but also it will mean cost savings, as the temperature of the feedstock is not required to be reduced (Tang, Li *et al.* 2011).

The key findings of adsorptive sulphur removal research published to date, including experimental conditions (e.g., Temperature, LHSV), initial sulphur concentrations and sulphur adsorption capacities, are summarized in TABLE 3.2, below. The highest adsorption capacity listed in the table pertains to thiophene adsorption in n-octane solution, using Cu(I)-Y (LPIE) zeolite, at approximately 2.6 mmol-S/g. Although this is an impressive adsorption capacity, it is not for refractory sulphur compounds that are commonly targeted in more recent research work, such as dibenzothiophene and methylated dibenzothiophene (e.g., 4,6 dimethyldibenzothiophene). As mentioned earlier,

these compounds, especially the 4,6 DMDBT, are amongst the most challenging compounds to be eliminated/removed through HDS and/or adsorption methods, mainly due to the steric hindrance caused by the methyl groups of the benzene rings. The maximum reported adsorption capacity for key refractory sulphur compound (4,6 dimethyldibenzothiophene) is at 0.52 mmol-S/g, which was achieved using an activated carbon based sorbent (see Table 3.2) (Liu *et al.*, 2010).

Table A-1 in Appendix A summarizes the description and findings of some of the key sulphur adsorption work/methods that have been researched and/or are currently commercialized.

The focus of this research work is on adsorptive removal of dibenzothiophene and 4,6 dimethyldibenzothiophene as well as key organo-nitrogen compounds including, quinoline and carbazole.

TABLE 3.2 – ADSORBENTS INVESTIGATED FOR ADSORPTIVE REMOVAL OF SULPHUR FROM FUEL – RESEARCH STAGE

Sorbent	Fuel Description	Sulphur in Fuel (ppmw)	Adsorption Conditions	Saturated Capacity (mg-S/g)	Saturated Capacity (mmol-S/g)	Reference
Ni/Si-Al	Gasoline	305	200 °C LHSV = $4.8h^{-1}$	>9.5	>0.30	Ma *et al.*
Ni-Al	Gasoline	210	Ambient Temperature	>1.7	>0.05	Ma *et al.*
Ni-Al	Real jet fuel	210	200 °C LHSV = $4.8h^{-1}$	>>4.4	>>0.14	Ma *et al.*
Cu(I)-Y (VPIE)	Jet fuel	364	Ambient Temperature	23.1	0.72	Hernandez-Maldonado *et al.*
Zn(II)-Y (LPIE-RT)	Jet fuel	364	Ambient Temperature	3.7	0.12	Hernandez-Maldonado *et al.*
Zn(II)-X (LPIE-RT)	Jet fuel	364	Ambient Temperature	6.3	0.20	Hernandez-Maldonado *et al.*
CuCl/AC	JP-5	1172	Ambient Temperature, LHSV = $2.3h^{-1}$	4.8	0.15	Wang *et al.*
$PdCl_2/Al_2O_3$	JP-5	1172	Ambient Temperature, LHSV = $2.3h^{-1}$	9.1	0.28	Wang *et al.*
$PdCl_2$/AC	JP-5	1172	Ambient Temperature, LHSV = $2.3h^{-1}$	19.7	0.62	Wang *et al.*

Sorbent	Fuel Description	Sulphur in Fuel (ppmw)	Adsorption Conditions	Saturated Capacity (mg-S/g)	Saturated Capacity (mmol-S/g)	Reference
Ni/Si-Al	JP-8	736	220 °C LHSV = $2.4h^{-1}$	-	-	Velu *et al.*
Ni/Si-Al	Light JP-8	380	220 °C LHSV = $2.4h^{-1}$	-	-	Velu *et al.*
KYNiIE-3 (red)	Light JP-8	380	80°C	~6	~0.19	Velu *et al.*
KYNi8lWl (red)	Light JP-8 Real diesel	380	80°C	~7	~0.12	Velu *et al.*
Activated Carbon	Diesel	297	Ambient Temperature	9.41	0.29	Hernandez-Maldonado and Yang
Selexsorb CDX (AL_2O_3)	Diesel	297	Ambient Temperature	12.17	0.38	Hernandez-Maldonado and Yang
Ce(IV)-Y (LPIE-80)	Diesel	297	Ambient Temperature	3.91	0.12	Hernandez-Maldonado and Yang
Cu(I)-Y (LPIE-RT)	Diesel	297	Ambient Temperature	11.97	0.37	Hernandez-Maldonado and Yang
AC/Cu(I)-Y (LPIE-RT)	Diesel	297	Ambient Temperature	13	0.41	Hernandez-Maldonado and Yang
CDX/Cu(I)-Y (LPIE-RT)	Diesel	297	Ambient Temperature	10.97	0.34	Hernandez-Maldonado and Yang

Sorbent	Fuel Description	Sulphur in Fuel (ppmw)	Adsorption Conditions	Saturated Capacity (mg-S/g)	Saturated Capacity (mmol-S/g)	Reference
CDX/Cu(I)-Y (LPIE-RT)	Diesel	297	Ambient Temperature	13.63	0.43	Hernandez-Maldonado and Yang
Cu(I)-Y (VPIE)	Diesel	297	Ambient Temperature	13.12	0.41	Hernandez-Maldonado and Yang
CDX/Cu(I)-Y (VPIE)	Diesel	297	Ambient Temperature	14.02	0.44	Hernandez-Maldonado and Yang
Ni(II)-Y (LPIE-RT)	Diesel	297	Ambient Temperature	6.53	0.20	Hernandez-Maldonado and Yang
Ni(II)-Y (LPIE-135)	Diesel	297	Ambient Temperature	6.82	0.21	Hernandez-Maldonado and Yang
Na-Y	T in n-octane (model fuel)	760	Ambient Temperature	33.6	1.05	Hernandez-Maldonado *et al.*
Na-Y	T in benzene	760	Ambient Temperature	3.2	0.10	Hernandez-Maldonado *et al.*
H-Y	T in n-octane	760	Ambient Temperature	36.8	1.15	Hernandez-Maldonado *et al.*
Ag-Y (LPIE)	T in n-octane	760	Ambient Temperature	29	0.91	Hernandez-Maldonado *et al.*
Ag-Y (LPIE)	T in benzene	760	Ambient Temperature	5.5	0.17	Hernandez-Maldonado *et al.*

Sorbent	Fuel Description	Sulphur in Fuel (ppmw)	Adsorption Conditions	Saturated Capacity (mg-S/g)	Saturated Capacity (mmol-S/g)	Reference
Cu(I)-Y (LPIE)	T in n-octane	760	Ambient Temperature	81.8	2.56	Hernandez-Maldonado *et al.*
			re-estimated based on provided breakthrough curve.	-	-	Hernandez-Maldonado *et al.*
Cu(I)-Y (LPIE)	T in benzene	760		17.3	0.54	Hernandez-Maldonado *et al.*
Cu(I)-Y (LPIE)	T in n-octane	190	Ambient Temperature	41	1.28	Hernandez-Maldonado *et al.*
Cu(I)-Y (LPIE)	T in 20% benzene, 80% n-octane	190	Ambient Temperature	14.1	0.44	Hernandez-Maldonado *et al.*
Cu(I)-Y (LPIE)	T in isooctane	190	Ambient Temperature, LHSV = $12h^{-1}$	~23	0.72	Ma *et al.*
Ni(II)-Y (LPIE)	BT,DBT, and 4,6-DMDBT in n-octane	150	Ambient Temperature	-	-	Ko *et al.*
Ni(II)-Y (LPIE)	BT,DBT, and 4,6-DMDBT in n-octane with 5 v/v % benzene	150	Ambient Temperature	-	-	Ko *et al.*
Ni(II)-Y (LPIE)	BT,DBT, and 4,6-DMDBT in n-octane with 5000 ppmw H_2O	150	Ambient Temperature	-	-	Ko *et al.*

Sorbent	Fuel Description	Sulphur in Fuel (ppmw)	Adsorption Conditions	Saturated Capacity (mg-S/g)	Saturated Capacity (mmol-S/g)	Reference
Ni-Al	T+BT in paraffins with 8% toluene	400	Ambient Temperature, LHSV = $24h^{-1}$	14.2	0.44	Ma *et al.*
Ni-Al	T+BT in paraffins with 8% toluene + 5.1% olefin	400	Ambient Temperature, LHSV = $24h^{-1}$	4	0.13	Ma *et al.*
Ni-Al	DBT and 4,6-DMDBT in paraffins with 10% *t*-butybenzene and 303 ppmw N	687	Ambient Temperature, LHSV = $4.8h^{-1}$	2.4	0.08	Ma *et al.*
KYNi30lWl (reduced)	BT+ 2-BT+ 5-BT in decane with 19% *n*-butylbenzene	506	Ambient Temperature	11	0.34	Velu *et al.*
KYNi30lWl (reduced)	BT+ 2-BT+ 5-BT in decane with 19% *n*-butylbenzene	506	80°C	11.5	0.36	Velu *et al.*
Activated alumina	DBT and 4,6-DMDBT in paraffins with 10% *t*-butybenzene and 303 ppmw N	687	Ambient Temperature, LHSV = $4.8h^{-1}$	3.4	0.11	Kim *et al.*
AC	DBT and 4,6-DMDBT in paraffins with 10% *t*-butybenzene and 303 ppmw N	687	Ambient Temperature, LHSV = $4.8h^{-1}$	16.3	0.51	Kim *et al.*
AC (ACNU)	BT, DBT, 4-MDBT, 4,6-DMDBT in paraffins with 10% butybenzene	398	Ambient Temperature, LHSV = $4.8h^{-1}$	13.1	0.41	Zhou *et al.*

Sorbent	Fuel Description	Sulphur in Fuel (ppmw)	Adsorption Conditions	Saturated Capacity (mg-S/g)	Saturated Capacity (mmol-S/g)	Reference
AC [8]	BT, DBT, 4-MDBT, 4,6-DMDBT in paraffins with 10% butybenzene	398	Ambient Temperature, LHSV = $4.8h^{-1}$	16.7	0.52	Zhou *et al.*
Cu(I)-Y (LPIE-RT)	Real gasoline	335	Ambient Temperature	12.61	0.39	Hernandez-Maldonado and Yang
Cu(I)-Y (LPIE)	Gasoline	305	Ambient Temperature, LHSV = $4.8h^{-1}$	0.64	0.02	Ma *et al.*
AC/Cu(I)-Y (LPIE-RT)	Gasoline	335	Ambient Temperature	15.87	0.50	Hernandez-Maldonado and Yang
Ni/Si-Al	Gasoline	305	Ambient Temperature, LHSV = $4.8h^{-1}$	1.5	0.05	Ma *et al.*
Ni(II)-X (LPIE-RT)	Diesel	297	Ambient Temperature	8.03	0.25	Hernandez-Maldonado and Yang
Ni(II)-Y (SSIE)	Diesel	297	Ambient Temperature	9.25	0.29	Hernandez-Maldonado and Yang
CDX/Ni(II)-Y (SSIE)	Diesel	297	Ambient Temperature	10.59	0.33	Hernandez-Maldonado and Yang
NaY	DBT in Hexadecane	900	30 °C	48	1.5	Ng *et al.*
NiY	DBT in Hexadecane	900	30 °C	32	1.0	Ng *et al.*

Sorbent	Fuel Description	Sulphur in Fuel (ppmw)	Adsorption Conditions	Saturated Capacity (mg-S/g)	Saturated Capacity (mmol-S/g)	Reference
CsY	DBT in Hexadecane	900	30 °C	32	1.0	Ng *et al.*
Ni(II)-Y (LPIE)	Diesel	186	Ambient Temperature	~0.5	0.02	Ko *et al.*

Source: Hydrogen and Syngas Production and Purification Technologies, 2010, pp.248 – 252.

Note:
T: Thiophene, BT: Benzothiophene, DBT: Dibenzothiophene, 4,6 DMDBT: 4,6 dimethyldibenzothiophene
JP-8, JP: reference to jet fuel specifications based on U.S. Gov. publication (1990)
AC: Activated Carbon, Y: Y-zeolite
LHSV: Liquid hourly space velocity (unit: 1/hour)

3.3 Adsorption

The process of adsorption is based on three main types of intermolecular interactions between a sorbate (also referred to as adsorbate) and sorbent (also referred to as adsorbent): (1) dispersion (van der Waals) energy, (2) electrostatic interactions and (3) chemical bond. The dispersion energy consists of an intermolecular interaction which is highly repulsive when in near-field, weakly attractive at intermediate separation and non-existing at large separation distances. A weaker form of energy, known as induction, resulting from dipole and induced-dipole interaction is typically grouped implicitly with the dispersion energy. The van der Waals' weak intermolecular attractive force increases with an increase in molecular density (i.e., increase in number of moles or decrease in volume). Also important to dispersion (van der Waals) energy is the ability to polarize, or polarizability of the interacting pair (both sorbate and sorbent). The higher the polarizability of the surface atom of a sorbent, the higher the potential for dispersion and adsorptive interaction (Do, 1998).

The electrostatic energy is the interaction of permanent dipoles/multipoles with the electric field. For this type of interaction, the charges and van der Waals radii of the surface atoms of the sorbate-sorbent are key, as they determine the strength of the electric field, based on Coulomb's equation:

$$F = K_c [q_1.q_2] / r^2 \qquad (3\text{-}1)$$

Where:

$F =$	magnitude of electric force
q_1 and $q_2 =$	charges on interacting pair (i.e., charges on sorbate and sorbent)
$r =$	distance between centers of interacting pair (sum of their van der Waals' radii)
$K_c =$	electrostatic constant

The two commonly distinguished forms of adsorption are physisorption and chemisorption. In physisorption, a molecule is adsorbed onto a surface without undergoing a significant change in its electronic structure, whereas in case of chemisorption, the electronic structure

of the adsorbate (i.e., molecule being adsorbed on to the surface) is significantly perturbed. It is common to assume that an adsorbate is chemisorbed when the adsorbate's bond energy to the surface is greater than 10 kcal/mol and physisorbed when it is at or below 10 kcal/mol (Masel, 1996). Nevertheless, it is important to note that distinguishing between chemisorption and physisorption may not be as clear in every case, especially in cases were a particulate adsorbate can be adsorbed to a surface both physically and chemically, due to variability in adsorptive sites and/or the nature of the adsorbate molecule. There are also instances were an adsorbate is initially physisorbed to the surface and then converted to a chemisorbed state (Masel, 1996).

Another distinction that can be made for surface adsorption is based on the change that an adsorbate molecule will go through when adsorbed onto a surface. If the adsorbate molecules remain intact after adsorption the process can be considered a *non-dissociative adsorption* whereas if bond cleavage occurs in the adsorbate (i.e., formation of new molecules) it can be referred to as dissociative adsorption (Masel, 1996).

For some chemical bonds, a weak bond, involving for example π electrons (i.e., electrons that participate in π-complexation), is the driving force in an intermolecular interaction. The weak π-bonding between a sorbent and a sorbate is also referred to as π-complexation. This type of bonding is only applicable in the case of transition metals with d-orbitals. For these sorbents, in addition to their typical σ-bonds using their s-orbital electrons, π-bonds are also formed due to the ability of the d-orbital electrons to back-donate electron density to the π-orbital of the sorbate (Yang, 2003).

In case of transition metals, the furthest occupied electron levels are "d" orbitals. The "d" orbitals of the transition metals are more diffused and spatially delocalized in comparison to the "s" and "p" orbitals. The unique properties of the "d" orbital, including the angular orientation and radial distribution are responsible for the distinctive characteristics of the transition metals (Kiselev & Krylov, 1989).

The strength of attraction between sorbent and sorbate is dependent of the following factors:

- How empty is the "s" orbital of the outermost electron shell of the cation on the sorbent surface.
- Availability of π-electrons in the sorbate, which can be donated to the cation of the sorbent.
- Availability of "d" orbital electrons of the cation on the sorbent surface and ease of donating "d" orbital electrons to the sorbate (Yang, 2003).

Sorbents commonly consist of transition metals or metal oxides supported on porous structures such as alumina or activated carbons, or activated carbons which in addition to their porous structure inherently have functional groups such as carbonyls and carboxyls on the surface. The dispersion / near-field repulsion forces exists in all sorbate-sorbent interactions and is believed to be the dominant force in the case of activated carbon. For metal oxides and zeolites, the electrostatic interactions often dominate (Masel, 1996).

The adsorption performance of activated carbons depends on both physical and chemical properties of its surface. Physical properties, including surface area, pore size and distribution, are key in determining contact between the sulphur-bearing compounds and active functional groups (e.g., carbonyl) on the surface. Chemical properties such as the type and density of surface functional groups are key in determining the type of adsorption (chemisorption / physisorption), capacity, and the ability to regenerate. Both the physical and chemical properties of a carbon sorbent vary depending on the source, activation conditions and methodology (Bansal and Goyal, 2005).

Separation via adsorption is based on three fundamental mechanisms:

1- *Steric mechanism* – which is when the porous media of the sorbent has pore dimensions that prevent the larger molecules from entering the pores;

2- *Equilibrium mechanism* – which is based on variation in the ability of the sorbent to adsorb different species (i.e. stronger adsorbed species are removed more readily from the stream); and,

3- *Kinetic mechanism* – which is based on the variations in rate of diffusions of different species into the pores of the sorbent (i.e. by controlling the exposure time, one can preferentially remove faster diffusing species).

In many instances, more than one of the above listed mechanisms comes into play in the adsorptive separation process (Do, 1998).

3.4 Sorbent Selection for Sulphur Adsorption

In this section, the rationale for selecting sorbents for adsorptive removal of sulphur compounds is discussed. The focus of the discussion is on activated carbon, which as will become clear by the end of this sub-section, is a valuable and effective sorbent to be used for the purposes of sulphur removal from transportation fuel.

3.4.1. Activated Carbon - Background

Activated carbon is made up primarily of carbon, modified through chemical and physical treatments to have a porous structure with extremely high surface area. In many cases, a single sample of activated carbon can contain pore sizes that are macropores (dia.>50 nm), mesopores (2 nm<dia.<50 nm) and micropores (dia.< 2nm) (Do, 1998). The surface area of activated carbon can be in the thousands of square-metres per gram of activated carbon. For example, in his work on selective adsorption of refractory sulphur species, Farag reports an activated carbon with a surface area of 3,060 m^2/g (Farag 2007).

Activated carbons have many applications in the chemical, biological, medical and environmental fields. Some of the most common applications of activated carbon include water purification (e.g., drinking water treatment), gas purification (e.g., extraction of volatile organic compounds), air filtration (e.g., personal respirators), and flue gas cleaning (simultaneous removal of SO_2 and NO_x) (McGuire and Suffet, 1980). The adsorptive nature of activated carbon makes it a good candidate for removal of pollutants from air and water, in environmental applications such as spill cleanup, remediation of contaminated ground water, and capture of volatiles from painting/coating, fuel dispensing, dry cleaning and other processes, some of which are discussed below (Serp and Figueiredo, 2009).

In recent years, research has been undertaken in the use of activated carbon for storing natural gas and hydrogen gas. The porous nature of the activated carbon acts like a sponge for different gases including natural gas and hydrogen. In most cases, gases are attached to the carbon material via Van der Waals forces. The adsorbed gases can then be extracted / desorbed through application of heat. Natural gas can be combusted and hydrogen can be used in hydrogen fuel cell applications. The storage of gas in activated carbons is appealing mainly because the gas can be stored in a low pressure, low mass, low volume environment, which is considered to be more feasible and safer than bulky on board compression tanks in vehicles (Pfeifer *et al.* 2008).

In medical applications, activated carbon is commonly used for treating overdoses and poisoning. The activated carbon can bind / adsorb the poisoning agent (depending on the poison) and thus prevent absorption by the gastrointestinal tract (Serp and Figueiredo, 2009).

Activated carbon filters are also used to retain radioactive gases from a nuclear boiling water reactor turbine condenser. The air vacuumed from the condenser contains traces of radioactive gases. Activated carbon adsorption beds are used to adsorb and retain the trace radioactive gases (Serp and Figueiredo, 2009).

Iodine or sulphur impregnated activated carbon is commonly used to capture and retain mercury in the flue gas associated with the combustion of coal in coal-fired power plants and wastes in medical waste incinerators (Serp and Figueiredo, 2009).

In heterogeneous catalysis, activated carbon is used as a support for active sites (e.g., transition metals and/or transition metal oxides) and as a surface for facilitating chemical reactions. A few examples of such application are provided below:

- In their 2004 research work, Silva and Figueiredo used activated carbon with manganese(III) salen complexes bearing hydroxyl groups for epoxidation of styrene in acetonitrile, using iodosylbenzene as an oxygen source. The research showed that the heterogenized catalysts are chemo-selective towards the styrene epoxide compared to their homogeneous counterparts, and they are resistant to leaching and can be re-used without loss of their catalytic activity. (Silva *et al.* 2004).

- Iron-impregnated activated carbon was tested for its catalytic properties in the oxidation of 4-chlorophenol in aqueous solution with hydrogen peroxide. The authors suggested suitability of such a catalyst for such an application in a fixed-bed reactor (Lücking *et al.* 1998).

- It was demonstrated that Pd on activated carbon (Pd/C) is an active and selective single catalyst for multi-step reactions in domino and tandem reactions involving (1) Heck reactions and hydrogenations for the synthesis of (a) dibenzyl and (b) 2-styryl-phenylamine, (2) Sonogashira coupling and intramolecular heteroannulation to form indole ring systems, and (3) Heck and Suzuki coupling reactions to produce 4-styryl-biphenyl. The activated carbon based catalyst showed a yield of 72 to 93% (Gruber *et al.* 2004).

- A heterogeneous copper-impregnated activated carbon was used as a catalyst in wastewater treatment, for the purpose of oxidation of organic pollutants. Highly porous activated carbon was used as the catalyst support. The catalyst was designed to promote the oxidation of organic pollutants in dyeing and printing wastewater from the textile industry. The activated carbon based catalyst enhanced the conversion of organic compounds in dyeing and printing wastewater, shortened the reaction time, and lowered the reaction temperature and the system total pressure (Hu *et al.* 1999).

- Activated carbon was successfully used as a support for a molybdenum catalyst for hydrodesulphurization. It was determined that the catalytic activity for thiophene hydrodesulphurization increased with increases in porosity and surface area of the activated carbon (Serp and Figueiredo, 2009).

Activated carbons are produced from various sources including, biomass such as coconut shells, general nutshells and wood, as well as coal and petroleum coke (petcoke). The activation process varies resulting in different characteristics in the produced activated carbon, however, the process typically consists of steam and/or acid treatment followed by thermal treatment, which results in formation of various functional groups on the surface of the activated carbon, the most common ones being the oxygen functional groups such as carbonyl and carboxyl. Depending on the source of carbon and the activation process, other functional groups, such as nitrogen-containing ones including, pyridine, amide, imides, lactam and pyrrole can form on the surface of activated carbon. Halides and sulphur can also exist on the surface and form complexes with other surface functional groups (Jansen and van Bekkum 1995). The existence of sulphur species on the surface of the activated carbon is not desirable for many applications and is considered to be an impurity, especially for cases where the activated carbon is to be used as a substrate for transition metals (Gould, Baturina *et al.* 2009). Baker and Rolison have reported that Pt nanoparticles were fully poisoned by the sulphur in the activated carbon substrate (Vulcan) (Baker *et al.* 2004).

The particle size of activated carbon used in adsorption or catalytic applications plays a key role in its performance. The powdered form of activated carbon (particle sizes of less than 125 micron) presents a large surface area to volume ratio with a small diffusion distance (i.e., shallow pores). The granular activated carbon on the other hand has a relatively larger particle size compared to powdered activated carbon and consequently, presents a smaller external surface area and deeper pores. Therefore, diffusion of adsorbate for granular activated carbons can be an important rate determining step. As a result, granular forms of activated carbons are more commonly used for gaseous adsorbates due to their faster rate of diffusion.

In literature, smaller particle sizes are associated with improved activity for activated carbon when used for catalytic / adsorptive applications. For example, for hydrogen and formic acid oxidation, activated carbon with smaller particle size is shown to perform better than those with larger particle sizes. It should however be noted that smaller particle size catalyst/sorbent (activated carbon) does not always positively influence the reaction rate and/or adsorption capacity. For example, it is well documented that for reactions such as oxidation of carbon monoxide and methanol as well as the oxygen reduction reaction on Pt / activated carbon catalyst, the activity of the catalyst decreases with a decrease in particle size (Serp and Figueiredo, 2009).

For metal impregnation of activated carbon, a few key factors can influence the activity / capacity of the catalyst / sorbent, including:

- The structure and morphology of the support (i.e., activated carbon) can influence the dispersion of metal nanoparticles.

- The catalytic / adsorptive activity or capacity can be affected by the interaction between the metal and substrate as the functional groups on the surface of the activated carbon interact with the metal nanoparticles.

- The catalytic / adsorptive activity or capacity can be impacted by antagonistic interaction of metal nanoparticles with impurities of the activated carbon such as sulphur and/or halides, resulting in poisoning of metal active sites.

It is documented in the literature that the interaction of some of the surface functionalities (e.g., carboxyl group) with catalyst precursors affects the dispersion of active sites (i.e., metal particles). Some authors have also indicated that oxygen-containing functional groups on the surface can also influence the intrinsic catalytic activity of the metal particles on the surface (Serp and Figueiredo, 2009).

3.4.2. This Research Work

Activated carbons possess a high level of flexibility for use as sorbents and/or supports for adsorptive removal of organo-sulphur compounds. Several of the useful attributes of activated carbon are listed below:

- The physical attributes of the activated carbon, including surface area, degree of dispersion of active sites and pore size distribution vary significantly depending on the source of carbon and activation process. They can be modified to facilitate a particular purpose such as the diffusion of reactants and products to and from the active sites. Similarly, the chemical attributes of the surface include functional groups and acidic/basic properties can be modified to fit a particular purpose (Serp and Figueiredo, 2009).

- The structure of activated carbon is stable at high temperatures and is resistant to both acidic and basic media (Serp and Figueiredo, 2009).

- Activated carbons can be obtained from waste streams such as petroleum coke (petcoke) which is generated as a result of the coking process at petroleum processing facilities. The use of a waste stream for a useful application at petroleum refineries (e.g., adsorptive desulphurization) makes it an attractive option for the industry not only in terms of cost, but also in terms of accessibility.

- Generally, activated carbons are inexpensive and in most cases cheaper than conventional catalyst supports.

- The metal active sites (impregnated metals) can be recovered, if and when the sorbent's adsorptive properties diminish, through combustion of the activated carbon. This process can also be a source of energy.

Activated carbon therefore is an attractive sorbent for adsorptive desulphurization of transportation fuel. The research work presented here focuses on activated carbons and modified activated carbons. The modifications to the activated carbon include metal impregnation and thermal treatment in inert conditions. The purpose of activated carbon modification and impregnation is to enhance its performance in adsorptive removal of sulphur compounds.

4.0 Experimental Methods

As mentioned in the previous section, the overall objective of this research work was to identify, develop and characterize, based on sorbent characterization and underlying scientific principles, sorbents that are effective in removing refractory sulphur compounds from fuel, through the process of selective adsorption. In order to achieve the objectives, several sorbents were prepared based on information from relevant literature. A series of liquid phase adsorption isotherm experiments were completed using the prepared sorbents. The adsorption mechanisms were identified and a series of sorbent characterization experiments were completed on the best performing sorbent. In the end, a series of flow reactor experiments were completed using the best performing sorbent, in order to gain some insight into the kinetics of adsorption and impact of temperature on sulphur adsorption.

The following list provides the breakdown of experimental work completed as a part of this research:

1. ***Sorbent selection and preparation***

2. ***Liquid phase adsorption study:***
    a. Metal impregnation and adsorption performance
    b. Adsorption isotherm mechanism
    c. Organo-nitrogen adsorption
    d. Competitive adsorption and selectivity
    e. Sorbent regenerability

3. ***Heat of adsorption study***

4. ***Sorbent characterization:***
    a. Surface area and pore size
    b. Acidity strength
    c. Surface functional groups
    d. Surface morphology and dispersion
    e. Oxidation state and surface chemical bonds

5. Flow Reactor Experiment – A kinetic study

This chapter provides a brief explanation on the instruments and experimental methodologies used to carry out the above-mentioned experimental work, with the exception of the flow reactor experiments, which are discussed in Section 7. Also, more details regarding the experimental methods are provided in subsequent sections of this report, where the results of the experiments are discussed.

The model organo-sulphur compounds used in this study were: dibenzothiophene (DBT) and 4,6-dimethyldibenzothiophene (4,6-DMDBT), and the organo-nitrogen compounds were quinoline (QIN) and carbazole (CBZL). Hexadecane (model diesel compound) was used as the solvent for all the experimental work.

4.1 Sorbent Selection and Preparation

As mentioned in sub-section 3.4, the focus of this research work is on activated carbon and modified (i.e., impregnated) activated carbon. The activated carbon will have two functions (1) act as a support for active sites (i.e., metals) that would be impregnated on its surface, and (2) act as a sorbent (adsorptive interaction of sulphur compounds with the surface functionalities of the activated carbon).

Sorbent preparation as well as surface area and pore size determination techniques, commonly used for evaluating sorbents are discussed in this section.

4.1.1. Activated Carbon

Three activated carbons with varying characteristics, including source, surface area and pore size distribution were selected based on previous preliminary work carried out by our research group in 2003 and 2004. The three selected activated carbons and their supplier / manufacturer are summarized in TABLE 4.1.

TABLE 4.1 – SELECTED ACTIVATED CARBONS

Sorbent	ID	Manufacturer / Distributor
Activated Carbon - Centaur	ACC	CALGON
Activated Carbon - Norit	ACN	Aldrich Chemical
Acid-washed Activated Carbon	AAC	Aldrich Chemical

The preliminary evaluation of the three activated carbons was to determine if there is a correlation between the surface area and sulphur adsorption performance. The BET areas were correlated with the adsorption capacities for DBT (Table 5.1 and 5.2) to determine if greater surface area translates to higher adsorption capacity for sulphur compound (DBT). It should be noted that as mentioned previously, other factors such as surface functional groups also play a key role in the adsorption capacity of an activated carbon. This topic will be further explored in Section 5.

Metal Impregnation on Activated Carbon

A selection of alkaline earth and transition metals were selected based on their characteristics, the preliminary work completed by our research group and information gathered from relevant literature. The metals were used in preparing metal-impregnated activated carbon. The expected result is a sorbent with well dispersed active sites (metal

species) that can interact with the existing functional groups on the surface of the activated carbon as well as adsorbate species for improved performance.

To build on the previous work of our research group in terms of further improving the adsorption characteristics of activated carbon for sulphur adsorption, the best performing activated carbon amongst the selected three was used for metal impregnation experiments. The procedure to prepare metal impregnated activated carbon is discussed below.

The procedure for the metal impregnation on the activated carbons sorbent is as follows:

- For the selected metals, a 2% wt. (metal) solution was prepared using the corresponding water soluble salts. The metals and their corresponding salts are summarized in TABLE 4.2, below.

- Ground and dried activated carbon (< 125 μm) was added to the solution and stirred for 24 hours at ambient temperature and atmospheric pressure.

- The mixture was filtered (suction-filtration) and air dried for 24 hours.

- The air dried activated carbon was treated under helium (He) flow at 110 °C for 3 hours, followed by 1 hour thermal treatment at 400 ^{o}C. The initial thermal treatment at 110 °C was to ensure that most of the physisorbed materials (including moisture) are removed without inducing a structural modification of the sorbent at this initial stage. The subsequent thermal treatment at 400 °C was to induce a structural uniformity and improve crystalline structure in terms of pore accessibility. This is further discussed in sub-section 6.6.3 (HRTEM). The thermal treatment was done in a glass flow reactor with a 0.8 micron pore size frit supporting the activated carbon. The reactor was purged with helium for 10 minutes

before introducing heat. The helium flow was continuous throughout the thermal treatment at a flow rate of 90 mL/min.

This method of impregnation while different than wet impregnation is considered to be suitable for the purposes of this research work as it is relatively easy to implement and has shown to provide relatively good dispersion of metal species on the surface of the activated carbon.

The metals selected for the impregnation of activated carbon were based on the literature review for sulphur adsorption applications (e.g., used in ion-exchanged zeolites) and applications in which catalysts with acidic (Lewis acid) properties were prepared. This is discussed further below and in subsequent sections. The metals used for the impregnation of activated carbon and their respective water-soluble metal salts used in the impregnation process are listed in **TABLE 4.2**.

TABLE 4.2 - METALS USED FOR AC IMPREGNATION

Sorbent	ID	Metal Salt Used for Impregnation
Ag-impregnated Centaur Activated Carbon	Ag / ACC	$AgNO_3$
Fe-impregnated Centaur Activated Carbon	Fe / ACC	$FeSO_4$
Ta-impregnated Centaur Activated Carbon	Ta / ACC	TaF_5
Sn-impregnated Centaur Activated Carbon	Sn / ACC	$SnCl_2$
Ni-impregnated Centaur Activated Carbon	Ni / ACC	$Ni\ (NO_3)_2$
Co-impregnated Centaur Activated Carbon	Co / ACC	$CoNO_3$
Ga-impregnated Centaur Activated Carbon	Ga / ACC	$Ga(NO_3)_3$
Sr-impregnated Centaur Activated Carbon	Sr / ACC	$Sr(NO_3)_2$

4.1.2. Preliminary Sorbent Characterization

The following sections discuss some of the most commonly used techniques for characterizing a sorbent in terms of surface area, pore volume and particle size distribution and their impact on the intended purpose of the sorbent (in this case sulphur adsorption).

BET – Surface Area

As a part of the preliminary assessment the specific surface area (m^2/g) of the selected activated carbons were determined based on Brunauer-Emmett-Teller (BET) methodology. The methodology and the equations are discussed below and the results are presented in Table 4.1, above.

BET theory makes the following assumptions:

1. Gas molecules physically adsorb on solid surfaces in layers;
2. there is no interaction between each adsorption layer; and,
3. Langmuir adsorption theory can be applied to each layer.

The latter is in reference to monolayer and equal energies across the adsorption sites.

The BET equation is expressed as follows:

$$\frac{1}{\nu}\left[\frac{P_o}{P} - 1\right] = \left[\frac{(c-1)}{c\nu_m}\right]\left[\frac{P}{P_o}\right] + \frac{1}{c\nu_m} \qquad (4\text{-}1)$$

Where,

P = Equilibrium pressure of adsorbate at the temperature of adsorption (torr)

P_o = Saturation pressure of adsorbate at the temperature of adsorption (torr)

v = Quantity of adsorbed gas (cc/g)

v_m = Quantity of gas adsorbed in monolayer (cc/g)

c = BET constant, calculated as follows:

$$c = \exp\left[\frac{E_1 - E_L}{RT}\right] \tag{4-2}$$

Where,

E_1 = Heat of adsorption of the first layer

E_L = Heat of adsorption for second and higher layers

The BET equation (4-1) above can be plotted with the x-axis being $\left[\frac{P}{P_o}\right]$ and the y-axis being $\frac{1}{v}\left[\frac{P_o}{P} - 1\right]$. The v_m can then be calculated from the slope and the y-intercept of the linear plot, as follows:

$$v_m = \left[\frac{1}{(slope + y - \text{int})}\right] \tag{4-3}$$

The total surface area and the specific surface area (i.e., per unit mass) are calculated using equations (4-4) and (4-5), below:

$$S_{tot} = \left[\frac{v_m . N . s}{V}\right] \tag{4-4}$$

Where,

S_{tot} = Total surface area (m^2)

N = Avogadro's number (6.02×10^{23} /mol)

V = Molar volume of adsorbent gas (cc)

s = adsorption cross section area ($°A^2$) (10^{-20} m)

$$S = \frac{S_{tot}}{W} \qquad (4\text{-}5)$$

Where,

S = Specific surface area (m^2/g)

W = Weight of sorbent (g)

For the purposes of this study, a Micrometrics GEMINI® instrument was employed. The following procedures were followed:

1. Activated carbon samples were pre-treated for 2 hours under a flow of helium gas. The treatment consisted of heating under inert gas (He), at a temperature ramp-up rate of 3^oC/min to a maximum of 200 ^oC (held at this temperature for two hours).

2. The dry activated carbon sample weights were determined from the weights of the sample tubes with the samples before and after the pre-treatments. The samples were then transferred to the adsorption unit.

3. The BET surface area was calculated by adsorbing nitrogen gas at liquid nitrogen temperature, following a pre-programmed procedure built-in to the instrument for calculating the surface area and pore volumes for activated carbons (note: the pore volume determination is discussed in Section 6.3; for the preliminary assessment only surface area was determined).

Sorbent Particle Size

From the three selected activated carbons, the best performing one (i.e., highest adsorption capacity towards DBT) was selected for further analysis including assessment of adsorption performance as a function of particle size distribution.

In order to determine the level of impact that sorbent particle size (i.e., contact surface) has on adsorption performance, adsorption studies were undertaken for three different particle size ranges, as follows: (a) 250 μm – 500 μm; (b) 125 μm – 250 μm; and (c) less than 125 μm (powder).

The particle size impact analysis was completed with the activated carbon that had the highest adsorption capacity towards DBT (see Table 5.1). The liquid phase adsorption of a DBT-hexadecane mixture was carried out for each size fraction. The methodology for the liquid phase adsorption is described in the following sub-section. In addition, the heat of adsorption was measured for the three adsorbents with different particle sizes, using flow calorimetry, details of which are discussed in subsequent sections.

4.2 Liquid Phase Adsorption Study

Equilibrium adsorption of organo-sulphur and/or organo-nitrogen in a binary solution with hexadecane was employed to determine and compare the adsorption performances of the prepared sorbents. From these equilibrium adsorption experiments, adsorption isotherms were constructed for each sorbent. Adsorption isotherm provides insight into the adsorption mechanism of a particular sorbent-adsorbate interaction. The saturated adsorption capacity of a sorbent towards a particular adsorbate can also be determined from its adsorption isotherm. The equilibrium adsorption isotherm experiments were performed according to the following steps:

- The sorbent was thermally treated under helium (He) flow at 110 °C for 3 hours, followed by 1 hour at 400 ^{o}C. This was done in a fixed bed reactor with the sorbent being supported on a 0.8 μm glass frit.

- Approximately 5g of adsorbate mixture (hexadecane + adsorbate such as DBT and/or 4,6 DMDBT) for each concentration (see Table 4.3) was dispensed in labelled vials. For each adsorbate mixture vial an identical adsorbate mixture vial was also used as a blank.

- Dried sorbent was immediately added to the mixture, and placed in pre-heated (at 50 °C) water-bath. The adsorption temperature was maintained at 50^{o}C.

- Magnetic stir bars were used in each vial for continuous mixing.

- The adsorption experiment (mixing at 50 °C) was carried out continuously for 20 hours.

- At the end of each run, the vials were centrifuged to remove the sorbent particulates from suspension. Each vial was centrifuged at 3000 RPM for 10 minutes.

- Samples were extracted from each vial and analyzed for sulphur concentration using gas chromatography coupled with a flame ionization detector (GC/FID) (see below for details on GC/FID analysis).

- The measured sulphur concentration in each of the samples was compared against the corresponding concentration in the stock solution to determine the amount adsorbed. Calculation details are discussed in Section 5.1.

Mixtures of DBT in hexadecane or 4,6 DMDBT in hexadecane were prepared with target sulphur concentrations as summarized in Tables 4.3 and 4.4, respectively.

TABLE 4.3 - HEXADECANE/DBT SOLUTIONS PREPARED FOR ISOTHERMAL ADSORPTION

Solution No.	Calculated Gravimetric Concentration (ppmw-S)	GC / FID Analysis (mmol-S / L)
1	3000	66.39
2	2200	51.65
3	1800	41.68
4	1200	26.81
5	900	20.84
6	400	9.26
7	200	4.73
8	100	2.79

Note:
The calculated concentrations are based on the weight of solvent (hexadecane) and that of DBT, rounded to the nearest 10^{th}.
For the purposes of calculating adsorption capacity, measured (GC/FID) values were used (in mmol-S/L).

TABLE 4.4 - HEXADECANE/4,6 DMDBT SOLUTIONS PREPARED FOR ISOTHERMAL ADSORPTION

Solution No.	Calculated Gravimetric Concentration (ppmw-S)	GC / FID Analysis (mmol-S / L)
1	800	21.48
2	400	10.21
3	200	4.95
4	100	2.72
5	50	1.34
6	25	0.64

Note:
The calculated concentrations are based on the weight of solvent (hexadecane) and that of 4,6 DMDBT, rounded to the nearest 10^{th}.
For the purposes of calculating adsorption capacity, measured (GC/FID) values were used (in mmol-S/L).

Gas Chromatography Analysis

GC analysis was carried out using a Varian CP-3800 gas chromatograph equipped with an automatic sampler, a VF-5MS capillary column (30 m x 0.32 mm, film thickness;1.0mm) and three detectors: flame ionization detector (FID), thermionic specific detector (TSD) and pulsed flame photometric detector (PFPD). The FID was maintained at a temperature of 300°C, nitrogen specific TSD at 300°C, and sulphur specific PFPD at 200°C. The following temperature program was used to analyze the concentration of the adsorbate sulphur compounds:

For hexadecane – DBT mixture:

Initial temperature = 80^{o} C (for 0 minute)
Temperature ramp-up rate = 10^{o} C/min (17 minutes)
Temperature 2 = 250^{o} C (final temperature for 8 minutes)
Detector temperature (FID) = 300^{o} C
Detector temperature (PFPD) = 200^{o} C
Auto sampler injection volume = 0.5 μL

For the hexadecane – 4,6-DMDBT mixture, due to the higher boiling point of DMDBT the upper temperature was set at 265 ^{o} C for a duration of 2.5 minutes:

For hexadecane - 4,6-DMDBT mixture:

Initial temperature = 80^{o} C (for 0 minute)
First temperature ramp-up rate = 5^{o} C/min
Temperature 2 = 120^{o} C (for 0 minute)
Second temperature ramp-up rate = 2^{o} C/min
Temperature 3 = 170^{o} C (for 0 minute)
Third temperature ramp-up rate = 10^{o} C/min (17 minutes)
Temperature 4 = 265^{o} C (final temperature for 2.5 minutes)

Detector temperature (FID) = 300^{o} C

Detector temperature (PFPD) = 200^{o} C

Injection volume = 0.5 μL

The GC/FID data for the stock solution (DBT in hexadecane or 4,6 DMDBT in hexadecane) are presented in Tables 4.3 and 4.4, above. For each sample at least two (2) injections (i.e., runs) were completed. In cases where the two values were significantly different, three new runs were completed.

Supplementary data for GC/FID analytical method and calibration are provided in Appendix C.

4.3 Heat of Adsorption Study

One of the methods of obtaining insights into the nature of the adsorption, including bond strength is to measure heat of adsorption. To obtain this, the Flow Calorimetry method, which was pioneered by our research group in the area of sulphur adsorption, was used to determine the heat of adsorption. Details of this methodology and its implementation are discussed below and also in subsequent sections.

Flow Calorimetry

Heat of adsorption was measured using a flow microcalorimeter. A schematic diagram of the SETARAM C80 is provided in **FIGURE 4.1**. This microcalorimeter is equipped with an auxiliary thermostat and two percolation cells, one functions as a reference cell and the other as a sample cell. Three Teledyne ISCO D-Series high precision syringe pumps were used to pump the solvent and adsorbate mixture through the percolation cells (both reference and sample cells). Approximately 0.25g of the heat-treated sorbent was loaded into the sample cell, which was promptly placed in the calorimeter under the solution (hexadecane) in order to minimize exposure to air. Pure solvent (hexadecane) was pumped through both the empty reference cell and over the adsorbent bed in the sample cell at a flow rate of 4.00 mL/h. The calorimeter and auxiliary heater were set to 30°C to preheat the feed. All the syringe pumps and pumping lines were maintained at an isothermal temperature of 30°C. The solvent was pumped through the calorimeter until thermal equilibrium was reached. The thermal equilibrium condition was characterized by a constant heat flow output ('baseline') seen in the resident Setsoft® software that was integrated with the Setaram C80 Flow Microcalorimeter. The feed to the sample cell in the calorimeter was then switched to the adsorbate solution (21.8 mmol of adsorbate (DBT) per liter of solution (hexadecane)) by the three way valve, while the flow of pure solvent (i.e. hexadecane) continued through the reference cell at the same flow rate. As the adsorbate solution passes over the sorbent bed, the heat evolved upon the

displacement of solvent by solute (adsorbate) molecules on the adsorbent was measured by the calorimeter. Samples of the calorimeter effluent were collected periodically. The sulphur concentrations in the collected samples were determined by GC analysis. The DBT heat of adsorption for each adsorbent was determined by integrating the area under heat flow curve. The amounts adsorbed were also determined from the breakthrough curves, constructed using the GC-determined sulphur concentrations. Molar heat of adsorption for sulphur in DBT was determined from these two values. As adsorption solution passes over the sorbent bed, the heat evolved upon the displacement of solvent by adsorbate molecules or adsorbate-solvent complex (heat of displacement) was measured by the resident Setsoft® software which was integrated with the calorimeter. The effluent samples were collected periodically at regular intervals and analyzed using gas chromatography.

FIGURE 4.1 - SETARAM C80 FLOW CALORIMETRY – A SCHEMATIC DIAGRAM

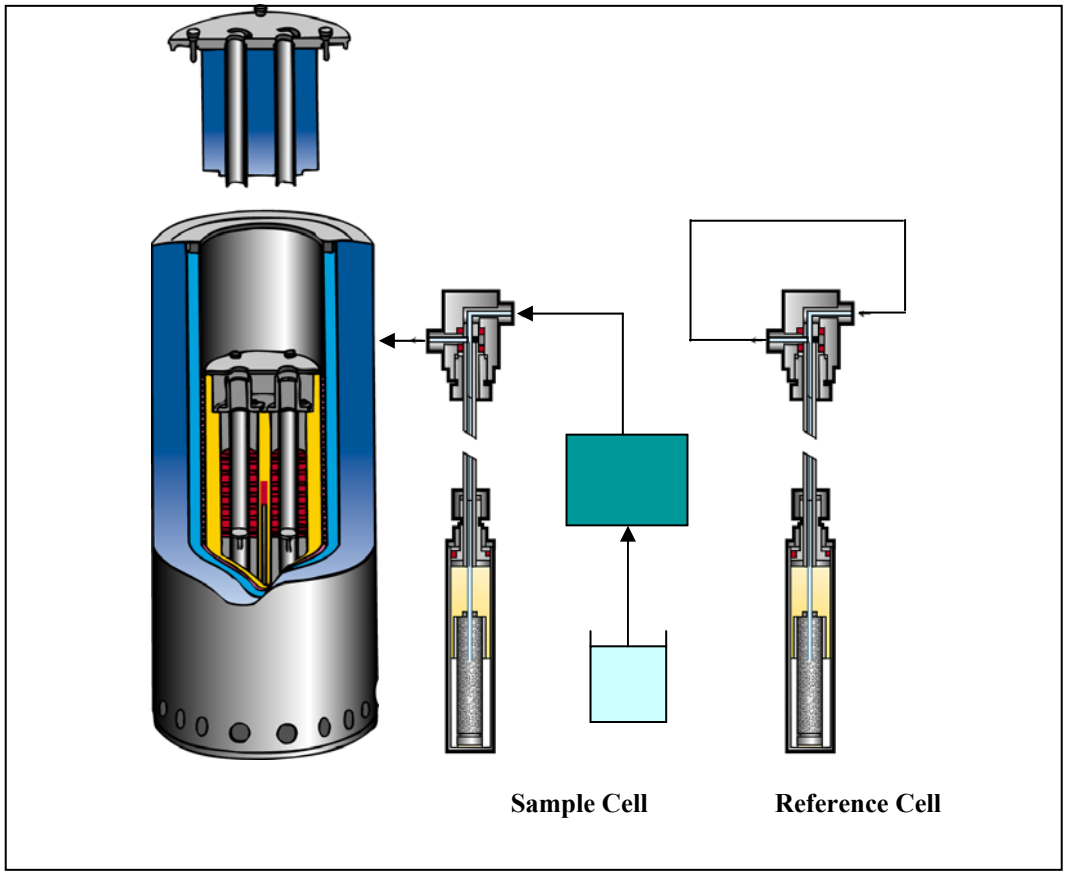

4.4 Best performing sorbent and additional analysis

The results from the equilibrium adsorption study was used to identify the sorbent with the highest adsorption capacity for DBT and/or 4,6-DMDBT (note: as a part of competitive adsorption study, adsorption analysis was conducted on a mixture solution containing both DBT and 4,6 DMDBT). The identified sorbent (i.e., best performing) was studied further in order to determine surface characteristics and/or material properties that resulted in the observed performance improvement as well as to gain a better understand of the adsorption mechanism. Subsequent studies on the best performing sorbent included: effect of metal loading (i.e., percent by weight of impregnated metal) on the adsorption capacity, study of adsorption isotherm mechanisms, organo-nitrogen adsorption study, competitive adsorption and selectivity analysis, sorbent regeneration analysis, sorbent acidity study, assessment of change in surface functional groups as a result of sulphur compound adsorption, oxidation state of impregnated metal on the surface of the sorbent and surface bonds formed after adsorption, heat of adsorption analysis, surface morphology and qualitative assessment of degree of dispersion of the impregnated metal on the surface of the sorbent. These studies are briefly discussed below and additional explanations and the results are presented in Sections 5 and 6.

1- Effect of Percent Metal Loading

In order to better determine the impact of metal impregnation on the adsorption performance (in this case the adsorption capacity), equilibrium adsorption isotherm study was undertaken for sorbents with different metal loadings (i.e., percent metal weight used in impregnation).

The initial metal impregnation was 2% by weight for all the metals examined in this study. Subsequently, the adsorption of DBT and 4,6 DMDBT in hexadecane was performed on activated carbon sorbents with 2wt%, 5wt% and 10wt% metal loadings. This was completed for the impregnated activated carbon that had the best adsorption capacity towards the sulphur compounds.

2- Adsorption Isotherm Mechanism

Since the initial analysis indicated improved adsorption performance as a result of metal impregnation (for some of the selected metals) additional adsorption isotherm studies were undertaken to determine an adsorption mechanism that best fits the metal-modified activated carbon. The study included curve fitting of the adsorption data, linearization of adsorption isotherm and linear regression analysis.

3- Organo-Nitrogen Adsorption Study

The organo-nitrogen compounds co-exist in the precursors of transportation fuel and often inhibit the sulphur removal by blocking the active sites on the adsorbent used for hydrodesulphurization or sulphur adsorption. Removal of organo-nitrogen compounds such as quinoline and carbazole from the untreated fuel is therefore an important step in adsorptive removal of sulphur. Therefore, equilibrium adsorption analysis was conducted for selected organo-nitrogen compounds, employing the best performing adsorbents.

4- Competitive Adsorption and Selectivity Analysis

Given that in petroleum refining application precursors of transportation fuel include a mixture of organo-sulphur and organo-nitrogen compounds along with aromatics, a competitive adsorption and selectivity study was undertaken for the best performing sorbent. The analysis consisted of equilibrium adsorption analysis for an equi-molar (21.8 mmol/L each) mixture of DBT, quinoline and naphthalene in hexadecane.

5- Sorbent Regeneration

The regenerability of the spent adsorbent was conducted to assess its feasibility for industrial scale petroleum refining. A combination of solvent wash, ultrasonic treatment and thermal treatment were used to test the regenerability of the spent sorbents. The adsorption capacity of the regenerated sorbent was determined through equilibrium adsorption analysis. The spent (i.e., used) sorbent was washed with toluene while under ultrasonic treatment. The sorbent was subsequently dried and heat treated under helium (He) flow at 110 °C for 3 hours, followed by 1 hour at 400 °C.

6- Sorbent Characterization

Sorbent characterization including surface analysis was completed for the best performing sorbent as well as virgin activated carbon (i.e., un-impregnated activated carbon) in order to better understand the mechanism and properties that led to the improved adsorption performance. The characterization included:

- BET Surface Analysis – The specific surface area (m^2/g-sorbent), pore volume and pore diameter analysis was also completed for the three different metal loadings and compared against un-impregnated activated carbon (i.e., virgin AC).

- HRTEM – EDX Analysis – The surface of the sorbent was examined for morphology and dispersion of impregnated metal on the surface using high resolution transmission electron microscopy (HRTEM). Also, the surface elements were identified using energy dispersive X-ray (EDX) spectroscopy.

- XPS Analysis – The oxidation state and potential bond forming between the adsorbate and adsorbent species was investigated using X-ray Photoelectron Spectroscopy (XPS).

- TPD Ammonia Analysis – The acidity strength of the sorbent was analyzed using Temperature Programmed Desorption (TPD) with Ammonia.

- FTIR Analysis – The surface functional groups of the sorbent were analyzed using Fourier Transform Infrared (FTIR) spectroscopy.

Additional details for the above-mentioned characterization methods and equipment are provided below and in subsequent sections (Section 5 and Section 6).

HRTEM

The TEM analysis of the sorbents was performed at the Canadian Centre for Electron Microscopy at the McMaster University. The TEM analysis was carried out on a FEI Titan 80-300 Cubed TEM equipped with a CEOS-designed hexapole-based aberration corrector for the image-forming lens and one for the probe-forming lens. The instrument operates a high-resolution monochromator allowing 0.1eV energy resolution with improved spectrometer optics (Gatan 866 model), stable spectrometer electronics and high-tension supply. The instrument is fitted with a Super-Twin lens in order to achieve sub-Angstrom resolution both for phase contrast imaging and Scanning Transmission Electron Microscopy (STEM). Additional explanation is provided along with the results in Section 5.

XPS

The XPS analysis was conducted at the University of Waterloo's Chemistry Department. The analysis was performed using a Thermo-VG Scientific ESCALab 250 Microprobe, equipped with a monochromatic Al Kα X-ray source with an energy rating of 1486.6 eV and a typical energy resolution of 0.4-0.5 eV full-width. The principles of measurement and details of the experimental setup are discussed Section 5.

TPD-Ammonia

Temperature programmed desorption of NH_3 was carried out using a Altamira TPD adsorption system. In a typical experiment, approximately 0.1 g of adsorbent sample was pre-treated in a U-shaped quartz sample tube attached to the sample port in a flow of argon (carrier gas) for 30 minutes at 200 ^{o}C. Then the sample was cooled to room temperature under the argon flow and NH_3 gas was adsorbed onto the sample in pulses until it was saturated. Saturation of the adsorbent with the ammonia gas was ensured by observing Thermal Conductivity Detector (TCD) signal of the instrument's software. After this step sample was flushed using the carrier gas at room temperature for 5 minutes

to remove the physisorbed NH_3. Then the sample was gradually heated at a rate of 10 ^oC/min to 1000 ^oC, followed by cooling of the sample back to room temperature. The desorption of NH_3 was monitored by a response signal from the thermal conductivity detector. The TCD response was plotted against time and temperature to give the desorption pattern of NH_3 (see Figure 6.10).

FTIR

A qualitative assessment of surface functional groups present on the surface of the activated carbon and changes to these functional groups after impregnation and sulphur adsorption was undertaken using FTIR. As infrared light hits the sample, it is absorbed much like in the UV spectroscopy. Unlike in UV spectroscopy, the molecule must experience a change to the dipole moment as it absorbs the light. The energy causes either a vibration or rotation in a bond, which we see in the IR spectrum. Each peak represents a specific stretch, bend, or rotation in the molecule. Some very intensely seen peaks are due to O-H, N-H, C=C and C=O stretches. Peaks are not seen for N_2 or O_2, because these bonds do not experience a net change in dipole as a result of their vibration. There are often times that different peaks correspond to the same bond in a molecule. This is because the bond can vibrate in many different ways that induce a change to the dipole moment. In general an IR spectrum is divided into two sections: the functional group area and the fingerprint area. In this study the focus will mostly be on the functional group area. This is the area where peaks are associated with characteristic functional groups like O–H or C=O. In this assessment IR spectra are examined for the presence or absence of peaks in the IR spectrum to confirm the presence or absence of certain functional groups in the selected activated carbon based sorbents.

The interpretation of infrared spectra involves the correlation of absorption bands in the spectrum of an unknown compound with the known absorption frequencies for the types of bonds. The characteristic infrared adsorption frequencies for various bonds (compounds) are summarized in Table 4.5. The infrared absorbencies for some key

functional groups are illustrated in Figure 4.2. To identify the source of an absorption band one would need to assess the intensity (weak, medium or strong), shape (broad or sharp), and position (cm^{-1}) of the band in the spectrum. Additional explanations as well as results are provided in Section 5.

TABLE 4.5 - CHARACTERISTIC INFRARED ABSORPTION FREQUENCIES

Bond	Compound Type	Frequency range, cm^{-1}
C-H	Alkanes	2960-2850(s) stretch 1470-1350(v) scissoring and bending
	CH3 Umbrella Deformation	1380(m-w) - Doublet - isopropyl, *t*-butyl
C-H	Alkenes	3080-3020(m) stretch 1000-675(s) bend
	Aromatic Rings	3100-3000(m) stretch
C-H	Phenyl Ring Substitution Bands	870-675(s) bend
	Phenyl Ring Substitution Overtones	2000-1600(w) - fingerprint region
C-H	Alkynes	3333-3267(s) stretch 700-610(b) bend
C=C	Alkenes	1680-1640(m,w)) stretch
CºC	Alkynes	2260-2100(w,sh) stretch
C=C	Aromatic Rings	1600, 1500(w) stretch
C-O	Alcohols, Ethers, Carboxylic acids, Esters	1260-1000(s) stretch
C=O	Aldehydes, Ketones, Carboxylic acids, Esters	1760-1670(s) stretch
	Monomeric -- Alcohols, Phenols	3640-3160(s,br) stretch
O-H	Hydrogen-bonded -- Alcohols, Phenols	3600-3200(b) stretch
	Carboxylic acids	3000-2500(b) stretch
N-H	Amines	3500-3300(m) stretch 1650-1580 (m) bend
C-N	Amines	1340-1020(m) stretch
CºN	Nitriles	2260-2220(v) stretch
NO_2	Nitro Compounds	1660-1500(s) asymmetrical stretch 1390-1260(s) symmetrical stretch

Note:
v - variable, m - medium, s - strong, br - broad, w - weak

Source: (Young, 1996)

FIGURE 4.2 - INFRARED ABSORBANCE FOR COMMON FUNCTIONAL GROUPS

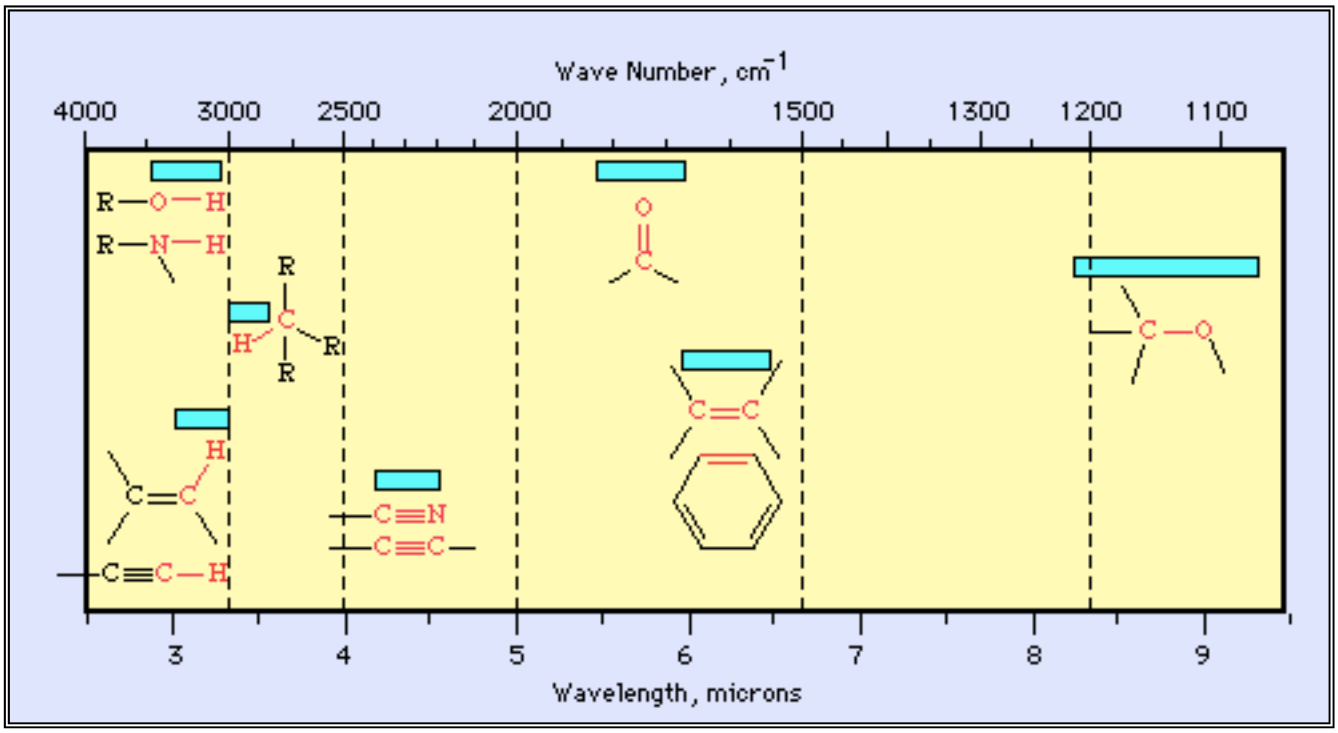

Source: (Young, 1996).

In this study, the samples were pre-treated at 120°C and inert gas (He) for one (1) hour prior to IR analysis.

5.0 Results & Discussion

This section includes an initial background review of key adsorption isotherm mechanisms. The latter part of this section includes the experimental data and discussion of the results and findings.

5.1 Adsorption Isotherms – A Background Review

The key adsorption isotherm mechanisms that will be utilized to fit experimental data in this study are discussed below. The data fitting details for all isotherms are provided in Appendix C. In all cases the data was fitted to more than one mechanism in order to determine the mechanism that best represents the experimental data. The isotherm mechanisms were selected based on relevant information from the literature review (i.e., Langmuir and Freundlich) and the adsorption scheme postulated by the author for sulphur adsorption on metal-impregnated activated carbon (i.e., Sips).

Langmuir Adsorption Isotherm

The Langmuir Isotherm is the most commonly used isotherm to describe adsorption. The Langmuir Isotherm can be derived from the thermodynamics of the equilibrium state of the following reaction:

$$\mathbf{S + A} \rightleftharpoons \mathbf{SA}$$

where S represents the adsorbate, A represents the empty active sites on the adsorbent, and SA represents the complex of an active site with the adsorbate adsorbed to its surface. The equilibrium constant, K (L/mol), for this reaction can be written as:

$$K = \frac{[SA]}{[S][A]} \qquad (5\text{-}1)$$

Where:

[S] = concentration of adsorbate

[A] = concentration of active sites

[SA] = concentration of adsorbate adsorbed on active sites

The concentration of the active-site and adsorbate complex, [SA], can be written as:

$$[SA] = \frac{q_e}{q_m} \tag{5-2}$$

Where,

q_m = Maximum adsorption capacity (mmol/g)

q_e = Actual amount of moles of adsorbate per unit adsorbent at equilibrium (mmol/g).

q_m is simply the total number of moles of adsorbate per unit adsorbent that theoretically could be adsorbed onto the surface of the adsorbent if every active site was filled. The concentration of the remaining empty active sites at equilibrium, [A], can therefore be written as $[A] = 1 - \frac{q_e}{q_m}$. If the equilibrium adsorbate concentration, [S], is replaced with the concentration of adsorbate at equilibrium [C_e, (mmol/L)] and equation (5-1) is rewritten, it yields:

$$K = \frac{\frac{q_e}{q_m}}{C_e\left(1 - \frac{q_e}{q_m}\right)} \tag{5-3}$$

which can be rearranged to yield the *Langmuir Isotherm*:

$$q_e = \frac{q_m K C_e}{1 + K C_e} \tag{5-4}$$

Where,

C_e = Concentration of adsorbate within the solution at equilibrium (mmol/L)

K = Equilibrium constant

In this equation, C_e and q_e can both be experimentally determined and q_e can be calculated by the equation:

$$q_e = \frac{(C_o - C_e)\rho_s m_s}{m_a} \tag{5-5}$$

Where,

C_o = Initial solution concentration (mmol/L)

ρ_s = Solution density (g/L)

m_s = Mass of solution (g)

m_a = Mass of adsorbent (g)

Also in equation (5-4) is the equilibrium constant K, and the maximum adsorption capacity q_m. These values can both be experimentally determined by linear regression of equation (5-4). A popular form of linear regression is to rewrite equation (5-4) as:

$$\frac{C_e}{q_e} = \frac{1}{q_m} C_e + \frac{1}{K q_m} \tag{5-6}$$

When a plot of $\frac{C_e}{q_e}$ versus C_e is made the maximum adsorption capacity (qm) and the Langmuir equilibrium constant (K) can be calculated as follows:

$$q_m = \frac{1}{slope} \tag{5-7}$$

$$K = \frac{1}{q_m \times (y - \text{intercept})} = \frac{slope}{(y - \text{intercept})} \tag{5-8}$$

Also, note that $K = k_{ads} / k_{des}$, where K_{ads} and K_{des} correspond to adsorption and desorption rate constants, respectively.

Freundlich Adsorption Isotherm

The Freundlich isotherm is one of the earlier empirically derived equations used to describe multi-layer adsorption. The Freundlich isotherm is the most important multi-site adsorption isotherm for rough surfaces (e.g., activated carbon) (Masel, 1996). The Freundlich equation has the form:

$$C_n = K\, C^{1/n} \qquad (5\text{-}9)$$

Where:

C_n = concentration of adsorbed species (mmol /g)

K = fitting parameter (generally temperature dependent) ($mmol^{1-1/n}\, L^{1/n}$ /g)

n = fitting parameter (generally temperature dependent)

The larger the n value, the more the isotherm's behaviour deviates from linear isotherm (Do, 1996).

The linearized version of Freundlich's equation (5-9) is obtained by taking the logarithm of the original equation, above:

$$\log_{10} C_n = \log_{10} (K) + 1/n \log_{10}(C) \qquad (5\text{-}10)$$

The values of 'K' and 'n' are obtained from the slope and y-intercept of the linear plot of $\log C_n$ versus logC, as follows (Do, 1998):

$$n = 1 / \text{Slope} \qquad (5\text{-}11)$$

$$K = 10^{\,(\text{y-intercept})} \qquad (5\text{-}12)$$

Modified Langmuir Isotherm (Sips Equation)

An isotherm equation that has received some attention is a modified version of the Langmuir equation, which also incorporates the multi-layer / multi-site characteristics of Freundlich isotherm (Do, 1998).

In their 2005 research work, Sohn ad Kim state there are two possible reasons why the Langmuir isotherm, which was originally used to describe gaseous-solid systems, may not work as well for liquid-solid systems: (1) when a species is adsorbed from a solution there will be accompanying desorption of another species for charge balance considerations; and (2) an adsorptive surface can be heterogeneous and result in island type adsorption which is different than Langmuir's uniform, monolayer adsorption (Sohn and Kim 2005).

The equation for this isotherm is as follows:

$$\theta = \frac{KC^x}{(1 + KC^x)} \qquad (5\text{-}13)$$

Where:

C = Solute concentration

θ = surface coverage ($\theta = q / q_{max}$)

K = Langmuir equilibrium constant ($K = k_{ads}/k_{des}$)

X = fitting parameter

Through rearranging, equation (5-13) can be written in its linear form as follows:

$$\frac{1}{q} = \left[\frac{1}{Kq_{max}}\right]\left[\frac{1}{C}\right]^x + \frac{1}{q_{max}} \qquad (5\text{-}14)$$

The values of K and q_{max} (same as q_m in the Langmuir equation 5-4, above) can be obtained from the slope and y-intercept of the linear plot of 1/q versus $[1/C]^x$. X is a fitting parameter, which when it equals 1, the adsorption resembles that of Langmuir, when less than 1, the adsorbate-sorbent system shows less dependency on concentration (C) and when greater than 1, the system shows a greater dependency on concentration (Sohn and Kim 2005).

5.2 Sorbent Selection & Preparation

The three selected Activated Carbons (ACs) were analyzed for adsorption performance, including adsorption capacity and equilibrium constant. For this assessment, adsorption isotherms, fitted to the linearized version of the Langmuir adsorption isotherm, were used.

Adsorption performances for the selected ACs consisting of maximum adsorption capacity, q_m (from equation 5-4) and equilibrium constant K (from equation 5-3) were calculated using the above mentioned linearization of Langmuir isotherms (equation 5-6). The particle size distribution for the three selected ACs was kept the same (i.e., 125μ - 250μ). In the case of Activated Carbon Centaur (ACC), multiple runs were performed to ensure repeatability. The adsorption capacity (q_m in mmol-S/g-sorbent) and equilibrium constant (K in L/mmol) for the three selected ACs are summarized in **TABLE 5.1**. Results indicate that the ACC has the highest adsorption capacity of the three selected activated carbons. Also presented in Table 5.1 are the regression values (R^2) for the linearization of the Langmuir equation (equation 5-6). The R^2 values (~0.99) for all three ACs indicate that the experimental data fits well with the Langmuir isotherm model.

TABLE 5.1 - ADSORPTION ISOTHERM DATA FOR DBT ON SELECTED ACTIVATED CARBON SORBENTS AT 50 °C

Sorbent	ID	Particle size	Isotherm		DBT in Hexadecane	
			Type*	Linear Regression (R^2)	q_{max} ** (mmol-S/g-sorbent)	K (L/mmol)
Activated Carbon - Centaur	ACC	125 - 250 μ	Langmuir	0.988 ± 0.002	0.57 ± 0.05	1.02 ± 0.20
Activated Carbon - Norit	ACN	125 - 250 μ	Langmuir	0.997	0.47	0.79
Acid-washed Activated Carbon	AAC	125 - 250 μ	Langmuir	0.992	0.37	0.81

Note:

* The isotherm that best fit the data is presented in this table. Details, including R^2 for other isotherm types are presented in Appendix C.

** The q_{max} values are based on Langmuir isotherm equation and in reference to DBT adsorption.

Standard Deviation is provided for experiments with 3 or more repeats.

Sorbent Particle Size Effect on Sulphur Adsorption

In order to determine the impact of particle size on the sulphur adsorption, adsorption performance was assessed for different sorbent particle size distributions. Finer particle sizes means higher surface area, which would facilitate more contact between the sorbent and sorbate and thus improve adsorptive activity of the sorbent (Serp and Figueiredo, 2009). Therefore, it is expected that finer particles sizes would result in better adsorption performance (i.e., higher q_{max}).

Based on it adsorption performance (Table 5.1), the ACC was selected for this analysis. Three particle size distribution ranges were examined: (1) 250µ - 500µ; (2) 125µ - 250µ and (3) < 125µ (powder). At least 2 runs were completed for each particle size fraction range. The mean adsorption capacities and equilibrium constants for both DBT and 4,6-DMDBT are summarized in **TABLE 5.2**.

TABLE 5.2 - ADSORPTION ISOTHERM DATA FOR DBT ON ACC OF VARIOUS PARTICLE SIZES AT 50 °C

Sorbent	ID	Particle size	Isotherm		DBT in Hexadecane	
			Type*	Linear Regression (R^2)	q_{max} ** (mmol-S/g-sorbent)	K (L/mmol)
Activated Carbon - Centaur	ACC-500	250 - 500 μ	Langmuir	0.984	0.45	1.27
Activated Carbon - Centaur	ACC-125	125 - 250 μ	Langmuir	0.988 ± 0.002	0.57 ± 0.05	1.02 ± 0.20
Activated Carbon - Centaur	ACC-PWDR	<125μ	Langmuir	0.992	0.74	0.42

Note:

* The isotherm that best fit the data is presented in this table. Details, including R^2 for other isotherm types are presented in Appendix C.

** The q_{max} values are based on Langmuir isotherm equation and in reference to DBT.

Standard Deviation is provided for experiments with 3 or more repeats. Values without standard deviation are mean values for two runs.

The finer particle size fraction (<125μ) had a q_m that is approximately 33.7% and 34.4% higher for DBT and 4,6-DMDBT, respectively, in comparison to the 500μ particle sizes. The results are therefore in accordance with the expected outcome.

5.3 BET – Surface Area

As a part of sorbent characterization, the three initially selected activated carbons were analyzed for total surface area using BET methodology (see Section 4.5 for details on the theory and methodology). The results are summarized in **TABLE 5.3**.

TABLE 5.3 - BET SURFACE AREA MEASUREMENT

Sorbent	ID	BET Surface Area (m^2/g)			
		run 1	run 2	run 3	Mean
Ni-impregnated Centaur Activated Carbon	Ni / ACC	629.5	627.4	n/a	628
Activated Carbon - Centaur	ACC	635.13	641.2	n/a	638
Acid-washed Activated Carbon	AAC	396.4	415.3	n/a	406
Activated Carbon - Norit	ACN	928.2	916.1	918	921 $\pm$ 7

The mean total surface area values indicate that acid-washed activated carbon (AAC) has the lowest surface area. This correlates well with its lower adsorption capacity. However, ACC is shown to have lower surface area than AC Norit (ACN), yet it is shown that ACC has higher adsorption capacity than ACT. One may conclude that although ACC has lower surface area than ACT, it may have more favourable

morphology (i.e. larger pore sizes) and/or a higher concentration of surface functional groups which can effectively interact with sulphur compounds in the adsorption process. Assessment of pore size distribution may provide more insights into this matter.

The BET surface area for metal-impregnated activated carbon (in this case, nickel on ACC) was also measured in order to determine how much of a reduction in surface area results from metal impregnation. The sample analyzed was 2% by weight Ni-impregnated ACC. Comparison of the surface areas for the impregnated and non-impregnated ACC indicates a reduction of approximately 1.6% (for 2% wt. impregnation). This expected reduction in surface area is considered to be relatively low. Therefore, improved adsorption due to metal impregnation (introduction of new adsorptive sites) is expected to result in an overall improvement of the sulphur adsorption capacity.

5.4 Effect of Impregnation on Sulphur Adsorption

Further adsorption performance assessment was carried out for transition metal impregnated ACC. The first set of assessments was completed for a sorbent particle size range of 125μ - 250μ (also referred to as 125μ). For impregnation, the transition metals were selected based on previous work completed in our research group as well as those published in the literature. As mentioned in previous sections of this thesis, nickel is considered to enhance sulphur adsorption due to its ability (because of its partially filled 'd' orbital) to form π bonding with sulphur of DBT and DMDBT (Hernández-Maldonado, Yang *et al.* 2005). Iron (Fe) and cobalt (Co) also have partially filled "d" orbitals and have been used in zeolite impregnation for sulphur adsorption work. In the case of copper (Cu), due to difficulties in maintaining a Cu^{+1} oxidation state when preparing the sorbent, it was not considered for this assessment. Silver (Ag) also has an unsaturated "d" orbital and has also been used in published sulphur adsorption research work (Chen, Wang *et al.* 2009). Tantalum was used as a catalyst for applications which

required presence of strong Lewis acid sites. With the sulphur in DBT and DMDBT having a lone pair of electrons, tantalum interaction with the lone pair could effectively contribute to sulphur adsorption. Additional explanation regarding other metal candidates used for the impregnation of the activated carbon is provided below.

A preliminary set of liquid phase adsorption experiments were completed using the ACC with a particle size range of 125μ - 250μ (hereby referred to as ACC-125). The ACC-125 was impregnated with Fe and Ag and the sulphur adsorptions were compared with the un-impregnated ACC-125. The resulting isotherms are presented in **FIGURE 5.1**. Isotherms and linearization plots for these runs and repeat runs are provided in Appendix C.

The linearization of the Langmuir isotherm for virgin ACC and the Freundlich isotherm for the impregnated ACC (i.e., Fe/ACC-125 and Ag/ACC-125 (see Appendix C) was used to establish maximum adsorption capacity and the equilibrium constant for each sorbent. These values are summarized in Table 5.4. The R-squared values for the best-fit line of linearized Langmuir / Freundlich isotherms were high, ranging from 0.97 to 0.99, indicating good fit of the experimental data with the corresponding isotherm model.

FIGURE 5.1 - ADSORPTION ISOTHERMS FOR ACC AND IMPREGNATED ACC (PARTICLE SIZE 125μ << 250μ, DBT-C16 BINARY MIXTURE AT 50 °C)

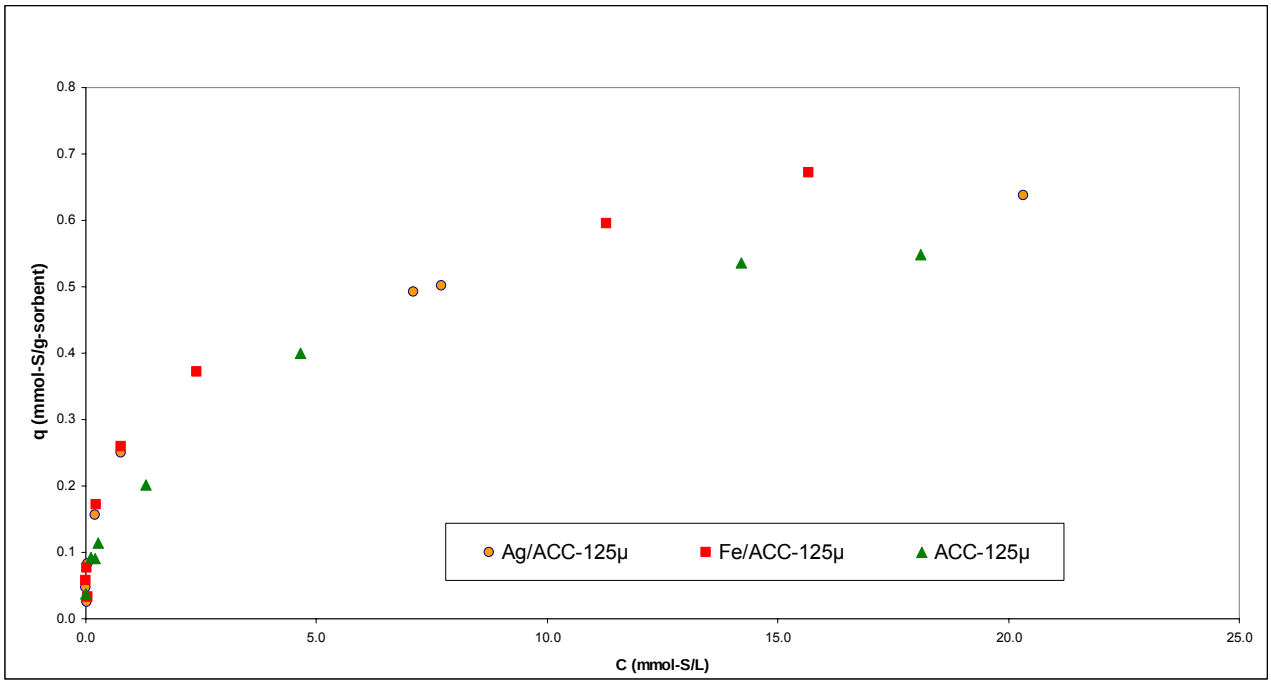

Results indicate that the metal impregnation of the ACC improves the adsorption performance in the following order: Fe/ACC > Ag/ACC > ACC. This can be said about the adsorption capacity as well as the equilibrium constant (see Table 5.4).

TABLE 5.4 - COMPARISON OF ADSORPTION ISOTHERM DATA FOR DBT ON ACTIVATED CARBON BASED SORBENTS AT 50 °C

Sorbent	ID	Impregnation Salt & (Percent Weight Loading)	Particle size	Isotherm		DBT in Hexadecane	
				Type*	Linear Regression (R^2)	q_{max} ** (mmol-S/g-sorbent)	K (L/mmol)
Ag-impregnated Activated Carbon - Centaur	Ag / ACC	$AgNO_3$ (2% by Wt. loading)	125 - 250 µ	Freundlich	0.987	0.637	1.127
Fe-impregnated Activated Carbon - Centaur	Fe / ACC	$FeSO_4$ (2% by Wt. loading)	125 - 250 µ	Freundlich	0.987	0.678	1.190
Activated Carbon - Centaur (Virgin)	ACC	n/a	125 - 250 µ	Langmuir	0.57 ± 0.05	0.57 ± 0.05	1.02 ± 0.20

Note:

* The isotherm that best fit the data is presented in this table. Details, including R2 for other isotherm types are presented in Appendix C.

** The q_{max} values are based on Langmuir or modified Langmuir isotherm equations and in reference to 4,6 DMDBT.

The 2% by Wt. metal loading is based on calculations.

Standard Deviation is provided for experiments with 3 or more repeats.

Given the impact of particle size on adsorption performance (established earlier on) further metal impregnation was carried out using finer particle sizes (i.e., <125μ).

DBT Adsorption Isotherms

Additional transition, alkaline-earth, group III and group IV metals were employed to modify the activated carbons to study their efficiency in sulphur removal. They include, tantalum (Ta), tin (Sn), gallium (Ga) and strontium (Sr). Some of the metal species have unfilled "d" orbitals, some do not have any "d" electrons and some are strongly electrophilic (see explanation below). The adsorption performances of the impregnated ACC (<125μ) sorbents (i.e., Ni/ACC, Ta/ACC, Sn/ACC, Ga/ACC, Sr/ACC and Co/ACC) were investigated by liquid phase adsorption of adsorbate sulphur (DBT and DMDBT in hexadecane) mixtures (see Appendix C for isotherm data, isotherm plots and linearization plots).

This experimental data for the liquid phase adsorption was analyzed with the following adsorption mechanisms: (1) Langmuir; (2) Freundlich; and, (3) Modified Langmuir or Sips. As discussed in sub-section 5.1, the Sips isotherm combines the Freundlich's multi-site approach with Langmuir's layered approach, realizing that the unlimited Freundlich adsorption (increase in adsorption 'q' with increase in concentration 'c') is not realistic.

The results are summarized **TABLE 5.5**, below. The table includes the isotherm mechanism that the experimental data fits best, the associated linear regression value, the maximum adsorption capacity (q_{max}) and the associated equilibrium constant. The data are presented in reducing order, in terms of adsorption capacity.

In general, the data supports the following observation: as the active sites associated with the impregnated metal species play a more significant role in sulphur adsorption (i.e., are more effective in improving the adsorption capacity), the more the adsorption mechanism moves away from Langmuir's isotherm model and more towards Freundlich's isotherm model.

This observation adds more validity to the postulation that the metal sites introduce new sulphur adsorption sites that interact differently with the sulphur species than the existing functional groups on the surface of the activated carbon.

Additional explanation for each of the sorbents is provided below.

TABLE 5.5 - COMPARISON OF ADSORPTION ISOTHERM DATA FOR DBT ON ACTIVATED CARBON BASED SORBENTS AT 50 °C

Sorbent	ID	Impregnation Salt & (Percent Weight Loading)	Particle size	Isotherm		q_{max} ** (mmol-S/g-sorbent)	K (L/mmol)
				Type*	Linear Regression (R^2)		
Ta-impregnated Centaur Activated Carbon	Ta-2 / ACC	TaF_5 (2% by Wt. loading)	Powder (<125µ)	Modified Langmuir	0.992 ± 0.003	1.10 ± 0.04	0.28 ± 0.04
Sn-impregnated Centaur Activated Carbon	Sn / ACC	$SnCl_2$ (2% by Wt. loading)	Powder (<125µ)	Freundlich	0.985	0.87	0.19
Ni-impregnated Centaur Activated Carbon	Ni / ACC	Ni $(NO_3)_2$ (2% by Wt. loading)	Powder (<125µ)	Freundlich	0.994 ± 0.004	0.81 ± 0.02	0.24 ± 0.01
Co-impregnated Centaur Activated Carbon	Co / ACC	$CoNO_3$ (2% by Wt. loading)	Powder (<125µ)	Langmuir	0.968	0.77	0.54
Activated Carbon - Centaur (Virgin)	ACC	n/a	Powder (<125µ)	Langmuir	0.992	0.74	0.42
Ga-impregnated Centaur Activated Carbon	Ga / ACC	$Ga(NO_3)_3$ (2% by Wt. loading)	Powder (<125µ)	Langmuir	0.987	0.74	0.76
Sr-impregnated Centaur Activated Carbon	Sr / ACC	$Sr(NO_3)_2$ (2% by Wt. loading)	Powder (<125µ)	Langmuir	0.994	0.67	0.47
Ag-impregnated Centaur Activated Carbon	Ag / ACC	$AgNO_3$ (2% by Wt. loading)	Powder (<125µ)	Langmuir	0.987	0.64	1.13

Note:

* The isotherm that best fit the data is presented in this table. Details, including R^2 for other isotherm types are presented in Appendix C.

** The q_{max} values are based on Langmuir or modified Langmuir isotherm equations and in reference to 4,6 DMDBT.

The 2% by Wt. metal loading is based on calculations.

Standard Deviation is provided for experiments with 3 or more repeats.

From the adsorption performances summarized in **TABLE 5.5** the following can be concluded:

- Ta/ACC (2 wt.% Ta impregnated Centaur activated carbon) has the highest adsorption capacity amongst the selected sorbents. The data had good repeatability, adding confidence to this conclusion. It is presumed that since tantalum is a strong Lewis acid, when dispersed on the surface of the ACC support, it would enhance the adsorption capacity of ACC by introducing additional active sites that have high affinity for the lone pair of electrons of sulphur present in DBT.

- For Ni/ACC, the electron deficiency in its "d" orbital and the spatial distribution of the "d" orbital, make Ni a good active site for π-complexation.

- Sn/ACC has the second highest adsorption capacity, which may be due to its relatively higher electronegativity (1.96) in comparison to other metal species in this study. However, there are no vacant "d" orbitals in Sn to form π-complexation. The improved adsorption capacity of Sn/ACC in comparison to virgin ACC is therefore attributed to mechanisms other than the common ones such as Lewis acid coordination or formation of π-electron interactions (Cotton and Wilkinson, 1972).

- Sr/ACC has the second lowest adsorption capacity amongst the selected sorbents, even lower than ACC. The latter may be due to some pore blockage (Sr has the largest metallic radius amongst the metals studied here). Obvious spatial limitations of "s" orbital electrons in comparison to "d" orbitals limits the extent of potential interactions with sulphur species, however, once formed, the bond strength would most likely be higher (Cotton and Wilkinson, 1972), which was further investigated by measuring the heat of adsorption (see sub-section 5.5).

4,6 DMDBT Adsorption Isotherms

Similar to DBT, liquid phase adsorption experiments were also completed for 4,6 DMDBT, using the same sorbents as above (i.e., metal impregnated ACC, <125μ). It should be noted that due to limited solubility of 4,6-DMDBT in C16, the maximum DMDBT concentration used in this study was 800 ppmw-S (~ 19 mmol-S/L).

The same general observation as above (for DBT) can be said about 4,6 DMDBT adsorption, i.e., as the active sites associated with the impregnated metal species play a more significant role in sulphur adsorption (i.e., are more effective in improving the adsorption capacity), the more the adsorption mechanism moves away from Langmuir's isotherm model and more towards Freundlich's isotherm model.

The adsorption isotherm data, isotherm plots and linearization plots are provided in Appendix C. The data are summarized in **TABLE 5.6**, in reducing order of the adsorption capacity. Similar to DBT, the highest q_{max} was for tantalum impregnated ACC.

TABLE 5.6 - ADSORPTION ISOTHERM DATA FOR 4,6 DMDBT ON ACTIVATED CARBON BASED SORBENTS AT 50 °C

Sorbent	ID	Impregnation Salt & (Percent Weight Loading)	Particle size	Isotherm		q_{max} ** (mmol-S/g-sorbent)	K (L/mmol)
				Type*	Linear Regression (R^2)		
Ta-impregnated Centaur Activated Carbon	Ta-2 / ACC	TaF_5 (2% by Wt. loading)	Powder (<125µ)	Modified Langmuir	0.991 ± 0.007	0.75 ± 0.04	0.78 ± 0.34
Ni-impregnated Centaur Activated Carbon	Ni / ACC	$Ni(NO_3)_2$ (2% by Wt. loading)	Powder (<125µ)	Freundlich	0.995 ± 0.006	0.67 ± 0.02	0.26 ± 0.03
Co-impregnated Centaur Activated Carbon	Co / ACC	$CoNO_3$ (2% by Wt. loading)	Powder (<125µ)	Freundlich	0.997	0.66	0.26
Ag-impregnated Centaur Activated Carbon	Ag / ACC	$AgNO_3$ (2% by Wt. loading)	Powder (<125µ)	Freundlich	0.986	0.65	0.27
Sn-impregnated Centaur Activated Carbon	Sn / ACC	$SnCl_2$ (2% by Wt. loading)	Powder (<125µ)	Freundlich	0.993	0.62	0.26
Centaur Activated Carbon	ACC	n/a	Powder (<125µ)	Langmuir	0.976 ± 0.013	0.58 ± 0.01	1.75 ± 0.57
Sr-impregnated Centaur Activated Carbon	Sr / ACC	$Sr(NO_3)_2$ (2% by Wt. loading)	Powder (<125µ)	Langmuir	0.95	0.57	1.42
Ga-impregnated Centaur Activated Carbon	Ga / ACC	$Ga(NO_3)_3$ (2% by Wt. loading)	Powder (<125µ)	Freundlich	0.989	0.56	0.26

Note:

* The isotherm that best fit the data is presented in this table. Details, including R2 for other isotherm types are presented in Appendix C.

** The q_{max} values are based on Langmuir or modified Langmuir isotherm equations and in reference to 4,6 DMDBT.

The 2% by Wt. metal loading is based on calculations.

Standard Deviation is provided for experiments with 3 or more repeats.

From the adsorption performances summarized in **TABLE 5.6**, the following can be concluded:

- Ta/ACC (2 wt.% Ta impregnated Centaur activated carbon), similar to the DBT adsorption, has the highest adsorption capacity amongst the selected sorbents. The data had good repeatability, adding confidence to this conclusion. The same explanation (i.e. strong Lewis acid) as that provided above (for DBT) can be said for 4,6-DMDBT as well. However, steric hindrance of alkyl groups my result in lower overall adsorption of 4,6-DMDBT in comparison to DBT.

- Ni/ACC had the second highest adsorption capacity and the lowest equilibrium constant. As mentioned above, electron deficiency in its "d" orbital and the spatial spread of the "d" orbital, make Ni a good active site for π-complexation for adsorption of organo-sulphur compounds.

- The difference observed between the adsorption capacity of plain ACC and sorbents impregnated with Ag, Sn, Sr and Ga are not considered to be significant. Therefore, although these species may create new active sites for the adsorption of 4,6-DMDBT, their interaction with surface morphology of the ACC support seems to cause pore blockage and also do not seem to notably overcome the steric hindrance associated with the methyl groups of 4,6-DMDBT.

5.5 Flow microcalorimetry

As discussed above, in order to determine adsorption strength between the sorbent and sorbate, flow microcalorimetry (calorimetry) was used to measure the heat of adsorption. This is the heat released when a sulphur compound (in this case DBT) replaces an already adsorbed compound (in this case C16). More energy is released (in the form of heat) when DBT is adsorbed onto the active sites of the sorbent than when C16 is adsorbed. Therefore, this thermodynamically favoured displacement continues until it reaches saturation, at which point the amount of DBT adsorbed and the amount of DBT desorbed reach equilibrium and the amount of heat released drops to the baseline. The higher heat release would typically be associated with stronger interaction (adsorption strength) between the sulphur compound (DBT) and the active sites.

The resident Setsoft® software linked with the Setaram C80 Flow calorimeter was used to generate heat flow curves. The integration of the heat flow curve (area under the curve) was also performed using the Setsoft® software. The area under the heat flow curve (baseline to baseline) is equal to the total heat of adsorption associated with DBT and the sorbent. It should be noted that the amount of heat released is also a function of sorbent weight (note: the concentration of DBT in hexadecane was kept approximately the same for all the runs). Therefore, to ensure that heat-releases can be compared, total heat of adsorption values were normalized based on the dry weight of the sorbents. The normalized heat of adsorption values are presented in **TABLE 5.7**.

The outflow from the calorimeter was collected at regular intervals and analyzed for sulphur content using GC/FID. The sulphur concentrations were plotted versus time (the time the sample was collected) to generate a breakthrough curve. When the sorbent reaches saturation, the *net* adsorption of sulphur compound will diminish and therefore,

the sulphur concentration in the outflow reaches that of the bulk solution which enters the calorimeter cell, hence the term breakthrough.

The heat flow curve and the breakthrough curve for each sorbent were plotted on the same graph (time matched). The combined curves for virgin ACC (un-impregnated) and that of Sr-ACC (Strontium 2% Wt. impregnated ACC), which had the highest heat of adsorption, are presented in Figure 5.2 and Figure 5.3, respectively. The plots for other sorbents are presented in Appendix C.

FIGURE 5.2 - CALORIMETRY HEAT FLOW AND BREAKTHROUGH CURVES FOR DBT IN HEXADECANE ON ACC (<125 μ) AT 30 °C

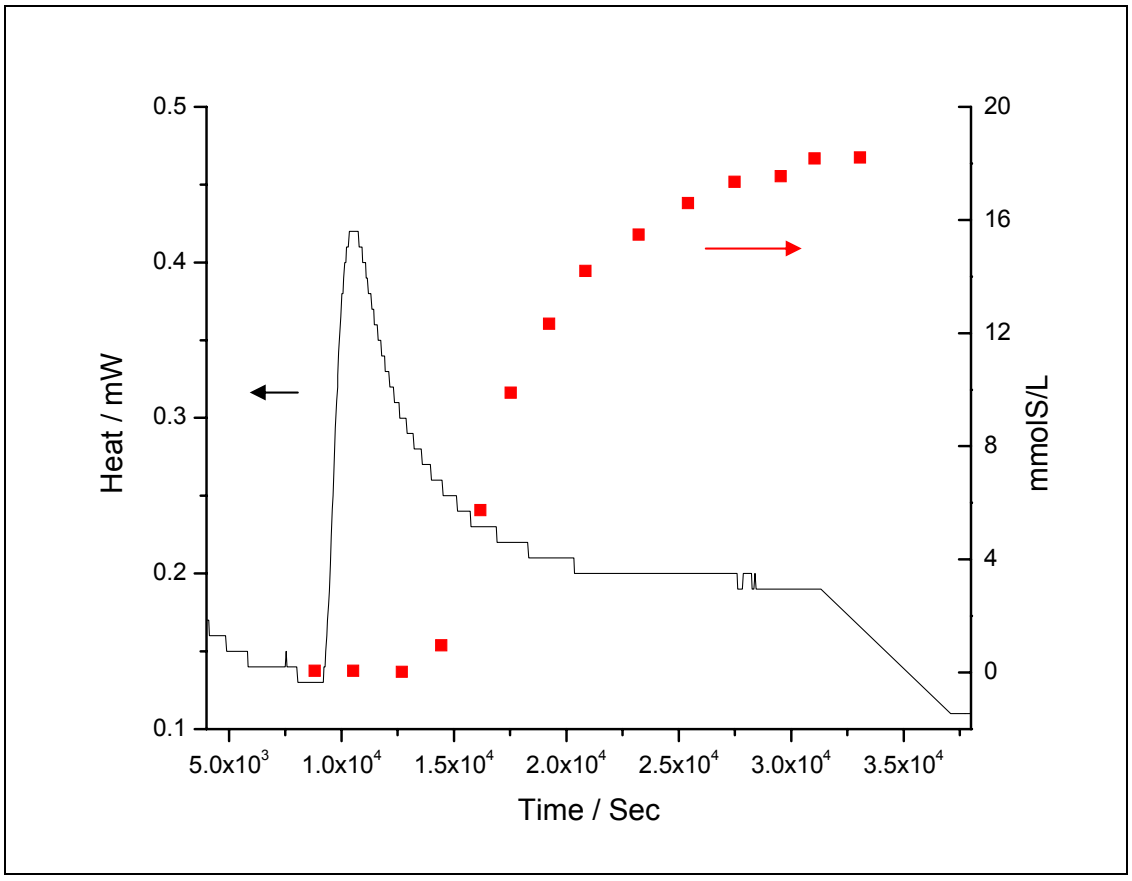

The heat flow and breakthrough plots illustrate that the peak of the heat of adsorption correlates with the initial part of the adsorption process when the sorbent has maximum capacity. The heat curve tapers-off back to the baseline as the sorbent reaches saturation (no net sulphur adsorption).

FIGURE 5.3 - CALORIMETRY HEAT FLOW AND BREAKTHROUGH CURVES FOR DBT IN HEXADECANE ON Sr-ACC (<125 μ) AT 30 °C

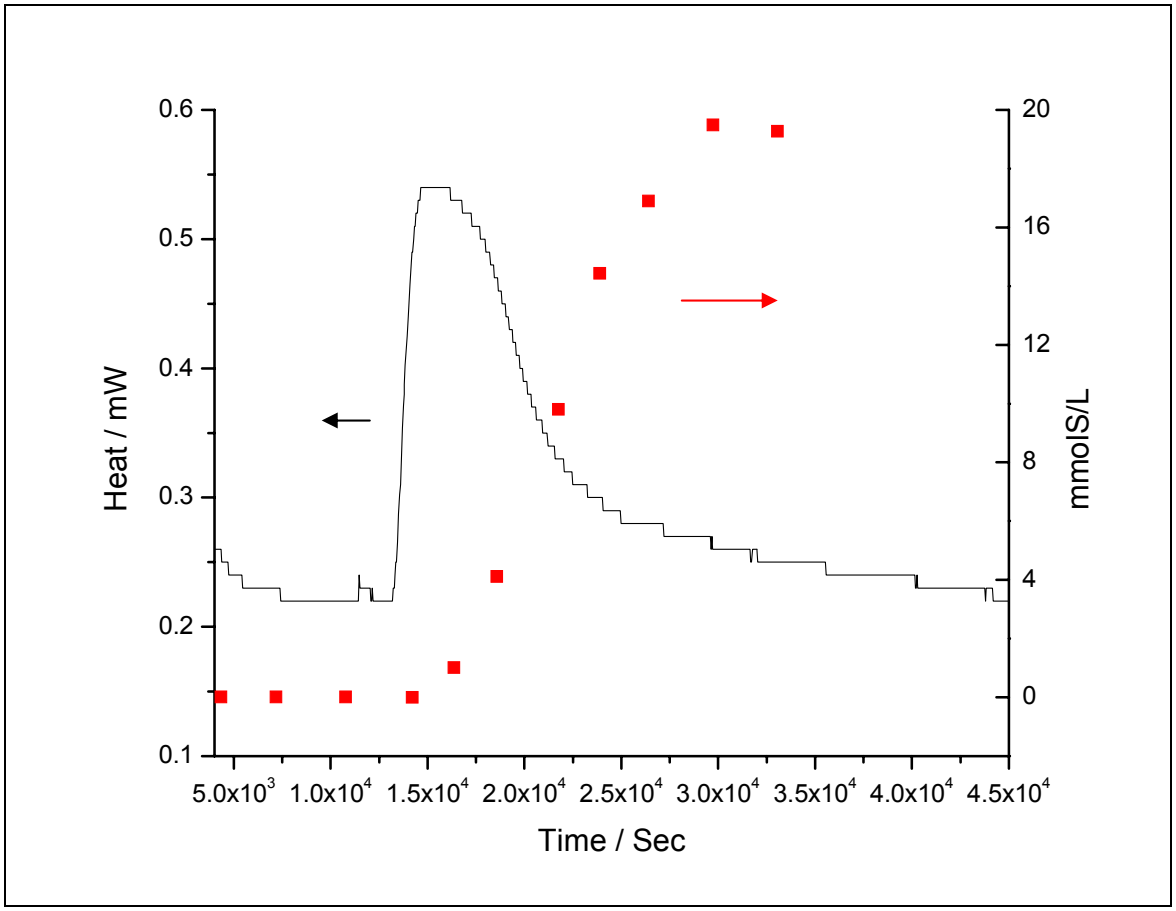

The normalized heat of adsorption values (**TABLE 5.7**) indicate that the Sr-ACC has the highest heat of adsorption, thus having the strongest adsorption strength towards DBT amongst the selected sorbents. As mentioned above, this maybe due to the interaction

with the electrons in the "s" orbital of Sr, which although they do not have the spatial spread of the "d" orbital, they are capable of forming stronger (but less of) bonding with the sulphur compound (i.e., DBT). As expected Ta/ACC also has a reasonably high heat of adsorption towards DBT. This is expected to be associated with the strong Lewis acid characteristic of Ta and its affinity for sulphur's lone pair of electrons.

Also presented in Table 5.7 are the molar heats of adsorption in kJ per mole of sulphur adsorbed. The molar heats of adsorption clearly reveal the strong interaction of DBT with Sr sites.

TABLE 5.7 - HEAT OF ADSORPTION VALUES FOR ACTIVATED CARBON AND IMPREGNATED ACTIVATED CARBONS (BINARY SOLUTION OF APPROXIMATELY 900 ppmw-S DBT IN HEXADECANE AT 30 °C)

Sorbent Description	Sorbent ID	Metal Impregnation (% by Weight)	Sorbent Particle Size	Normalized Heat (J/g-sorbent)	Molar Heat (kJ/mol-S)
Sr-impregnated Centaur Activated Carbon	Sr-ACC	2%	<125 u (powder)	16.57	24.65
Ta-impregnated Centaur Activated Carbon	Ta-ACC	2%	<125 u (powder)	11.13	10.12
Co-impregnated Centaur Activated Carbon	Co-ACC	2%	<125 u (powder)	9.98	12.92
Activated Carbon - Centaur (Virgin)	ACC	0%	<125 u (powder)	6.78	9.11
Ag-impregnated Centaur Activated Carbon	Ag-ACC	2%	<125 u (powder)	6.02	9.45
Ga-impregnated Centaur Activated Carbon	Ga-ACC	2%	<125 u (powder)	5.18	6.97
Ni-impregnated Centaur Activated Carbon	Ni-ACC	2%	<125 u (powder)	4.9	6.05
Activated Carbon - Centaur (Virgin)	ACC125	0%	125 - 250	3.24	5.68
Activated Carbon - Centaur (Virgin)	ACC 500	0%	250 - 500	0.98	2.20

Another observation was the impact of sorbent particle size on the adsorption heat. Three particle size factions of ACC, were analyzed using the calorimeter. The particle size fractions were:

- ACC500 (particle size range: 250µm - 500µm);
- ACC125 (particle size range: 125µm - 250µm); and,
- ACC Powder (particle size <125µm).

The combined heat flow and breakthrough curves for the ACC Powder (<125 µm) are presented in Figure 5.2, above. The plots for ACC500 and ACC125 are presented in **FIGURE 5.4** and **FIGURE 5.5**, respectively.

FIGURE 5.4 - CALORIMETRY HEAT FLOW AND BREAKTHROUGH CURVES FOR DBT IN HEXADECANE ON ACC500 (250µm << 500µm) AT 30 °C

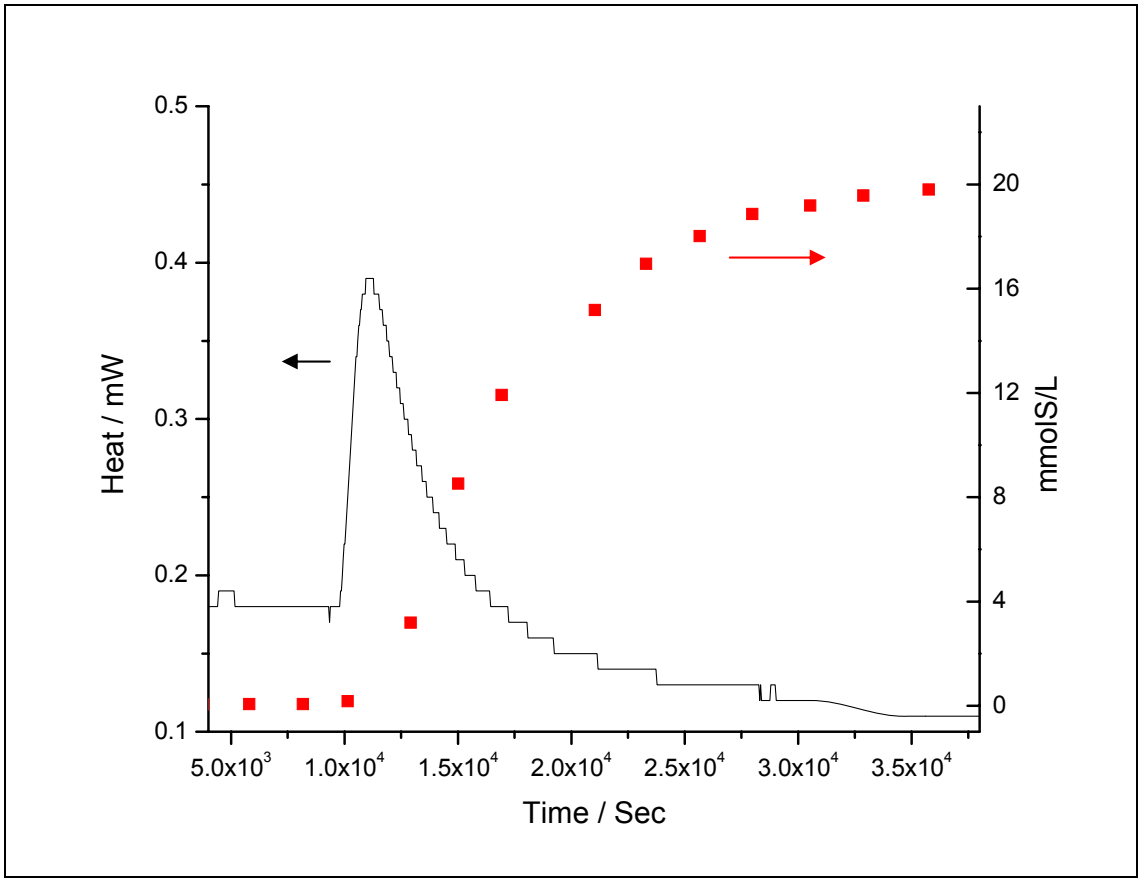

FIGURE 5.5 - CALORIMETRY HEAT FLOW AND BREAKTHROUGH CURVES FOR DBT IN HEXADECANE ON ACC-125μm (125μm<<250μm) AT 30 °C

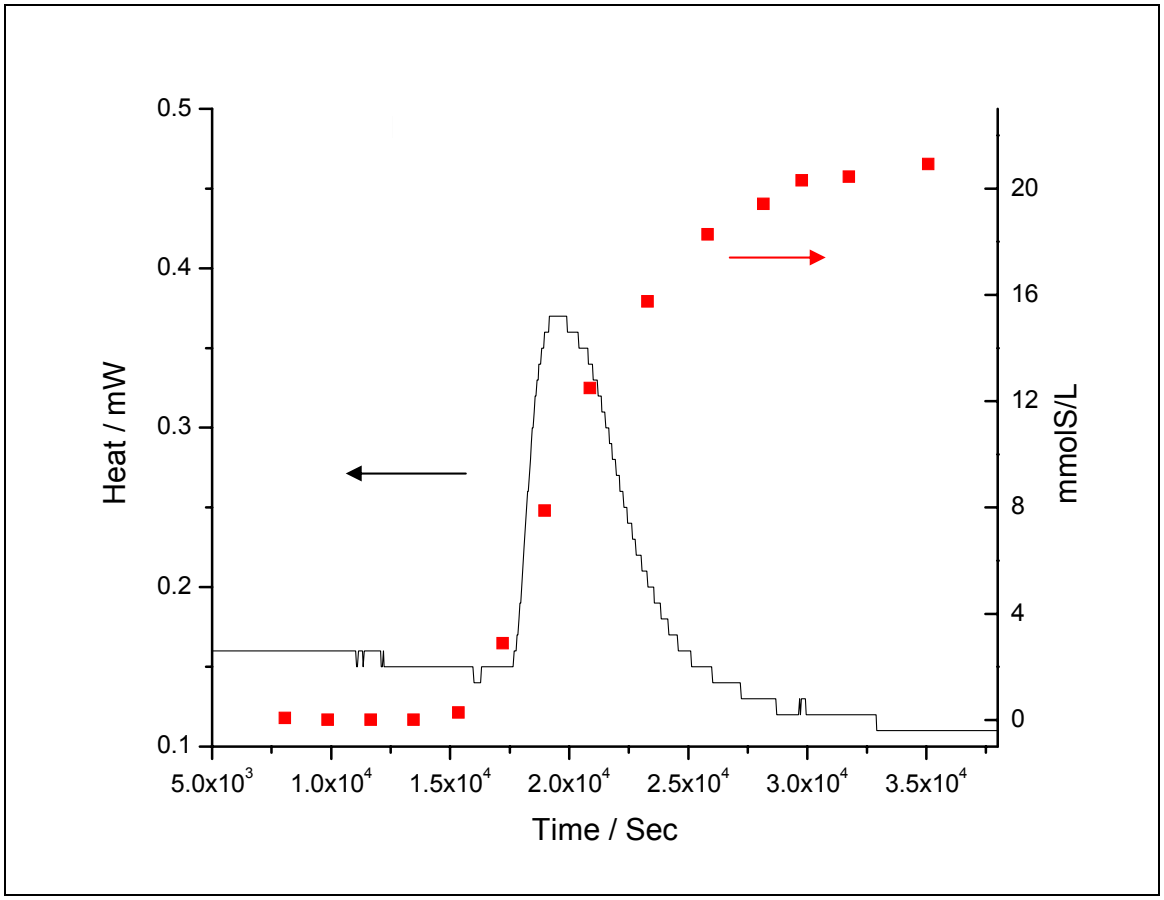

The normalized heat of adsorption results indicate almost 7 times higher heat release for the powder ACC versus the 500μm size fraction (see **TABLE 5.7**). This is evidence that more contact surface area resulting from finer particle sizes promotes more adsorptive interactions.

6.0 Study of Tantalum Impregnated Activated Carbon

It was ascertained through wet adsorption analysis that tantalum impregnation of activated carbon (Ta/ACC) boosts the adsorption capacity of virgin activated carbon by approximately 50% for DBT and 30% for 4,6 DMDBT. Also, the analysis showed that amongst the metal-impregnated activated carbons analyzed tantalum had the highest adsorption capacity for both sulphur compounds (i.e., DBT and 4,6 DMDBT). The sulphur adsorption capacity of Ta/ACC is quite high when compared against the adsorption performances published in the literature and those currently deployed in the industry (see Section 3). As such, more detailed analysis and characterization of tantalum impregnated activated carbon is warranted to determine key factors that influence its performance and to obtain insight into the potential adsorption type / mechanism by which it adsorbs sulphur species. To accomplish this following analysis were completed:

- *Effect of tantalum loading* – In order to determine the effect of tantalum on sulphur adsorption, sorbents with varying percent weight loading of tantalum on activated carbon were prepared and analyzed for their adsorption performance. In addition, the impact of tantalum loading on sorbent surface area and pore volume was assessed. Potential adsorption mechanisms for organo-sulphur compounds on tantalum impregnated sorbent were also investigated.

- *Effect of fluoride and acid* – TaF_5 salt readily dissociates in water and forms an acidic solution (pH ~ 2). Through the impregnation process, fluoride and/or its complexes can form sites on the surface of the activated carbon that can influence adsorption. Also, the acidic nature of the solution may physically and/or chemically alter the activated carbon. To determine any of such effects, sorbents were prepared using the hydrofluoric acid (HF) and sulphuric acid (H_2SO_4). The adsorption performances of the acid treated sorbents were

determined through isothermal wet adsorption analysis. The results were compared against Ta-impregnated activated carbon.

- *Heat of adsorption* – The heat of adsorption for the tantalum impregnated activated carbon was compared with that of virgin activated carbon in order to establish insight into type(s) of adsorptive sites that may exists on the surface of the sorbent as a result of the impregnation. Change in normalized heats of adsorption (between the virgin and impregnated activated carbon) can reveal existence of new / different adsorptive sites on the surface of tantalum-impregnated activated carbon. This can help explain the improved adsorption performance and possible adsorption type (i.e., physisorption or chemisorption) for the tantalum sites.

- *Competitive Adsorption* – The industrial use of the developed sorbent for adsorptive desulphurization would mean exposure to numerous chemical species that can compete for the adsorptive sites of the sorbent. These species include coexisting sulphur compounds, with DBT and 4,6 DMDBT being the most difficult to remove, as well as aromatics such as naphthalene and organo-nitrogen compounds such as quinoline and carbazole. To determine its adsorptive performance in a competitive environment (i.e., numerous adsorbates co-existing) sulphur, aromatic and nitrogen adsorption on tantalum impregnated activated carbon was investigated.

- *Characterization* – When physical and/or chemical changes to a sorbent are assessed together with its adsorptive performance, one can establish links between certain properties / characteristics of the sorbent and the change in its performance it order to expand the understanding of the adsorption process and key factors that influence it. To establish a better understanding of the physical and chemical changes that take place as a result of metal impregnation, a series of systematic characterizations were completed, as follows:

- HRTEM was used to determine physical characteristics of the sorbent and changes as a result of tantalum impregnation process. The physical features including surface morphology and dispersion of tantalum on the surface of the activated carbon were evaluated. The analysis was carried out on tantalum impregnated activated carbon as well as virgin activated carbon.

- Along with HRTEM, EDX analysis was also conducted to determine elements (e.g., tantalum) that exist on the surface of the sorbents. The analysis was carried out on tantalum impregnated activated carbon as well as virgin activated carbon.

- FTIR analysis was used to identify functional groups on the surface of the sorbents and determine if the impregnation process influences those functional groups. The analysis was carried out on tantalum impregnated activated carbon as well as virgin activated carbon.

- TPD – Ammonia analysis was used to determine a change in the acidic strength of the sorbent as a result of tantalum impregnation. The analysis was carried out on tantalum impregnated activated carbon as well as virgin activated carbon.

- XPS analysis was carried out to determine the oxidation state of tantalum on the surface of the sorbent, tantalum complexes that may form, and functional groups that may exist on the surface of the sorbent. The analysis was also used to gain insights into the bonds that may form between the active sites of the sorbent (e.g., tantalum sites) and adsorbates (e.g., DBT, carbazole). The analysis was carried out on virgin activated carbon, unused (fresh) tantalum-impregnated activated

carbon and used tantalum-impregnated activated carbon (i.e., used in an equilibrium adsorption experiment for organo-sulphur or organo-nitrogen compounds).

6.1 Tantalum Chemistry and Impregnation

The metal impregnation procedure was briefly discussed in previous sections. The impregnation process used for tantalum is different that the rest of the metals due to the chemical properties of tantalum and its halide/oxide complexes. As such, a more detailed explanation of the impregnation process and the chemical/physical properties of tantalum and its complexes are provided in this section.

Tantalum Chemistry

Tantalum is a rare refractory metal which naturally exists in the form of oxide complexes along with other transition metals such as, iron, manganese and niobium (i.e., columbite-tantalite: $(Fe, Mn)(Nb, Ta)_2O_6$). Although a metal, tantalum has chemical properties in its V oxidation state that is quite typical of non-metal elements. This includes formation of numerous anionic species instead of cationic ones (virtually no cationic chemistry). The columbite-tantalite dissociates in hydrofluoric acid, producing fluorinated tantalum and niobium as well as oxyfluoride complexes such as, $TaOF_5^{2-}$. Sulphuric acid is also used in combination with HF, during the acid digestion processing of the columbite-tantalite. For a reasonable dissolution rate, concentrated HF (up to 70%) at temperatures of 70 – 90 °C is required. Highly concentrated HF includes very reactive species such as HF^{2-} which can result in formation of anionic complexes such as TaF_6^- and TaF_7^{2-}. In case of H_2SO_4 and HF mixed acid solution, the chemistry is more complex but it is likely that H_2SO_4 interacts mainly with iron and manganese, while the HF interacts mainly with niobium and tantalum. The dissolved fluorinated refractory metals are then separated through liquid-liquid extraction using aqueous solutions and organic solvents (Agulyansky 2004).

Production of tantalum oxide includes precipitation of tantalum hydroxide ($Ta_2O_5.nH_2O$) in an aqueous solution and subsequent thermal treatment of tantalum hydroxide to form tantalum oxide. The strip solution of tantalum includes oxyfluoro acid complexes including oxyfluorotantalic acid (H_2TaOF_5) and fluorotantalic acid (H_2TaF_7) (Buslaev, Nikolaev *et al.* 1985). For conversion of the liquid acids into solid (i.e., precipitate) tantalum oxide, three key steps are commonly performed: (1) substitution of fluoride ions, (2) precipitation of insoluble tantalum compounds formed (e.g., tantalum hydroxide), and (3) decomposition of precipitate through thermal treatment, to form tantalum oxides (Agulyansky 2004). Fluoride substitution step is key in determining the quality / purity of the tantalum oxide formed. Fluoride impurities, which exist mainly in the form of oxyfluorides such as TaO_2F and Ta_3O_7F, can have deterring effects on tantalum oxide applications. For the thermal treatment, it is shown that higher temperature during the thermal treatment leads to less water molecules incorporated in the oxide complex (Titov, Krokhin *et al.* 1995).

The oxides of tantalum can exist in the form of Ta_2O_5 (which is the most stable) or TaO_x with x being less than or equal to 2.5. The tantalum oxide is a dense white powder which is relatively inert and insoluble in water. Tantalum fluoride (TaF_5) on the other hand readily dissociates in water forming a strong acidic solution (if not diluted) which helps to prevent the formation of precipitates at low pH.

Tantalum Impregnation

Use of a support (in this case, inexpensive support such as activated carbon) to disperse adsorptively active metals makes the sorbent more economical while improving its performance as a sorbent or catalyst through electronic interaction of metal with the substrate (Park and Keane 2003).

An effective impregnation of transition metals on the surface of a support consists of well dispersed metal species on the surface with minimal clustering of the metal species. This

is to minimize overlapping active sites and to maximize the interaction between adsorbate and the active sites (i.e., metal sites). To achieve this, the metal species are to be fully dissolved in a carrier solvent (e.g., aqueous) so that they can penetrate the pores and cavities of the support (i.e., activated carbon) in a wet impregnation process and subsequently precipitate out of solution and form active sites on the surface of the sorbent.

As mentioned above, tantalum oxide is insoluble in water, while tantalum pentaflouride dissociates in water, forming an acidic solution (i.e., HF, H_2TaOF_5), which keeps the formed tantalum hydroxide in solution, allowing it to infiltrate the pores and cavities of the activated carbon. Therefore, for the purposes of this study, TaF_5 was used for the tantalum impregnation of the activated carbon.

The wet impregnation of activated carbon was done over 24 hours to ensure that the process is not limited by mass transfer. Also, the mixture was under continuous agitation for the 24-hour period to help with surface wetting, contact (active site and support) and dispersion. The wet activated carbon was filtered using suction filtration and washed with distilled water several times to reduce acidity and help with formation of hydroxide precipitates on the surface of the activated carbon. The air dried Ta-impregnated activated carbon was then dried under helium flow as follows:

- continuous thermal treatment at 150 °C for 3 hours, with a temperature ramp-up rate of 10 °C /min for 25 – 100 °C, a 30 minute hold at 100 °C followed by a second ramp-up (same rate as before) to 150 °C (hold for 2 hours and 15 minutes).
- Continuous thermal treatment at 400 °C for 1 hour, with a temperature ramp-up rate of 10 °C /min.

The thermally treated sorbent was cooled under helium flow. Any exposure to air at the above mentioned temperatures can result in full or partial oxidization of the activated carbon, which voids its use as a sorbent and sorbent structure.

The cooled sorbent (Ta-impregnated activated carbon) was then weighed and immediately transferred to vials / cells with adsorbate solution to ensure minimum exposure to air. This is due to the hydrophilic nature of activated carbon. In fact in our experiments it was observed that longer exposures to ambient air / moisture in the air significantly inhibited the adsorptive performance of the sorbent, while no exposure (e.g., in case of the flow reactor experiments, where an in-situ thermal treatment was undertaken under helium flow) showed noticeable improvement in adsorption performance.

6.2 Adsorption Performance as a Function of Tantalum Loading

The effect of tantalum on sulphur adsorption was investigated through equilibrium adsorption of DBT and 4,6 DMDBT on sorbents with different percent tantalum loadings. For this analysis, sorbents with tantalum loadings of 2%, 5% and 10% by weight were prepared and identified as follows:

- Ta-2/ACC – 2% Ta (by weight) on Activated Carbon Centaur
- Ta-5/ACC – 5% Ta (by weight) on Activated Carbon Centaur
- Ta-10/ACC – 10% Ta (by weight) on Activated Carbon Centaur

The adsorption isotherm data, isotherm plots and linearization plots for multiple runs for each sorbent are provided in Appendix C.

A third party measurement of tantalum content for the 5% and 10% impregnated sorbents were performed. The analysis was conducted at Cambridge Materials Testing Limited

using ICP method. The results indicated a percent by weight concentration of 3.14% and 8.04% for the 5% and 10% Ta-impregnated sorbents.

The DBT adsorption isotherms for the three sorbents as well as that of un-impregnated activated carbon (i.e., virgin ACC) are presented in Figure 6.1. The maximum adsorption capacities for DBT as well as K values are presented in **TABLE 6.1**.

FIGURE 6.1 - DBT ADSORPTION ISOTHERMS FOR Ta-IMPREGNATED ACC AT DIFFERENT TANTALUM LOADINGS

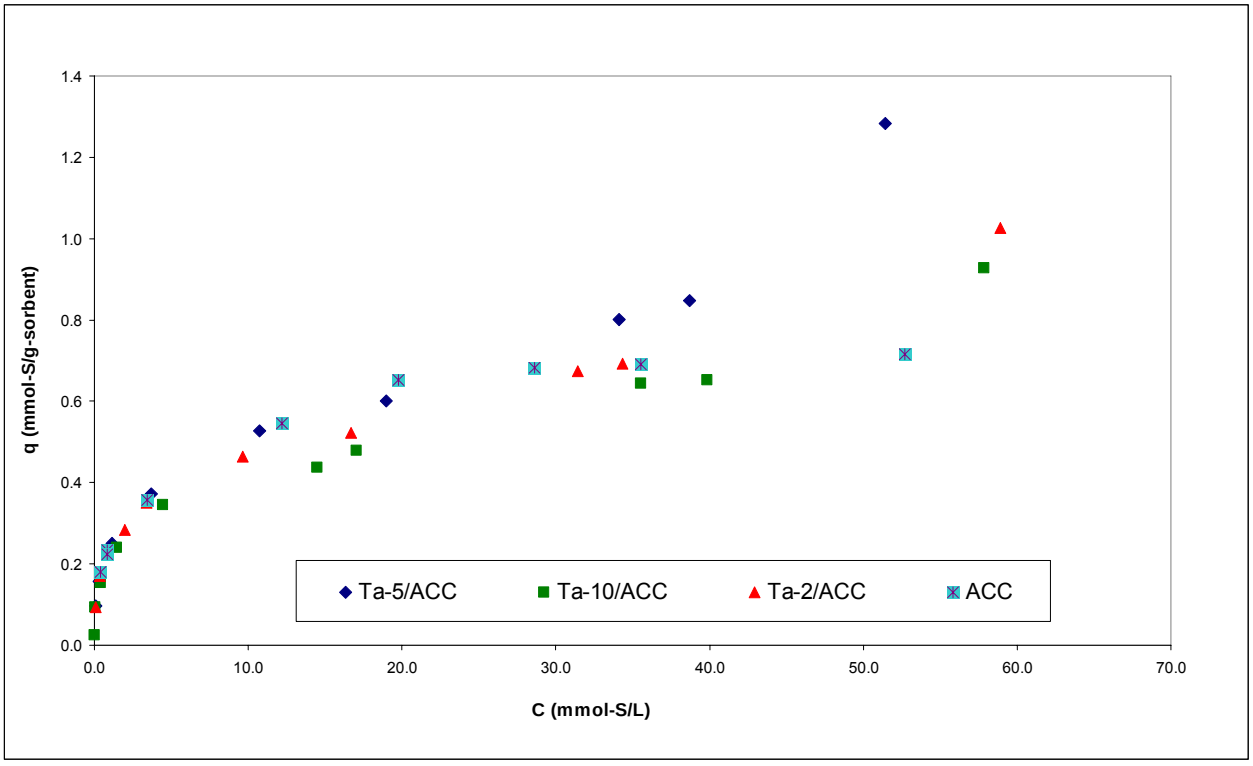

NOTE:
Ta-2/ACC – 2% Ta (by weight) on Activated Carbon Centaur
Ta-5/ACC – 5% Ta (by weight) on Activated Carbon Centaur
Ta-10/ACC – 10% Ta (by weight) on Activated Carbon Centaur
ACC – Un-impregnated (virgin) ACC
Isotherms for repeat runs are provided in Appendix C

TABLE 6.1 - ADSORPTION ISOTHERM DATA FOR DBT ON ACTIVATED CARBON BASED SORBENTS AT DIFFERENT TANTALUM LOADINGS, AT 50 °C

Sorbent	ID	Impregnation Salt & (Percent Weight Loading)	Particle size	Isotherm		q_{max} ** (mmol-S/g-sorbent)	K (L/mmol)
				Type*	Linear Regression (R^2)		
Activated Carbon - Centaur (Virgin)	ACC	n/a	Powder (<125µ)	Langmuir	0.992	0.74	0.42
Ta-impregnated Activated Carbon - Centaur	Ta-2 / ACC	TaF_5 (2% by Wt. loading)	Powder (<125µ)	Modified Langmuir (Sips Equation)	0.992 ± 0.003	1.10 ± 0.04	0.28 ± 0.04
Ta-impregnated Activated Carbon - Centaur	Ta-5 / ACC	TaF_5 (5% by Wt. loading)	Powder (<125µ)	Modified Langmuir (Sips Equation)	0.993 ± 0.003	1.49 ± 0.16	0.32 ± 0.06
Ta-impregnated Activated Carbon - Centaur	Ta-10 / ACC	TaF_5 (10% by Wt. loading)	Powder (<125µ)	Modified Langmuir (Sips Equation)	0.984 ± 0.012	1.00 ± 0.07	0.39 ± 0.06

Note:

* The isotherm that best fit the data is presented in this table. Details, including R^2 for other isotherm types are presented in Appendix C.

** The q_{max} values are based on Langmuir or modified Langmuir isotherm equations and in reference to DBT.

The percent by Wt. tantalum loading is based on calculations.

Standard Deviation is provided for experiments with 3 or more repeats. Values without standard deviation are mean values for two runs.

Through adsorption isotherm analysis, a difference between the adsorption mechanism of sulphur compounds on to ACC (virgin) and tantalum impregnated ACC was discovered. This is clearly visible from the isotherms shown in Figure 6.1. The virgin ACC follows the Langmuir's monolayer isotherm while all three tantalum impregnated ACCs do not show a good fit with Langmuir's isotherm. Instead all three tantalum impregnated sorbents show a better fit with Freundlich isotherm, which is based on independent, multi-site adsorption mechanism. The experimental data for the tantalum impregnated ACC fitted best with Sips model, which is a combination of Freundlich and Langmuir isotherms (as per sub-section 5.1). This will be discussed further in the following sections. Linearization and regression coefficients support this conclusion. The calculation details and linearization plots are provided in Appendix C.

It is believed that the modification of activated carbon with Ta results in the introduction of new adsorption sites which interact strongly with the adsorbate's electrons. This interaction is believed to be due to the Lewis acid characteristics that the tantalum species on the surface possess. In the sulphur adsorption process, these sites interact with the lone pair of electrons of sulphur in DBT and DMDBT.

The maximum adsorption capacities of the three impregnated sorbents clearly show improvements in capacity in comparison to virgin ACC. The sulphur adsorption capacity for DBT followed the trend: ACC < Ta-10ACC < Ta-2/ACC < Ta-5/ACC. The 5% Ta-impregnated ACC (Ta-5/ACC) had an adsorption capacity approximately 100% higher than that of virgin ACC. This further confirms the formation of additional active sites that adsorb sulphur compounds.

The reduction in DBT adsorption capacity for Ta-10/ACC is attributed to clustering and pore blockage and thus reduced access to adsorptive sites due to overload of tantalum species. This is further discussed in the following sections.

Adsorption of 4,6 dimethyldibenzothiophene (4,6 DMDBT) in hexadecane (C16) was also conducted in liquid phase using 2%, 5% and 10% Ta-impregnated ACC. The results were compared against virgin ACC. The adsorption isotherms are presented in **FIGURE 6.2** and the adsorption capacities are presented in **TABLE 6.2**.

The findings are similar to those mentioned above for DBT adsorption: (1) adsorption mechanism of tantalum impregnated ACC is likely different than virgin ACC, (2) the virgin ACC follows Langmuir's isotherm mechanism while Ta-impregnated ACC seems to fit best with Sips model (also referred to as modified Langmuir).

The density of the sorbent changes with higher loading of tantalum. Since the adsorption is a function of surface area comparison of amount adsorbed per unit weight of sorbent amongst the four sorbents may be conservative in determining the adsorption performance of the sorbents. In other words, the actual adsorption capacities would likely be higher.

FIGURE 6.2 - 4,6 DMDBT ADSORPTION ISOTHERMS FOR Ta-IMPREGNATED ACC AT DIFFERENT TANTALUM LOADINGS (BINARY SOLUTION OF 4,6 DMDBT AND HEXADECANE AT 50 °C)

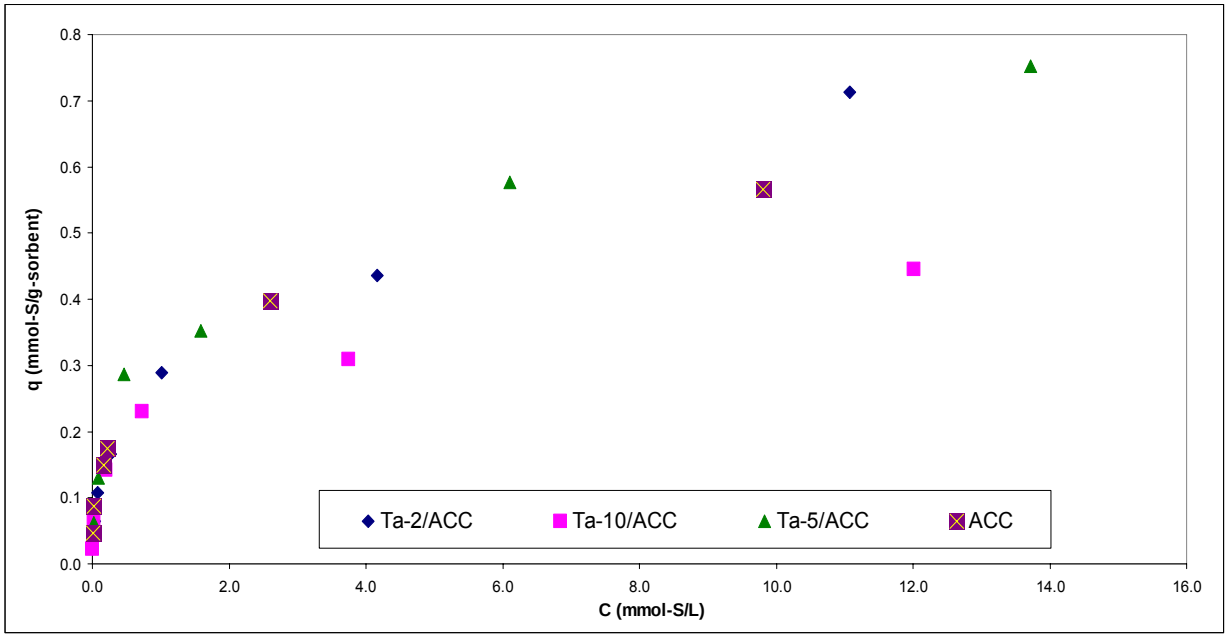

NOTE:
Ta-2/ACC – 2% Ta (by weight) on Activated Carbon Centaur
Ta-5/ACC – 5% Ta (by weight) on Activated Carbon Centaur
Ta-10/ACC – 10% Ta (by weight) on Activated Carbon Centaur
ACC – Un-impregnated (virgin) ACC
Isotherms for repeat runs are provided in Appendix C

TABLE 6.2 - ADSORPTION ISOTHERM DATA FOR 4,6 DMDBT ON ACTIVATED CARBON BASED SORBENTS AT DIFFERENT TANTALUM LOADINGS, AT 50 °C

Sorbent	ID	Impregnation Salt & (Percent Weight Loading)	Particle size	Isotherm		q_{max} ** (mmol-S/g-sorbent)	K (L/mmol)
				Type*	Linear Regression (R^2)		
Centaur Activated Carbon	ACC	n/a	Powder (<125µ)	Langmuir	0.976 ± 0.013	0.58 ± 0.01	1.75 ± 0.57
Ta-impregnated Centaur Activated Carbon	Ta-2 / ACC	TaF_5 (2% by Wt. loading)	Powder (<125µ)	Modified Langmuir (Sips Equation)	0.991 ± 0.007	0.75 ± 0.04	0.78 ± 0.34
Ta-impregnated Centaur Activated Carbon	Ta-5 / ACC	TaF_5 (5% by Wt. loading)	Powder (<125µ)	Modified Langmuir (Sips Equation)	0.994 ± 0.005	0.76 ± 0.07	0.92 ± 0.29
Ta-impregnated Centaur Activated Carbon	Ta-10 / ACC	TaF_5 (10% by Wt. loading)	Powder (<125µ)	Modified Langmuir (Sips Equation)	0.994 ± 0.002	0.48 ± 0.03	1.28 ± 0.18

Note:

* The isotherm that best fit the data is presented in this table. Details, including R^2 for other isotherm types are presented in Appendix C.

** The q_{max} values are based on Langmuir or modified Langmuir isotherm equations and in reference to 4,6 DMDBT.

The percent by Wt. metal loading is based on calculations.

Standard Deviation is provided for experiments with 3 or more repeats.

The sulphur adsorption capacity for 4,6 DMDBT followed the trend: ACC < Ta-10/ACC < Ta-2/ACC < Ta-5/ACC, which is similar to that observed for DBT adsorption. The best performing sorbent (i.e., Ta-5/ACC) has approximately 31% higher adsorption capacity in comparison to virgin ACC. Similar to DBT, the adsorption mechanism is best described by the Sips equation, which further confirms the above-indicated hypothesis (i.e., formation of adsorptive sites that function independently of those already existing on the surface of the activated carbon). The Sips equation curbs (i.e., defines a q_{max}) the continuous increase in adsorption with increase of sorbate concentration, which is a characteristic of Freundlich's empirical mechanism. The Ta-impregnated ACC consists of a heterogeneous surface consisting of patches of adsorption sites with similar adsorption energies grouped together and with no interaction between the patches (i.e., independent active/adsorptive sites). One can assume that each patch adsorbs only one adsorbate molecule and thus the Langmuir equation applies to each patch and Freundlich applies to the heterogeneous surface as a whole.

Similar to DBT adsorption capacity, the reduction in 4,6 DMDBT adsorption capacity for Ta-10/ACC is attributed to clustering and pore blockage and thus reduced access to adsorptive sites due to overload of tantalum species. This is further investigated in the following sections.

The maximum adsorption capacity calculated using Sips equation and experimental data (0.76 mmol-sulphur/g_{ads}) at 50 °C is higher (by a significant margin) than any other adsorption capacity reported in the literature for the particularly difficult to remove 4,6 DMDBT. This higher adsorption capacity observed for DMDBT is believed to be due to the introduction of tantalum adsorption sites which to some extend can overcome the steric hindrance of 4,6-DMDBT. The strength of this interaction with Ta may result in ortho methyl groups present on the DMDBT molecule to orient in such way that facilitates interaction between the tantalum site and the sulphur atom of DMDBT molecule (Agulyansky 2004).

6.3 Impact of Tantalum Loading on Surface Area and Pore Volume

In order to better explain some of the observed trends in adsorption capacity of the tantalum impregnated activated carbon discussed in the previous section, the impact of tantalum impregnation on surface area and pore volume was investigated.

The surface areas and pore volumes were determined using BET surface area analysis. The analysis was completed for virgin ACC along with the three tantalum impregnated ACCs, i.e., Ta-2/ACC, Ta-5/ACC and Ta-10/ACC. The results are summarized in Table 6.3. The results indicate that as the percentage of tantalum loading on to the activated carbon increases there is a corresponding decrease in the BET surface area and pore volume. The 5% Ta impregnation results in approximately 3% reduction in BET surface area in comparison to the 2% Ta loading, whereas, 10% Ta impregnation results in approximately 34% reduction in surface area, compared to the 2% Ta loading. Similar reductions are also observed for pore volume.

This anticipated result confirms one part of the above-mentioned hypothesis regarding the reduction in adsorption capacity of Ta-10/ACC: Overloading of tantalum species, resulting in pore blockage and thus reduced access to adsorptive sites.

TABLE 6.3 - BET SURFACE AREA AND PORE VOLUME ANALYSIS

Adsorbent	BET SA (m^2/g)	Pore Volume (cc/g)
ACC	646	0.265
Ta-2/ACC	597	0.127
Ta-5/ACC	578	0.098
Ta-10/ACC	445	0.056

6.4 Impact of Acid Treatment on Adsorption Performance

As mentioned earlier, for tantalum impregnation process, TaF_5 in aqueous solution was used, which resulted in formation of an acidic solution that may potentially impact physical and/or chemical nature of the activated carbon and thus influence the adsorption performance. In order to determine if the observed improvement in sulphur adsorption capacity of the Ta-impregnated ACC is due to the presence of tantalum adsorption sites or due to the presence of any residual fluoride ion layer that might be present on the ACC surface or simply the acidification of ACC during the impregnation process, acid treated sorbents were prepared and tested for DBT adsorption. The acid treatments were done using hydrofluoric acid (HF) and sulphuric acid (H_2SO_4). For this purpose HF and H_2SO_4 treated ACC were synthesized in a liquid acid treatment procedure as follows:

- ACC of <125μ particle size was added to 1.0 M HF acid and stirred using a Teflon covered magnetic stir bar, overnight (18 hours);
- The mixture was suction filtered and the recovered ACC was dried in air for 24 hours; and,
- The air dried ACC was thermally treated in the same way as other sorbents (i.e., 110 °C for 3 hours followed by 1 hour at 400 °C), before being used in liquid adsorption study.

The same procedure was used for sulphuric acid.

The DBT adsorption isotherms for the two acid-treated ACCs are presented in Figure 6.3. The maximum adsorption capacities and Langmuir equilibrium constant (K) values are summarized in **TABLE 6.4**.

FIGURE 6.3 - DBT ADSORPTION ISOTHERM FOR ACID TREATED ACC (ACC<125μ, BINARY SOLUTION OF DBT IN HEXADECANE AT 50 °C)

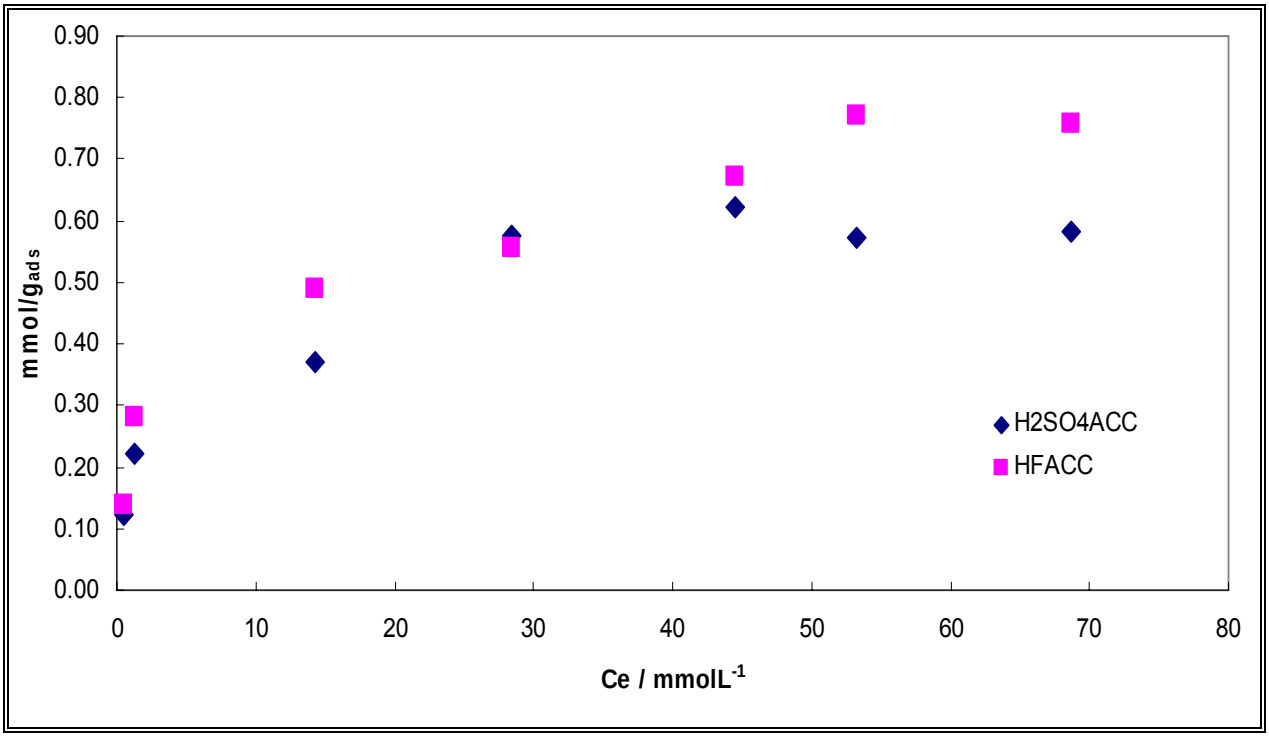

TABLE 6.4 - DBT ADSORPTION RESULTS FOR ACID TREATED ACC

Acid Treatment	q_{max} (mmol-S/g-sorbent)	K (L/mmol)
HF Treated ACC	0.82	0.15
H_2SO_4 Treated ACC	0.63	0.27

For both acid treated ACCs, there was a minor change in the maximum adsorption capacity (DBT) when compared to virgin ACC. Research on activated carbons has shown that structurally they are typically resistant to acids and bases (Serp and

Figueiredo, 2009). Therefore, it is not anticipated that the acid treatment would result in disruption of the activated carbon structure. Moreover, the results were not indicative of formation of secondary adsorption sites as a result of acid treatment since the experimental data fits the Langmuir adsorption isotherm model better than the Freundlich model (see Appendix C). Although acid treatment may potentially alter the surface chemistry of the activated carbon, one may argue that the observed change in q_{max} (when compared with virgin ACC) is relatively minor and thus acid treatment has little or no impact on sulphur adsorption capacity of ACC.

6.5 Competitive Adsorption

As mentioned above the industrial applications for the developed sorbent for adsorptive desulphurization would require maintaining a good adsorption capacity in the presence of other chemical species that can potentially compete for the adsorption sites. These species include coexisting sulphur compounds, with DBT and 4,6 DMDBT being the most difficult to remove and thus most important for this study, as well as aromatics, such as naphthalene and organo-nitrogen compounds, such as quinoline and carbazole. To determine the adsorptive performance of the tantalum impregnated ACC in a competitive environment (i.e., numerous co-existing adsorbates) the adsorption of sulphur, aromatic and nitrogen compounds as well as combination thereof, on tantalum impregnated activated carbon (i.e., Ta-5/ACC) was investigated.

6.5.1. Adsorption of Organo-Nitrogen Compounds

Adsorption of organo-nitrogen compounds from a mixture of quinoline and hexadecane was investigated using the best performing tantalum impregnated ACC, i.e., 5% by weight Ta-impregnated ACC (Ta-5/ACC). The investigation consisted of liquid adsorption isotherm analysis for both virgin ACC and Ta-5/ACC. This was to ascertain

the impact that Ta impregnation has on quinoline adsorption. The isotherms are presented in Figure 6.4 and the adsorption capacities and K values are presented in **TABLE 6.5**.

FIGURE 6.4 - QUINOLINE ADSORPTION ISOTHERMS FOR TA-IMPREGNATED ACC AND VIRGIN ACC

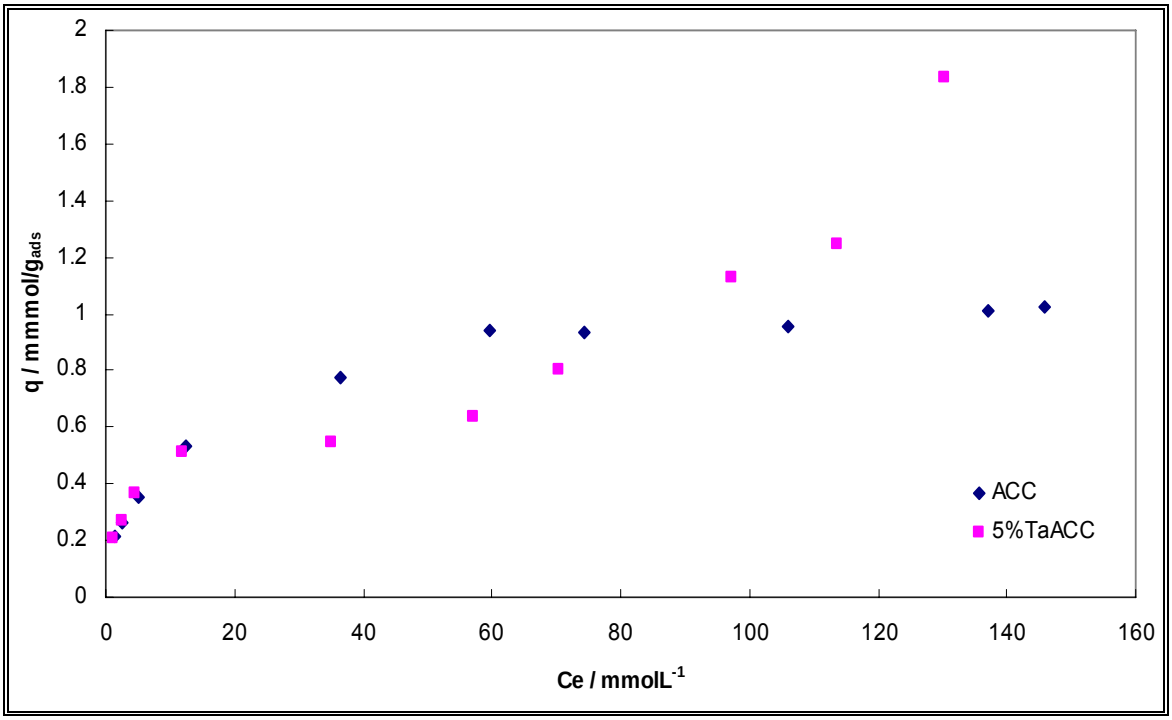

TABLE 6.5 - QUINOLINE ADSORPTION ON TA-IMPREGNATED ACC AND VIRGIN ACC (BINARY SOLUTION OF QUINOLINE IN HEXADECANE AT 50 °C)

Adsorbent	Adsorption Capacity (mmol-N/g-sorbent)	K (L/mmol)
Ta-5/ACC	1.84	0.189
ACC (virgin)	1.36	0.062

Note:
Results are mean values based on two runs.

The results indicate that similar to that of sulphur adsorption, nitrogen adsorption is improved as a result of tantalum impregnation. The improvement in adsorption capacity is approximately 35%, which is considered to be significant. Similar to sulphur adsorption, the isotherm for Ta-5/ACC seems to fit the Freundlich equation while virgin ACC best fits the Langmuir adsorption equation. The linearization and regression analysis are provided in Appendix C.

In addition to the liquid isotherm study of quinoline adsorption on virgin ACC and Ta-5/ACC (above), a single point adsorption study was conducted for carbazole. For each sorbent two separate runs were completed. The results of each run and the average adsorption capacity in mmol-N/g-sorbent is provided in Table 6.6, below.

Similar to quinoline, the tantalum impregnated ACC illustrates higher adsorption capacity towards carbazole (approximately 21% higher) in comparison to virgin ACC.

TABLE 6.6 - CARBAZOLE ADSORPTION CAPACITY ANALYSIS FOR ACC AND TA/ACC (BINARY SOLUTION OF CARBAZOLE IN TETRALIN AT 50 °C)

Sorbent Use	Run ID	GC/FID (mmol-N/L)		Adsorption Capacity (mmol-N / g-sorbent)
		Stock Solution	After Adsorption	
ACC (Virgin)	Run 1	23.5	14.5	0.41
	Run 2	23.5	15.1	0.37
5%-Ta/ACC	Run 1	23.5	15.7	0.47
	Run 2	23.5	16.1	0.48

Note:
Based on 300 ppmw-N carbazole in tetralin.

The strong Lewis acid characteristic of Ta is believed to be responsible for this greater adsorption capacity for both quinoline and carbazole. It is postulated that the new adsorptive sites (i.e., tantalum species) interact strongly (strong Lewis acid) with the lone pair of electrons of nitrogen in quinoline and carbazole and thus improve adsorption performance.

6.5.2. Adsorption of Aromatic Compounds

The adsorption capacity of sorbents towards aromatic compounds was assessed using a mixture of naphthalene and hexadecane. The investigation consisted of liquid adsorption isotherm analysis for both virgin ACC and Ta-5/ACC. This was to ascertain the impact that Ta impregnation of ACC has on naphthalene adsorption.

The isotherms are presented in **FIGURE 6.5** and the adsorption capacities and K values are presented in Table 6.7. Amounts of naphthalene adsorbed are significantly less compared to that of sulphur and nitrogen compounds. Little change in adsorption capacity of naphthalene was observed for the Ta-5/ACC when compared with virgin ACC. The lower adsorption capacity for naphthalene on these sorbents is not clearly understood, however, one may hypothesize that the surface functionalities of the activated carbon and tantalum species on the surface of the ACC interact primarily with the sulphur and nitrogen atoms in organo-sulphur (DBT and 4,6 DMDBT) and organo-nitrogen (quinoline and carbazole) compounds, respectively, rather than their aromatic rings.

The adsorption isotherms for both virgin ACC and Ta-5/ACC fit the Langmuir's adsorption mechanism.

FIGURE 6.5 - NAPHTHALENE ADSORPTION ISOTHERMS FOR Ta-IMPREGNATED ACC AND VIRGIN ACC (BINARY SOLUTION OF NAPHTHALENE IN HEXADECANE AT 50 °C)

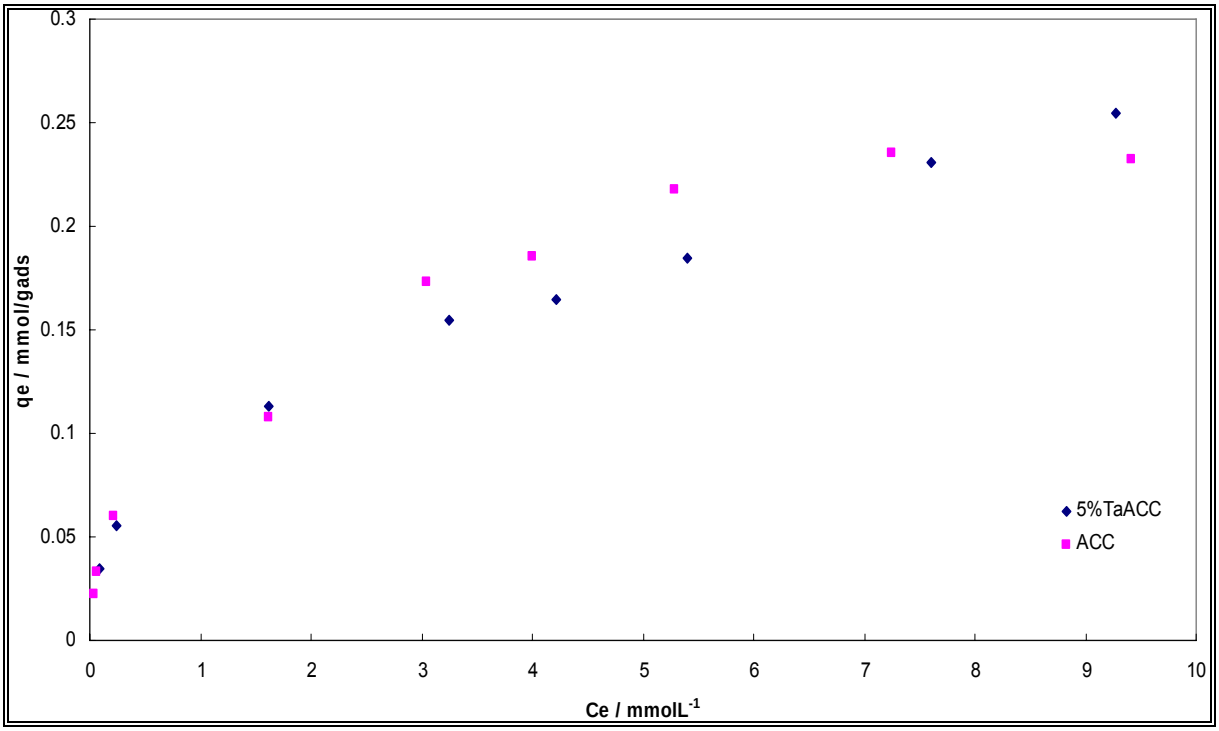

TABLE 6.7 - NAPHTHALENE ADSORPTION ON Ta-IMPREGNATED ACC AND VIRGIN ACC (BINARY SOLUTION OF NAPHTHALENE IN HEXADECANE AT 50 °C)

Adsorbent	q_{max} (mmol/g-sorbent)*	K (L/mmol)
Ta-5/ACC	0.25	0.095
ACC (virgin)	0.23	0.973

Note:
Results are mean values based on two runs.
* mmol of naphthalene per gram of sorbent

6.5.3. Competitive Adsorption – Sulphur / Nitrogen / Aromatics

A study of competitive adsorption and selectivity was carried out to determine adsorption behaviour of Ta-impregnated ACC in a mixture (which tends to be the case in industrial applications). Equilibrium adsorption of a mixture of sulphur (DBT), nitrogen (quinoline) and aromatic (naphthalene), containing equi-molar amounts of each compound was studied using 5% by weight Ta-impregnated ACC. The results indicate higher selectivity towards quinoline than DBT and naphthalene for both virgin ACC and Ta-5/ACC. The least selectivity is observed for naphthalene, which again is similar for both sorbents.

The order of amounts adsorbed is in a similar trend as that of adsorption of individual adsorbates. Results of this experiment are presented in Table 6.8, below.

TABLE 6.8 - COMPETITIVE ADSORPTION – DBT, QUINOLINE AND NAPHTHALENE ON TA-5/ACC

Adsorbate	Adsorption Capacity (mmol/g)	
	ACC (virgin)	Ta-5/ACC
DBT	0.39	0.47
Quinoline	0.46	0.48
Naphthalene	0.09	0.18

Note:
Equi-molar concentrations of each adsorbate (at approximately 22 mmol/L) was used, adsorption time: 24 hours, temperature: 50 °C

6.6 Sorbent Regenerability

Regenerability of the best performing sorbent, Ta-5/ACC was studied to determine its feasibility for industrial applications. The regenerability consisted of solvent wash, ultrasonic treatment and heat treatment. The spent/used sorbent was washed with toluene while under ultrasonic treatment.

In order to determine regeneration temperature for the thermal treatment of the used sorbent a thermogravimetric analysis was undertaken on a used, tantalum impregnated activated carbon sorbent. The analysis consisted of a temperature ramp-up rate of 10 °C per minute, and a 30-minute hold (isothermal) at 400 °C, followed by a final temperature ramp-up (at the same rate of 10 °C / min) to a maximum temperature of 600 °C. The result is presented graphically in Figure 6.6, below.

The results indicate a 4.46% mass reduction in the temperature range of approximately 312 °C and 397 °C. The result was compared with that of unused Ta-5/ACC and the mass reduction observed for used sorbent did not appear for unused sorbent. It was therefore concluded that the mass loss detected at those temperatures can potentially be associated with the residual organo-sulphur compound, in this case, DBT (boiling point ~ 332 °C). It should be noted the used sorbent sample used in themogravimetric analysis was not washed with toluene or sonicated.

FIGURE 6.6 - THERMOGRAVIMETRIC ANALYSIS OF USED Ta-5/ACC

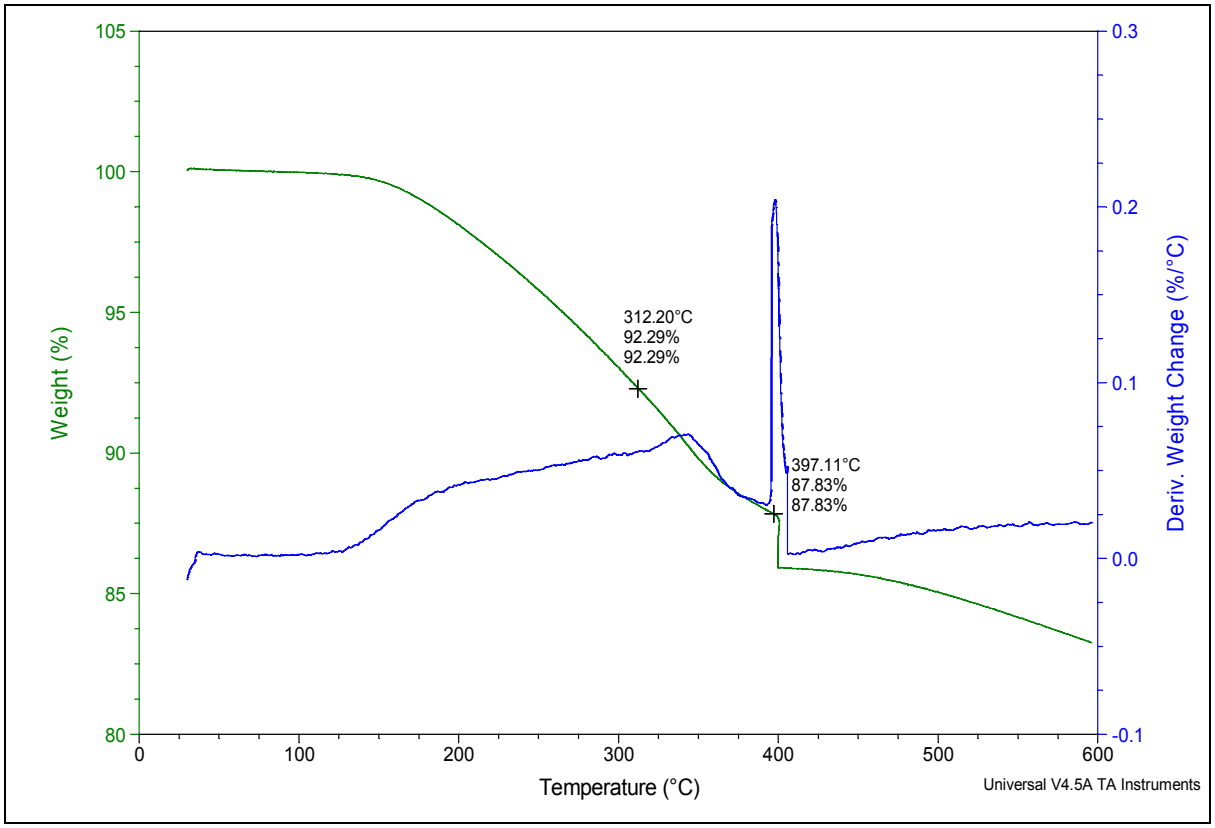

The sorbent was subsequently heat treated at 400°C under He flow. The results of the analysis are presented in Table 6.9. After the sorbent regeneration process, the sulphur adsorption capacity was decreased by approximately 6%.

TABLE 6.9 - SORBENT REGENERABILITY ANALYSIS – TA-5/ACC

Adsorbent	q_{max} / $mmolg_{ads}^{-1}$
Fresh	1.14
Reuse-1	1.07

As we will see in Section 7, the regenerability of Ta-5/ACC is near 100% (i.e., the adsorption capacity is fully restored) when sorbent treatment and activation is conducted in-situ (See Section 7).

6.7 Heat of Adsorption Analysis – Ta-5/ACC

The heat of adsorption for 5% by weight Ta-impregnated ACC was studied using a flow calorimeter (DBT in hexadecane mixture). The results were compared to that of virgin ACC in order to determine the impact of Ta impregnation on heat of adsorption. The results are presented in Figure 6.7 and Table 6.10. Results indicated a molar heat of adsorption that is more than three times higher for Ta-5/ACC in comparison to virgin ACC. This observation is expected and it is believed to be due to (1) introduction of new adsorption sites and (2) the stronger adsorption bond (i.e., chemisorption) that is formed between the Lewis acid Ta and the electron pair of sulphur in DBT.

The Ta sites tend to form stronger adsorption bonds with organo-sulphur compounds than those formed between the surface functional groups and the organo-sulphur compounds. As we will see in subsequent sections (i.e., XPS), formation of a tantalum – sulphur bond is detected in used Ta-5/ACC sorbent, indicating a chemisorption interaction between Ta sites and sulphur.

FIGURE 6.7 - HEAT FLOW CURVES FOR ACC, 5%TAACC ADSORBENTS

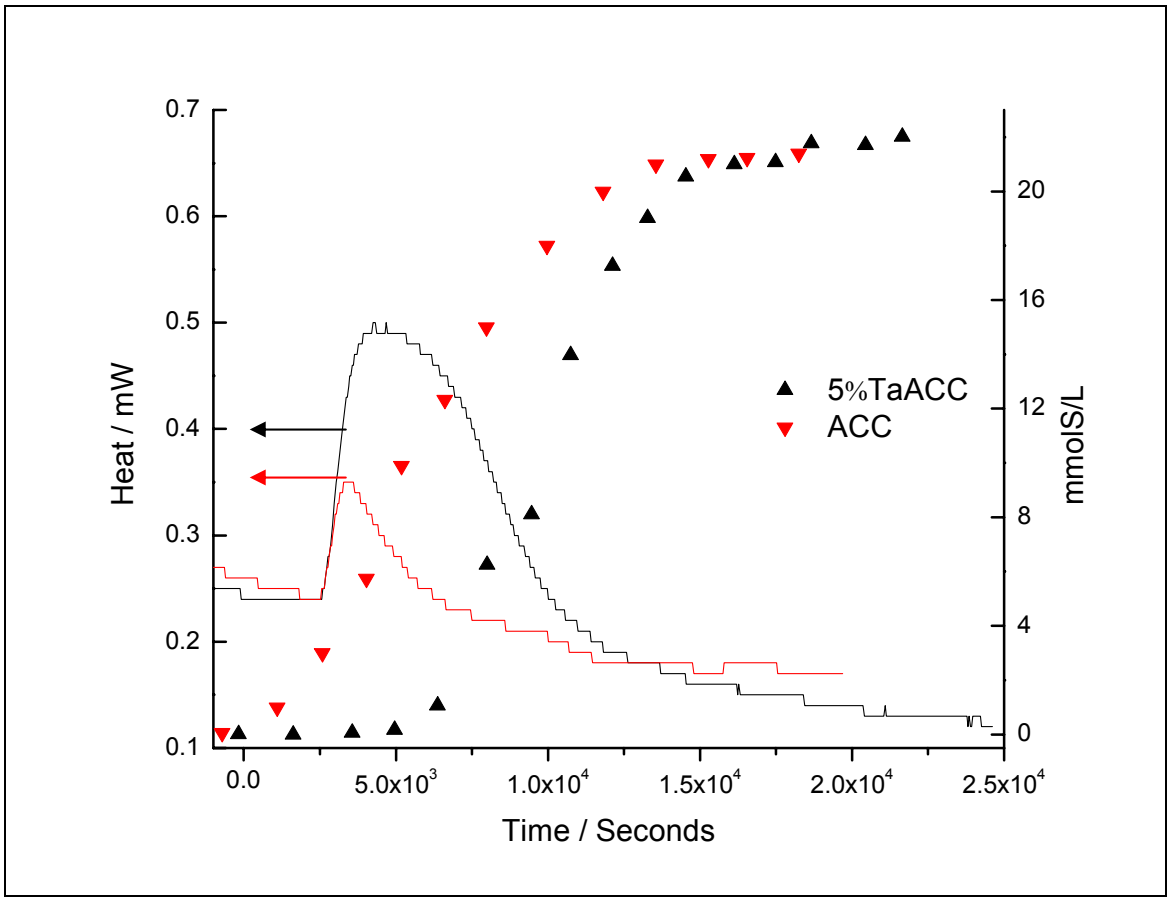

TABLE 6.10 - COMPARISON OF HEAT OF ADSORPTION TA-5/ACC VERSUS ACC

Adsorbent	Normalized Heat (J/g-sorbent)	Molar Heat (kJ/mol)	Adsorption Capacity (mmol/g-sorbent)
Ta-5/ACC	11.15	13.60	0.82
ACC	1.35	3.86	0.35

6.8 Sorbent Characterization

When physical and/or chemical changes to a sorbent are assessed together with its adsorptive performance, one can establish links between certain properties / characteristics of the sorbent and the change in its performance in order to gain a better understanding of the adsorption and key factors that influence it. To establish a better understanding of the physical and chemical changes that take place as a result of metal impregnation, series of systematic characterizations were completed which are further discussed in the following subsections.

6.8.1. FTIR – Surface Functional Groups

A qualitative assessment of the selected sorbents was carried out using FTIR, in order to identify surface functional groups that exist on the surface of the activated carbons. Furthermore, comparative assessments were conducted to qualitatively determine possible interactions between impregnation metal species (i.e., tantalum species) and the existing surface functional groups.

The results of FTIR analysis for the sorbents ACC (virgin), Ta-2/ACC and Ta-5/ACC are presented in Figure 6.8, below. In the literature, a description of FTIR bands for various activated carbons is reported. Figure 4.2 provides the infrared absorption bands assigned to various functional groups (Young, 1996). The functional groups present on surfaces of various activated carbons vary depending on the source of the activated carbon.

FIGURE 6.8 - FTIR ANALYSIS OF SORBENTS

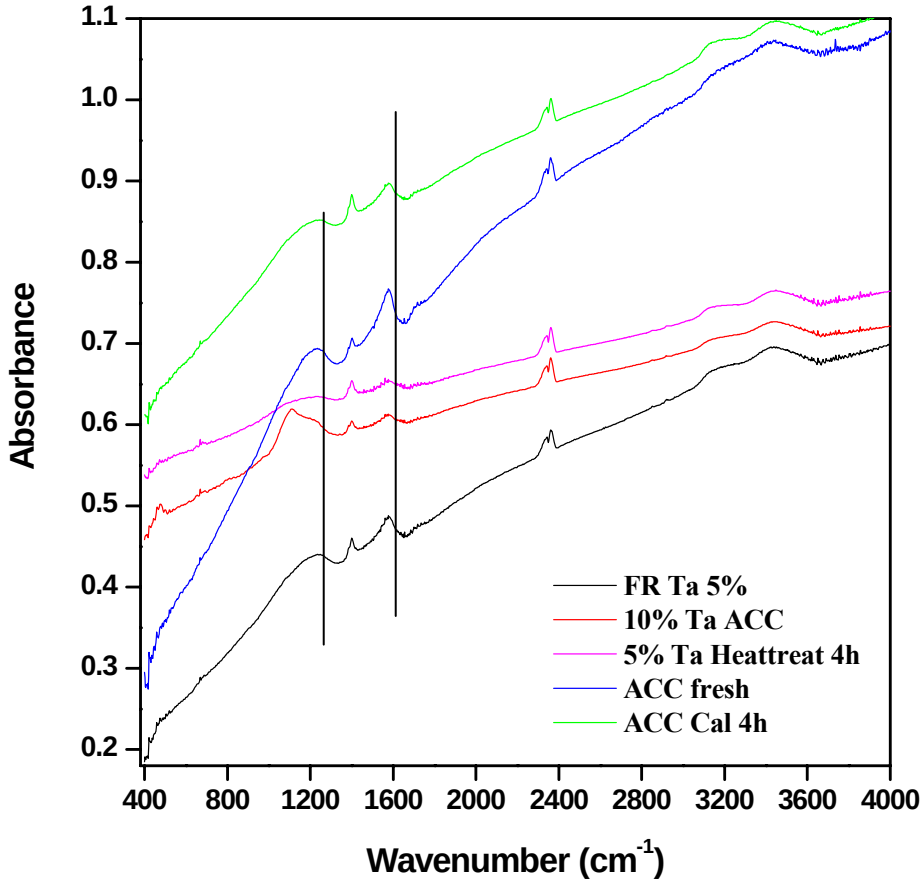

In the case of ACC, several characteristic bands of activated carbon are observed in the FTIR spectra. Peaks corresponding to oxygen functional groups of highly conjugated C-O stretching (1152 cm^{-1}, 1360 cm^{-1}), aromatic ring stretching coupled to highly conjugated carbonyl groups (1565 cm^{-1}), C-C triple bond stretching (2300 cm^{-1}), C-H stretching in aliphatic methylene and methyl groups (2384 cm^{-1}), broad O-H stretching band in hydroxyl, carboxyl and phenolic groups (3420 cm^{-1}) and O-H stretching band (3570 cm^{-1}) are evident. The FTIR was also completed for Ta-2/ACC and Ta-5/ACC. The characteristic vibration bands described above (oxygen functional groups) were found to be present in the FTIR spectra of all three adsorbents indicating little or no impact on the active functional groups of activated carbon as a result of tantalum impregnation. Also, it was determined that the thermal treatment of the activated carbon

to a maximum temperature of 400 °C does not impact the surface functional groups of the activated carbon. This is the case for both virgin and impregnated ACC.

6.8.2. Temperature-Programmed Desorption – Ammonia

Information regarding the strength of the acidity of the sorbent was obtained via the quantitative and qualitative analysis of the temperature programmed desorption (TPD) of ammonia. The sorbent was activated in situ by prolonged thermal treatment while exposed to carrier gas and were subsequently saturated with ammonia. The adsorbed ammonia was removed by thermal treatment. The sorbent bed was heated according to a predetermined thermal profile (see below). The signal peaks resulting from desorption of ammonia as a function of temperature provided information regarding the relative strength of acidity of the adsorption sites.

Sample Preparation

Sorbents of a particle size range 125µ - 250µ were prepared using crushing and sieving. Approximately 0.1g of catalyst meeting this size specification was precisely weighed using a Sartorius balance (± 0.00005 g). The sorbent was transferred into a quartz U-tube reactor, which utilizes a small amount of quartz wool on both ends of the tube to ensure that the sorbent remains inside the U-tube during the analysis and as the carrier gas flows through the U-tube. The U-tube was then secured to the sample station of an Altamira AMI-200 Catalyst Characterization System using ultra-torr fittings with o-ring seals provided by Altamira Instruments.

Once the U-tube was inserted into the sample station of the Altamira AMI-200 and sealed, an 800 W heating mantle was raised into position to surround the U-tube. The U-tube was enclosed at the top of the mantle with insulation and insulation tape. The AMI-200 is equipped with multiple gas input ports capable of accommodating up to 4 carrier gases, 4 treatment gases and 4 blend gases. The volumetric flow rates of the carrier,

treatment and blend gas streams are controlled by three Brooks mass flow controllers within the AMI-200 apparatus. UHP 5.0 Argon was used as a carrier gas and anhydrous ammonia was connected to a treatment gas inlet. No blend gases were used in these experiments.

The direction of gas flow within the apparatus was controlled by two multi-port sampling valves as illustrated in the schematic representation of the Altamira AMI-200 Figure 6.9. The AMI-200 was equipped with a thermal conductivity detector (TCD) downstream of the analytical vent enabling the quantification of ammonia desorbing from the specimen (i.e., sorbent).

FIGURE 6.9 - A SCHEMATIC DIAGRAM OF TPD FLOWS AND CONTROL SYSTEM

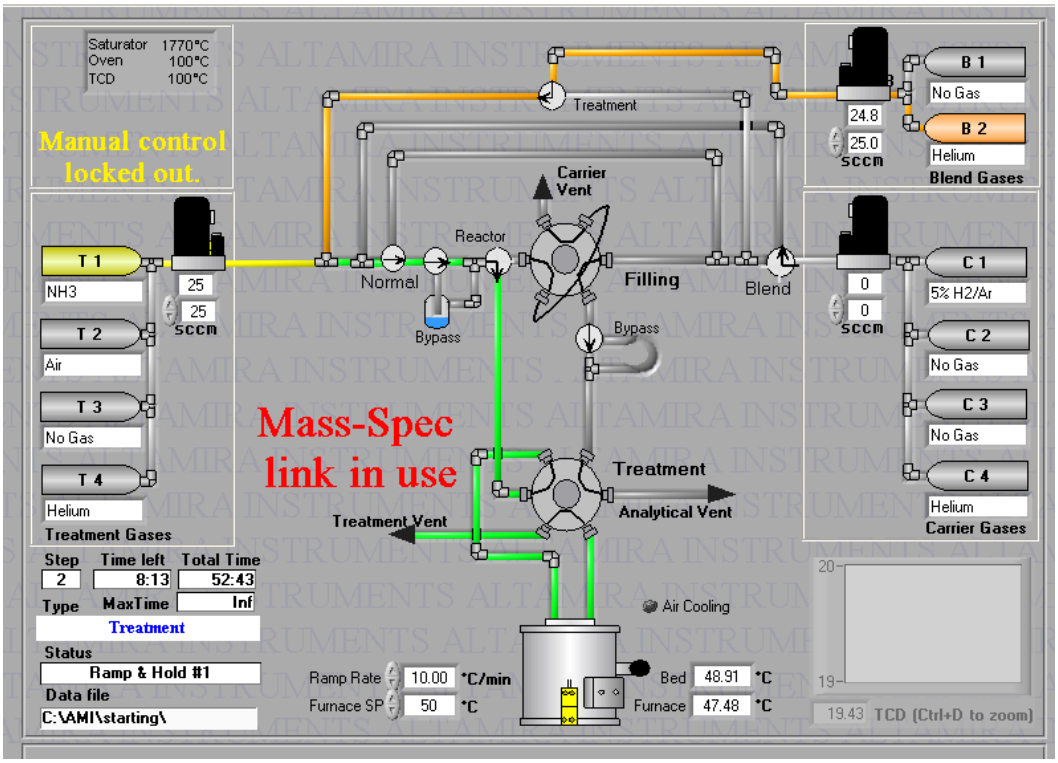

The pre-treatment and analysis steps are listed below:

- Flow of argon (carrier gas) for 30 minutes at 200 ^{o}C;

- Cool to room temperature under the argon flow;
- NH_3 gas adsorption onto the sample in pulses until it was saturated (saturation of the adsorbent with the ammonia gas confirmed by TCD);
- Flush sample using the carrier gas at room temperature for 5 minutes to remove the excess and loosely bonded NH_3;
- Heat up sample at a rate of 10 ^oC/min to 1000 ^oC; and,
- Cool the sample back to room temperature.

The desorption of NH_3 was monitored by a response signal from the thermal conductivity detector. The TCD response was plotted against time and temperature to give the desorption pattern of NH_3. The plots for ACC and Ta/ACC are presented in Figure 6.10.

Generally, the higher the temperature at which desorption of ammonia takes place, the stronger the acidity of the sorbent. ACC and tantalum impregnated ACC were analyzed for acidity. Results are shown graphically in **FIGURE 6.10**.

FIGURE 6.10 - TPD-AMMONIA FOR Ta-IMPREGNATED AND NON-IMPREGNATED ACTIVATED CARBON (ACC)

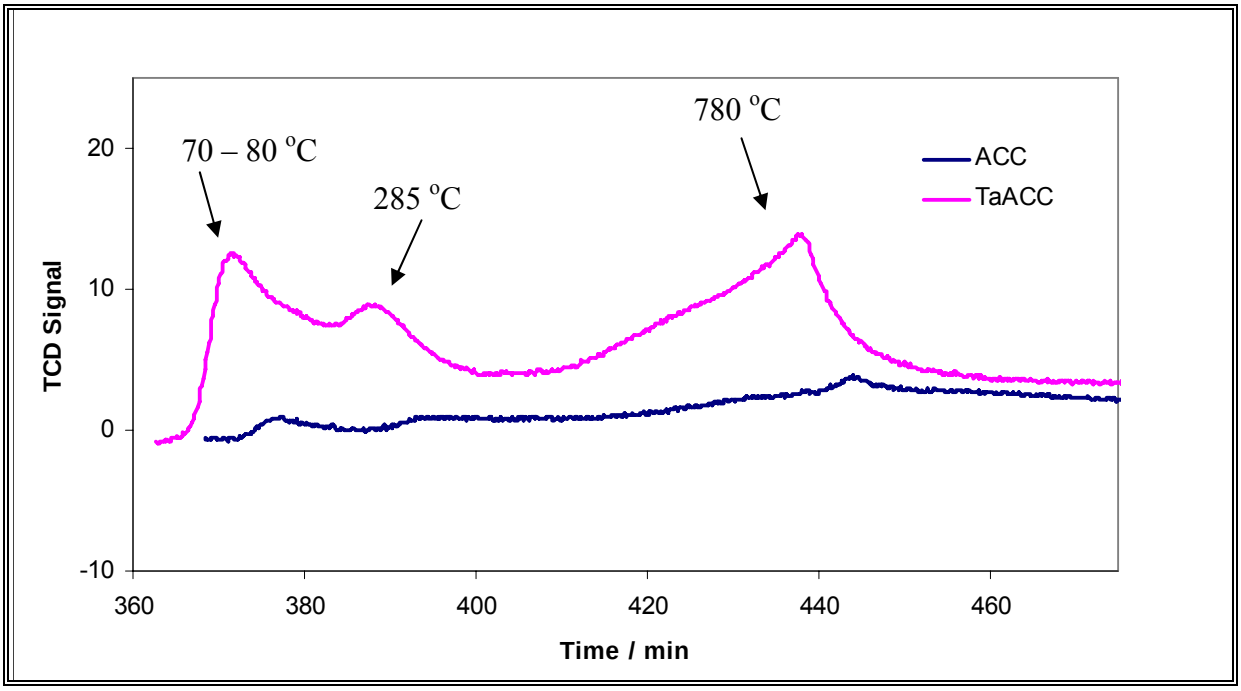

The results indicate that although ACC has some acidic properties, impregnation with Ta significantly improved the acidity of the sorbent. The desorption of ammonia at lower temperature ranges (e.g., 70 – 80 °C) is indicative of weakly adsorbed (likely physisorbed) ammonia. Significant ammonia desorption was detected, which was determined to peak at a bed temperature of approximately 780 °C. This is indicative of a strong ammonia-sorbent bond for Ta/ACC, which is otherwise absent for virgin ACC (un-impregnated). Thus the strong interaction is considered to be between the tantalum on the surface of the activated carbon and ammonia.

It should be noted that this technique does not reveal the nature of the acidity since NH_3 will adsorb indiscriminately on both Lewis and Bronsted acid sites. However, tantalum is well known for its Lewis acid properties (Howarth and Gillespie 1996). This is

particularly useful since Lewis acid sites provide good adsorption sites for thiophenic compounds, due to the interaction with the lone pair of electrons of sulphur.

6.8.3. HRTEM Analysis

HRTEM was used to determine physical characteristics of the sorbent and changes as a result of tantalum impregnation process. The physical features including surface morphology and dispersion of tantalum on the surface of the activated carbon were evaluated. The analysis was carried out on tantalum impregnated activated carbon as well as virgin activated carbon.

Along with HRTEM, EDX analysis was also conducted to determine elements (e.g., tantalum) that exist on the surface of the sorbents. The analysis was carried out on tantalum impregnated activated carbon as well as virgin activated carbon.

The results are illustrated in **FIGURE 6.11** (a) to (d). It can be seen from the figures that the thermal treatment at 400 °C induces structural uniformity in the activated carbon support and is believed to improve its crystalline structure in terms of pore accessibility. In addition, the thermal treatment of sorbent at 400 °C is believed to improve the dispersion of various tantalum species and a more uniform array of lattice structure.

The improved dispesion of tantalum species as a result of heat treatment can potentially be due to the differences in the crystallographic structures of various Ta oxide species (Sata *et al.* 2010). As we will discuss later on, the tantalum species on the surface of the activated carbon consist mainly of various tantalum oxide species such s Ta_2O_5 and TaO_x with $x<2.5$.

FIGURE 6.11 - HRTEM FOR VIRGIN ACC AND Ta-5/ACC

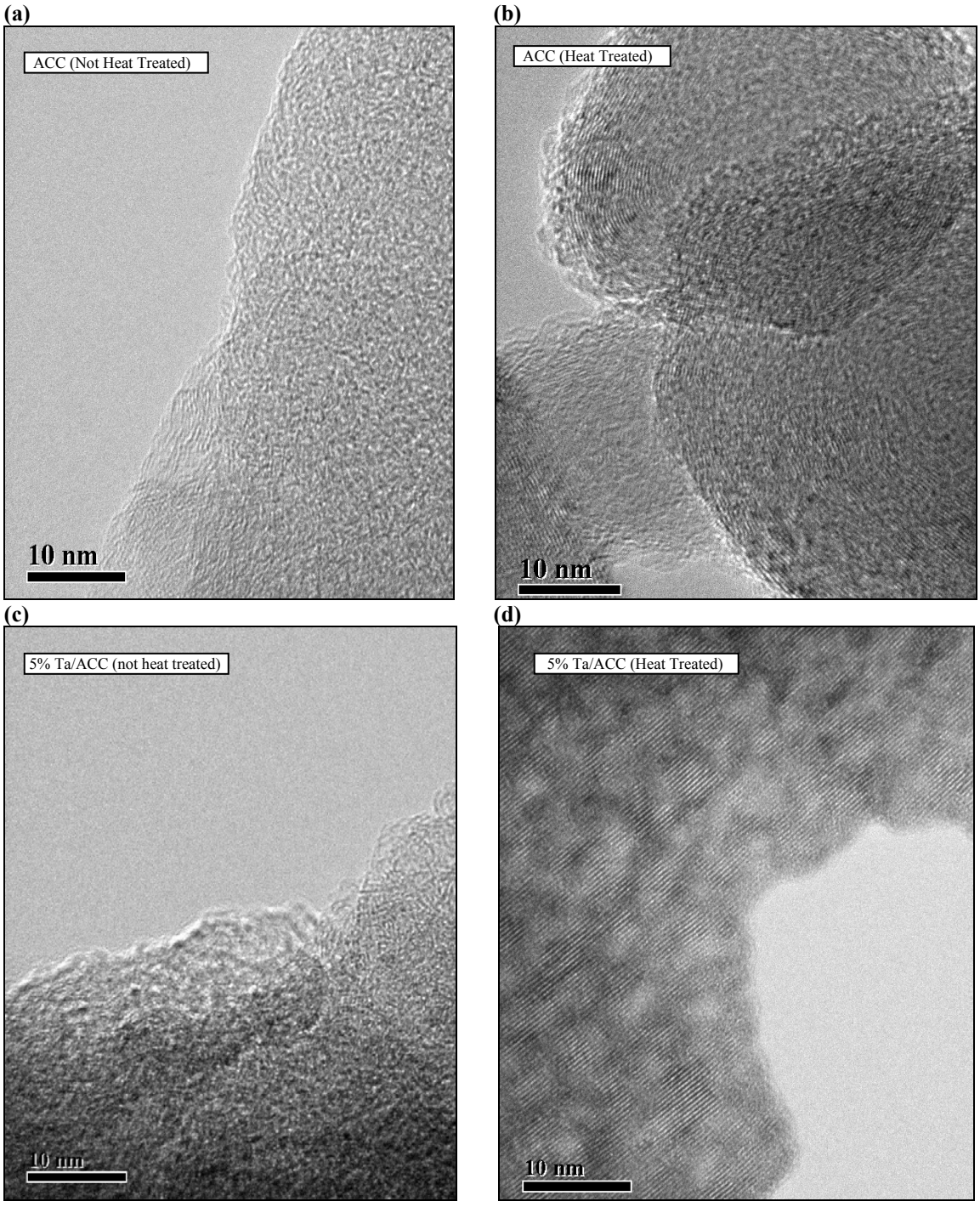

The existence of the tantalum onto activated carbon is confirmed through HRTEM-EDX analysis. The EDX results for un-impregnated ACC and 5% Ta/ACC are presented in **FIGURE 6.12** (a) and (b), respectively. The results unambiguously confirm the incorporation of the tantalum species onto the surface or in the pores of the activated carbon.

FIGURE 6.12 – HRTEM-EDX ANALYSIS FOR (a)VIRGIN ACC AND (b)Ta-5/ACC

(a)

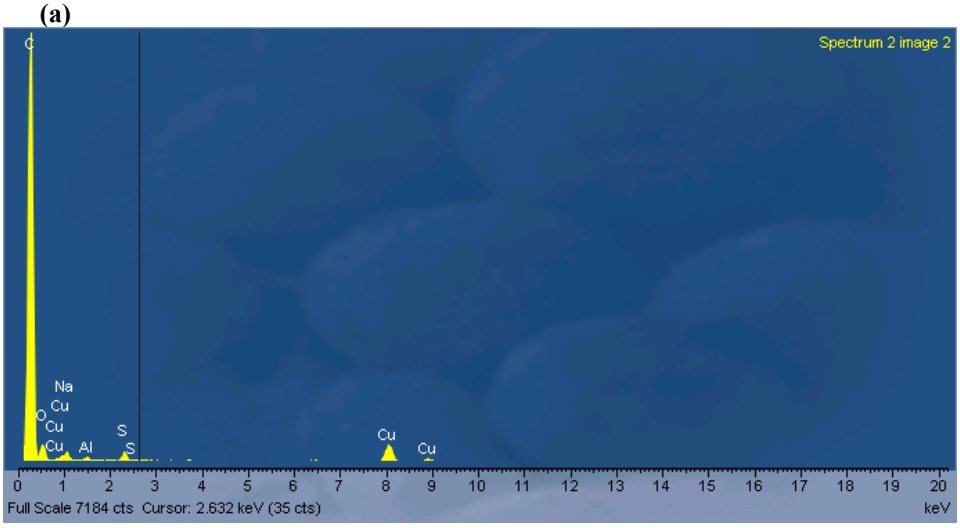

(b)

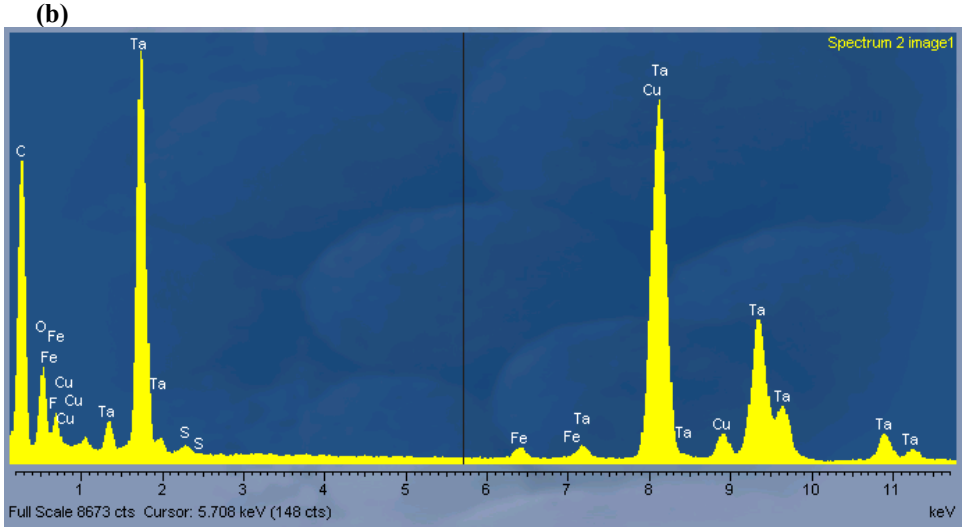

Although tantalum species are found in the porous structure of ACC, the combined TEM and EDX analysis of zoomed in segments of the sorbent indicate that the distribution of tantalum species on the surface of the activated carbon is relatively inhomogeneous, with some areas showing well dispersed tantalum species (spectrum 1 in Figure 6.13) and others showing large clusters of tantalum species, pointing to a relatively low dispersion (spectrum 1 in Figure 6.14). Improving the dispersion of tantalum species on the surface can potentially improve the already high (highest to date by a significant margin) adsorption capacity of Ta-5/ACC.

FIGURE 6.13 - TEM OF Ta-5/ACC AND EDX ANALYSIS FOR THE DISPERSED Ta

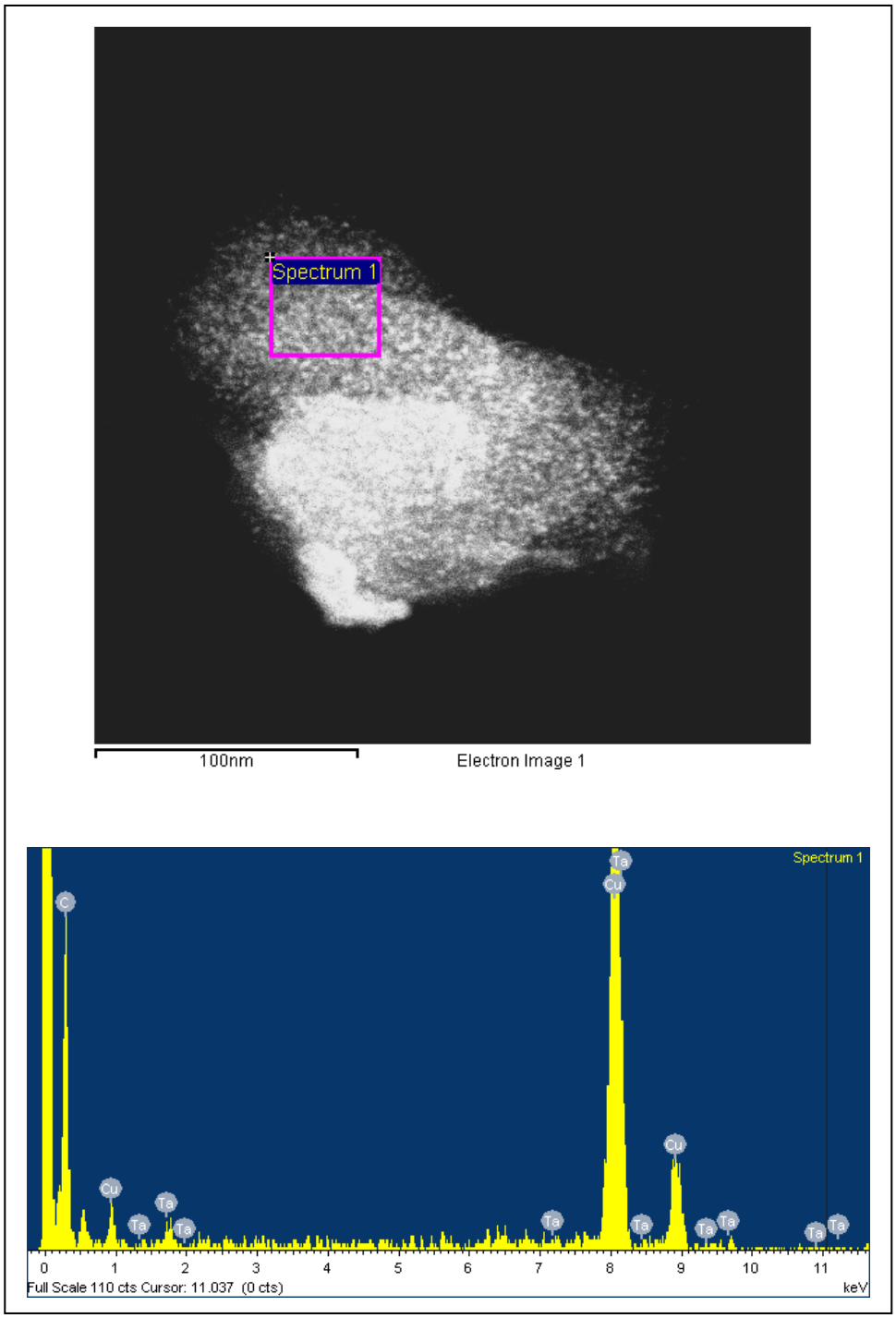

FIGURE 6.14 - TEM OF Ta-5/ACCAND EDX ANALYSIS FOR THE CLUSTERED Ta

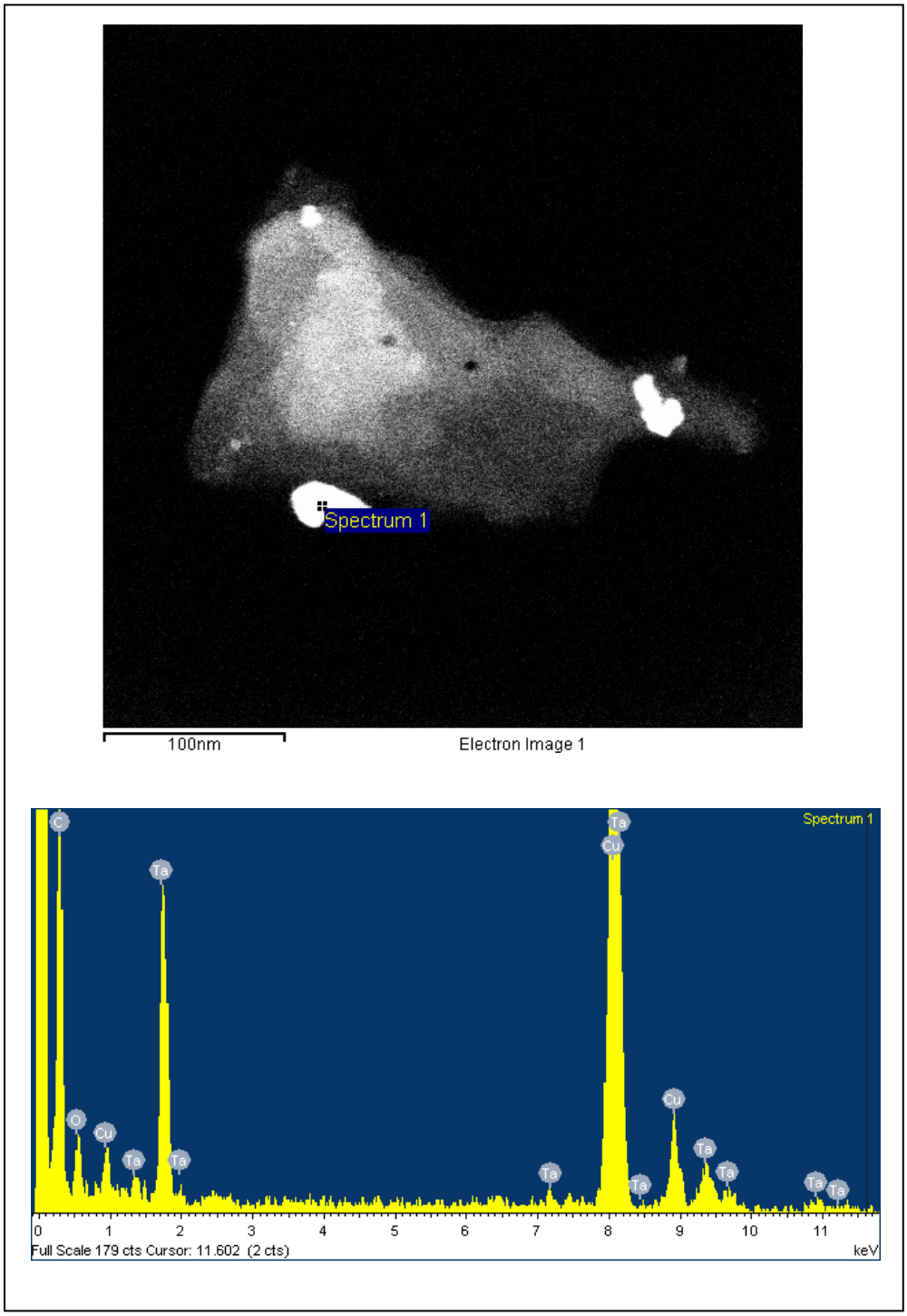

6.8.4. XPS Analysis

X-ray photoelectron spectroscopy (XPS) is based on photo-ionization and dispersive energy analysis. The photoelectrons that are emitted for a sample are analyzed in order to determine the composition and oxidation state of the sample. XPS is a surface analysis method and thus the composition and oxidation state pertain to the surface of the sample. XPS allows the study of the energy levels of atomic cores, based on Einstein's equation:

$$\tau_e = h\nu - E_b,$$

Where:

τ_e : kinetic energy of the photoemitted electron

E_b : binding energy of the core level

h: Plank's constant (6.62×10^{-34} J s)

ν: rediation frequency (Hz)

Different chemical bonds are associated with different binding energies. This difference can determine types of binding sites for similar atoms based on their binding energies. This type of analysis is achieved through XPS. The photon absorbed by an atom in a molecule leads to the ionization and emission of inner shell electron.

The exact value of the binding energy of an emitted electron depends on the following key factors:

(1) The level from which the photoemission is occurring from;

(2) The oxidation state of the atom; and,

(3) The local chemical and physical environment.

Changes in the oxidation state and/or chemical and physical environment of the sample result in small shifts in peak positions in the spectrum, commonly referred to as chemical shifts. Such shifts are readily detected and interpreted through XPS analysis. The XPS

technique is of high intrinsic resolution since the core levels have discrete and well defined energy levels (Perkin Elmer, 1990).

Through observation it is determined that in analyzing elements using XPS, spin orbit splitting occurs which leads to additional peaks in the binding energy spectra. This is the case for p, d and f orbitals, resulting in doublets in XPS spectra. In case of s orbital, splitting does not occur (i.e., single peak in XPS spectrum). The splittings are distinguished by total angular momemtum of the electron which is a combination of its orbital angular momentum 'l' and spin angular momentum 's'. For orbitals with doublets (i.e., p, d and f) the quantum numbers referring to total angular momentum, 'j' are listed in Table 6.11, below (Moulden *et al.* 1995).

TABLE 6.11 - TOTAL ANGULAR MOMENTUM VALUES FOR ORBITS IN XPS

subshell	j values
s	1/2
P	1/2 , 3/2
d	3/2 , 5/2
f	5/2 , 7/2

Note: $j = |l \pm s|$

The photoelectron lines for each peak are expressed in reference to the associated energy level, orbital shell and its 'j'. For example, Ta $4f_{7/2}$ refers to energy level 4 (i.e., n = 4), 'f' orbital and 'j' value of 7/2.

The XPS analysis was completed using an Al Kα radiation source ($\mathbf{h}\nu$ = 1486.6 eV). Therefore, the kinentic energy of the emitted photoelectrons will have a range of 0 to ~1486 (energy resolution of 0.4-0.5 eV). The analysis was completed under ultra-high vacuum, at 10^{-9} torr.

The XPS analysis was completed in order to determine and/or confirm, (1) chemical species and/or functional groups that exist on the surface of the activated carbon; (2) tantalum species and oxidation state of tantalum that exists on the surface of the activated carbon; (3) the change in tantalum species / oxidation state after the sorbent is exposed to adsorbates (in this case, DBT and CBZL); and, (4) bonding strength of sulphur (in DBT) and nitrogen (in CBZL) with tantalum adsorption sites.

The XPS analysis was completed for the following samples:

(1) *Unused virgin ACC* – Unused, heat treated activated carbon sorbent with no metal impregnation;
(2) *Unused Ta-5/ACC* – Unused, heat treated activated carbon with 5% Ta impregnation;
(3) *Used (DBT) Ta-5/ACC* – Used (for dibenzothiophene adsorption), heat treated activated carbon with 5% Ta impregnation; and,
(4) *Used (CBZL + DBT) Ta-5/ACC* – Used (for carbazole adsorption), heat treated activated carbon with 5% Ta impregnation.

A full elemental survey of virgin ACC and unused Ta-5/ACC was completed to determine elemenal species that exist on the surface of the sorbent. The survey scans are provided in Appendix C. The results indicate existence of carbon and oxygen for both ACC and Ta-5/ACC and tantalum for Ta-5/ACC. Fluoride was not detected in Ta-5/ACC. This is in line with the expected dissolution of tantalum pentafluoride and formation of tantalum oxides (Ta_2O_5 and TaO_x, $x<2.5$) during the impregnation procedure.

Carbon – C 1s

The deconvoluted XPS spectra for C 1s ½, for samples: (1) Used (DBT) Ta-5/ACC and (2) Used (CBZL + DBT) Ta-5/ACC are presented in Figures 6.15 and 6.16, respectively. The binding energies corresponding to carbon 1s peaks are also presented in the figures. The deconvolution for the first sample results in four (4) peaks and in the second sample results in three (3) peaks. The carbon peak with highest intensities (at 58.7% and 65.5%, respectively) for both figures appears at approximately 284 eV, and corresponds to polymeric carbon (Benndorf, Grischke *et al.* 1988). The carbon 1s peak at approximately 284.3 eV in Used (CBZL + DBT) Ta-5/ACC corresponds to carbon in carbazole (Kessel and Schultze 1990). Similarly, the C 1s peak at approximately 284.5 eV is considered to correspond to carbon in dibenzothiophene. The peak at approximately 285 eV also apprears in both cases and corresponds to C-C bonding. The peak at approximately 288 eV also exists in both spectra, and corresponds to caboxylic functionalities, which is expected to exist on the surface of the activated carbon. The binding energy at approximately 286 eV for the first sample can be attributed to single bonds to both S and O. The intensity of this peak is at 9.1%, suggesting there S from DBT is adsorbed at carbon functional groups on the surface of the activated carbon. Generally, oxygen can induce a primary substitution effect on the C 1s line, shifting the higher binding energy side by approximately 1.5 eV for each C-O bond. Therefore, a O-C-O and a C=O have similar C 1s ½ binding energies. (Sarac, Tofail *et al.* 2004).

The carbon 1s peak corresponding to carbon in tantalum cabide is at 282.7 eV (Gruzalski, Zehner *et al.* 1985). As can be seen this peak position does not exist in either of the XPS spectra, leading to the conclusion that tantalum oxides do not form complexes with carbon of the substrate.

The results point to the fact that majority of the functional groups on the surface of the activated carbon (ACC) are oxygen based.

Results also indicated that similar carbon species with similar intensities (excluding C-S) were observed on the surface of the virgin (without metal impregnation) ACC. This re-confirms that the impregnation process has little or no impact on the oxygen functional groups on the surface of the activated carbon.

FIGURE 6.15 - DECONVOLUTED XPS SPECTRUM FOR USED (DBT) TA-5/ACC CURVE FITTING FOR C 1S 1/2

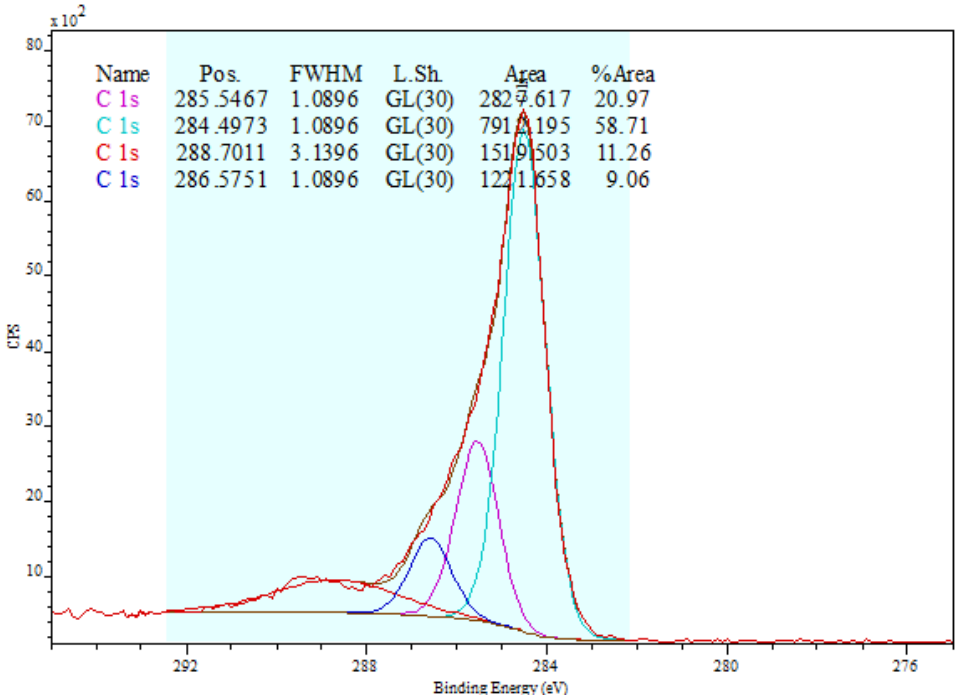

FIGURE 6.16 - DECONVOLUTED XPS SPECTRUM FOR USED (CBZL+DBT) TA-5/ACC CURVE FITTING FOR C 1S 1/2

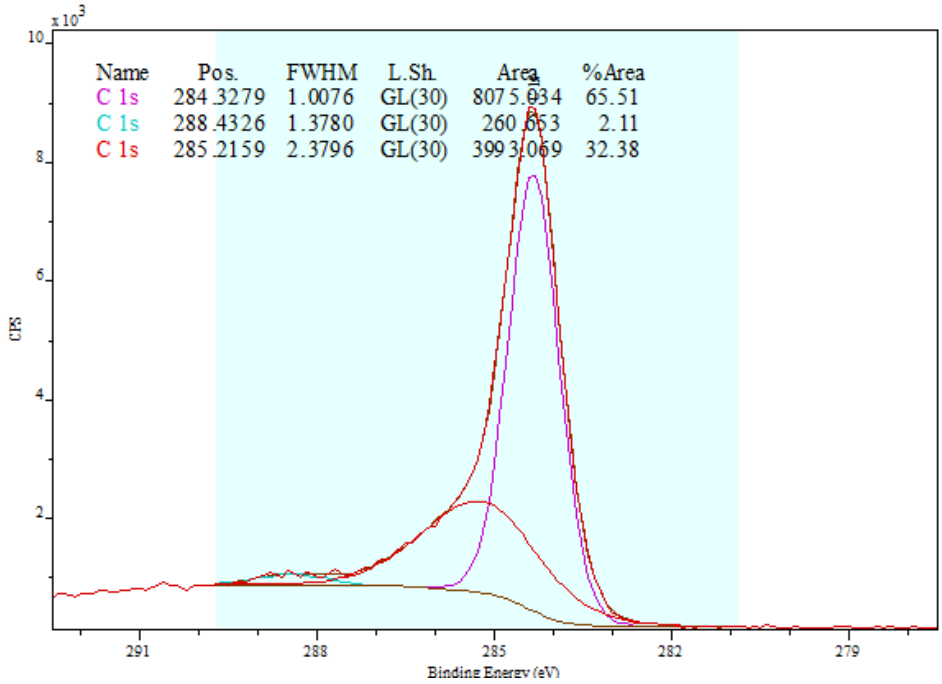

Oxygen – O 1s

The XPS spectra for O 1s ½ , for samples: (1) Unused virgin ACC, (2) Unused Ta-5/ACC, (3) Used (DBT) Ta-5/ACC and (4) Used (CBZL + DBT) Ta-5/ACC are presented in Figures 6.17 to 6.20, respectively. The binding energies corresponding to oxygen 1s peaks are also presented in the figures.

The O 1s binding energy falls within a relatively narrow range of approximately 2 eV, at a peak of approximately 533 eV, which when deconvoluted, represent single and double bonds with carbon (i.e., C-O and C=O) (Sarac, Tofail *et al.* 2004) as well as O 1s corresponding to O in Ta_2O_5 / TaO_x, which is documented to occur at 530.9 eV (Chun, Ishikawa *et al.* 2003). The deconvoluted O 1s for sample (4) is presented in Figure 6.21.

Comparing the XPS spectra for the used and unused samples indicates that the interaction between the oxygen functional groups on the surface of the activated carbon and adsorbate species (i.e., dibenzothiophene and carbazole) do not result in formation of new bonds, which reconfirms physisorption of the adsorbate species on the activated carbon surface.

FIGURE 6.17 - FITTED XPS SPECTRUM FOR UNUSED VIRGIN ACC CURVE FITTING FOR O 1S 1/2

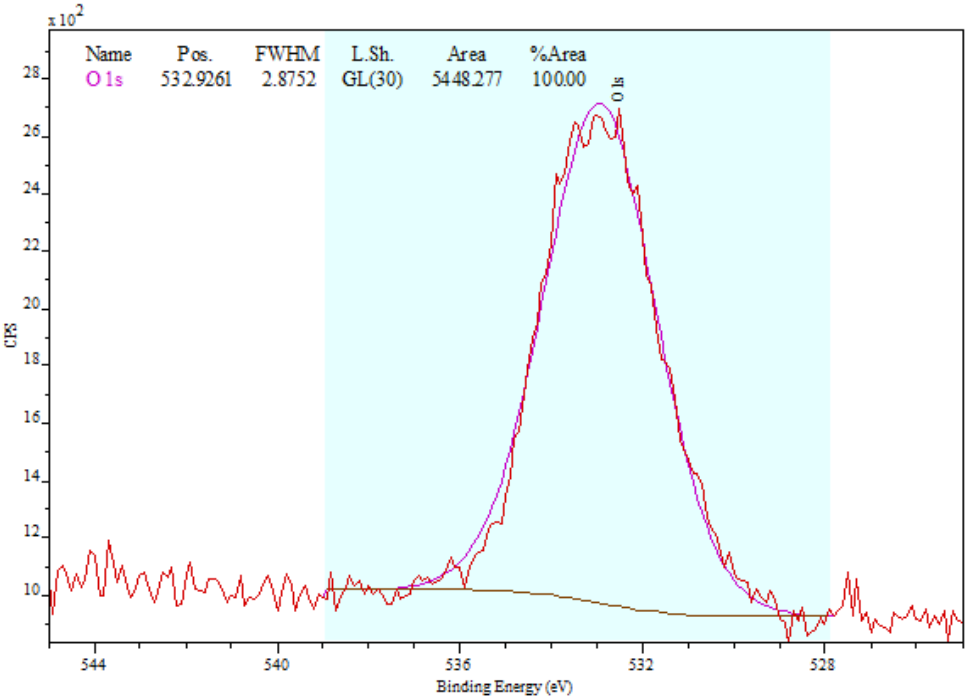

FIGURE 6.18 - FITTED XPS SPECTRUM FOR UNUSED TA-5/ACC CURVE FITTING FOR O 1S 1/2

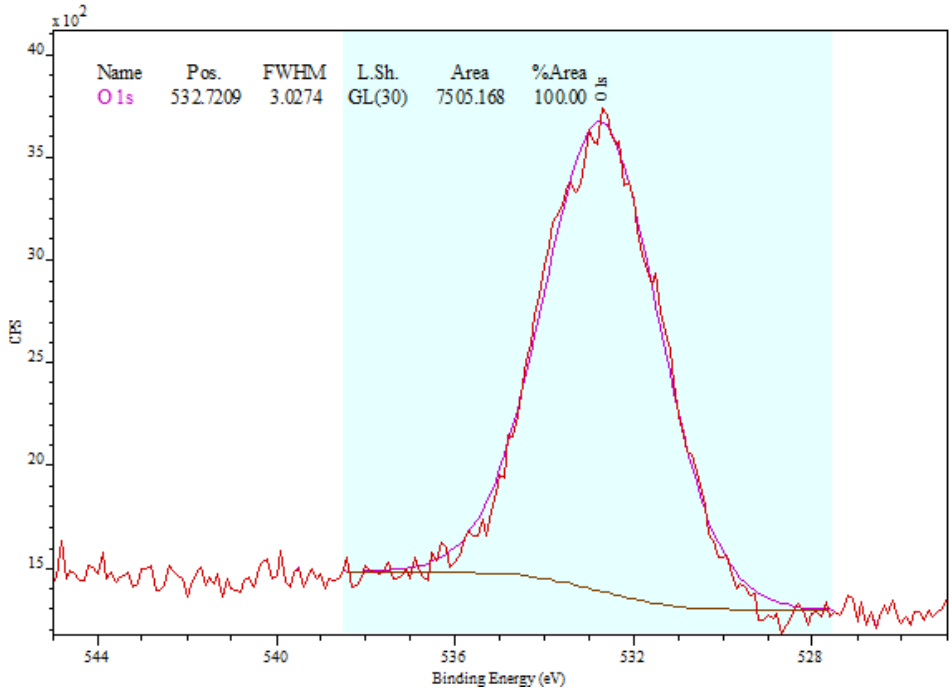

FIGURE 6.19 - FITTED XPS SPECTRUM FOR USED (DBT) TA-5/ACC CURVE FITTING FOR O 1S 1/2

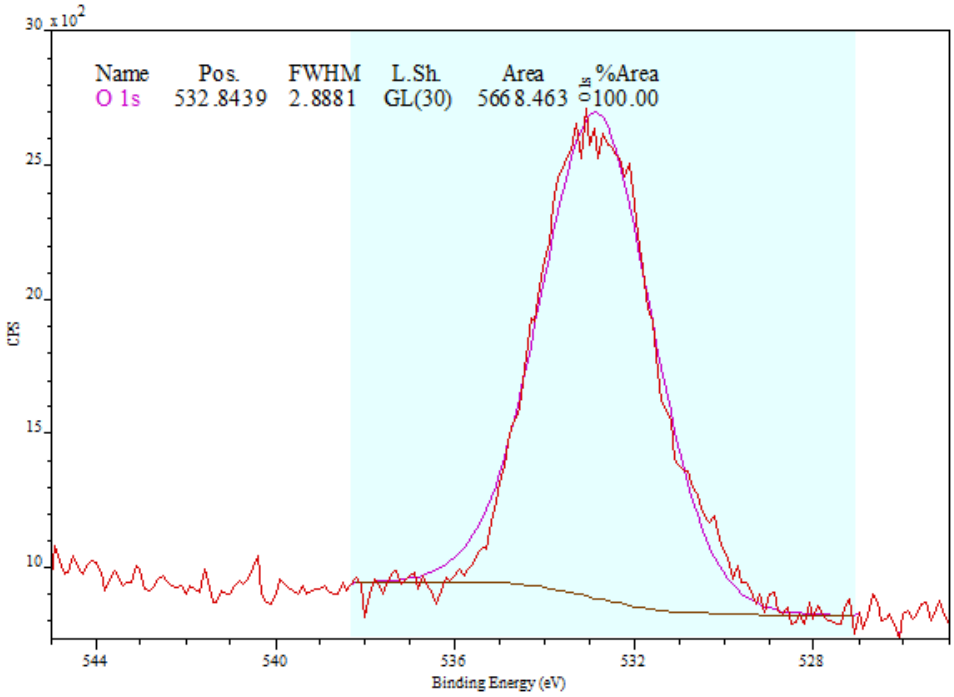

FIGURE 6.20 - FITTED XPS SPECTRUM FOR USED (CBZL+DBT) TA-5/ACC CURVE FITTING FOR O 1S 1/2

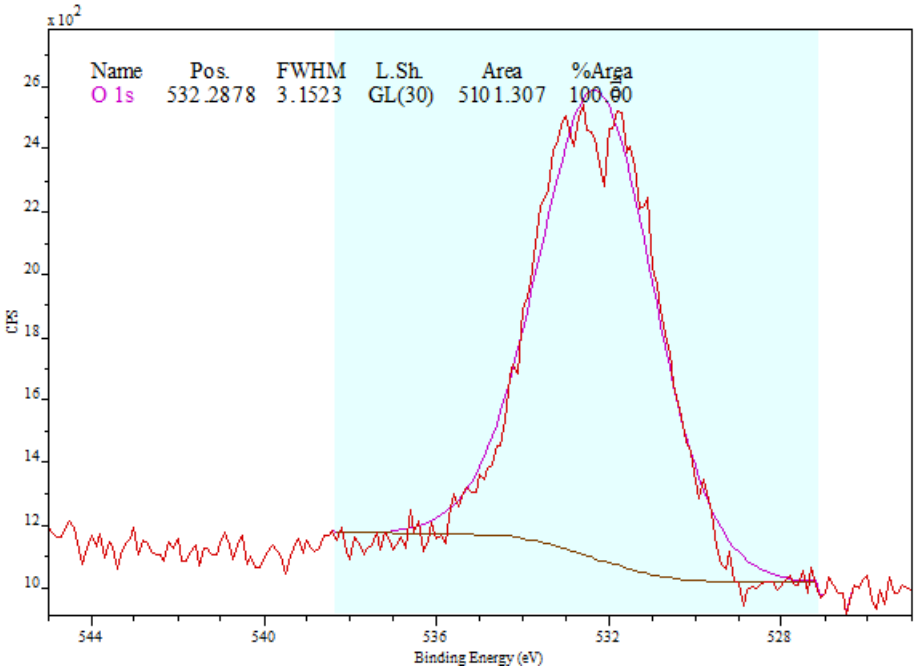

FIGURE 6.21 - DECONVOLUTED XPS SPECTRUM FOR USED (CBZL+DBT) TA-5/ACC CURVE FITTING FOR O 1S 1/2

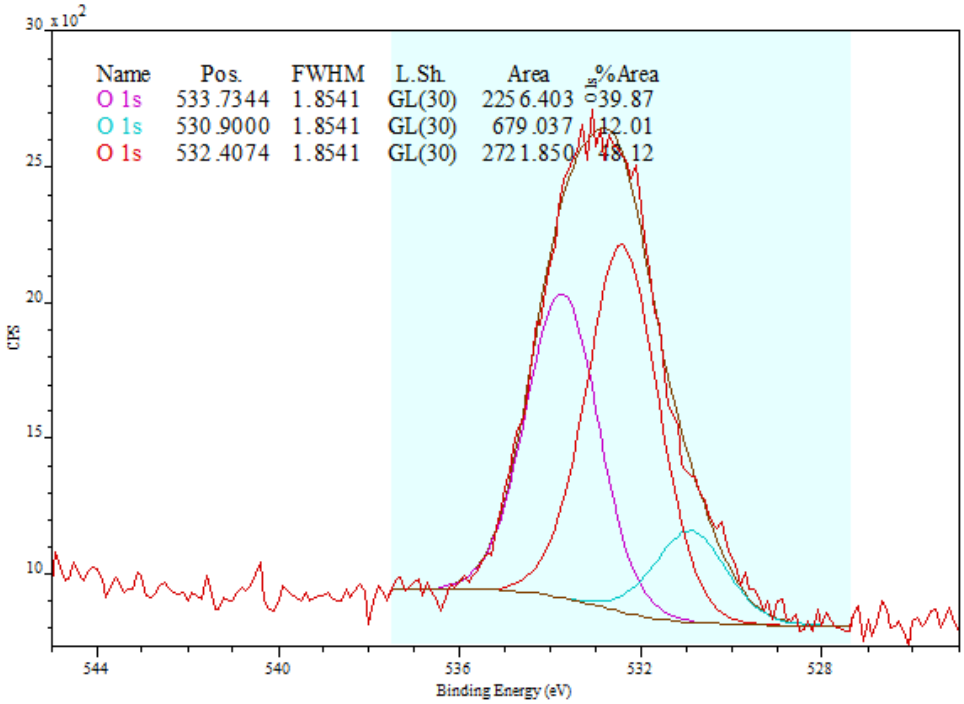

Sulphur – S 2p

The deconvoluted XPS spectra for S 2p ½ and 2p ¾ , for samples: (1) Used (DBT) Ta-5/ACC and (2) Used (CBZL + DBT) Ta-5/ACC are presented in Figures 6.22 and 6.23, respectively.

The S 2p binding at 163.6 eV corresponds to S in CS_2 and at 164.7 eV corresponds to organic sulphur, possibly aromatic. The binding energy of sulphur in dibenzothiophene is at 168.2 eV, which corresponds with S 2p measured for Used (CBZL + DBT) Ta-5/ACC.

FIGURE 6.22 - DECONVOLUTED XPS SPECTRUM FOR USED (DBT) TA-5/ACC CURVE FITTING FOR S 2P

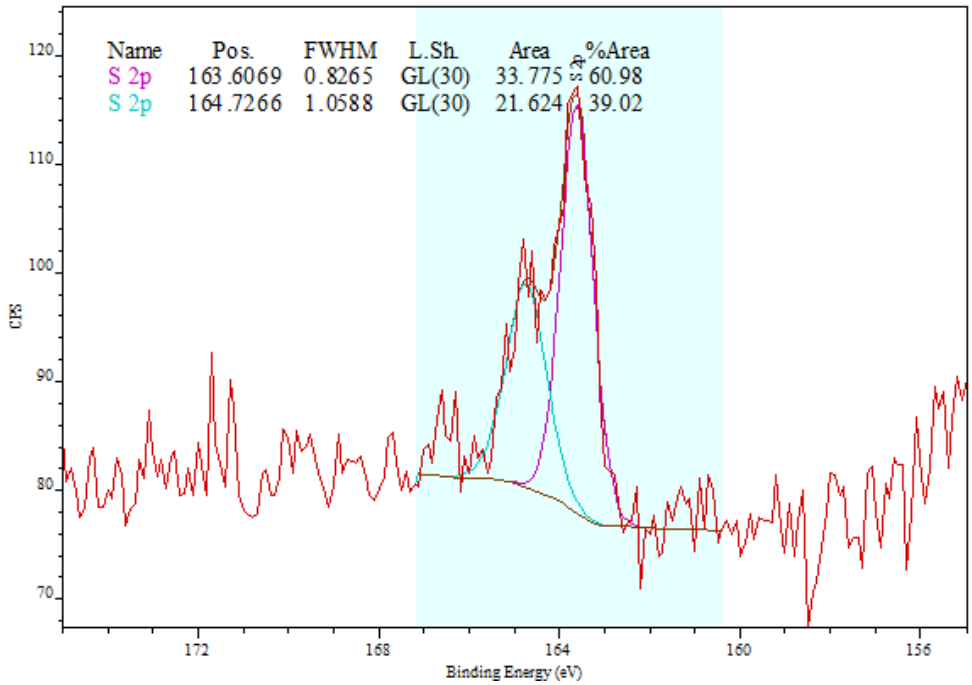

FIGURE 6.23 - DECONVOLUTED XPS SPECTRUM FOR USED (CBZL+DBT) TA-5/ACC CURVE FITTING FOR S 2P

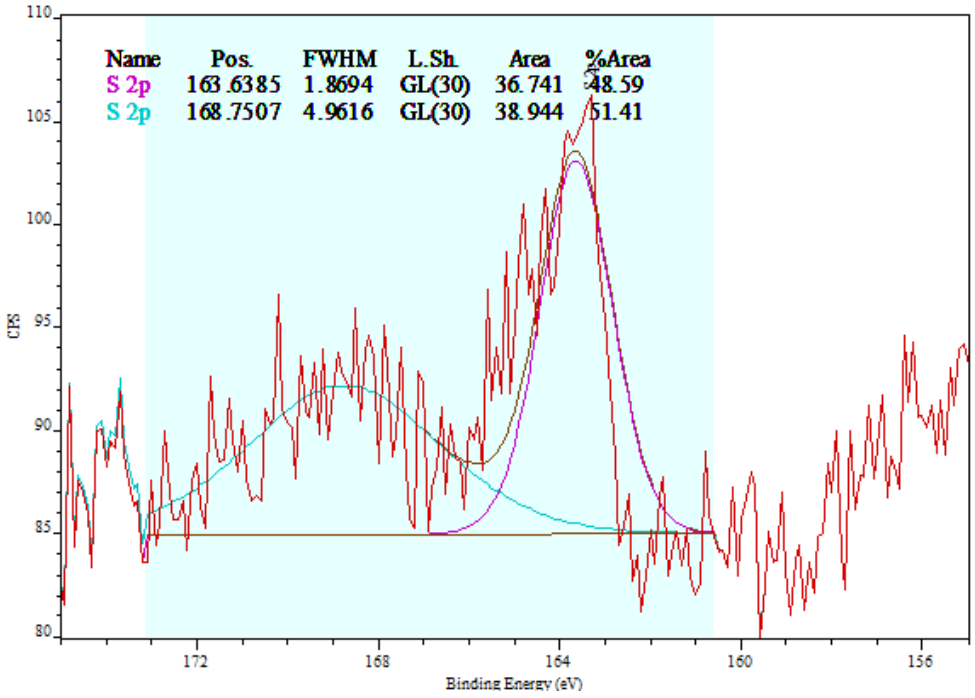

Tantalum – Ta 4f

The deconvoluted XPS spectra for Ta 4f (5/2 and 7/2), for samples: (1) Unused Ta-5/ACC, (2) Used (DBT) Ta-5/ACC and (3) Used (CBZL + DBT) Ta-5/ACC are presented in Figures 6.24 to 6.26, respectively.

The fact that the tantalum peaks are relatively broad suggests that more than one tantalum species are present on the surface of the sorbent (Skadtchenko, Trudeau *et al.* 2003). The peaks corresponding to Ta 4f 5/2 and 4f 7/2 in TaO_x (x = 2, 4) are at approximately 28 eV and 26 eV, respectively (Demiryont, Sites *et al.* 1985). For Ta_2O_5, the peaks corresponding to Ta 4f 5/2 and 4f 7/2 are documented at 28.5 eV and 26.7 eV, respectively (Demiryont, Sites *et al.* 1985).

The peaks corresponding to Ta 4f 7/2 in TaS and TaS_2 are at approximately 26.6 eV and 26.7 eV, respectively (McGuire, Schweitzer *et al.* 1973). The peak at 26.1 eV for the used (DBT) Ta-5/ACC sample is considered to be associated with the Ta-S bond, with S remaining as a part of DBT, and the observed reduction can potentially be due to electronic interactions with the organic sulphur molecule.

Generally, when comparing the peaks corresponding to Ta 4f (both 5/2 and 7/2) in the unused sorbent (Figure 6.24) and used sorbents (6.25 and 6.26), the binding energies have shifted lower by 0.4 eV to 1.6 eV. This can potentially be due to induced negative charge on Ta associated with the sulphur in DBT and/or nitrogen in carbazole (Masud, Alam *et al.* 2011).

The peak corresponding to Ta^0 metal is at 23.7 eV for 4f 5/2 and 21.8 eV for 4f 7/2. (Chun, Ishikawa *et al.* 2003). These peaks did not exist in any of the three tantalum spectra.

FIGURE 6.24 - DECONVOLUTED XPS SPECTRUM FOR UNUSED TA-5/ACC CURVE FITTING FOR TA 4F

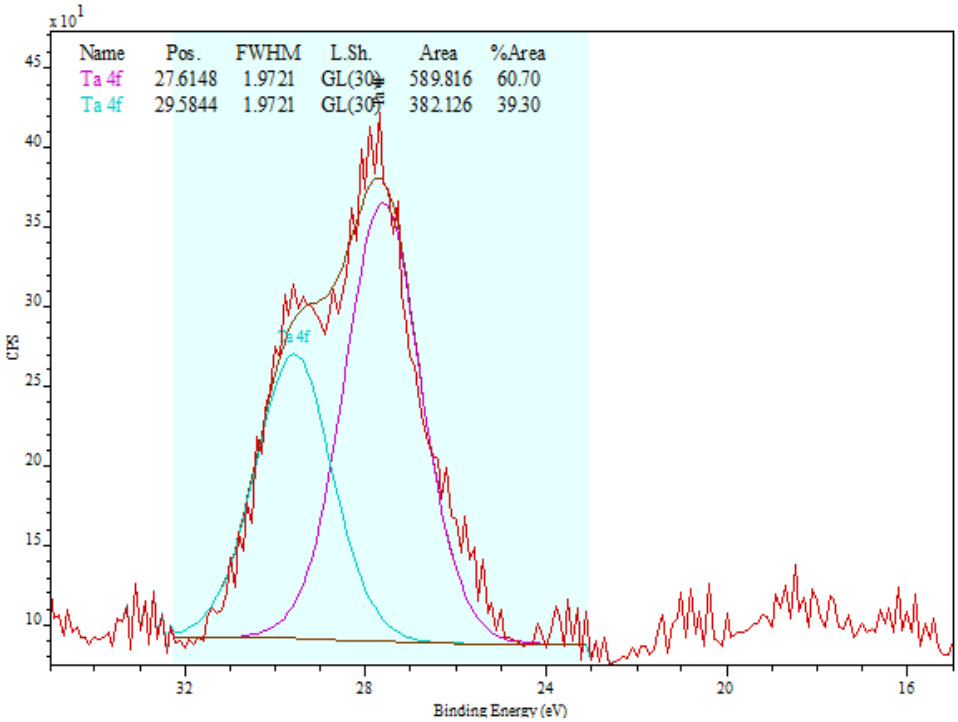

FIGURE 6.25 - DECONVOLUTED XPS SPECTRUM FOR USED (DBT) TA-5/ACC CURVE FITTING FOR TA 4F

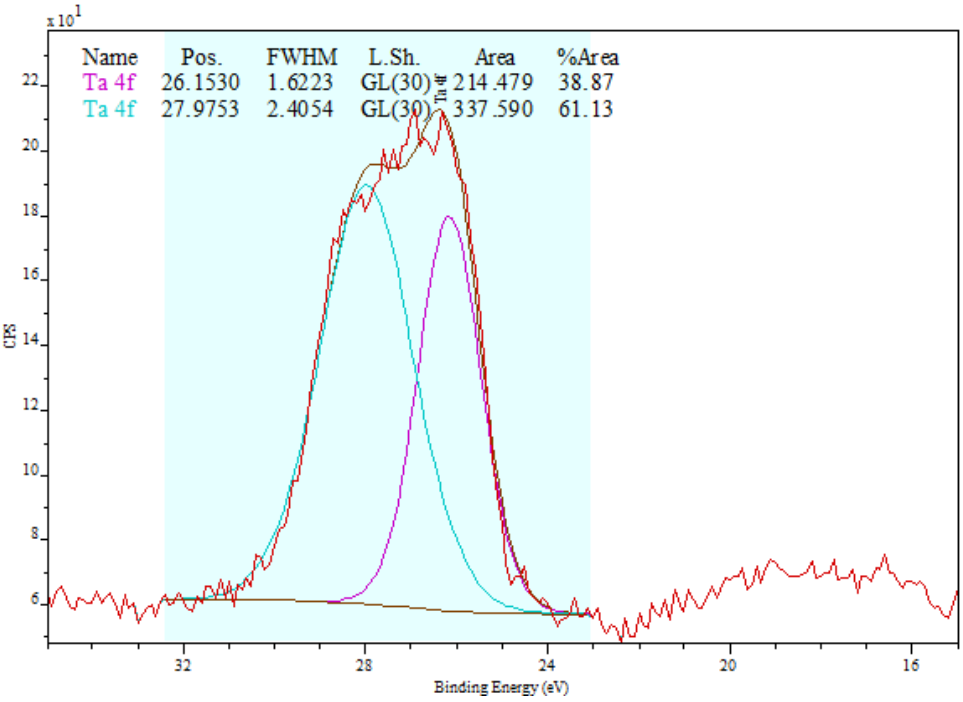

FIGURE 6.26 - DECONVOLUTED XPS SPECTRUM FOR USED (CBZL+DBT) TA-5/ACC CURVE FITTING FOR TA 4F

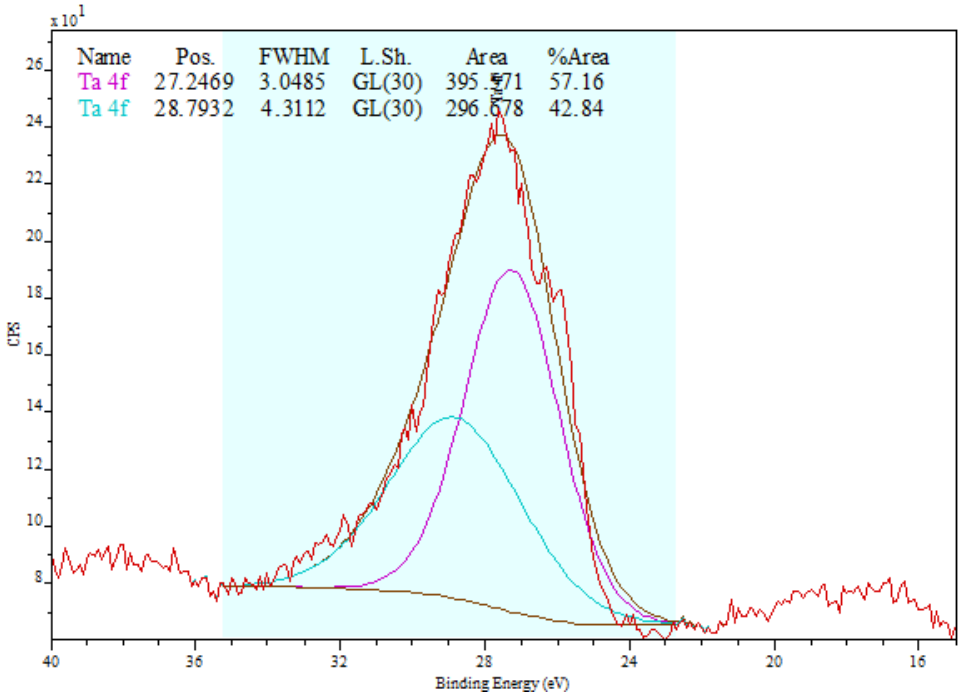

Nitrogen – N 1s

The fitted XPS spectrum for N 1s, for Used (CBZL + DBT) Ta-5/ACC is presented in **FIGURE 6.27**. The binding energy corresponding to the nitrogen 1s peak is also presented in the figure.

The nitrogen in the Ta-N bond has a 1s peak at 398.2 eV (Chuang and Chen 1998). This is the closest binding energy that matches the observed value at 399.7 eV. As mentioned above, it is likely that the nitrogen bond in carbazole remains intact and the electron cloud of carbazole rings resulted in a shift of approximately 1.5 eV. It is therefore concluded that tantalum species on the surface from a bond (chemisorb) the carbazole molecule as a whole, through bonding to its nitrogen.

FIGURE 6.27 -FITTED XPS SPECTRUM FOR USED (CBZL+DBT) TA-5/ACC CURVE FITTING FOR N 1S

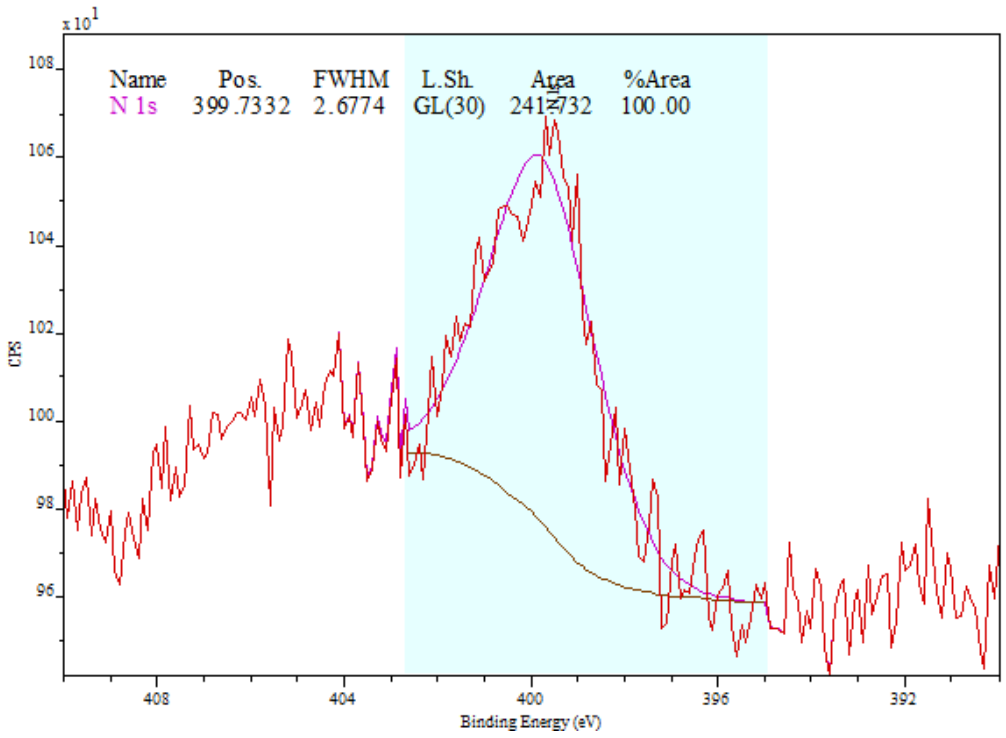

7.0 Flow Reactor Experiment

The purpose of the flow reactor experiments was to gain some insights into the kinetics of sulphur adsorption onto tantalum impregnated activated carbon. This includes determining the kinetic model that best fits the sulphur adsorption, and determining mechanisms and process parameters that influence and/or control the adsorbate uptake rate.

7.1 Background

The performance of a sorbent in sulphur removal is dependent on four main factors:

1. The maximum capacity of the sorbent towards sulphur compounds, (in this case DBT and/or 4,6 DMDBT), which may or may not be fully realized under actual process conditions;
2. The equilibrium behaviour, which influences the efficiency by which the capacity is reached and in many cases controls the maximum capacity of a sorbent;
3. The kinetics behaviour, which pertains to mechanisms such as diffusion and adsorption (e.g., reaction rate in case of chemisorption) that control the overall rate of adsorption; and,
4. The process conditions, such as temperature and contact time between sorbate and sorbent which can influence both kinetics and thermodynamics of the adsorption process and thereby affect the performance of a sorbent.

7.2 Experimental

The equipment and experimental setup and procedure was developed and improved upon, through several experimental iterations and trial and errors. The 'perfected' setup and

experimental procedure used in collecting the presented data / results are summarized below.

For the purposes of the flow reactor experiment, a fixed bed reactor system consisting of the following components was prepared:

- 0.6mm inside diameter, glass reactor, with built-in 0.9µm glass frit for sorbent support and a bulge segment for sorbent bed;
- High Performance Liquid Chromatography (HPLC) pump, equipped with line pressure indicator (up to 6000 psi) and flow range of 0.1 mL/min to 10 mL/min;
- Vertical tubular furnace with built-in dual heating elements;
- Programmable temperature controller system with dual logic input for bed temperature and furnace temperature;
- Stainless steel tubes and fittings, including a four-way connector with needle valves and purge port;
- Gas flow controller system consisting of a flow indicator and control valves;
- Thermocouple wire;
- Sample collection system consisting of a sample holder ring and motorized rotor; and,
- Quartz wool.

A schematic diagram of the flow reactor setup is provided in Figure 7.2, below.

The experimental procedure for the flow reactor experiments are as follows:

- The dried sorbent was weighed and placed into the flow reactor on top of the glass frit.
- Glass wool was inserted into the reactor and placed within the bulge portion of the reactor. The sorbent particles, attached to the microfibers of the glass wool forming a well dispersed sorbent bed. This was to improve contact efficiency between the adsorbate and adsorbent. Figure 7.2 is a photograph of 1000x

magnification of the bed, illustrating the attachment of sorbent particles (black activated carbon particles) to the exterior of the see-through glass microfibers.

FIGURE 7.1 – SORBENT ENTRAPPED IN GLASS MICROFIBER IN THE FLOW REACTOR BED

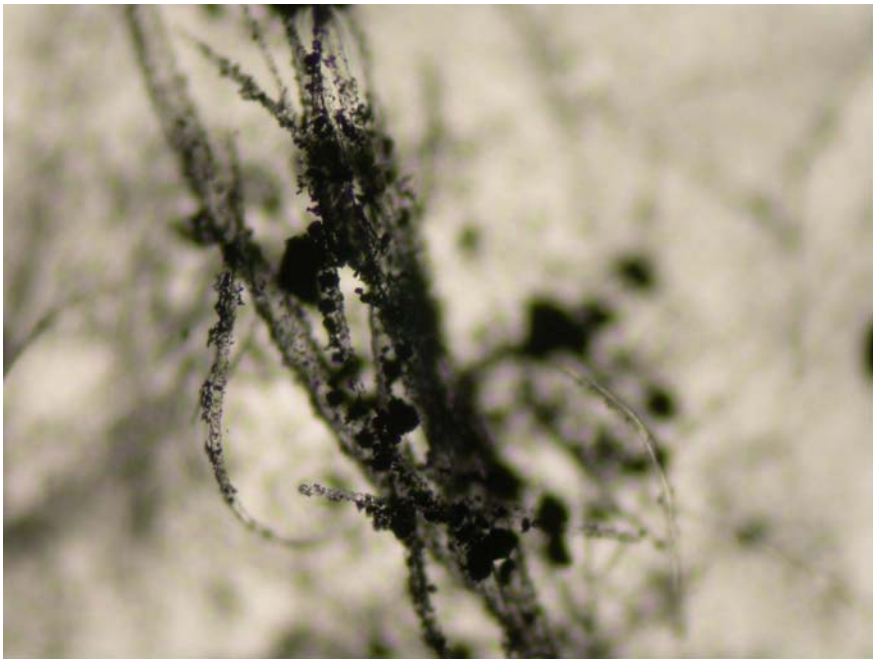

- A second glass wool cluster was compacted and inserted into the reactor, just above the bulge portion to prevent entrainment of sorbent in the reactor outflow.
- The thermocouple wire was twisted around the reactor. The reactor was placed inside the tubular furnace with the bottom connected to the four-way connector and the top connected to the sample connection port, a 1/8" S.S. tube connecting to the sample collection system.
- The reactor was purged and kept under helium (ultra pure 5.0) flow at a flow rate of 80 mL/min.
- The programmable temperature controller was set to raise the temperature from ambient (25 °C) to 110 °C at 10 °C/min. The temperature was held at 110 °C for 60 minutes. It was then raised to 150 °C at the same rate and kept at this

temperature for 120 minutes. This was followed by a temperature ramp up to 400 °C at the same ramp-up rate of 10 °C/min and held at 400 °C for 60 minutes. The reactor was then cooled to the desired temperature (in this case, ambient or 25 °C, 40 °C, 70 °C and 100 °C) while under helium flow.

- Once the temperature of the bed stabilized, the flow of gas was stopped and the flow of DBT in hexadecane (at ~ 900 ppmw-S) was initiated. The respective valves were adjusted accordingly. The HPLC pump was set to operate at the desired flow rate (in this case 0.1 mL/min).
- Sample collection was started approximately 25 minutes after the solution (i.e., DBT in hexadecane) came into contact with the sorbent bed, taken at regular time intervals, in this case, every 12.5 minutes. Samples were collected until the concentration of sulphur (i.e., DBT) in the outflow stabilized.
- The samples were analyzed using Varian 3800, GC/FID, according to the heating program discussed in Section 4.

A photograph illustrating the instruments and setup of the flow reactor apparatus is provided in Figure 7.3, below.

FIGURE 7.2 - A SCHEMATIC DIAGRAM OF THE FLOW REACTOR EXPERIMENT

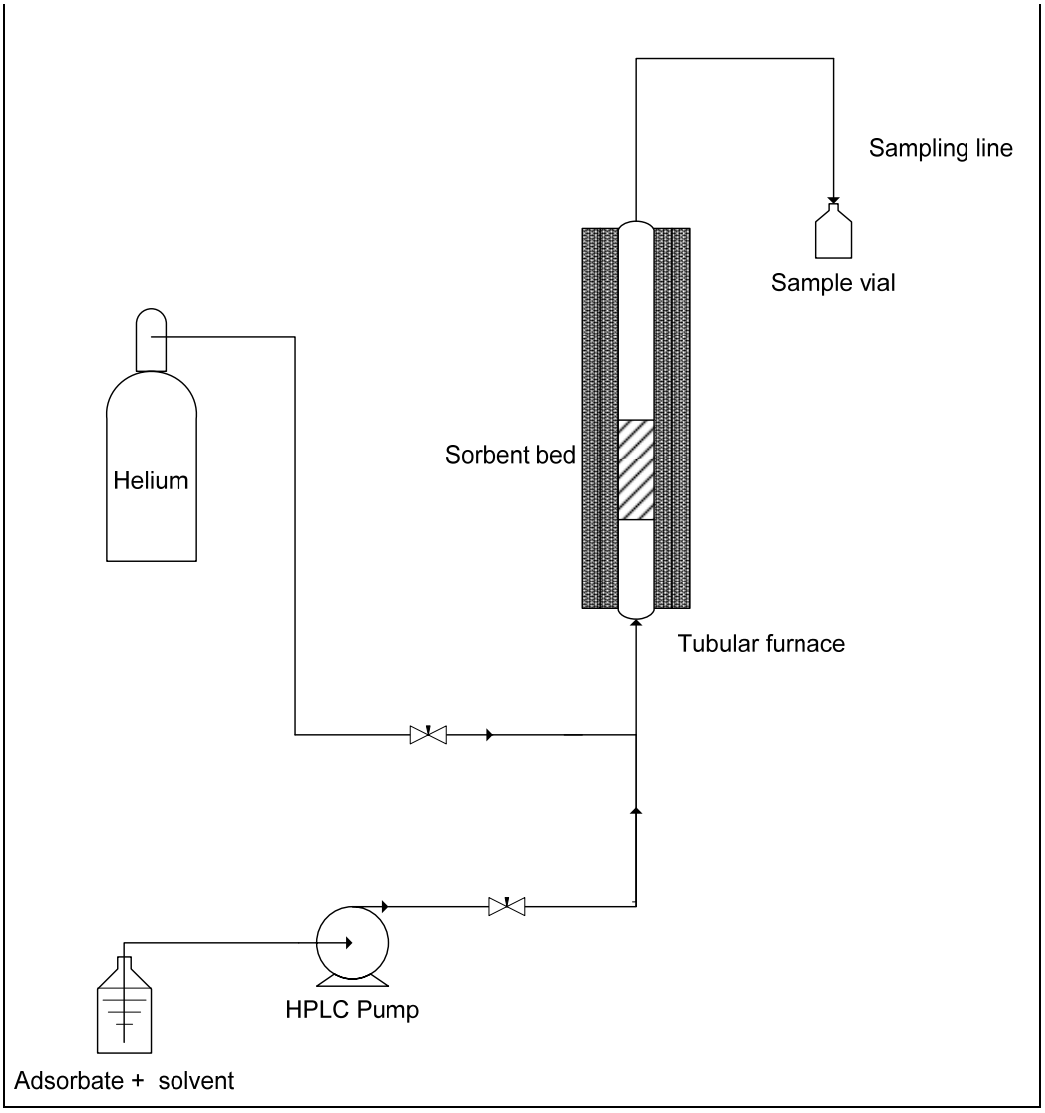

Note:
HPLC pump: High Performance Liquid Chromatography pump
Adsorbate: Dibenzothiophene, Solvent: Hexadecane
Helium: Ultra pure 5.0

FIGURE 7.3 – FLOW REACTOR APPARATUS

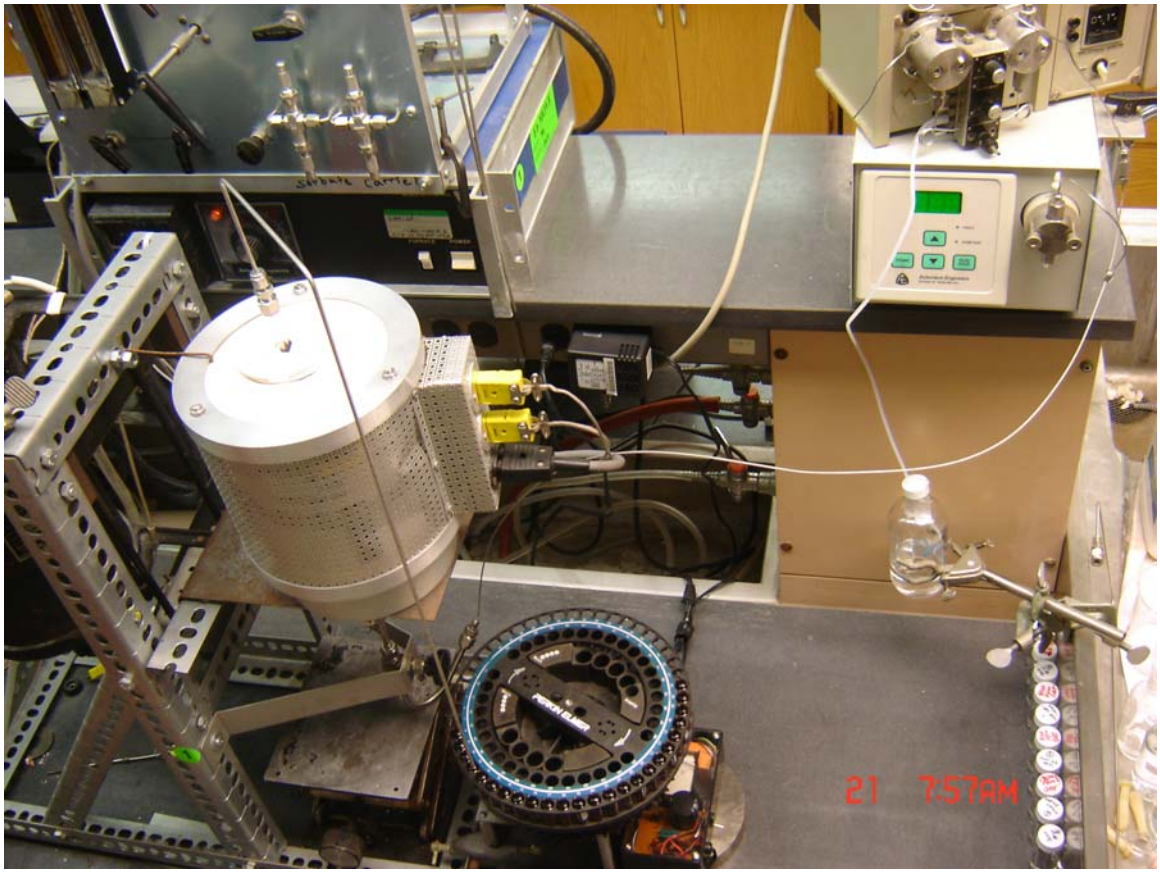

7.3 Adsorption Kinetics

Generally, the kinetics of a reaction that occurs on the surface, such as sulphur adsorption, is significantly different than typical reaction kinetics in the gas or liquid phase. Therefore, the rate equations tend to be quite different (Zhao, Zhang *et al.* 2008). Adsorption onto porous media consists of a transfer from the liquid phase to the solid phase through (1) boundary layer mass transfer from the bulk to interface film, (2) internal diffusion within the sorbent pore and (3) adsorption within the sorbent pore or on its external surface (Poots, McKay *et al.* 1976).

As mentioned in previous chapters, adsorption consists of a collision of a molecule with a surface such that the molecule sticks to the surface. The trapping of a molecule occurs when its translational energy loss due to a collision with a surface is such that the molecule stays on the surface. The sticking of a molecule occurs when upon collision a molecule loses energy and converts into a state where the molecule remains on the surface. It is important to note that trapping and sticking processes are different in that the rate of trapping is the rate at which the energy is transferred between the incoming molecule and the surface whereas the rate of sticking is the rate at which the incoming molecules (after collision) find an active site to adsorb to either through physisorption or chemisorption (Masel, 1996). In other words, in sticking a molecule not only has to lose its energy upon collision with a lattice, it also has to interact with active sites on the surface (e.g., form a bond) such that it is adsorbed by the surface. Sticking is commonly expressed as a probability $S(\theta)$ as a function of surface coverage, θ:

$$S(\theta) = \frac{[number\ of\ molecules\ that\ stick]}{[number\ of\ molecules\ that\ impinge\ on\ surface]} \tag{7-1}$$

If the surface flux of incoming molecules is defined as I_z, it is easy to see that adsorption rate would then depend on the product of the surface flux (molecules/cm^2 sec) and the probability of adsorption $S(\theta)$, as follows:

$$r_a = S(\theta).I_z \tag{7-2}$$

The flux of incoming molecules is dependent on the speed and density of the molecules (Masel, 1996).

In addition to the above basic collision scenarios, a molecule can also have an initial collision, followed by movement along the surface until it finds and sticks to an

adsorption site. This scenario, which is also referred to as precursor-moderated adsorption, is more complex to model but, in principle consists of an initial collision where the molecule loses most of its energy to the lattice and is trapped. The molecule then needs to diffuse over the surface to find a bare site to fill (Masel, 1996).

A molecule can also have an elastic collision with the surface and scatter or come into contact with an already occupied adsorption site (also referred to as active site), and replace the already adsorbed molecule. The latter occurs when the replacement is favoured from an energy perspective, i.e., associated with a decrease in surface free energy (ΔG) (Do, 1998).

In addition to the above, mass transfer or diffusion, i.e., transport of adsorbate to the surface of the sorbent, plays a key role in adsorption kinetics. It should be noted that diffusivity can be on the surface (external mass transfer) or can be within pore volumes (internal mass transfer). The two diffusivities are significantly different in mechanism and how they are impacted by variables such as loading, adsorbate molecular size and temperature (Do, 1998). This topic will be discussed further in subsequent sections.

7.4 Adsorption Kinetic Model

The rate of adsorption or the rate of sulphur (DBT) uptake by the selected sorbents was analyzed using pseudo first-order and pseudo second-order kinetic models. The flow reactor experiment was conducted for virgin and impregnated activated carbon. The experimental data for the flow reactor experiments for virgin activated carbon (ACC – virgin) and 5% tantalum impregnated activated carbon (Ta-5/ACC) was fitted into both kinetics models in order to determine which model would best fit the experimental data. The flow reactor experiment was also completed for the best performing sorbent (i.e., Ta-5/ACC) at reactor temperatures of 25 °C (ambient), 40 °C, 70 °C and 100 °C. Variables such as contact time and loading rates that can potentially impact the rate were kept the same. For all the runs, a binary solution of approximately 900 ppmw-S DBT in hexadecane was used. The flow rate of the binary solution was kept constant at 0.1 mL/min.

Pseudo First-Order Kinetic Model

For the purposes of this study, Lagergren's pseudo first-order rate equation was used, as follows:

$$\frac{dq_t}{dt} = k_{1ad}\,(q_e - q_t) \qquad (7\text{-}3)$$

Where:

q_e = amount of sulphur adsorbed at equilibrium (mmol-S/g-sorbent)
q_t = amount of sulphur adsorbed at time t (mmol-S/g-sorbent)
k_{1ad} = pseudo first-order adsorption rate constant (min^{-1}).

When integrated, at boundary conditions, i.e., t = 0 to t; q_t = 0 to q_t, equation (7-3) will become:

$$\log(q_e - q_t) = \log q_e - \frac{k_{1ad}.t}{2.303} \quad (7\text{-}4)$$

The values of q_e and k_{1ad} can be obtained from the y-intercept and slope of the linear plot for 'log ($q_e - q_t$)' versus 't', as follows:

$q_e = 10^{(\text{Y-intercept})}$

k_{1ad} = 2.303 x Slope

The initial rate of adsorption can be obtained by multiplying the rate constant (k_{1ad}) by the calculated equilibrium adsorption capacity (q_e). The initial rate of adsorption is referred to as 'h_1' (mmol/g/min) in this document (1 for first-order) (Wen, Han *et al.* 2010).

Pseudo Second-Order Kinetic Model

For the purposes of this study, the experimental data were also fitted to a pseudo second-order rate equation, as follows:

$$\frac{dq_t}{dt} = k_{2ad}(qe - qt)^2 \quad (7\text{-}5)$$

Where:

k_{2ad} = pseudo second-order adsorption rate constant (mmol/g/min).

When integrated, the equation (7-5) will become:

$$\frac{t}{q_t} = \frac{1}{k_{2ad}.q_e^{\,2}} + \frac{t}{q_e} \quad (7\text{-}6)$$

The values of q_e and k_{2ad} can be obtained from the y-intercept and slope of the linear plot for '(t/q_t)' versus 't', as follows:

q_e = 1 / Slope

k_{2ad} = (Slope)^2 / y-intercept

The initial rate of adsorption can be obtained by multiplying the rate constant (K_{2ad}) by the square of the calculated equilibrium adsorption capacity (q_e). The initial rate of adsorption is referred to as 'h_2' (mmol/g/min) in this document (2 for first-order) (Wen, Han *et al.* 2010).

7.5 Tantalum Impregnation and Adsorption Kinetics

The impact of tantalum impregnation on adsorption kinetics was studied. The flow reactor analysis was completed for virgin ACC and Ta-5/ACC. In total, five runs were completed, two for ACC-virgin and three for Ta-5/ACC. The third run for Ta-5/ACC was completed for regenerated sorbent. The results are summarized in Table 7.1, and details are provided in Appendix C.

For all the runs, the experimental data were fit to both pseudo first-order and pseudo second-order kinetic models (as described above). The linear regressions indicate that for both virgin and impregnated activated carbon, the data best fit the pseudo second-order kinetic model, with R^2 values ranging from 0.975 to 0.997 (see Table 7.1 and Appendix C).

On average the tantalum impregnated ACC exhibited a higher initial rate of adsorption. This is expected as the adsorption on tantalum sites is shown to be of chemisorption type (forming Ta-S bond as per XPS analysis). The adsorption onto tantalum sites tends to be more exothermic than adsorption (mainly physisorption) on activated carbon (as per the microcalorimetry analysis presented in Section 5 of this report). Therefore, more

thermodynamically favoured chemisorption (lowering of surface free energy at a faster rate) is expected to occur more rapidly than physisorption.

The equilibrium adsorption capacities of the sorbents were calculated based on the pseudo second-order kinetic equation (7-6). The observed better fit for pseudo second order is indicative of the fact that the sulphur adsorption is much dependent on the concentration of available adsorptive sites on the surface of the activated carbon. On average, the tantalum impregnation showed an approximately 137% increase in adsorption capacity compared to the activated carbon. It should be noted that the adsorption capacities calculated from the flow reactor experimental data are higher than those calculated from isotherm experiments for the same sorbents. In addition to the difference in estimation/calculation methods, it is believed that the in-situ activation of the sorbent, which prevents exposure to air and moisture, improves the adsorption capacity of the sorbents. This is further confirmed by the results of the virgin activated carbon presented in Table 7.1. The sorbent for the first ACC-virgin run was dried and activated in a separate reactor and was then weighed and transferred to the flow reactor. However, the sorbent for the second run was dried and activated in-situ under helium (no exposure to air / moisture prior to exposure to the binary solution). This has contributed to the approximately 25% higher adsorption capacity observed for run II versus run I.

The sorbents for all other flow reactor runs in this study were activated in-situ, in accordance to the procedure described in sub-section 7.2, above.

Another interesting observation is the regenerability of the tantalum impregnated activated carbon. As mentioned above, the third run for the Ta-5/ACC was with regenerated sorbent. For sorbent regeneration, the same procedure as before (discussion in Section 6) was applied, consisting of a toluene wash, sonication and thermal treatment. The thermal treatment of the sorbent however, was completed in-situ. The results indicate almost 100% regeneration.

In their 2009 research work, Zhou *et al.* indicated that the adsorption capacity of the activated carbon was able to be fully recovered through solvent regeneration and thermal treatment (Zhou, *et al.* 2009). As mentioned above, adsorption on activated carbon is mainly physisorption, which is considered to be fully reversible, thus easily regenerated. Nevertheless, the sulphur bond on Ta-5/ACC is considered chemisorption and thus more difficult to regenerate. The results of this study indicate that the tantalum impregnated activated carbon can almost be fully regenerated. From an industrial application point of view, this adds more value to an already superior sorbent for adsorptive desulphurization.

TABLE 7.1 - KINETICS RESULTS – FLOW REACTOR EXPERIMENTS FOR VIRGIN ACC AND TA-5/ACC AT REACTOR TEMPERATURE OF 25 °C

Sorbent	Run ID	Volumetric Flow Rate (mL/min)	Adsorption Kinetics	Linear Regression (R^2)**	Initial Rate of Adsorption (mmol/g/min)	Adsorption Capacity (mmol-S/g-sorbent)
ACC - Virgin	Run I	0.1	Pseudo second order	0.9746	0.0155	0.66
	Run II	0.1	Pseudo second order	0.9784	0.0091	0.83
Ta-5/ACC	Run I	0.1	Pseudo second order	0.9898	0.0156	1.79
	Run II	0.1	Pseudo second order	0.9763	0.0158	1.73
	Run III*	1.1	Pseudo second order	0.9973	0.0161	1.78

Note:

All runs were completed using approximately 900 ppmw-S (~21.3 mmol-S/L) DBT in hexadecane (binary solution).

All runs consisted of in-situ activated (i.e., no exposure to air) for approximately 4 hours prior to each run.

* The third flow reactor run for 25 °C reactor temperature was completed on regenerated sorbent.

** The R2 values pertain to the linearized pseudo second order equation (t/q_t vs. t).

7.6 Adsorption Temperature and Adsorption Kinetics

The impact of adsorption temperature on the kinetics of adsorption was studied. For this study, Ta-5/ACC was used. The flow reactor experiment was completed at reactor temperatures (i.e., sorbent bed temperature) of 25 °C (ambient), 40 °C, 70 °C and 100 °C. Variables such as contact time and loading rates that can potentially impact the rate were kept the same. The binary solution (approximately 900 ppmw-S DBT in hexadecane) was pumped through the reactor / sorbent bed at a constant flow rate of 0.1 mL/min. The results are summarized in Table 7.2, below. Details of calculations including graphs are provided in Appendix C.

The experimental data were fit to both pseudo first-order and pseudo second-order kinetics to determine which one better fits the experimental data. Results for both fittings are provided in Appendix C. It was determined based on linear regression that for all the temperatures, the experimental data better fits the pseudo second-order kinetic model, with R^2 values ranging from 0.976 to 0.997 (see Table 7.2). The two key finding of the temperature varying flow reactor experiments are:

1. On average the initial adsorption rate did not change significantly with temperature, with the exception of the rate at 70 °C, which was lower than the rest, all others rates were on average similar.

2. The sulphur adsorption capacity decreases with increase in reactor temperature. In fact the adsorption capacity drops approximately 60% when the temperature of the sorbent bed was increased from 40 °C to 70 °C. The highest adsorption capacity was obtained for ambient (25 °C) reactor temperature.

In order to explore these results further, we will need to look at the expected impact of temperature on diffusivity and adsorptive interaction.

Surface diffusion is defined as the thermal motion of adsorbed molecules on a surface (Do, 1998). The mobility of adsorbed molecules at the surface is a function of distance between adjacent sites, and the average time that a site is occupied between jumps. One can define 'E_s' as the activation energy needed for each jump, and write the following equation for surface diffusivity:

$$D_s = D_{s0} \exp\left[-\frac{E_s}{RT}\right] \tag{7-7}$$

Where,

D_s = surface diffusivity

D_{s0} = pre-exponential factor

R = Gas constant

T = Temperature (K)

Surface flux can be defined as mass transfer along the surface induced by a surface concentration gradient, per unit length or area. Therefore if 'J_s' represents surface flux, we can express the following proportionality:

$$Js \ \alpha \ D_s K \left[\frac{dC}{dz} \right] \tag{7-8}$$

Where,

α = proportionality

K = equilibrium constant [$K = K_o \exp(-\Delta H / RT)$]

dC/dz = concentration gradient

From the above equation (7-7) and proportionality (7-8), as well as the expression for K, one can derive the following proportionality for surface flux:

$$Js \ \alpha \ D_s Ko \exp\left[-\frac{Es + \Delta H}{RT} \right] \frac{dC}{dz} \tag{7-9}$$

Now a few key points:

- For thermodynamically favourable adsorption, the associated surface free energy should decrease ($\Delta G<0$); and,
- Adsorption is associated with a decrease in entropy ($\Delta S<0$), as the molecules adsorbing into the surface of the sorbent gain orderliness;

Therefore, in the expression $\Delta G = \Delta H - T\Delta S$, ΔH would be negative. It should be noted that the exothermic aspect of sulphur adsorption was shown in previous sections of this report, based on the heat of adsorption data measured through microcalorimetry experiments.

Heat of adsorption is typically greater than the activation energy for jumping between the sites on the surface (i.e., E_s). Therefore, in the proportionality (7-9), the term $-(Es + \Delta H)$ will be positive. This means that for a given concentration gradient, although the surface diffusivity (equation 7-7) increases with an increase in temperature, the surface flux decreases with an increase in temperature (Do, 1998).

For pore volume diffusion, the diffusion flux can be expressed as follows:

$$J_p = -D_{eff}\left[\frac{dC}{dz}\right] \tag{7-10}$$

Where,

J_p = pore diffusion flux for porous media

D_{eff} = effective diffusivity based on total cross-sectional area

dC/dz = concentration gradient

We also know that the pore diffusion flux is inversely proportional to temperature (based on Knudson pore diffusion):

$$J_p \ \alpha \ \frac{1}{\sqrt{2\pi MRT}} \tag{7-11}$$

Where,

M = Molecular weight

R = Gas constant

T = Temperature (K)

Pore diffusivity can increase or decrease with an increase in temperature, however, in both cases its rate of change is not as fast as surface diffusion. In other words, the diffusivity at the surface dominates over pore diffusivity (Do, 1998).

Now the two main findings mentioned above can be explained as follows:

- The net rate of adsorption is the difference between the rate of adsorption and rate of desorption. The rate of adsorption can depend on mass transfer (diffusion) and adsorptive interactions between the adsorbate and sorbent (physisorption or chemisorption). It was established above that the increase in temperature increases surface diffusivity but impedes diffusion flux. Therefore, one may postulate that the impediment of the diffusion flux will result in reduction in adsorbed quantity, and hence adsorption capacity, while the impact on adsorptive interactions (exothermic) is offset by improved diffusivity. Hence there are minor changes in the rate of adsorption due to changes in reactor temperature.

TABLE 7.2 - KINETICS RESULTS – FLOW REACTOR EXPERIMENTS FOR TA-5/ACC AT VARIOUS REACTOR TEMPERATURES

Reactor Temperature	Run ID	Volumetric Flow Rate (mL/min)	Best Fit Kinetic	Linear Regression (R2)**	Initial Rate of Adsorption (g/mmol/min)	Adsorption Capacity (mmol-S/g-sorbent)	
						per run	Mean
25 °C	Run I	0.1	Pseudo second order	0.9898	0.0156	1.79	1.77
	Run II	0.1	Pseudo second order	0.9763	0.0158	1.73	
	Run III*	0.1	Pseudo second order	0.9973	0.0161	1.78	
40 °C	Run I	0.1	Pseudo second order	0.9951	0.0155	1.56	1.58
	Run II	0.1	Pseudo second order	0.9951	0.0161	1.61	
70 °C	Run I	0.1	Pseudo second order	0.9870	0.0115	0.96	0.98
	Run II	0.1	Pseudo second order	0.9982	0.0091	1.00	
100 °C	Run I	0.1	Pseudo second order	0.9922	0.0189	0.86	0.90
	Run II	0.1	Pseudo second order	0.9973	0.0121	0.95	

Note:

All runs were completed using approximately 900 ppmw-S (~21.3 mmol-S/L) DBT in hexadecane (binary solution).

All runs consisted of in-situ activated (i.e., no exposure to air) for approximately 4 hours prior to each run.

* The third flow reactor run for 25 °C reactor temperature was completed on regenerated sorbent.

** The R^2 values pertain to the linearized pseudo second order equation (t/q_t vs. t).

7.7 Intra-particle Diffusion and Adsorption

As mentioned above, the overall adsorption process for sulphur compounds onto the sorbent can be influenced by several mechanisms, including surface and pore diffusion, as well as adsorptive interaction with the surface (i.e., physisorption or chemisorption). In order to determine the impact of intra-particle (pore) diffusion on adsorption, the Weber-Morris Intra-particle model (1964) was utilized, according to the following equation:

$$q_t = K_{id} t^{0.5} + C \qquad (7\text{-}12)$$

Where,

K_{id} = rate constant for intra-particle transport (mmol / g / $min^{1/2}$)

t = Time (min)

C = y-intercept (constant)

q_t = amount adsorbed at time, t (mmol/g)

If the Weber-Morris plot of q_t versus $t^{0.5}$ generates a linear plot, which passes through the origin, it is a good indication that the intra-particle diffusion is the key controlling mechanism for the adsorption. This analysis was completed for the tantalum impregnated activated carbon and for all the reactor temperatures that were assessed in this study. The results are summarized in Table 7.3, below. All data and calculation spreadsheets are provided in Appendix C.

The plots of q_t versus $t^{0.5}$ were linear with reasonable R^2, however, none of the plots passed through the origin. This indicates that intra-particle diffusion exists, but it is not likely that the overall adsorption is controlled nor noticeably impacted by it.

As the temperature of the reactor increases, the y-intercept value 'C' increases, indicating that the plot is moving away from the origin, and thus intra-particle diffusion is becoming less of a controlling mechanism. This can further point to the fact that the boundary layer (i.e., surface diffusion) and, potentially, surface adsorption are the dominating mechanisms in the sulphur adsorption onto Ta-5/ACC (Sutherland, 2010).

For the highest reactor temperature tested (100 °C), the plot consists of two linear zones, with the first zone representing external surface adsorption derived by surface diffusion and surface adsorption (see Appendix C). In the second zone, adsorption reaches the later stage and the intra-particle diffusion seems to have more influence on the adsorption (Wen, Han *et al.* 2010).

TABLE 7.3- WEBER-MORRIS MODEL RESULTS FOR INTRA-PARTICLE DIFFUSION

Sorbent	Flow Reactor Temperature (°C)	K_{id} * (mmol/g $min^{1/2}$)	C ** (mmol/g)
Ta-5/ACC	25	0.069	0.101
	40	0.057	0.196
	70	0.040	0.073
	100	0.015	0.489

Note:

* The K_{id} (rate constant of intra-particle transport) values are averages of two runs for each reactor temperature.

** C is the y-intercept for the linearized plot, based on Weber-Morris model: $q_t = K_{id} (t^{1/2}) + C$

q_t is the adsorption at time t in mmol of sulphur per gram of sorbent.

8.0 Conclusions and Recommendations

8.1 Conclusions

Changes in regulations concerning sulphur content of fuel in the developed nations including Canada and United States have resulted in extensive research to improve existing technologies or to come up with new processes to further reduce the total sulphur content in fuel such as gasoline, diesel and jet fuel. From the production of crude oil to the end use of refinery products, sulphur has always been a source of pollution, occurring initially in the form of hydrogen sulphide (H_2S) or sour gas and other organically bonded sulphur compounds naturally occurring in crude oil. Therefore, in order to curb its unfavourable direct and indirect environmental impacts as well as the adverse effects on human health, governments have taken the initiative to bring about regulations to limit sulphur emissions from the combustion of fossil fuels.

Regulatory agencies have and continue to implement stringent guidelines and regulations on sulphur content in fuels (especially transportations fuels including diesel, gasoline and jet fuel). This encompasses not only fuel used for on-road vehicles (requiring maximum of 10 ppmw-Sulphur), but also diesel used in non-road vehicles, locomotives and marine engines (requiring 15 ppmw-Sulphur). Furthermore, use of existing transportation fuels for fuel cell applications is considered a convenient and suitable future option. However, this application would require sulphur content in fuel less than 1 ppmw-S (ideally less than 0.2 ppmw-S). As a result extensive research work has gone into improving the existing technologies or to come up with new processes/technologies to further reduce the sulphur content in fuel.

As mentioned above, the overall objective of this research was to identify, develop and characterize, based on underlying scientific principles, sorbents that are effective in removal of refractory sulphur compounds from fuel through the process of selective adsorption. Many physical attributes and chemical characteristics of both sorbent and

sorbate determine their interaction in an adsorption process. Research work completed here illustrates that:

- Activated carbon is a suitable sorbent for sulphur removal via adsorption. It is relatively inexpensive and abundant, has very large surface area per unit mass, has functional groups on the surface that can interact (physisorption) with target sulphur and nitrogen compounds, is easy to manufacture, and if not reusable after numerous regenerations, it can be combusted under controlled conditions to generate energy. The physical and chemical attributes of activated carbon can be modified to better fit a particular purpose. Activated carbons can be obtained from waste streams such as petroleum coke (petcoke), which is generated as a result of coking process at petroleum processing facilities. The use of a waste stream for a useful application at petroleum refineries (e.g., adsorptive desulphurization) makes it an attractive option for the industry not only in terms of cost, but also in terms of accessibility.

- The best performing sorbent, Ta-5/ACC, which was developed as a part of this research work, had maximum adsorption capacities of approximately 1.77 and 0.76 mmol-S/g-sorbent for DBT and 4,6 DMDBT, respectively. These capacities are significantly higher than those published to date. The sorbent also has good adsorption capacities for organo-nitrogen compounds (i.e., quinoline and carbazole) and a low selectivity towards aromatics, which is desired in adsorptive desulphurization. The surface morphology of the activated carbon, the oxygen functional groups on the surface of the activated carbon, as well as strong (chemisorption) interaction between tantalum's partly vacant and far reaching 'd' orbital and lone pair electrons on sulphur and nitrogen are considered to be the main contributing factors to the observed enhancement. The benefit of Ta impregnation is three fold: (1) increase of overall sulphur adsorption capacity; (2) the impact on the adsorption sites of ACC are likely minor as a result of the Ta

impregnation; and (3) formation of more stable adsorption bond with organo-sulphur compounds, evident from measured higher adsorption energy.

- It was uniquely established in this study that the adsorption isotherms of the impregnated activated carbons best fit Sips isotherm equation, which is a combination of the Langmuir and Freundlich equations. This finding fits well with our initial hypothesis regarding the introduction of new adsorptive sites as a result of tantalum impregnation and that the sites did not fit well with Langmuir's monolayer and uniform adsorption mechanism.

- While Ta-5/ACC has more active sites than Ta-2/ACC, it is believed that the reduction in adsorption capacity of Ta-10/ACC is mainly due to pore blockage and reduction of surface area, as well as, blockage of active sites on the surface of the activated carbon. The Ta-5/ACC sorbent has shown remarkable selectivity towards organo-sulphur (i.e. DBT) and organo-nitrogen (i.e. quinoline) compounds and has a regenerability rate of 94% for batch process and approximately 100% (i.e., fully restored adsorption capacity) when regenerated and used for adsorption in-situ.

- The TEM results illustrate that heat treatment of the activated carbon induces regularity in the pore structure. Thermal treatment at 400 °C induces a structural uniformity in the activated carbon support and improves its crystalline structure in terms of pore accessibility. In addition, the thermal treatment of sorbent at 400 °C results in better dispersion of various tantalum species and a more uniform array of lattice structure.

- XPS analysis indicates formation of Ta-S and Ta-N bonds thus supporting the initial hypothesis of chemisorption for the tantalum sites. In other words, DBT, 4,6 DMDBT, quinoline and carbazole maintain their molecular structure but simply adsorb to the active sites.

- The HRTEM-EDX analysis of zoomed-in segments of the sorbent indicate that the distribution of tantalum species on the surface of the activated carbon is relatively inhomogeneous, with some areas showing well dispersed tantalum species while other areas showing large clusters of tantalum species, pointing to a relatively low dispersion.

- The FTIR results indicate that the characteristic vibration bands describing oxygen functional groups (present on the surface of the activated carbon) for virgin and impregnated (tantalum) activated carbon, thus indicating little or no impact on the active functional groups of ACC as a result of tantalum impregnation. Additionally, results indicate that the thermal treatment of the activated carbon up to 400 °C does not impact the surface functional groups of the activated carbon.

The purpose of the flow reactor experiments was to gain some insights into the kinetics of sulphur adsorption onto tantalum impregnated activated carbon. This includes determining the kinetic model that best fits the sulphur adsorption, and determining mechanisms and process parameters that influence and/or control the adsorbate update rate. The key finding of the flow reactor experiments are as follows:

- The flow reactor data fitted well with the pseudo second order kinetic model.

- On average, as expected, the tantalum impregnated ACC exhibited a higher initial rate of adsorption in comparison to virgin ACC. This is expected as the adsorption on tantalum sites is shown to be of chemisorption type. The adsorption onto tantalum sites tends to be more exothermic than adsorption (mainly physisorption) on activated carbon. Therefore, more thermodynamically favoured chemisorption is expected to occur more rapidly than physisorption. On

average, the tantalum impregnation showed approximately 137% increase in adsorption capacity over the activated carbon.

- The in-situ thermal treatment of the spent tantalum impregnated activated carbon resulted in almost 100% regeneration.

- The data indicated that on average the initial adsorption rate did not change significantly with temperature. With the exception of the rate at 70 °C which was lower than the rest, all others rates were on average similar. The data also indicate that the sulphur adsorption capacity decreases with an increase in reactor temperature. In fact the adsorption capacity drops approximately 60% when the temperature of the sorbent bed increases from 40 °C to 70 °C. The highest adsorption capacity was obtained for ambient (25 °C) reactor temperature. The net rate of adsorption is the difference between the rate of adsorption and rate of desorption. Rate of adsorption depends on mass transfer (diffusion) and adsorptive interactions between the adsorbate and sorbent (physisorption or chemisorption). We established that the increase in temperature increases surface diffusivity but impedes diffusion flux. Therefore, one may postulate that the impediment of the diffusion flux will result in reduction in adsorbed quantity, hence adsorption capacity, while impact on adsorptive interactions (exothermic) is offset by improved diffusivity, hence minor change in rate of adsorption due to change in reactor temperature.

- Based on Weber-Morris intra-particle diffusion model, intra-particle diffusion exists in the adsorption of DBT on tantalum impregnated activated carbon, however, it is not likely that the overall adsorption is controlled or noticeably impacted by it. Also, as the temperature of the reactor increases the y-intercept value 'C' increases, indicating that the plot is moving away from the origin, and thus intra-particle diffusion is becoming less of a controlling mechanism. This can further point to the fact that the boundary layer (i.e., surface diffusion) and

potentially surface adsorption are play a key role in the sulphur adsorption onto Ta-5/ACC.

8.2 Recommendations

One of the key factors in determining potential commercial usage of an effective sorbent is its performance in a mixture of numerous competing compounds. Therefore, continued work on competitive adsorption, using a larger group of compounds (e.g., a commercially available diesel fuel sample) is recommended. Also, actual testing of the developed sorbent, Ta-5/ACC with actual diesel fuel with high sulphur content is recommended.

The analysis in this research work indicated that the dispersion of tantalum on the surface was relatively inhomogeneous. Better dispersion has shown to improve adsorption performance. Ways of improving the dispersion of tantalum species on the surface of the activated carbon can be investigated further. Methods such as wet adsorption may prove to be more effective in improving dispersion of metal species on the surface of the activated carbon.

Also, the adsorption kinetics may be different for other sulphur compounds such as 4,6 DMDBT and nitrogen compounds. The assessment of the kinetics will provide insight into the adsorption process, which one can use to optimize the process. This includes assessment of contact time (i.e., flow rate through the sorbent bed) and sorbate loading.

REFERENCES

Babich I.V., J.A. Moulijn, "Science and technology of novel processes for deep desulphurization of oil refinery streams: a review." Fuel 82 (2003) 607–631

Bansal R. C. and Goyal M. Activated Carbon Adsorption. Taylor & Francis, 2005.

Cotton F.A. and Wilkinson G. Advanced Inorganic Chemistry – A Comprehensive Text, 3rd Edition, Wiley, 1972.

Cretoiu L., J.C. Gentry, K. Sam, R. Wright-Wytcherley. "Sulphur Reduction with no Octane Loss- GT-DeSulf." ERTC 7th Annual Meeting, Paris, France, Nov. 18-20, 2002

Cullen, M.; Avidan, A.; "SulphCo – Desulphurization via Selective Oxidation", AM-01-55, NPRA 2001 Annual Meeting.

Do D.D. Adsorption Analysis: Equilibria and Kinetics. Imperial College Press, 1998.

Fujikawa T., K. Idei, K. Ohki, H. Mizuguchi and K. Usui, 2001. "Kinetic behavior of hydrogenation of aromatics in diesel fuel over silica-alumina-supported bimetallic Pt-Pd catalyst." Applied Catalysis A: General 205 (2001) 71 – 77.

García-Gutiérreza J. L., G. A. Fuentesb, M. E. Hernández-Teránb, F. Murrietaa, J. Navarretea and F. Jiménez-Cruza. "Ultra-deep oxidative desulphurization of diesel fuel with H_2O_2 catalyzed under mild conditions by polymolybdates supported on Al_2O_3." Instituto Mexicano del Petróleo, Programa de Procesos y Reactores, Eje Central Lázaro Cárdenas 152, 07730 México D.F., MexicoÁrea de Ingeniería Química, Universidad A. Metropolitana-Iztapalapa, 09340 México D.F., Mexico. 2006.

Gentry J. And Fu-Ming Lee, 2000. "Novel process for FCC gasoline desulphurization and benzene reduction to meet clean fuels requirements." GTC Technology Corp. Houston, TX.

Hamid H. S., Abu Bakr S.H Saleem. "Removal of Sulphur Compounds from Naphtha Solutions Using Solid Adsorbents." Chem. Eng. Technol. 20 (1997) 342-347

Hernandez-Maledonado., A. and R. T. Yang. "New Sorbents for Desulphurization of Diesel Fuels Via π-Complexation." AIChE Journal, April 2004, Vol 50, No. 4

Hernandez-Maledonado A. and R.T. Yang. "Desulphurization of Commercial Jet Fuels by Adsorption Via π-Complexation with Vapor Phase Ion Exchanged Cu(I)-Y Zeolites." Ind. Eng. Chem. Res. 2004, 43m 6142-6149

Irvine Robert L., "Process for desulphurizing gasoline and hydrocarbon feedstocks. U.S. Patent 1998.

Ji., Y, P. Afanasiev, M. Vrinatb, W. Lia and C. Lia. "Promoting Effects in Hydrogenation and Hydrodesulphurization Reactions on the Zirconia and Titania Supported Catalysts." Applied Catalysis A: General 257 (2004) 157-164

Kabe T., A. Ishihara, Q. Zhang, 1993. "Deep Desulphurization of light oil 2. Hydrodesulphurization of dibenzothiophene 4-methyldibenzothiophene and 4,6-dimethyldibenzothiophene." Applied Catalysis A: General 97 (1993) 1 – 9.

Heidi Karjalainen Ulla Lassi, Katariina Rahkamaa-Tolonen Virpi Kröger and Riitta L. Keiskia**. "**Thermodynamic equilibrium calculations of sulphur poisoning in Ce–O–S and La–O–S systems." 2004. University of Oulu, Department of Process and Environmental Engineering, Oulu, Finland.

Laredo, G. C., Cortes, C. M., "Kinetics of Hydrodesulphurization of Dimethylbenzothiophenes *in* a Gas Oil Narrow-Cut Fraction and Solvent Effects." Applied Catalysis 252 (2003) 295-304

Larrubia, M. A., A. Gutièrrez-Alejandreb, J. Ramìrez, and G. Buscaa. "A FTIR study of the adsorption of Indole, Carbozale, Benzothiophene, Dibenzotiophene and 4,6,-dibenzotiophene Over Solid Adsorbents and Catalysts." Applied Catalysis, General (2002) 224 167-178

Liang., C., F. Tian, Z. Li, Z. Feng, Z. Wei (2003). "Preparation and Adsorption Properties for Thiophene of Nanostructured W2Con Ultrahigh-Surface-Area Carbon Materials." Chem. Mater. American Chemical Society.

Liu K., Song C. and Subramani V., Hydrogen and Syngas Production and Purification Technologies. Wiley, 2010.

Ma X., Sun L. and Song C., 2002. "A new approach to deep desulphurization of gasoline, diesel fuel and jet fuel by selective adsorption for ultra-clean fuel and for fuel cell application." Catalysis Today 77 (2002) 107 – 116.

Ma X., Sun L. and Song C., 2003. "Adsorptive desulphurization of diesel fuel over a metal sulfide-based adsorbent." Pennsylvania State University, Department of Energy and Geo-Environmental Engineering and The Energy Institute.

Mali Taylor, "Removal of Sulphur Compounds , Liquid Phase Adsorption." University of Waterloo, Department of Chemical Engineering, 2002.

Manoilova. O. "Influence of Acid-Base and Redox Properties of Metal Oxides on Thiophene Trapping; an Infrared Study." Institute of Physics, St. Petersburg University. 1985.

Mochida Isao, Yosuke Sano, Ki-Hyouk Choi, Yozo Korai. "Adsorptive removal of sulphur and nitrogen species from a straight run gas oil over activated carbons for its deep hydrodesulphurization." Applied Catalysis B: Environmental 49 (2004) 219–225.

Murata. S, *K. Murata, K. Kidena, M. Nomura*. "A Novel Oxidative Desulphurization System for Diesel Fuels with Molecular Oxygen in the Presence of Cobalt Catalysts and Aldehydes." American Chemical Society, July 29 2003.

Ng, Flora T. T.; Rahman, Ataur; Ohasi, Tomotsugu; Jiang, Ming. "A study of the adsorption of thiophenic sulphur compounds using flow calorimetry." Applied Catalysis, B: Environmental (2005), 56(1-2), 127-136. CODEN: ACBEE3 ISSN:0926-3373. CAN 142:222182 AN 2005:106432 CAPLUS

Phillips Petroleum Company, 2001. http://www.fuelstechnology.com/szorbdiesel.htm.

Sakanishi Kinya, Farag Hamdy, Sato Shinya, Matsumura Akimitsu, Saito Ikuo. "Adsorptive removal of sulphur compounds from naphtha fractions by using Carbon adsorbents." National Institute of Advanced Industrial Science and Technology, Ibaraki Japan. American Chemical Society, Division of Fuel Chemistry, 2003, 48(2).

Sata S., M. I. Awad, M. S. El Deab, T. Okajima and T. Ohsaka, "Hydrogen spillover phenomenon: Enhanced Reversible hydrogen adsorption/desorption at Ta2O5-coated Pt electrode in acidic media." Electrochimica Acta, 2010, 55, 3528 – 3536.

Serp P. and Figueiredo J.L. Carbon Materials for Catalysis. Wiley, 2009.

Shaker Haji , Can Erkey, "Removal of Dibenzothiophene from Model Diesel by Adsorption on Carbon Aerogels for Fuel Cell Application." Ind. Eng. Chem. Res. 2003, 42, 6933-6937.

Song, Chunshan. "Fuel Processing for low-temperature and high-temperature fuel cells; Challenges, and opportunities for sustainable development in the 21st Century." *Catal. Today* 2002, *77*, 17.

Song Chunshan. and X. Ma, 2003. "New design approaches to ultra-clean diesel fuels by deep desulphurization and deep dearomatization." Applied Catalysis B: Environmental 41 (2003) 207 – 238.

Song, Chunshan, X. Ma, Anning Zhau. *Liquid-phase adsorption of multi-ring thiophenic sulphur compounds on carbon materials with different surface properties.* Journal of Physical Chemistry B 2006, 110 pp. 4699 – 4707.

Sotleo J.L., M. A. Uguina, M.D. Romero, J.M.Gomez, V.I. Agueda and M.A. Ortiz, 2001. *Dibenzothiophene adsorption over zeolites with faujasite structure.* Studies in Surface Science and Catalysis (2001) 135.

Sprague. M. J, J. Zheng, L. Sun, C. Song. "Effect of Sulphur Removal from Naphthalene on its Hydrogenation over Mordenite-Supported Pd Catalyst." Am. Chem. Soc. Div. Petrol. Chem. Prep., 2002, 47 (2), 103-105.

Song Chunshan, S. Velu, Xiaoliang Ma, "Selective Adsorption for Removing Sulphur from Jet Fuel over Zeolite-Based Adsorbents." Ind. Eng. Chem. Res. 2003, 42, 5293-5304

Song Chunshan., Velu S., S. Watanabe, X. Ma, L. Sun and, 2003. "Development of selective adsorbents for removing sulphur from gasoline for fuel cell applications." Pennsylvania State University, Department of Energy and Geo-Environmental Engineering and The Energy Institute.

Torrisi S. Jr., T. Remans, J. Swain. "The Challenging Chemistry of Ultra-Low-Sulphur Diesel." World Refining – December 2002.

Agulyansky, A. (2004). Main principals of the chemistry of tantalum and niobium fluoride compounds. Chemistry of Tantalum and Niobium Fluoride Compounds. Amsterdam, Elsevier Science**:** 339-340.

Baker, W. S., J. W. Long, R. M. Stroud, D. R. Rolison (2004). "Sulphur-functionalized carbon aerogels: a new approach for loading high-surface-area electrode nanoarchitectures with precious metal catalysts." Journal of Non-Crystalline Solids **350**: 80-87.

Benndorf, C., M. Grischke (1988). "Identification of carbon and tantalum chemical states in metal-doped a-C:H films." Surface and Coatings Technology **36**(1-2): 171-181.

Buslaev, Y. A., A. I. Nikolaev (1985). "Investigation of Nb(V) and Ta(V) state in fluoride solutions." Journal of Fluorine Chemistry **29**(1-2): 51-51.

Chen, H., Y. Wang, F.H. Yang, R.T. Yang (2009). "Desulphurization of high-sulphur jet fuel by mesoporous [pi]-complexation adsorbents." Chemical Engineering Science **64**(24): 5240-5246.

Chuang, J.-C. and M.-C. Chen (1998). "Properties of thin Ta-N films reactively sputtered on Cu/SiO2/Si substrates." Thin Solid Films **322**(1-2): 213-217.

Chun, W.-J., A. Ishikawa, Hideki Fujisawa, Tsuyoshi Takata, J. N. Kondo, M. Hara, M. Kawai, Y. Matsumoto, and K. Domen. (2003). "Conduction and Valence Band Positions of Ta2O5, TaON, and Ta3N5 by UPS and Electrochemical Methods." The Journal of Physical Chemistry B **107**(8): 1798-1803.

Demiryont, H., J. R. Sites, K. Geib (1985). "Effects of oxygen content on the optical properties of tantalum oxide films deposited by ion-beam sputtering." Appl. Opt. **24**(4): 490-495.

Farag, H. (2007). "Selective adsorption of refractory sulphur species on active carbons and carbon based CoMo catalyst." Journal of Colloid and Interface Science **307**(1): 1-8.

Gould, B. D., O. A. Baturina, K. E. Swider-Lyons. (2009). "Deactivation of Pt/VC proton exchange membrane fuel cell cathodes by SO2, H2S and COS." Journal of Power Sources **188**(1): 89-95.

Gruber, M., S. Chouzier, K. Koehler, L. Djakovitch (2004). "Palladium on activated carbon: a valuable heterogeneous catalyst for one-pot multi-step synthesis." Applied Catalysis A: General **265**(2): 161-169.

Gruzalski, G. R., D. M. Zehner, G.W. Ownby (1985). "Electron spectroscopic studies of tantalum carbide." Surface Science **157**(2-3): L395-L400.

Hernández-Maldonado, A. J. Qi, F. Yang, R. Yang (2005). "Desulphurization of transportation fuels by [pi]-complexation sorbents: Cu(I)-, Ni(II)-, and Zn(II)-zeolites." Applied Catalysis B: Environmental **56**(1-2): 111-126.

Howarth, J. and K. Gillespie (1996). "Investigations into the use of niobium and tantalum complexes as Lewis acids." Tetrahedron Letters **37**(33): 6011-6012.

Hu, X., L. Lei, H.P. Chu, P.L. Yue (1999). "Copper/activated carbon as catalyst for organic wastewater treatment." Carbon **37**(4): 631-637.

Jansen, R. J. J. and H. van Bekkum (1995). "XPS of nitrogen-containing functional groups on activated carbon." Carbon **33**(8): 1021-1027.

Kessel, R. and J. W. Schultze (1990). "Surface analytical and photoelectrochemical investigations of conducting polymers." Surface and Interface Analysis **16**(1-12): 401-406.

Lücking, F., H. Köser, M. Jank, A. Ritter (1998). "Iron powder, graphite and activated carbon as catalysts for the oxidation of 4-chlorophenol with hydrogen peroxide in aqueous solution." Water Research **32**(9): 2607-2614.

Masel R. I., Principles of Adsorption and Reaction on Solid Surfaces. Wiley series in Chemical Engineering, Wiley, 1996.

Masud, J., M. T. Alam, R. Miah, T. Okajima, T. Ohsaka (2011). "Enhanced electrooxidation of formic acid at Ta2O5-modified Pt electrode." Electrochemistry Communications **13**(1): 86-89.

McGuire, G. E., G. K. Schweitzer, T.A. Carlson (1973). "Core electron binding energies in some Group IIIA, VB, and VIB compounds." Inorganic Chemistry **12**(10): 2450-2453.

McGuire M.J. and Suffet I.H., Activated carbon adsorption of organics from aqueous phase Volume 2. Ann Arbor Science, 1980.

Moulden J. F., W. F. Stickle, P. E. Sobol, and K. D. Bumben. *Handbook of X-ray Photoelectron Spectroscopy*, Physical Electronics Inc. (1995).

Park, C. and M. A. Keane (2003). "Catalyst support effects: gas-phase hydrogenation of phenol over palladium." Journal of Colloid and Interface Science **266**(1): 183-194.

Poots, V. J. P., G. McKay, J.J. Healy (1976). "The removal of acid dye from effluent using natural adsorbents--II Wood." Water Research **10**(12): 1067-1070.

Rosa Silva, A., J. LuIs Figueiredo, C. Freire, B. de Castro (2004). "Manganese(III) salen complexes anchored onto activated carbon as heterogeneous catalysts for the epoxidation of olefins." Microporous and Mesoporous Materials **68**(1-3): 83-89.

Sarac, A. S., S. A. M. Tofail, et al. (2004). "Surface characterisation of electrografted random poly[carbazole-co-3-methylthiophene] copolymers on carbon fiber: XPS, AFM and Raman spectroscopy." Applied Surface Science **222**(1-4): 148-165.

Sata, S., M. I. Awad, M. S. El-Deaba, T. Okajimaa and T. Ohsaka (2010). "Hydrogen spillover phenomenon: Enhanced reversible hydrogen adsorption/desorption at Ta_2O_5-coated Pt electrode in acidic media." Electrochimica Acta **55**(10): 3528-3536.

Sekar, M., V. Sakthi, S. Rengaraj (2004). "Kinetics and equilibrium adsorption study of lead(II) onto activated carbon prepared from coconut shell." Journal of Colloid and Interface Science **279**(2): 307-313.

Serp P. and Figueiredo J.L. *Carbon Materials for Catalysis*, John Wiley & Sons, Inc. (2009).

Skadtchenko, B. O., M. Trudeau, M.J. Willans, D. Antonelli. (2003). "Structural and Spectroscopic Studies on Mesoporous Tantalum Oxide–Sodium Fulleride Composites

with Conducting Fulleride Columns in the Pores." Advanced Functional Materials **13**(9): 671-681.

Sohn, S. and D. Kim (2005). "Modification of Langmuir isotherm in solution systems--definition and utilization of concentration dependent factor." Chemosphere **58**(1): 115-123.

Sutherland C, Venkobachar C. (2010) "A diffusion-chemisorption kinetic model for simulating biosorption using forest macro-fungus, fomes fasciatus." International Research Journal of Plant Science Vol. 1(4): 107-117.

Titov, A. A., V. A. Krokhin, N. K. Zhulanov and D. L. Melnikov (1995). "Preparation of chemically active powders of niobium and titanium oxides and synthesis of dielectric ceramic materials." Journal of Materials Processing Technology **55**(3-4): 249-253.

Wen, J., X. Han, Xue Han, Hongfei Lin, Ying Zheng, Wei Chu (2010). "A critical study on the adsorption of heterocyclic sulphur and nitrogen compounds by activated carbon: Equilibrium, kinetics and thermodynamics." Chemical Engineering Journal **164**(1): 29-36.

Yang R. T. 2003. Adsorbents: Fundamentals and Applications. New York: Wiley-Interscience.

Yang, R. T.; Herna´ndez-Maldonado, A. J.; Yang, F. H. Desulphurization of Transportation Fuels with Zeolites under Ambient Conditions. Science 2003, 301, 79-81.

Yang R.T. and Yuhe Wang. *Desulphurization of Liquid Fuels by Adsorption on Carbon-Based Sorbents and Ultrasound-Assisted Sorbent Regeneration.* Langmuir 2007, 23 pp. 3825 – 3831.

Young Paul R. Organic Chemistry OnLine 1996. University of Illinois at Chicago. www.chem.uic.edu/web1/ocol/spec/IRTable.htm

Zhao, D., Juan Zhanga, Erhong Duana and Jinlong Wanga (2008). "Adsorption equilibrium and kinetics of dibenzothiophene from n-octane on bamboo charcoal." Applied Surface Science 254(10): 3242-3247.

Zhou, A., Xiaoliang Ma and Chunshan Song (2009). "Effects of oxidative modification of carbon surface on the adsorption of sulphur compounds in diesel fuel." Applied Catalysis B: Environmental **87**(3-4): 190-199.

Zhang J.C. L. F. Songa, J. Y. Hua, S. L. Onga, W. J. Nga, L. Y. Leea, Y. H. Wangb, J. G. Zhaob and R. Y. Mab In*vestigation on Gasoline Deep Desulphurization for Fuel Cell Applications.* Energy Conservation and Management No. 46 (2005).

APPENDIX A

TABLE A-1 SUMMARY OF CURRENT SULPHUR REMOVAL TECHNIQUES

TABLE A-1
SUMMARY OF CURRENT SULPHUR REMOVAL TECHNIQUES

Ref	Year	Compound	Sorbents	Solution	Experimental Condition	Removal %	Observations/ Comments
1	-	Thiophene	CeO_2, CeO_2-ZrO_2, ZrO_2, Ga_2O_3, TiO_2, ZnO, Al_2O_3,SiO_2 and CaO	-	Infrared Method T= 300-670 K Samples were preheated at 670-970 K in vacuum and O_2 Adsorption in presence /absence of H_2	N/R	The amount of sulphate species diminishes in the following sequence: CeO_2> CeO_2-ZrO_2> ZrO_2> Ga_2O_3> TiO_2> ZnO> Al_2O_3>SiO_2 The sulphur retention is highest for metal oxides with strong redox and basic properties
2	1997	Sulphur Compounds	Activated Carbon & Zeolite 13X	Naphtha	T= 80 C	N/R	Adsorption in the range of practical interest (550ppm) can be achieved effectively by using activated carbon at 80 C. Zeolite 13 X maybe more effective for low concentration ranges (<50 ppm) at ambient temperatures
3	2002	Thiophene	NaY Zeolite	Hexadecane	Adsorption takes place in a heat shaker at 45 C and 150 rpm. Two series of experiment with regeneration performed.	1) Initial Ads.: 53.36; Reads.:59.09 2) Initial Ads.: 67.7; Reads.1: 55.96; Reads.2:14.75	Previous experiments indicate that zeolites (NaY and 13 X) out perform all other sorbents tested. The regeneration process suggests that NaY have a superior advantage in large scale applications.
			Zeolite 13X			1) Initial Ads.: 62.68; Reads.:26.37 2) Initial Ads.: 45.94; Reads1.: 36.75; Reads2.: 6.72	
4	2001	DMDBT	Alumina, zirconia and magnesia	-	Study by IR spectroscopy	N/R	The main adsorption process is due to adsorption on Lewis sites or on acid-base pairs. On alumina the adsorption is strongest. Adsorption of 4,6,-DMDBT is definitely limited in extent likely due to steric hindrance.
5	2004	Thiophene	Zeolite 13X	Hexadecane	Adsorption takes place in a heat shaker at 48 C and 150 rpm for 20 hours. For 13 X and NaY a regeneration study was performed as well.	1) 1.47mmol S sorbed / g adsorbent 2) 1st ads.: 0.3166; 2nd ads.: 0.2721	Adsorption in the range of 200 to 3000 wppm can be achieved effectively by using type 13 X, NaY, Acidic and USY zeolites at moderate temperature. Adsorption patterns follows this manner: USY> Acidic> NaY> 13 X
			NaY zeolite			1) 1.89 2) 1st ads.: 0.4724; 2nd ads.: 0.4157	
			USY zeolite			1.52	
			Acidic zeolites			1.54	
6	2002	Benzothiophene	Raney NiAl alloy (Aldrich)	Naphthalene in methanol	The solution was eluted through a packed bed of Raney Ni in a glass column at 45 C. The column was kept under nitrogen to prevent base metal oxidation.	100	
7	2000	Sulphur Compounds	S Zorb	Gasoline	Gasoline is combined with hydrogen and heated, the vaporized gasoline is injected into a fluid bed. T= 650- 775 F; P= 100-300 PSIG	Low sulphur case:97 High sulphur case: 99.3	S Zorb Technology by Conoco Philips Petroleum Company

Ref	Year	Compound	Sorbents	Solution	Experimental Condition	Removal %	Observations/ Comments
8	2003	Benzothiophene and its substituted aromatic sulphur compounds	Y Zeolites (with Cu, Ni, Pd and Ce ions)	Model jet fuel (MJF) & real jet fuel (JP-8)	The process is called : PSU-SARS T= 80 C	CeY: 10 mg S sorbed / g adsorbent for MJF (510 ppmw S) and 4.5 mg/g for JP-8 (750 ppm S)	In static condition, with a residence time of 5 h, the selectivity order is 2-MBT (Methyl benzothiophene) >= 5-MBT > BT Under dynamic condition with a residence time of 0.4 h, the selectivity order is 5-MBT> BT> 2-MBT
9	2003	Thiophene	Nanostructured W_2C on ultrahigh-surface-area carbon (HSAC)	Fuel oil	30 min for W/HSAC and WC/HSAC and 60 min for W_2C/HSAC	no sulphur detected in the product	Adsorption capacity is in the order of: W_2C/HSAC> W/HSAC> WC/HSAC >> HSAC
10	2003	Dibenzothiophene	4 nm and 22 nm Carbon Aerogels	n-hexadecane	Ambient temperature and pressure	over 4 nm: 86 over 22 nm: 93	selective adsorption of dibenzothiophene using carbon aerogels is feasible. The carbon aerogel with the larger average pore size had higher adsorption capacity and faster adsorption kinetics.
11	2004	Sulphur Compounds	AC/Cu(I)-Y, CU(I)-Y, Selexsorb, CDX (Alumina), CuCl/γ-Al_2O_3, Activated carbon, Cu(I)-ZSM-5	Commercial diesel fuel	Fixed bed adsorbent operated at ambient temperature and pressure	with the CU(I)Y the product will contain as low as 0.15 ppmw-S	Copper (auto-reduced) type-Y zeolites are superior adsorbents for the removal of all sulphur compounds from commercial diesel fuels. Total sulphur adsorption capacity at breakthrough follow the order:AC/Cu(I)-Y> CU(I)-Y> Selexsorb> CDX (Alumina)> CuCl/γ-Al2O3> Activated carbon> Cu(I)-ZSM-5 The Cu(I)-ZSM-5 is promising for application with selectivity toward small thiophene molecules
12	2004	Sulphur Compounds	Cu(I)- Y (VPIE), Selexsorb CDX, Selexsorb CDX/Cu(I)-Y(VPIE)	Commercial Jet fuels	Fixed bed adsorbent operated at ambient temperature and pressure The activated alumina was used as guard bed to Cu(I)-Y(VPIE).	The best adsorbent produces 38 m3 of jet fuel per gram of sorbent with a weighted average content of 0.071 ppmw-S	Vapor Phase Ion Exchanged copper (I) type Y zeolites are superior adsorbent for removal of all sulphur compounds from commercial jet fuels. Total sulphur adsorption capacity at breakthrough follow the order: Selexsorb CDX< Cu(I)-Y (VPIE)< Selexsorb CDX/Cu(I)-Y(VPIE)
13	2003	Benzene and dibenzohiophene	Silica and alumina	Benzene, dibenzohiophene and n-octanol Diesel fuel	The Mixture and a cobalt salt (acetate or chloride) and an aldehyde was stirred at 40 C for 15 min. Then, the produces dibenzothiophene sulfone was removed by silica or alumina adsorption	For Diesel fuel : 97	Several organic sulfides including benzothiophene and 4,6- dimethyl dibenzothiophene also could be converted to the corresponding sulfones in almost quantitative yeilds.
14	2003	Dimethyl dibenzothiophenes	Catalysts: CoMo/ Al_2O_3	A Narrow cut gas oil fraction with octadecane as solvent	Hdrodesulphurization process T= 350-390 C, P= 5.2 Mpa	Adsorption constant for different solvent concentration: 35.75 - 52.32 l/mol	Dimethyl benzothiophene with a methyl group in position were the least reactive of the sulphur compounds present in the lump
15*	2002	Mercaptans, sulfides, thiophenic- type components	-	Cracked stock gasoline with Techtive-DS as solvent	GT- Desulf process: the primary operation is extractive distillation. Relative volataliry of the feed is altered and sulfu compounds extracted.	The product contains less than 10 ppmw of thiophenic-type sulphur compounds	The technology delivers zero octane loss and handles a wide range of feed composition

Ref	Year	Compound	Sorbents	Solution	Experimental Condition	Removal %	Observations/ Comments
16*	2003	Thiophene	Catalysts: MoS_2 and WS_2 sulfides, non-promoted or promoted with Co and Ni. The supports were ZrO_2, alumina stabilized TiO_2 and pure alumina	-	-	-	The nature of promoter plays determining role for the catalytic performance. The most active ones for hydrodesulphurization reactions were Ni-promoted Mo and W catalysts, supported on ZrO_2.

N/R: Not Reported

* Processes other than (passive) adsorption

References:

1 - Manoilova. O., *et al.* ,Influence of Acid-Base and Redox Properties of Metal Oxides on Thiophene Trapping; an Infrared Study, Institute of Physics, St. Petersburg University, Russia

2 - Abu Bakr S.H Saleem and Halim S. Hamid, Removal of Sulphur Compounds from Naphtha Solutions Using Solid Adsorbents, Chem. Eng. Technol. 20 (1997) 342-347

3 - Taylor Mali, Removal of Sulphur Compounds , Liquid Phase Adsorption, University of Waterloo, Department of Chemical Engineering, 2002

4 - Larrubia. M. A., *et al.* A FT_IR study of the adsorption of Indole, Carbozale, Benzothiophene, Dibenzotiophene and 4,6,-dibenzotiophene Over Solid Adsorbents and Catalysts, Applied Catalysis, General 224 (2002) 167-178

5 Ng F.T.T., *et al.* Adsorption of Sulphur Compound on Zeolites: A Calorimetry, TPD and Thermogravimetry Study. 2004

6 Sprague. M. J, *et al.* Effect of Sulphur Removal from Naphthalene on its Hydrogenation over Mordenite-Supported PD Catalyst, Petroleum Chemistry Division Preprints,J6 2002, 47(2)

7 - www.fuelstechnology.com/zsorb_processover.htm

8 - Velu. S, Xiaoliang Ma, Chunshan Song., Selective Adsorption for Removing Sulphur from Jet Fuel over Zeolite-Based Adsorbents, Ind. Eng. Chem. Res. 2003, 42, 5293-5304

9 - Liang., C. *et al.* Preparation and Adsorption Properties for Thiophene of Nanostructured W2C on Ultrahigh-Surface-Area Carbon Materials, Chem. Mater. American Chemical Society, Published on Web, 2003

10 - Shaker Haji , Can Erkey, Removal of Dibenzothiophene from Model Diesel by Adsorption on Carbon Aerogels for Fuel Cell Application, Ind. Eng. Chem. Res. 2003, 42, 6933-6937

11 - Hernandez-Maledonado., A. and Yang, R. T, New Sorbents for Desulphurization of Diesel Fuels Via π-Complexation, AIChE Journal, April 2004, Vol 50, No. 4

12 - Hernandez-Maledonado., A. and Yang, R. T, Desulphurization of Commercial Jet Fuels by Adsorption Via π-Complexation with Vapor Phase Ion Exchanged Cu(I)-Y Zeolites, Ind. Eng. Chem. Res. 2004, 43m 6142-6149

13 - Murata. S, *et al.* A Novel Oxidative Desulphurization System for Diesel Fuels with Molecular Oxygen in the Presence of Cobalt Catalysts and Aldehydes, American Chemical Society, July 29 2003, Published on web

14 - Laredo, G. C., Cortes, C. M. , Kinetics of Hydrodesulphurization of Dimethylbenzothiophenes in a Gas Oil Narrow-Cut Fraction and Solvent Effects, Applied Catalysis 252 (2003) 295-304

15 - Cretoiu L., *et al.* Sulphur Reduction with no Octane Loss- GT-DeSulf ^{TM}, ERTC 7th Annual Meeting, Paris, France, Nov. 18-20, 2002

16 - Ji., Y, *et al.* Promoting Effects in Hydrogenation and Hydrodesulphurization Reactions on the Zirconia and Titania Supported Catalysts, Applied Catalysis A: General 257 (2004) 157-164

APPENDIX B

MOLECULAR STRUCTURES OF KEY ORGANO-SULPHUR COMPOUNDS

BENZOTHIOPHENE

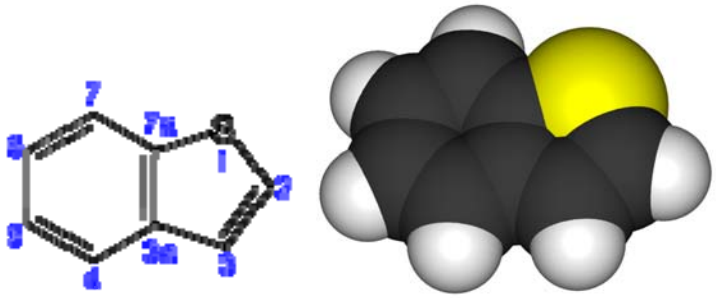

DIBENZOTHIOPHENE

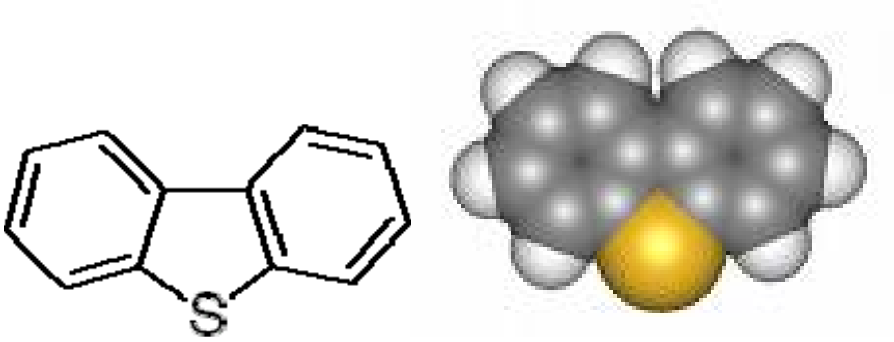

4,6-DIMETHYLDIBENZOTHIOPHENE

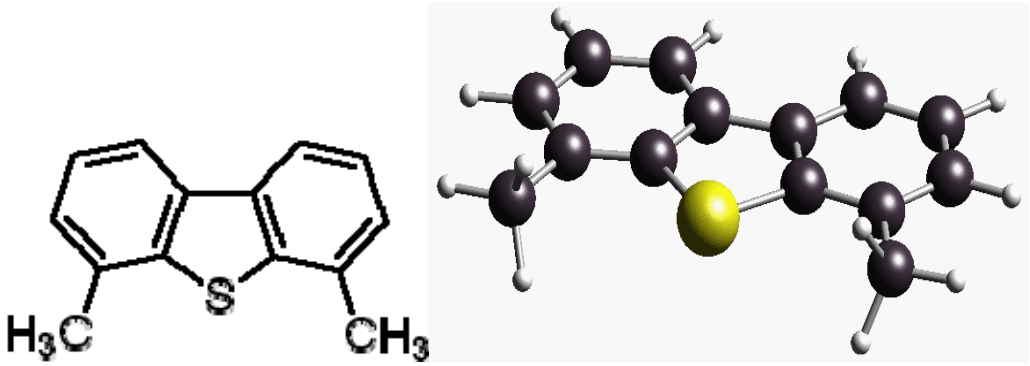

APPENDIX C

SUPPLEMENTARY DATA

APPENDIX C1 – ISOTHERMS AND LINEARIZATION
APPENDIX C2 – CALORIMETRY AND BREAKTHROUGH
APPENDIX C3 – XPS ANALYSIS – FULL SURVEY
APPENDIX C4 – GC/FID ANALYTICAL METHOD & CALIBRATION
APPENDIX C5 – FLOW REACTOR EXPERIMENTS

Adsorption Isotherm - DBT in Hexadecane

Sorbent: Ag (2% wt.) on ACC

Temperature = 50°C

Duration: 24 Hours

Sorbent particle size: 125μ << 250μ

Ag / ACC - 125 μ

Bulk Solution (DBT + C16)			Conc. Final		Sorbent	Plot data		Linear Plot - Langmuir	
C solution	*weight of Soln*	*n solution*	*C solution*	*n solution*	*weight*	*C solution*	*q*	C	C/q
mmol/L	*g*	*mmol*	*mmol/L*	*mmol*	*g*	*mmol/L*	*mmol/g*		
39.080	5.117	0.259	20.33	0.13458	0.1949	20.330	0.637	20.330	31.924
31.460	4.863	0.198	7.11	0.04473	0.3115	7.110	0.492	7.110	14.458
23.080	5.042	0.151	7.72	0.05036	0.1999	7.720	0.501	7.720	15.403
9.570	5.129	0.064	0.77	0.00511	0.2329	0.770	0.251	0.770	3.071
5.210	5.112	0.034	0.20	0.00132	0.2129	0.200	0.156	0.200	1.285
2.630	4.911	0.017	0.04	0.00025	0.1976	0.040	0.083	0.040	0.480
1.450	4.889	0.009	0.01	0.00006	0.1963	0.010	0.046	0.010	0.216
0.570	4.985	0.004	0.03	0.00019	0.1356	0.030	0.026	0.030	1.168
								Intercept	1.393
								Slope	1.570
								qm	0.637
								K	1.127
								R^2	0.987

Linear Plot - Freundlich	
log (C)	**log (q)**
1.308	-0.196
0.852	-0.308
0.888	-0.300
-0.114	-0.601
-0.699	-0.808
-1.398	-1.080
-2.000	-1.334
-1.523	-1.590
K	0.226
n	2.546
R^2	0.911

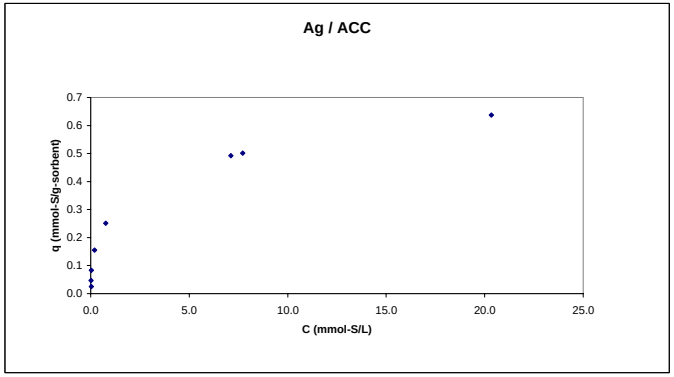

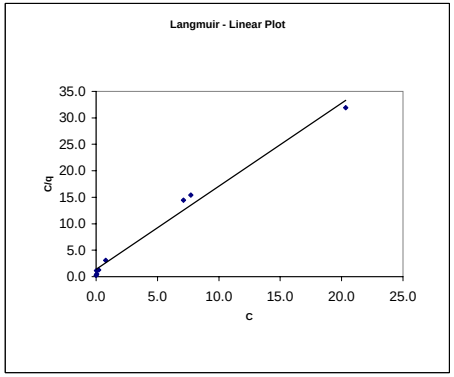

Adsorption Isotherm - DBT in Hexadecane

Sorbent: Ag (2% wt.) on ACC

Temperature = 50°C

Duration: 24 Hours

Sorbent particle size: <125μ

Ag/ACC (<125μ)

Bulk Solution (DBT + C16)			Conc. Final		Sorbent	Plot data		Linear Plot - Langmuir	
C solution	*weight of Soln*	*n solution*	*C solution*	*n solution*	*weight*	*C solution*	*q*	C	C/q
mmol/L	*g*	*mmol*	*mmol/L*	*mmol*	*g*	*mmol/L*	*mmol/g*		
72.370	5.216	0.488	63.310	0.42722	0.0877	63.310	0.697	63.310	90.817
56.640	4.791	0.351	41.350	0.25627	0.1303	41.350	0.727	41.350	56.857
46.330	5.437	0.326	20.790	0.14622	0.2640	20.790	0.680	20.790	30.556
30.640	5.447	0.216	18.170	0.12804	0.1378	18.170	0.638	18.170	28.494

Linear Plot - Freundlich	
log (C)	**log (q)**
1.801	-0.157
1.616	-0.138
1.318	-0.167
1.259	-0.195

22.400	4.861	0.141	10.190	0.06407	0.1436	10.190	0.535	10.190	19.060
10.740	5.325	0.074	2.040	0.01405	0.1849	2.040	0.324	2.040	6.294
5.350	5.398	0.037	1.060	0.00740	0.1149	1.060	0.261	1.060	4.065
2.560	4.987	0.017	0.150	0.00097	0.1264	0.150	0.123	0.150	1.220
1.420	4.946	0.009	0.020	0.00013	0.1261	0.020	0.071	0.020	0.282

Intercept	2.286
Slope	1.382
qm	0.724
K	0.605
R^2	0.997

1.008	-0.272
0.310	-0.489
0.025	-0.584
-0.824	-0.910
-1.699	-1.149
K	0.242
n	3.260
R^2	0.984

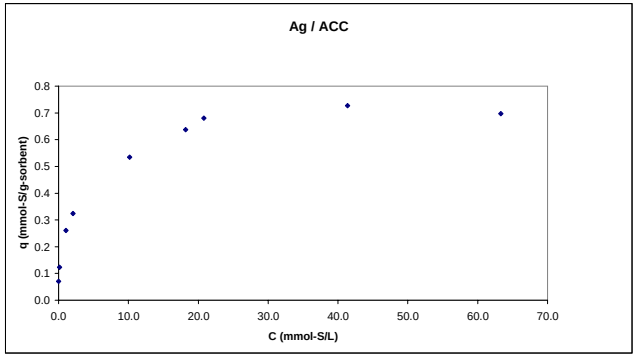

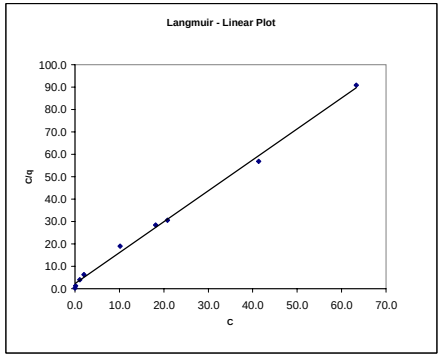

Adsorption Isotherm - DBT in Hexadecane

Sorbent: Fe (2% wt.) on ACC

Temperature = 50°C

Duration: 24 Hours

Sorbent particle size: 125μ << 250μ

Fe / ACC - 125 μ

Bulk Solution (DBT + C16)			Conc. Final		Sorbent	Plot data		Linear Plot - Langmuir	
C solution	*weight of Soln*	*n solution*	*C solution*	*n solution*	*weight*	*C solution*	*q*	C	C/q
mmol/L	*g*	*mmol*	*mmol/L*	*mmol*	*g*	*mmol/L*	*mmol/g*		
39.080	5.046	0.255	15.66	0.1022	0.227	15.660	0.673	15.660	23.283
31.460	4.931	0.201	11.29	0.0720	0.216	11.290	0.595	11.290	18.988
23.080	4.857	0.145	2.41	0.0151	0.349	2.410	0.372	2.410	6.475
9.570	4.849	0.060	0.77	0.0048	0.213	0.770	0.260	0.770	2.964
5.210	5.199	0.035	0.23	0.0015	0.195	0.230	0.172	0.230	1.336
2.630	4.964	0.017	0.03	0.0002	0.217	0.030	0.077	0.030	0.390
1.450	5.106	0.010	0.01	0.0001	0.164	0.010	0.058	0.010	0.173
0.570	5.020	0.004	0.04	0.0003	0.106	0.040	0.033	0.040	1.228
								Intercept	1.240
								Slope	1.476
								qm	0.678
								K	1.190
								R^2	0.987

Linear Plot - Freundlich	
log (C)	**log (q)**
1.195	-0.172
1.053	-0.226
0.382	-0.429
-0.114	-0.585
-0.638	-0.764
-1.523	-1.114
-2.000	-1.237
-1.398	-1.487
K	0.248
n	2.615
R^2	0.905

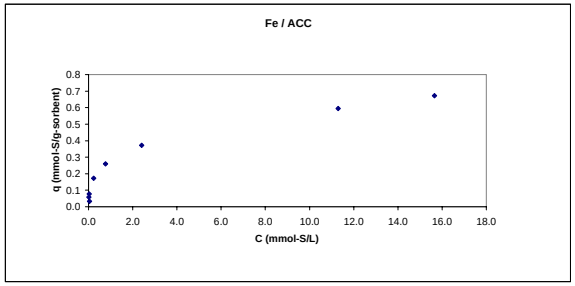

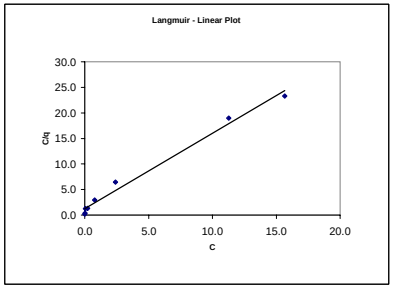

Adsorption Isotherm - DBT in Hexadecane

Sorbent: Co (2% wt.) on ACC

Temperature = 50°C

Duration: 24 Hours

Sorbent particle size: <125µ

Co / ACC

Bulk Solution (DBT + C16)			Conc. Final		Sorbent	Plot data		Linear Plot - Langmuir	
C solution	*weight of Soln*	*n solution*	*C solution*	*n solution*	*weight*	*C solution*	*q*	C	C/q
mmol/L	*g*	*mmol*	*mmol/L*	*mmol*	*g*	*mmol/L*	*mmol/g*		
39.080	5.573	0.282	15.34	0.1106	0.2241	15.340	0.764	15.340	20.086
31.460	5.262	0.214	11.42	0.0777	0.2101	11.420	0.649	11.420	17.587
23.080	5.017	0.150	6.61	0.0429	0.2261	6.610	0.473	6.610	13.980
9.570	5.284	0.065	2.41	0.0165	0.1431	2.410	0.342	2.410	7.046
5.210	5.359	0.036	0.58	0.0040	0.1530	0.580	0.210	0.580	2.765
2.630	5.136	0.017	0.06	0.0004	0.1901	0.060	0.090	0.060	0.668
1.450	5.148	0.010	0.02	0.0001	0.1466	0.020	0.065	0.020	0.308
0.570	5.152	0.004	0.02	0.0001	0.1541	0.020	0.024	0.020	0.841
								Intercept	1.850
								Slope	1.330
								qm	0.752
								K	0.719
								R^2	0.946

Linear Plot - Freundlich	
log (C)	**log (q)**
1.186	-0.117
1.058	-0.188
0.820	-0.325
0.382	-0.466
-0.237	-0.678
-1.222	-1.047
-1.699	-1.187
-1.699	-1.624
K	0.235
n	2.346
R^2	0.942

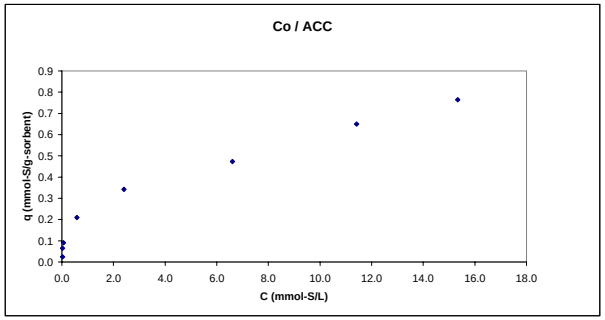

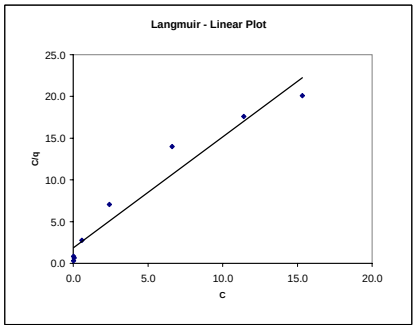

Adsorption Isotherm - DBT in Hexadecane

Sorbent: ACC

Temperature = 50°C

Duration: 24 Hours

Sorbent particle size: 125µ <<250µ

ACC - 125µ

Bulk Solution (DBT + C16)			Conc. Final		Sorbent	Plot data		Linear Plot - Langmuir	
C solution	*weight of Soln*	*n solution*	*C solution*	*n solution*	*weight*	*C solution*	*q*	C	C/q
mmol/L	*g*	*mmol*	*mmol/L*	*mmol*	*g*	*mmol/L*	*mmol/g*		
39.080	5.200	0.263	19.13	0.13	0.220	19.130	0.611	19.130	31.333
31.460	5.029	0.205	12.09	0.08	0.232	12.090	0.544	12.090	22.230
23.080	5.005	0.149	5.41	0.04	0.246	5.410	0.466	5.410	11.618
9.570	4.898	0.061	1.29	0.01	0.245	1.290	0.214	1.290	6.022
5.210	5.106	0.034	0.19	0.0013	0.160	0.190	0.208	0.190	0.914
2.630	5.093	0.017	0.10	0.0007	0.173	0.100	0.097	0.100	1.036
1.450	5.087	0.010	0.01	0.0001	0.323	0.010	0.029	0.010	0.341
0.570	4.996	0.004	0.02	0.0001	0.211	0.020	0.017	0.020	1.187
								Intercept	1.613
								Slope	1.616
								qm	0.619
								K	1.002
								R^2	0.986

Linear Plot - Freundlich	
log (C)	**log (q)**
1.282	-0.214
1.082	-0.265
0.733	-0.332
0.111	-0.669
-0.721	-0.682
-1.000	-1.015
-2.000	-1.533
-1.699	-1.773
K	0.205
n	2.271
R^2	0.898

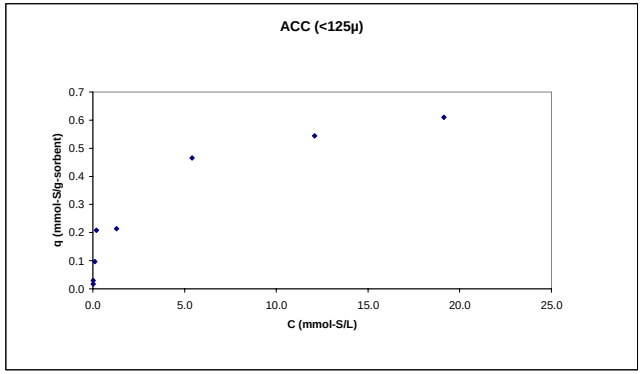

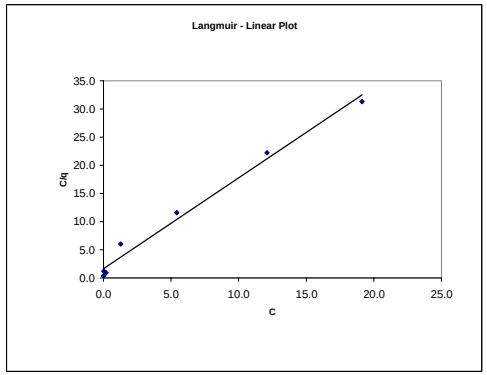

Adsorption Isotherm - DBT in Hexadecane

Sorbent: Acid-washed activated carbon

Temperature = 50°C

Duration: 24 Hours

Sorbent particle size: 125µ <<250µ

AAC (125µ)

Bulk Solution (DBT + C16)			Conc. Final		Sorbent	Plot data		Linear Plot - Langmuir	
C solution	*weight of Soln*	*n solution*	*C solution*	*n solution*	*weight*	*C solution*	*q*	C	C/q
mmol/L	*g*	*mmol*	*mmol/L*	*mmol*	*g*	*mmol/L*	*mmol/g*		
39.080	4.918	0.249	24.27	0.15	0.2589	24.270	0.364	24.270	66.692
31.460	5.003	0.204	18.81	0.12	0.2213	18.810	0.370	18.810	50.840
23.080	5.311	0.159	14.43	0.10	0.1847	14.430	0.322	14.430	44.846
9.570	5.195	0.064	1.88	0.01	0.3103	1.880	0.167	1.880	11.287
5.210	5.019	0.034	0.96	0.01	0.2096	0.960	0.132	0.960	7.292
2.630	5.110	0.017	0.17	0.0011	0.2168	0.170	0.075	0.170	2.267
1.450	5.079	0.010	0.06	0.0004	0.1590	0.060	0.057	0.060	1.045
0.570	5.374	0.004	0.02	0.0001	0.0712	0.020	0.054	0.020	0.372
								Intercept	2.938
								Slope	2.659
								qm	0.376
								K	0.905
								R^2	0.991

Linear Plot - Freundlich	
log (C)	**log (q)**
1.385	-0.439
1.274	-0.432
1.159	-0.492
0.274	-0.778
-0.018	-0.881
-0.770	-1.125
-1.222	-1.241
-1.699	-1.270
K	0.142
n	3.381
R^2	0.986

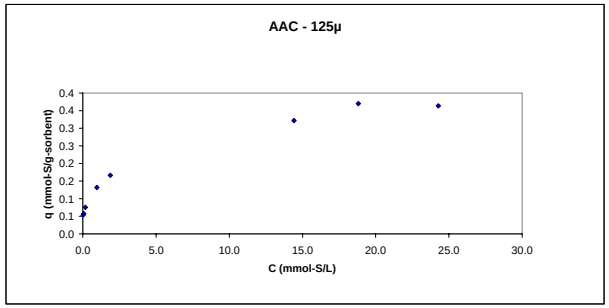

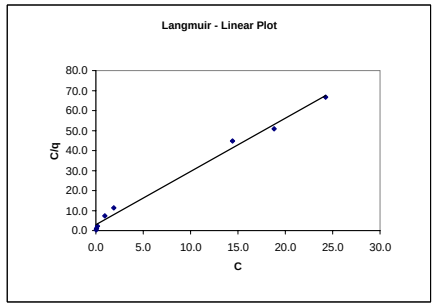

Adsorption Isotherm - DBT in Hexadecane

Sorbent: Ni (2% wt.) on ACC

Temperature = 50°C

Duration: 24 Hours

Sorbent particle size: <125µ

Ni/ACC

Bulk Solution (DBT + C16)			Conc. Final		Sorbent	Plot data		Linear Plot - Langmuir	
C solution	*weight of Soln*	*n solution*	*C solution*	*n solution*	*weight*	*C solution*	*q*	C	C/q
mmol/L	*g*	*mmol*	*mmol/L*	*mmol*	*g*	*mmol/L*	*mmol/g*		
72.370	5.031	0.471	56.63	0.37	0.1258	56.630	0.814	56.630	69.542
56.640	5.023	0.368	40.39	0.26	0.1452	40.390	0.727	40.390	55.536
46.330	5.031	0.302	29.16	0.19	0.1605	29.160	0.696	29.160	41.883
30.640	5.041	0.200	17.17	0.11	0.1429	17.170	0.615	17.170	27.934
22.400	5.004	0.145	6.33	0.04	0.2337	6.330	0.445	6.330	14.220
10.740	5.015	0.070	1.45	0.01	0.2101	1.450	0.287	1.450	5.054
5.350	5.039	0.035	0.98	0.01	0.1183	0.980	0.241	0.980	4.070
2.560	5.017	0.017	0.19	0.00	0.1179	0.190	0.130	0.190	1.456
1.420	4.799	0.009	0.05	0.00	0.1047	0.050	0.081	0.050	0.615
								Intercept	3.590
								Slope	1.234
								qm	0.810
								K	0.344
								R^2	0.989

Linear Plot - Freundlich	
log (C)	**log (q)**
1.753	-0.089
1.606	-0.138
1.465	-0.157
1.235	-0.211
0.801	-0.352
0.161	-0.542
-0.009	-0.618
-0.721	-0.884
-1.301	-1.090
K	0.232
n	3.057
R^2	0.995

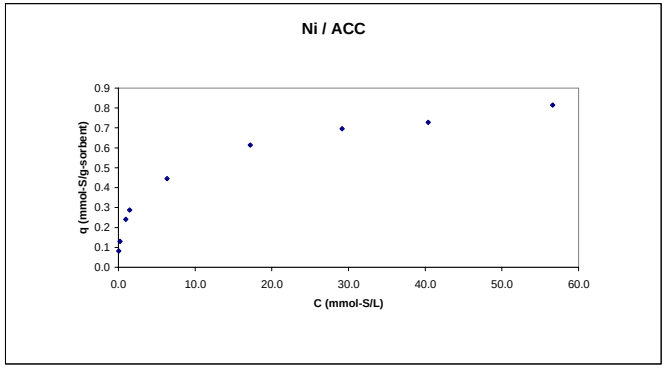

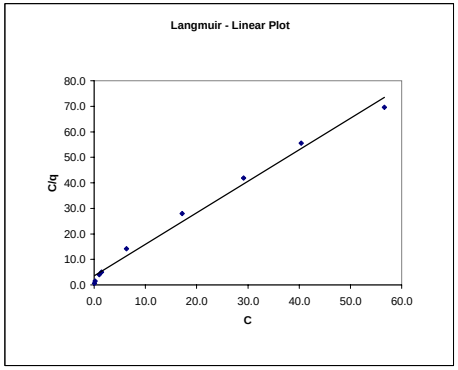

Adsorption Isotherm - DBT in Hexadecane

Sorbent: Activated Carbon - Norit

Temperature = 50°C

Duration: 24 Hours

Sorbent particle size: 125µ <<250µ

ACN - 125µ

Bulk Solution (DBT + C16)			Conc. Final		Sorbent	Plot data		Linear Plot - Langmuir	
C solution	*weight of Soln*	*n solution*	*C solution*	*n solution*	*weight*	*C solution*	*q*	C	C/q
mmol/L	*g*	*mmol*	*mmol/L*	*mmol*	*g*	*mmol/L*	*mmol/g*		
72.370	4.942	0.463	51.79	0.33	0.2867	51.790	0.459	51.790	112.855
56.640	5.177	0.379	38.47	0.26	0.2584	38.470	0.471	38.470	81.695
46.330	4.619	0.277	29.50	0.18	0.2320	29.500	0.433	29.500	68.060
30.640	4.571	0.181	17.24	0.10	0.1773	17.240	0.447	17.240	38.580
22.400	4.715	0.137	12.07	0.07	0.1560	12.070	0.404	12.070	29.886
10.740	5.187	0.072	3.94	0.03	0.1530	3.940	0.298	3.940	13.211
5.350	4.550	0.031	0.95	0.01	0.1620	0.950	0.160	0.950	5.943
2.560	4.946	0.016	0.13	0.0008	0.1161	0.130	0.134	0.130	0.971
1.420	5.097	0.009	0.04	0.0003	0.0972	0.040	0.094	0.040	0.427
								Intercept	2.700
								Slope	2.124
								qm	0.471
								K	0.787
								R^2	0.997

Linear Plot - Freundlich	
log (C)	**log (q)**
1.714	-0.338
1.585	-0.327
1.470	-0.363
1.237	-0.350
1.082	-0.394
0.595	-0.525
-0.022	-0.796
-0.886	-0.873
-1.398	-1.029
K	0.201
n	4.229
R^2	0.969

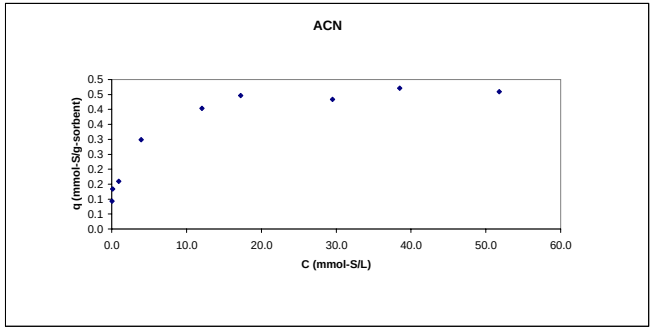

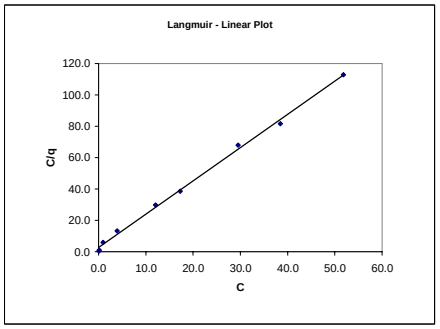

Adsorption Isotherm - DBT in Hexadecane

Sorbent: ACC

Temperature = 50°C

Duration: 24 Hours

Sorbent particle size: 250µ<<500µ

ACC-250 µ

Bulk Solution (DBT + C16)			Conc. Final		Sorbent	Plot data		Linear Plot - Langmuir	
C solution	*weight of Soln*	*n solution*	*C solution*	*n solution*	*weight*	*C solution*	*q*	C	C/q
mmol/L	*g*	*mmol*	*mmol/L*	*mmol*	*g*	*mmol/L*	*mmol/g*		
72.370	5.027	0.471	21.40	0.14	0.6877	21.400	0.482	21.400	44.403
56.640	4.989	0.366	17.30	0.11	0.5110	17.300	0.497	17.300	34.819
46.330	5.428	0.325	15.14	0.11	0.4500	15.140	0.487	15.140	31.110
30.640	5.209	0.206	10.25	0.07	0.3416	10.250	0.402	10.250	25.484
22.400	4.856	0.141	7.62	0.05	0.2412	7.620	0.385	7.620	19.797
10.740	5.361	0.074	0.72	0.0050	0.3662	0.720	0.190	0.720	3.794
5.350	5.022	0.035	0.13	0.0008	0.2231	0.130	0.152	0.130	0.855
2.560	4.293	0.014	0.10	0.0006	0.1343	0.100	0.102	0.100	0.983
1.420	4.827	0.009	0.01	0.0001	0.2255	0.010	0.039	0.010	0.256
								Intercept	1.684
								Slope	2.014
								qm	0.497
								K	1.196
								R^2	0.989

Linear Plot - Freundlich	
log (C)	**log (q)**
1.330	-0.317
1.238	-0.304
1.180	-0.313
1.011	-0.396
0.882	-0.415
-0.143	-0.722
-0.886	-0.818
-1.000	-0.993
-2.000	-1.408
K	0.206
n	3.226
R^2	0.972

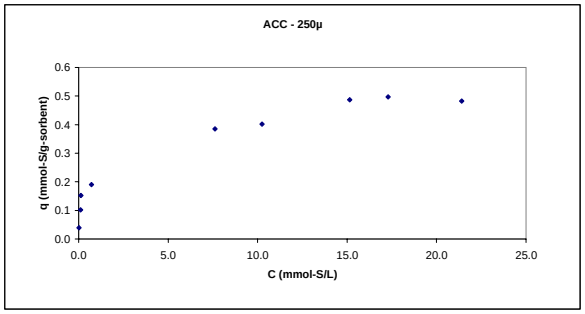

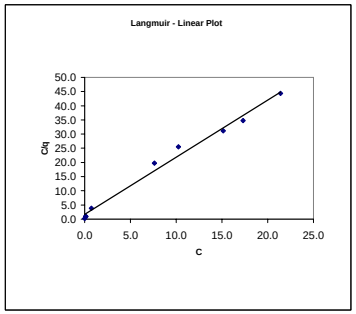

Adsorption Isotherm - DBT in Hexadecane

Sorbent: Ga (2% wt.) on ACC

Temperature = 50°C

Duration: 24 Hours

Sorbent particle size: <125µ

Ga/ACC

Bulk Solution (DBT + C16)			Conc. Final		Sorbent	Plot data		Linear Plot - Langmuir	
C solution	*weight of Soln*	*n solution*	*C solution*	*n solution*	*weight*	*C solution*	*q*	C	C/q
mmol/L	*g*	*mmol*	*mmol/L*	*mmol*	*g*	*mmol/L*	*mmol/g*		
72.370	5.095	0.477	55.39	0.37	0.164	55.390	0.685	55.390	80.920
56.640	5.138	0.376	37.04	0.25	0.166	37.040	0.785	37.040	47.195
46.330	5.243	0.314	30.78	0.21	0.133	30.780	0.795	30.780	38.725
30.640	5.300	0.210	21.08	0.14	0.096	21.080	0.683	21.080	30.875
22.400	5.263	0.152	8.24	0.06	0.183	8.240	0.527	8.240	15.642
10.740	5.076	0.071	1.78	0.01	0.183	1.780	0.321	1.780	5.540
5.350	4.636	0.032	1.20	0.01	0.092	1.200	0.271	1.200	4.426
2.560	4.965	0.016	0.30	0.00	0.091	0.300	0.160	0.300	1.879
1.420	5.376	0.010	0.02	0.00	0.141	0.020	0.069	0.020	0.289
								Intercept	1.761
								Slope	1.345
								qm	0.743
								K	0.764
								R^2	0.987

Linear Plot - Freundlich	
log (C)	**log (q)**
1.743	-0.165
1.569	-0.105
1.488	-0.100
1.324	-0.166
0.916	-0.278
0.250	-0.493
0.079	-0.567
-0.523	-0.797
-1.699	-1.160
K	0.248
n	3.177
R^2	0.984

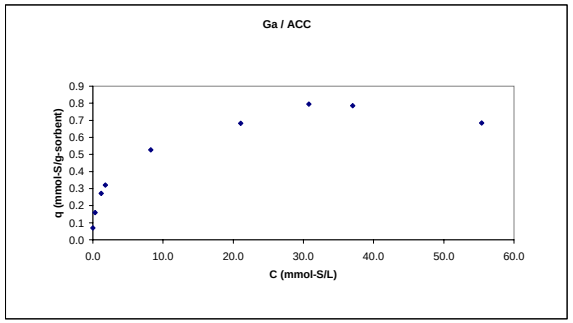

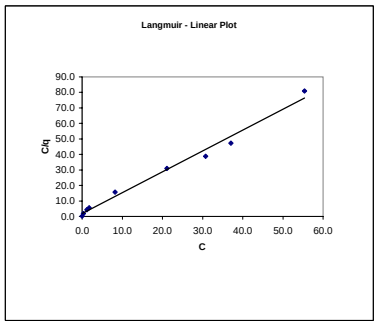

Adsorption Isotherm - DBT in Hexadecane

Sorbent: Sn (2% wt.) on ACC

Temperature = 50°C

Duration: 24 Hours

Sorbent particle size: <125µ

Sn/ACC

Bulk Solution (DBT + C16)			Conc. Final		Sorbent	Plot data		Linear Plot - Langmuir	
C solution	*weight of Soln*	*n solution*	*C solution*	*n solution*	*weight*	*C solution*	*q*	C	C/q
mmol/L	*g*	*mmol*	*mmol/L*	*mmol*	*g*	*mmol/L*	*mmol/g*		
72.370	5.159	0.483	58.34	0.39	0.1095	58.340	0.855	58.340	68.225
56.640	5.758	0.422	40.42	0.30	0.1514	40.420	0.798	40.420	50.649
46.330	5.090	0.305	31.02	0.20	0.1400	31.020	0.720	31.020	43.076
30.640	5.100	0.202	20.07	0.13	0.1132	20.070	0.616	20.070	32.576
22.400	4.966	0.144	12.80	0.08	0.1200	12.800	0.514	12.800	24.905
10.740	5.361	0.074	3.87	0.03	0.1198	3.870	0.398	3.870	9.732
5.350	4.761	0.033	1.51	0.01	0.0926	1.510	0.255	1.510	5.912
2.560	5.339	0.018	0.48	0.00	0.0869	0.480	0.165	0.480	2.903
1.420	4.907	0.009	0.06	0.00	0.1079	0.060	0.080	0.060	0.750
								Intercept	5.136
								Slope	1.142
								qm	0.876
								K	0.222
								R^2	0.979

Linear Plot - Freundlich	
log (C)	**log (q)**
1.766	-0.068
1.607	-0.098
1.492	-0.143
1.303	-0.210
1.107	-0.289
0.588	-0.400
0.179	-0.593
-0.319	-0.782
-1.222	-1.097
K	0.219
n	2.880
R^2	0.996

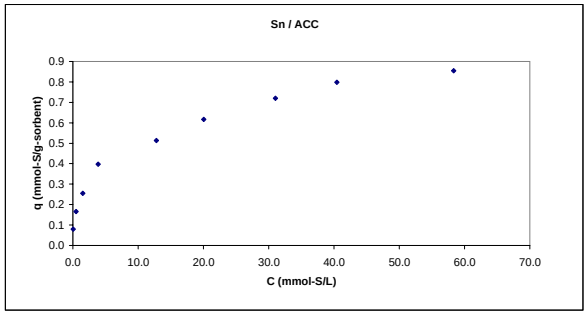

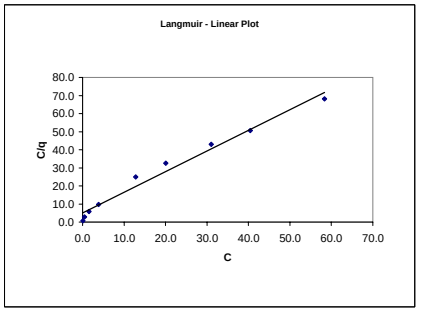

Adsorption Isotherm - DBT in Hexadecane

Sorbent: Sr (2% wt.) on ACC

Temperature = 50°C

Duration: 24 Hours

Sorbent particle size: <125µ

Sr/ACC

Bulk Solution (DBT + C16)			Conc. Final		Sorbent	Plot data		Linear Plot - Langmuir	
C solution	*weight of Soln*	*n solution*	*C solution*	*n solution*	*weight*	*C solution*	*q*	C	C/q
mmol/L	*g*	*mmol*	*mmol/L*	*mmol*	*g*	*mmol/L*	*mmol/g*		
72.370	5.261	0.493	61.40	0.418	0.1181	61.400	0.632	61.400	97.129
56.640	5.546	0.406	44.02	0.316	0.1339	44.020	0.676	44.020	65.096
46.330	5.120	0.307	37.93	0.251	0.0834	37.930	0.667	37.930	56.855
30.640	5.523	0.219	20.42	0.146	0.1257	20.420	0.581	20.420	35.153
22.400	5.758	0.167	17.64	0.131	0.0656	17.640	0.540	17.640	32.637
10.740	5.278	0.073	4.45	0.030	0.1121	4.450	0.383	4.450	11.615
5.350	4.848	0.034	1.67	0.010	0.0809	1.670	0.285	1.670	5.854
2.560	5.119	0.017	0.54	0.004	0.0668	0.540	0.200	0.540	2.697
1.420	5.660	0.010	0.20	0.001	0.0655	0.200	0.136	0.200	1.466
								Intercept	3.162
								Slope	1.487
								qm	0.672
								K	0.470
								R^2	0.994

Linear Plot - Freundlich	
log (C)	**log (q)**
1.788	-0.199
1.644	-0.170
1.579	-0.176
1.310	-0.236
1.246	-0.267
0.648	-0.417
0.223	-0.545
-0.268	-0.698
-0.699	-0.865
K	0.235
n	3.582
R^2	0.982

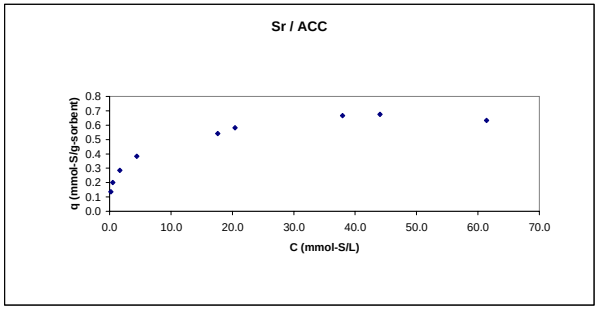

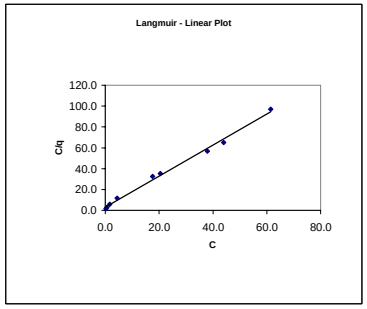

Adsorption Isotherm - DBT in Hexadecane

Sorbent: ACC

Temperature = 50°C

Duration: 24 Hours

Sorbent particle size: <125µ

ACC (<125µ)

Bulk Solution (DBT + C16)			Conc. Final		Sorbent	Plot data		Linear Plot - Langmuir	
C solution	*weight of Soln*	*n solution*	*C solution*	*n solution*	*weight*	*C solution*	*q*	C	C/q
mmol/L	*g*	*mmol*	*mmol/L*	*mmol*	*g*	*mmol/L*	*mmol/g*		
66.390	5.022	0.431	55.77	0.36	0.100	55.770	0.691	55.770	80.674
51.650	5.075	0.339	38.64	0.25	0.110	38.640	0.778	38.640	49.675
41.680	5.312	0.286	30.61	0.21	0.105	30.610	0.727	30.610	42.091
26.810	5.012	0.174	17.18	0.11	0.104	17.180	0.598	17.180	28.725
20.840	5.633	0.152	13.17	0.10	0.100	13.170	0.560	13.170	23.515
9.260	5.171	0.062	4.78	0.03	0.078	4.780	0.383	4.780	12.490
4.730	5.601	0.034	0.83	0.01	0.118	0.830	0.240	0.830	3.457
2.790	5.504	0.020	0.64	0.00	0.065	0.640	0.234	0.640	2.734
1.420	5.508	0.010	0.04	0.00	0.109	0.040	0.090	0.040	0.443
								Intercept	3.007
								Slope	1.341
								qm	0.746
								K	0.446
								R^2	0.987

Linear Plot - Freundlich	
log (C)	**log (q)**
1.746	-0.160
1.587	-0.109
1.486	-0.138
1.235	-0.223
1.120	-0.252
0.679	-0.417
-0.081	-0.620
-0.194	-0.631
-1.398	-1.044
K	0.249
n	3.372
R^2	0.988

Modified Langmuir		
$(1/C)^K$	1/q	X
0.134	1.447	0.500
0.161	1.286	
0.181	1.375	
0.241	1.672	
0.276	1.786	
0.457	2.613	
1.098	4.165	
1.250	4.272	
5.000	11.075	
Intercept	1.352	
Slope	1.991	
qmax	0.739	
K	0.679	
R^2	0.9862	

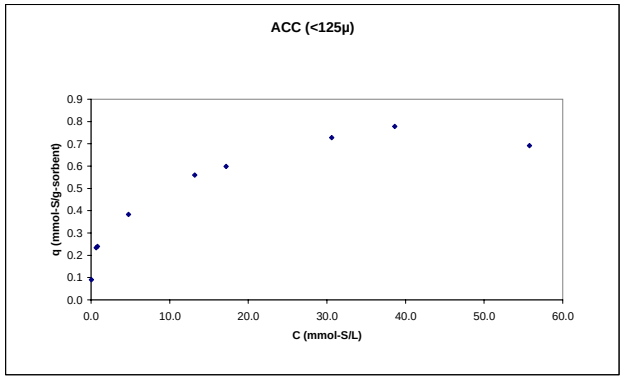

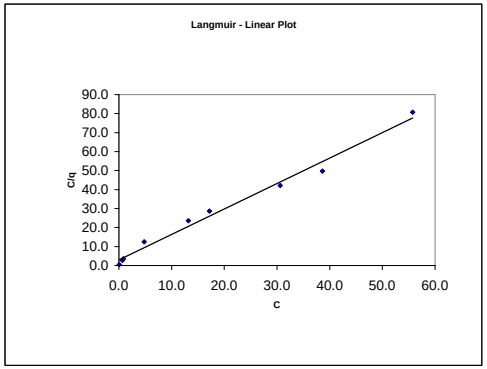

Adsorption Isotherm - DBT in Hexadecane

Sorbent: Ta (2% wt.) on ACC

Temperature = 50°C

Duration: 24 Hours

Sorbent particle size: <125µ

Ta - 2 / ACC

Bulk Solution (DBT + C16)			Conc. Final		Sorbent	Plot data		Linear Plot - Langmuir	
C solution	*weight of Soln*	*n solution*	*C solution*	*n solution*	*weight*	*C solution*	*q*	C	C/q
mmol/L	*g*	*mmol*	*mmol/L*	*mmol*	*g*	*mmol/L*	*mmol/g*		
66.390	4.650	0.399	50.87	0.3060	0.0814	50.870	1.147	50.870	44.349
51.650	5.392	0.360	34.20	0.2386	0.1513	34.200	0.805	34.200	42.511
41.680	5.559	0.300	26.62	0.1914	0.1500	26.620	0.722	26.620	36.872
26.810	5.111	0.177	13.61	0.0900	0.1673	13.610	0.522	13.610	26.089
20.840	4.874	0.131	12.31	0.0776	0.1021	12.310	0.527	12.310	23.369
9.260	5.054	0.061	3.29	0.0215	0.1196	3.290	0.326	3.290	10.081
4.730	4.766	0.029	0.65	0.0040	0.1355	0.650	0.186	0.650	3.501
2.790	4.453	0.016	0.40	0.0023	0.1002	0.400	0.137	0.400	2.911
								Intercept	8.211
								Slope	0.874
								qm	1.145
								K	0.106
								R^2	0.882

Linear Plot - Freundlich	
log (C)	**log (q)**
1.706	0.060
1.534	-0.094
1.425	-0.141
1.134	-0.283
1.090	-0.278
0.517	-0.486
-0.187	-0.731
-0.398	-0.862
K	0.203
n	2.506
R^2	0.987

Modified Langmuir		
$(1/C)^X$	**1/q**	**X**
0.102	0.872	0.580
0.129	1.243	
0.149	1.385	
0.220	1.917	
0.233	1.898	
0.501	3.064	
1.284	5.386	
1.701	7.277	
Intercept	0.874	
Slope	3.715	
qmax	1.144	
K	0.235	
R^2	0.9886	

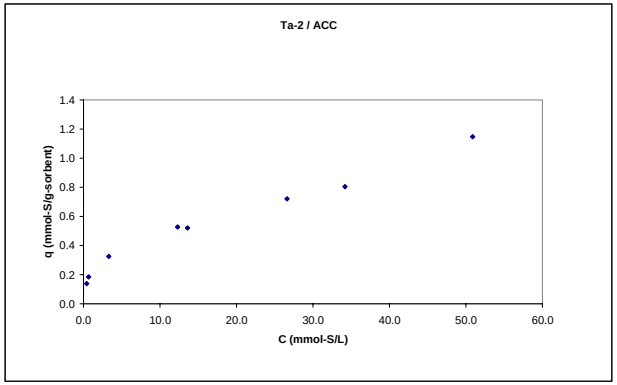

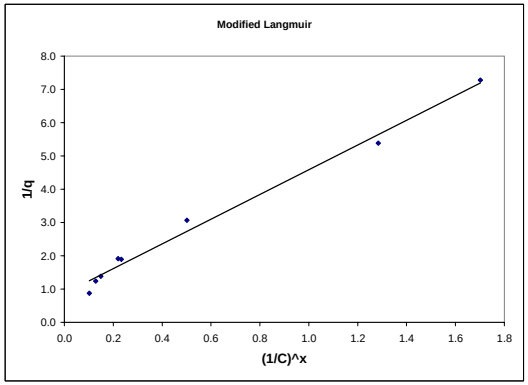

Adsorption Isotherm - DBT in Hexadecane

Sorbent: Ta (10% wt.) on ACC

Temperature = 50°C

Duration: 24 Hours

Sorbent particle size: <125µ

Ta-10 / ACC

Bulk Solution (DBT + C16)		Conc. Final		Sorbent	Sulfur in Solution		Langmuir	
C solution	*weight of Soln*	*C solution*	*n solution*	*weight*	*C (remaining)*	*C (removed)*	*q*	*C/q*
ppm	*g*	*ppm*	*ppm*	*g*	*mmol/L*	*mmol/L*	*mmol/g*	
3096.0	5.379	2394.96	701.05	0.127	57.853	16.935	0.928	62.348
2145.0	4.670	1648.93	496.07	0.111	39.832	11.983	0.652	61.078
1914.0	5.490	1469.88	444.13	0.118	35.507	10.728	0.644	55.170
1143.0	5.317	705.91	437.10	0.152	17.052	10.559	0.478	35.645
880.9	4.920	599.67	281.23	0.099	14.486	6.793	0.437	33.168
403.3	4.754	184.33	218.98	0.094	4.453	5.290	0.345	12.921
200.6	5.397	60.26	140.35	0.099	1.456	3.390	0.240	6.069
102.3	5.000	16.13	86.17	0.088	0.390	2.082	0.154	2.535
52.6	5.049	1.50	51.11	0.087	0.036	1.235	0.093	0.390
20.0	4.846	0.08	19.93	0.124	0.002	0.481	0.024	0.074
							Intercept	6.425
							Slope	1.199
							qm	0.834
							K	0.187
							R^2	0.911

Freundlich	
log (C)	**log (q)**
1.762	-0.032
1.600	-0.186
1.550	-0.191
1.232	-0.320
1.161	-0.360
0.649	-0.463
0.163	-0.620
-0.409	-0.813
-1.442	-1.033
-2.742	-1.613
K	0.211
n	3.127
R^2	0.987

Modified Langmuir		
$(1/C)^X$	**1/q**	**X**
0.189	1.078	0.410
0.221	1.533	
0.231	1.554	
0.313	2.090	
0.334	2.290	
0.542	2.902	
0.857	4.170	
1.472	6.506	
3.903	10.790	
13.310	41.061	
Intercept	1.031	
Slope	2.979	
qmax	0.970	
K	0.346	
R^2	0.9958	

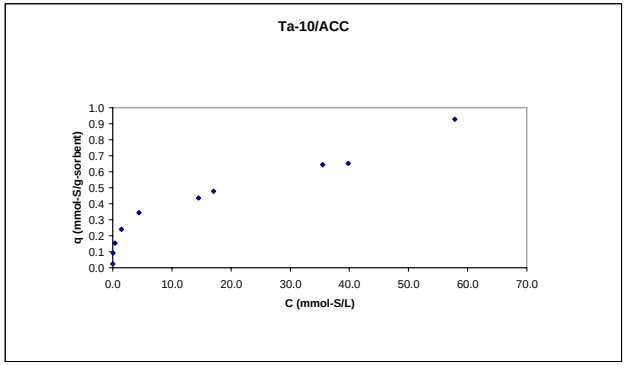

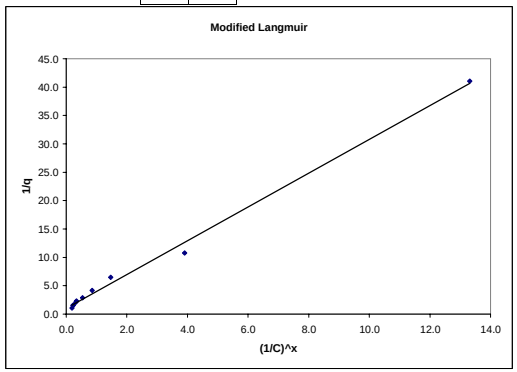

Adsorption Isotherm - DBT in Hexadecane

Sorbent: Ta (5% wt.) on ACC

Temperature = 50°C

Duration: 24 Hours

Sorbent particle size: <125µ

Ta-5 / ACC

Bulk Solution (DBT + C16)		Conc. Final		Sorbent	Sulfur in Solution		Langmuir	
C solution	*weight of Soln*	*C solution*	*n solution*	*weight*	*C (remaining)*	*C (removed)*	*q*	*C/q*
ppm	*g*	*ppm*	*ppm*	*g*	*mmol/L*	*mmol/L*	*mmol/g*	
3096.0	5.194	2128.21	967.80	0.1224	51.409	23.378	1.283	40.058
2145.0	5.583	1601.81	543.19	0.1117	38.694	13.121	0.848	45.608
1914.0	4.818	1412.35	501.65	0.0943	34.117	12.118	0.801	42.600
1143.0	5.438	785.74	357.27	0.1010	18.980	8.630	0.601	31.575
880.9	4.988	445.36	435.54	0.1288	10.758	10.521	0.527	20.410
403.3	5.370	153.46	249.85	0.1128	3.707	6.035	0.372	9.973
200.6	5.507	47.75	152.86	0.1048	1.153	3.692	0.251	4.595
102.3	5.527	12.20	90.10	0.0997	0.295	2.176	0.156	1.888
52.6	5.422	3.10	49.51	0.0860	0.075	1.196	0.098	0.767
							Intercept	6.232
							Slope	0.888
							qm	1.126
							K	0.143
							R²	0.869

Freundlich	
log (C)	**log (q)**
1.711	0.108
1.588	-0.071
1.533	-0.096
1.278	-0.221
1.032	-0.278
0.569	-0.430
0.062	-0.600
-0.531	-0.807
-1.126	-1.011
K	0.238
n	2.782
R²	0.982

Modified Langmuir		
$(1/C)^X$	**1/q**	**X**
0.170	0.779	0.450
0.193	1.179	
0.204	1.249	
0.266	1.664	
0.343	1.897	
0.555	2.690	
0.938	3.984	
1.733	6.407	
3.212	10.253	
Intercept	0.765	
Slope	3.050	
qmax	1.308	
K	0.251	
R²	0.9908	

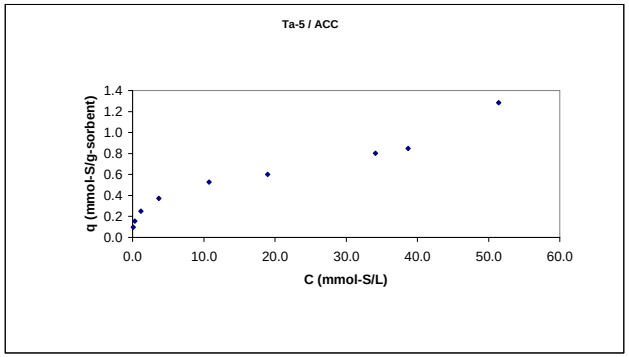

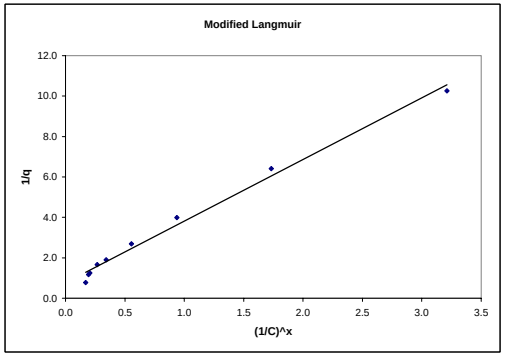

Adsorption Isotherm - DBT in Hexadecane

Sorbent: Co (2% wt.) on ACC

Temperature = 50°C

Duration: 24 Hours

Sorbent particle size: <125µ

Co/ACC

Bulk Solution (DBT + C16)			Conc. Final		Sorbent	Plot data		Linear Plot - Langmuir	
C solution	*weight of Sols*	*n solution*	*C solution*	*n solution*	*weight*	*C solution*	*q*	C	C/q
mmol/L	*g*	*mmol*	*mmol/L*	*mmol*	*g*	*mmol/L*	*mmol/g*		
72.370	5.425	0.508	64.700	0.4541	0.07	64.700	0.781	64.700	82.818
56.640	4.921	0.361	45.130	0.2873	0.09	45.130	0.778	45.130	58.015
46.330	5.476	0.328	35.930	0.2545	0.11	35.930	0.682	35.930	52.715
30.640	4.921	0.195	22.280	0.1418	0.08	22.280	0.630	22.280	35.377
22.400	5.322	0.154	10.730	0.0739	0.15	10.730	0.537	10.730	19.967
10.740	5.048	0.070	3.000	0.0196	0.14	3.000	0.359	3.000	8.351
5.350	4.809	0.033	0.910	0.0057	0.11	0.910	0.247	0.910	3.687
2.560	3.466	0.011	0.080	0.0004	0.11	0.080	0.101	0.080	0.794
1.420	5.084	0.009	0.030	0.0002	0.11	0.030	0.082	0.030	0.366
								Intercept	3.503
								Slope	1.261
								qm	0.793
								K	0.360
								R^2	0.990

Linear Plot - Freundlich	
log (C)	**log (q)**
1.811	-0.107
1.654	-0.109
1.555	-0.166
1.348	-0.201
1.031	-0.270
0.477	-0.445
-0.041	-0.608
-1.097	-0.997
-1.523	-1.086
K	0.240
n	3.265
R^2	0.994

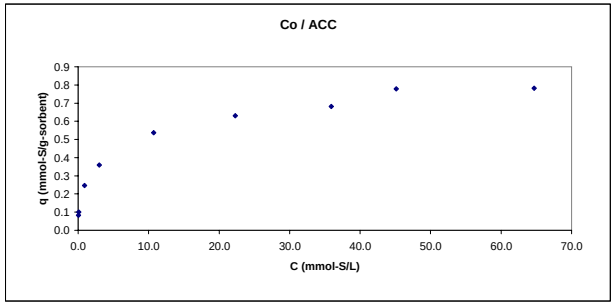

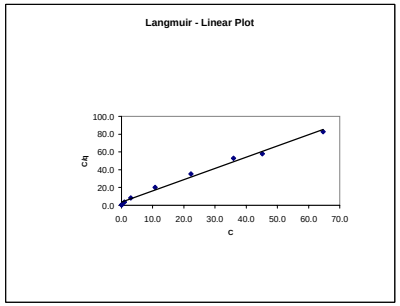

Adsorption Isotherm - DBT in Hexadecane

Sorbent: ACC

Temperature = 50°C

Duration: 24 Hours

Sorbent particle size: 125µ <<250µ

ACC - 125µ

Bulk Solution (DBT + C16)			Conc. Final		Sorbent	Plot data		Linear Plot - Langmuir	
C solution	*weight of Soln*	*n solution*	*C solution*	*n solution*	*weight*	*C solution*	*q*	C	C/q
mmol/L	*g*	*mmol*	*mmol/L*	*mmol*	*g*	*mmol/L*	*mmol/g*		
39.080	5.215	0.264	12.89	0.09	0.351	12.890	0.504	12.890	25.586
31.460	4.978	0.203	7.91	0.05	0.347	7.910	0.437	7.910	18.092
23.080	5.346	0.160	1.78	0.01	0.551	1.780	0.267	1.780	6.657
9.570	5.223	0.065	0.72	0.0049	0.304	0.720	0.196	0.720	3.665
5.210	4.871	0.033	0.38	0.0024	0.191	0.380	0.159	0.380	2.389
2.630	5.221	0.018	0.02	0.0001	0.352	0.020	0.050	0.020	0.399
1.450	5.170	0.010	0.02	0.0001	0.206	0.020	0.047	0.020	0.430
0.570	4.995	0.004	0.03	0.0002	0.197	0.030	0.018	0.030	1.689
0.310	5.172	0.002	0.02	0.0001	0.137	0.020	0.014	0.020	1.413
								Intercept	1.583
								Slope	1.938
								qm	0.516
								K	1.225
								R^2	0.987

Linear Plot - Freundlich	
log (C)	**log (q)**
1.110	-0.298
0.898	-0.359
0.250	-0.573
-0.143	-0.707
-0.420	-0.798
-1.699	-1.300
-1.699	-1.332
-1.523	-1.751
-1.699	-1.849
K	0.183
n	2.111
R^2	0.880

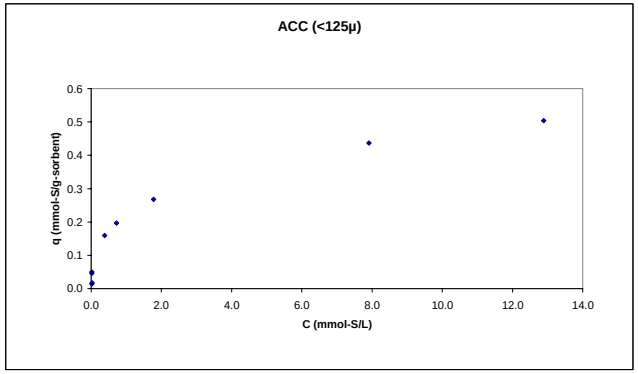

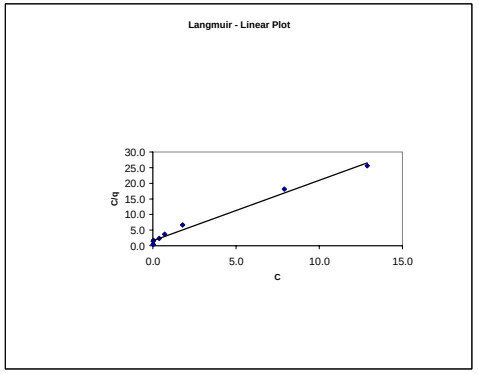

Adsorption Isotherm - DBT in Hexadecane

Sorbent: Acid-washed activated carbon

Temperature = 50°C

Duration: 24 Hours

Sorbent particle size: 125µ <<250µ

AAC (125µ) - Dried

Bulk Solution (DBT + C16)			Conc. Final		Sorbent	Plot data		Linear Plot - Langmuir	
C solution	*weight of Soln*	*n solution*	*C solution*	*n solution*	*weight*	*C solution*	*q*	C	C/q
mmol/L	*g*	*mmol*	*mmol/L*	*mmol*	*g*	*mmol/L*	*mmol/g*		
39.080	5.035	0.255	24.19	0.16	0.269	24.190	0.361	24.190	66.998
31.460	4.950	0.201	18.21	0.12	0.258	18.210	0.329	18.210	55.306
23.080	5.128	0.153	12.61	0.08	0.202	12.610	0.343	12.610	36.745
9.570	4.965	0.061	1.67	0.011	0.318	1.670	0.159	1.670	10.472
5.210	5.180	0.035	1.08	0.007	0.194	1.080	0.143	1.080	7.574
2.630	5.075	0.017	0.07	0.0005	0.178	0.070	0.094	0.070	0.741
								Intercept	3.754
								Slope	2.686
								qm	0.372
								K	0.715
								R²	0.993

Linear Plot - Freundlich	
log (C)	**log (q)**
1.384	-0.442
1.260	-0.482
1.101	-0.464
0.223	-0.797
0.033	-0.846
-1.155	-1.025
K	0.161
n	4.056
R²	0.956

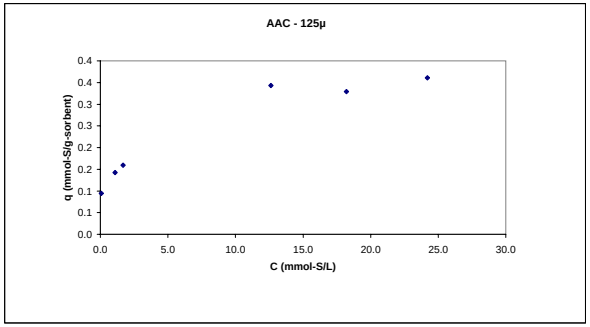

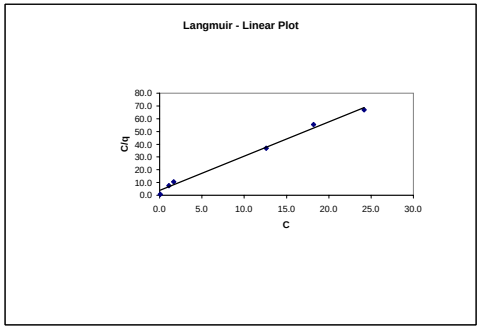

Adsorption Isotherm - DBT in Hexadecane

Sorbent: Ni (2% wt.) on ACC

Temperature = 50°C

Duration: 24 Hours

Sorbent particle size: <125µ

Ni/ACC

Bulk Solution (DBT + C16)			Conc. Final		Sorbent	Plot data		Linear Plot - Langmuir	
C solution	*weight of Soln*	*n solution*	*C solution*	*n solution*	*weight*	*C solution*	*q*	C	C/q
mmol/L	*g*	*mmol*	*mmol/L*	*mmol*	*g*	*mmol/L*	*mmol/g*		
72.370	5.610	0.525	56.270	0.41	0.1500	56.270	0.779	56.270	72.239
56.640	5.674	0.416	38.970	0.29	0.1842	38.970	0.704	38.970	55.342
46.330	5.347	0.320	34.860	0.24	0.1156	34.860	0.686	34.860	50.790
30.640	5.123	0.203	16.980	0.11	0.1429	16.980	0.634	16.980	26.800
22.400	5.028	0.146	13.280	0.09	0.1077	13.280	0.551	13.280	24.112
10.740	5.023	0.070	4.600	0.03	0.0990	4.600	0.403	4.600	11.414
5.350	5.107	0.035	1.790	0.01	0.0767	1.790	0.307	1.790	5.838
2.560	5.115	0.017	0.600	0.00	0.0640	0.600	0.203	0.600	2.961
1.420	5.164	0.009	0.160	0.00	0.0657	0.160	0.128	0.160	1.249
								Intercept	4.166
								Slope	1.273
								qm	0.785
								K	0.306
								R^2	0.991

Linear Plot - Freundlich	
log (C)	**log (q)**
1.750	-0.108
1.591	-0.152
1.542	-0.163
1.230	-0.198
1.123	-0.259
0.663	-0.395
0.253	-0.513
-0.222	-0.693
-0.796	-0.892
K	0.241
n	3.254
R^2	0.990

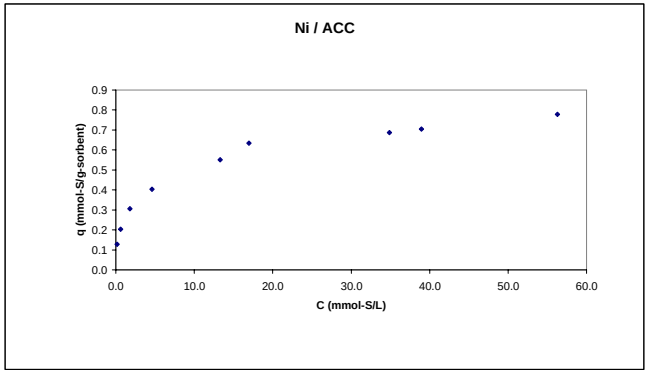

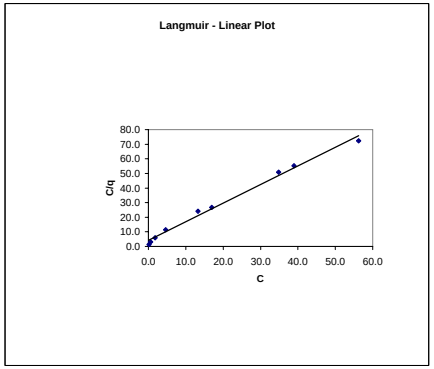

Adsorption Isotherm - DBT in Hexadecane

Sorbent: ACC

Temperature = 50°C

Duration: 24 Hours

Sorbent particle size: 250μ<<500μ

ACC-250 μ

Bulk Solution (DBT + C16)			Conc. Final		Sorbent	Plot data		Linear Plot - Langmuir	
C solution	*weight of Soln*	*n solution*	*C solution*	*n solution*	*weight*	*C solution*	*q*	C	C/q
mmol/L	*g*	*mmol*	*mmol/L*	*mmol*	*g*	*mmol/L*	*mmol/g*		
66.390	5.787	0.497	62.50	0.47	0.0814	62.500	0.358	62.500	174.701
51.650	5.826	0.389	46.28	0.35	0.0919	46.280	0.440	46.280	105.080
41.680	5.306	0.286	34.64	0.24	0.1132	34.640	0.427	34.640	81.139
26.810	5.056	0.175	21.40	0.14	0.0900	21.400	0.393	21.400	54.435
20.840	5.911	0.159	16.01	0.12	0.0997	16.010	0.370	16.010	43.217
9.260	5.631	0.067	5.88	0.04	0.0869	5.880	0.283	5.880	20.753
4.730	6.334	0.039	2.46	0.02	0.0801	2.460	0.232	2.460	10.593
2.790	6.294	0.023	1.20	0.01	0.0779	1.200	0.166	1.200	7.221
1.420	5.950	0.011	0.24	0.002	0.0751	0.240	0.121	0.240	1.984
								Intercept	1.886
								Slope	2.529
								qm	0.395
								K	1.341
								R^2	0.980

Linear Plot - Freundlich	
log (C)	**log (q)**
1.796	-0.446
1.665	-0.356
1.540	-0.370
1.330	-0.405
1.204	-0.431
0.769	-0.548
0.391	-0.634
0.079	-0.779
-0.620	-0.917
K	0.176
n	4.290
R^2	0.935

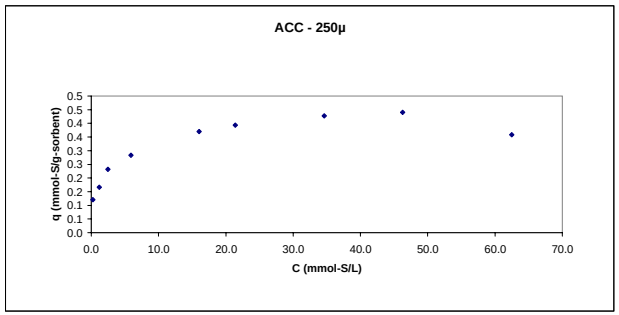

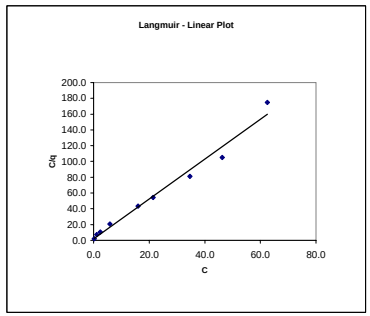

Adsorption Isotherm - DBT in Hexadecane

Sorbent: Sn (2% wt.) on ACC

Temperature = 50°C

Duration: 24 Hours

Sorbent particle size: <125µ

Sn/ACC

Bulk Solution (DBT + C16)			Conc. Final		Sorbent	Plot data		Linear Plot - Langmuir	
C solution	*weight of Soln*	*n solution*	*C solution*	*n solution*	*weight*	*C solution*	*q*	C	C/q
mmol/L	*g*	*mmol*	*mmol/L*	*mmol*	*g*	*mmol/L*	*mmol/g*		
72.370	5.159	0.483	52.890	0.35	0.1566	52.890	0.830	52.890	63.709
56.640	5.758	0.422	33.880	0.25	0.2331	33.880	0.727	33.880	46.582
46.330	5.090	0.305	30.610	0.20	0.1460	30.610	0.709	30.610	43.173
30.640	5.100	0.202	20.680	0.14	0.1221	20.680	0.538	20.680	38.423
22.400	4.966	0.144	15.720	0.10	0.0932	15.720	0.460	15.720	34.140
10.740	5.361	0.074	4.895	0.03	0.1320	4.895	0.307	4.895	15.941
5.350	4.761	0.033	0.995	0.01	0.1322	0.995	0.203	0.995	4.904
2.560	5.339	0.018	0.720	0.00	0.0869	0.720	0.146	0.720	4.923
1.420	4.907	0.009	0.250	0.00	0.1079	0.250	0.069	0.250	3.632
								Intercept	7.813
								Slope	1.152
								qm	0.868
								K	0.147
								R^2	0.949

Linear Plot - Freundlich	
log (C)	**log (q)**
1.723	-0.081
1.530	-0.138
1.486	-0.149
1.316	-0.269
1.196	-0.337
0.690	-0.513
-0.002	-0.693
-0.143	-0.835
-0.602	-1.162
K	0.156
n	2.338
R^2	0.975

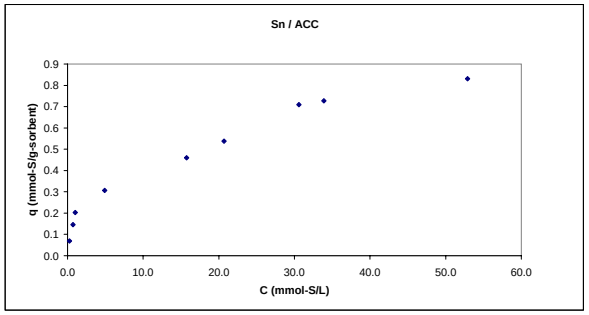

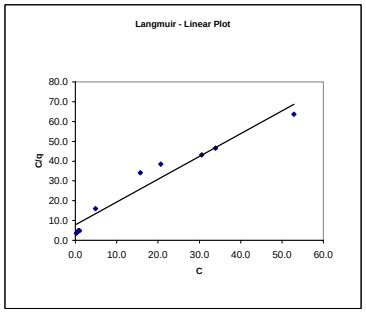

Adsorption Isotherm - DBT in Hexadecane

Sorbent: ACC

Temperature = 50°C

Duration: 24 Hours

Sorbent particle size: <125µ

ACC (<125µ)

Bulk Solution (DBT + C16)			Conc. Final		Sorbent	Linear Plot - Langmuir			
C solution	*weight of Soln*	*n solution*	*C solution*	*n solution*	*weight*	*C (remaining)*	*C (removed)*	*q*	*C/q*
mmol/L	*g*	*mmol*	*mmol/L*	*mmol*	*g*	*mmol/L*	*mmol/L*	*mmol/g*	
66.390	4.890	13.690	52.700	0.33	0.1211	52.700	13.690	0.715	73.698
51.650	5.194	16.100	35.550	0.24	0.1566	35.550	16.100	0.691	51.460
41.680	4.496	13.075	28.605	0.17	0.1114	28.605	13.075	0.683	41.903
26.810	4.883	7.040	19.770	0.12	0.0681	19.770	7.040	0.653	30.274
20.840	5.336	8.665	12.175	0.08	0.1096	12.175	8.665	0.546	22.311
9.260	4.739	5.815	3.445	0.02	0.0996	3.445	5.815	0.358	9.625
4.730	4.718	3.895	0.835	0.01	0.1020	0.835	3.895	0.233	3.582
2.790	4.513	1.955	0.835	0.00	0.0511	0.835	1.955	0.223	3.738
1.420	4.744	1.020	0.400	0.00	0.0347	0.400	1.020	0.180	2.217
								Intercept	3.427
								Slope	1.348
								qm	0.742
								K	0.393
								R^2	0.997

Freundlich	
log (C)	**log (q)**
1.722	-0.146
1.551	-0.161
1.456	-0.166
1.296	-0.185
1.085	-0.263
0.537	-0.446
-0.078	-0.632
-0.078	-0.651
-0.398	-0.744
K	0.244
n	3.335
R^2	0.989

Modified Langmuir		
$(1/C)^K$	1/q	X
0.079	1.398	0.640
0.102	1.448	
0.117	1.465	
0.148	1.531	
0.202	1.833	
0.453	2.794	
1.122	4.290	
1.122	4.477	
1.798	5.544	
Intercept	1.295	
Slope	2.552	
qmax	0.772	
K	0.507	
R^2	0.9802	

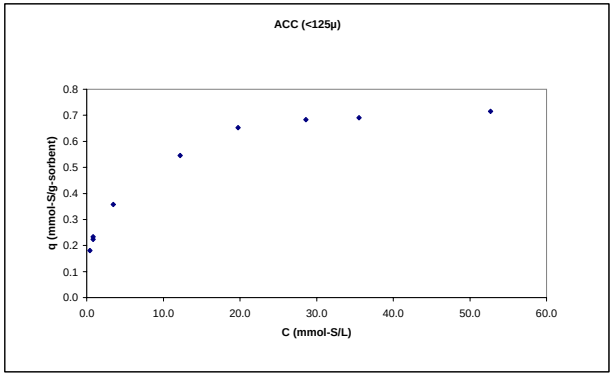

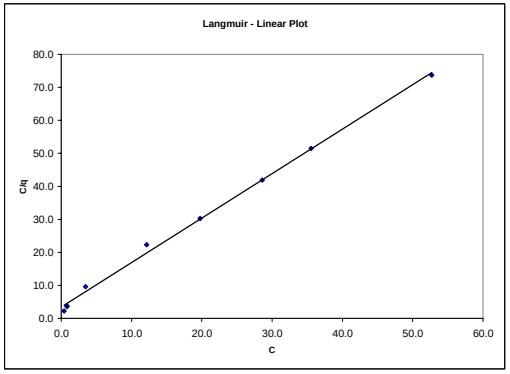

Adsorption Isotherm - DBT in Hexadecane

Sorbent: Ta (2% wt.) on ACC

Temperature = 50°C

Duration: 24 Hours

Sorbent particle size: <125µ

Ta-2 / ACC

Bulk Solution (DBT + C16)		Conc. Final		Sorbent	Sulfur in Solution		Langmuir	
C solution	*weight of Soln*	*C solution*	*n solution*	*weight*	*C (remaining)*	*C (removed)*	*q*	*C/q*
ppm	*g*	*ppm*	*ppm*	*g*	*mmol/L*	*mmol/L*	*mmol/g*	
3096.0	5.300	2438.700	657.30	0.1060	58.910	15.878	1.027	57.359
2145.0	5.087	1421.480	723.52	0.1660	34.338	17.478	0.693	49.559
1914.0	4.882	1301.975	612.03	0.1384	31.451	14.784	0.675	46.622
1143.0	5.185	690.520	452.48	0.1402	16.680	10.930	0.523	31.896
880.9	4.769	399.810	481.09	0.1543	9.658	11.621	0.465	20.787
403.3	5.284	140.030	263.27	0.1243	3.383	6.360	0.350	9.672
200.6	4.843	82.360	118.24	0.0631	1.990	2.856	0.284	7.015
102.3	5.363	15.490	86.81	0.0856	0.374	2.097	0.170	2.202
52.6	4.570	3.040	49.56	0.0760	0.073	1.197	0.093	0.789
							Intercept	7.150
							Slope	1.030
							qm	0.971
							K	0.144
							R^2	0.908

Freundlich	
log (C)	**log (q)**
1.770	0.012
1.536	-0.159
1.498	-0.171
1.222	-0.282
0.985	-0.333
0.529	-0.456
0.299	-0.547
-0.427	-0.770
-1.134	-1.031
K	0.225
n	3.006
R^2	0.990

Modified Langmuir		
$(1/C)^X$	**1/q**	**X**
0.160	0.974	0.450
0.204	1.443	
0.212	1.482	
0.282	1.912	
0.360	2.152	
0.578	2.859	
0.734	3.526	
1.556	5.884	
3.238	10.738	
Intercept	0.938	
Slope	3.076	
qmax	1.066	
K	0.305	
R^2	0.9943	

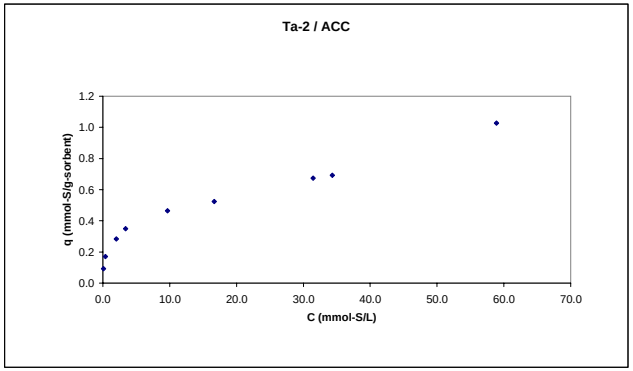

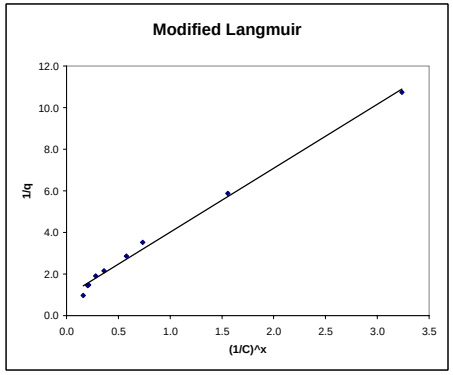

Adsorption Isotherm - DBT in Hexadecane

Sorbent: Ta (10% wt.) on ACC

Temperature = 50°C

Duration: 24 Hours

Sorbent particle size: <125µ

Ta-10 / ACC

Bulk Solution (DBT + C16)		Conc. Final		Sorbent	Sulfur in Solution		Langmuir	
C solution	*weight of Soln*	*C solution*	*n solution*	*weight*	*C (remaining)*	*C (removed)*	*q*	*C/q*
ppm	*g*	*ppm*	*ppm*	*g*	*mmol/L*	*mmol/L*	*mmol/g*	
3096.0	4.625	2140.40	955.60	0.1433	51.704	23.084	0.964	53.644
2145.0	4.822	1363.68	781.32	0.1767	32.941	18.874	0.666	49.436
1914.0	5.164	1300.06	613.94	0.1515	31.405	14.830	0.654	48.019
1143.0	4.906	726.69	416.32	0.1293	17.554	10.057	0.494	35.560
880.9	4.233	540.76	340.14	0.1013	13.063	8.217	0.444	29.407
403.3	4.317	222.62	180.69	0.0637	5.378	4.365	0.383	14.054
200.6	4.824	47.73	152.87	0.0929	1.153	3.693	0.248	4.648
102.3	5.225	12.98	89.32	0.0689	0.314	2.158	0.212	1.481
52.6	5.429	0.53	52.08	0.0848	0.013	1.258	0.104	0.122
							Intercept	7.051
							Slope	1.126
							qm	0.888
							K	0.160
							R²	0.887

Freundlich	
log (C)	**log (q)**
1.714	-0.016
1.518	-0.176
1.497	-0.184
1.244	-0.307
1.116	-0.352
0.731	-0.417
0.062	-0.605
-0.504	-0.674
-1.897	-0.982
K	0.274
n	4.079
R²	0.959

Modified Langmuir		
(1/C)^X	**1/q**	**X**
0.294	1.038	0.310
0.338	1.501	
0.344	1.529	
0.411	2.026	
0.451	2.251	
0.594	2.613	
0.957	4.031	
1.433	4.725	
3.873	9.599	
Intercept	1.052	
Slope	2.283	
qmax	0.951	
K	0.461	
R²	0.9715	

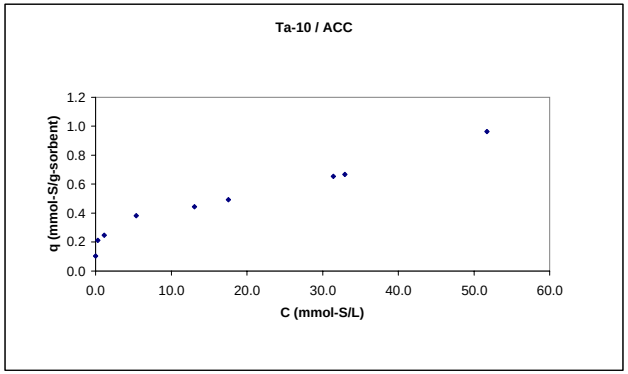

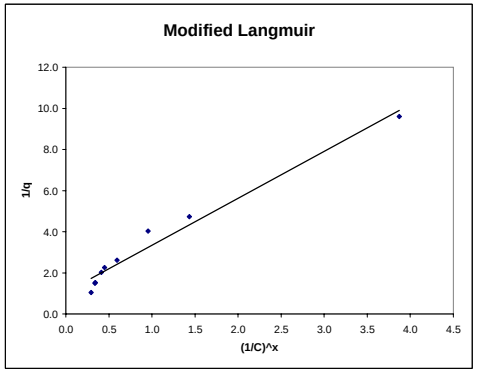

Adsorption Isotherm - DBT in Hexadecane

Sorbent: Ta (5% wt.) on ACC

Temperature = 50°C

Duration: 24 Hours

Sorbent particle size: <125µ

Ta-5 / ACC

Bulk Solution (DBT + C16)		Conc. Final		Sorbent	Sulfur in Solution		Langmuir	
C solution	*weight of Soln*	*C solution*	*n solution*	*weight*	*C (remaining)*	*C (removed)*	*q*	*C/q*
ppm	*g*	*ppm*	*ppm*	*g*	*mmol/L*	*mmol/L*	*mmol/g*	
3096.0	5.753	2344.24	751.76	0.0946	56.628	18.160	1.429	39.638
2145.0	5.120	1462.67	682.33	0.1200	35.333	16.483	0.910	38.835
1914.0	4.880	1239.74	674.27	0.1206	29.947	16.288	0.853	35.124
1143.0	4.881	749.79	393.21	0.0746	18.112	9.498	0.804	22.526
880.9	4.510	552.25	328.66	0.0674	13.340	7.939	0.687	19.411
403.3	4.875	75.19	328.11	0.1098	1.816	7.926	0.455	3.990
200.6	4.839	12.60	188.00	0.0989	0.304	4.541	0.287	1.059
102.3	4.719	0.62	101.69	0.1288	0.015	2.456	0.116	0.128
52.6	4.117	0.07	52.54	0.0984	0.002	1.269	0.069	0.023
							Intercept	3.894
							Slope	0.808
							qm	1.237
							K	0.208
							R²	0.885

Freundlich	
log (C solution)	*log (q)*
mmol/L	*mmol/g*
1.753	0.155
1.548	-0.041
1.476	-0.069
1.258	-0.095
1.125	-0.163
0.259	-0.342
-0.517	-0.541
-1.828	-0.934
-2.804	-1.163
K	0.378
n	3.720
R²	0.989

Modified Langmuir		
$(1/C)^X$	1/q	X
0.275	0.700	0.320
0.320	1.099	
0.337	1.173	
0.396	1.244	
0.436	1.455	
0.826	2.197	
1.463	3.479	
3.846	8.589	
7.894	14.559	
Intercept	0.632	
Slope	1.824	
qmax	1.582	
K	0.347	
R²	0.9923	

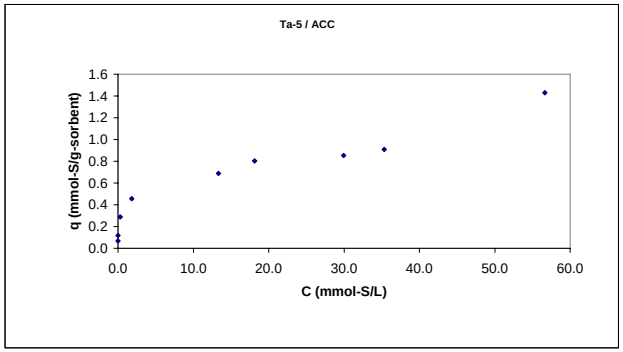

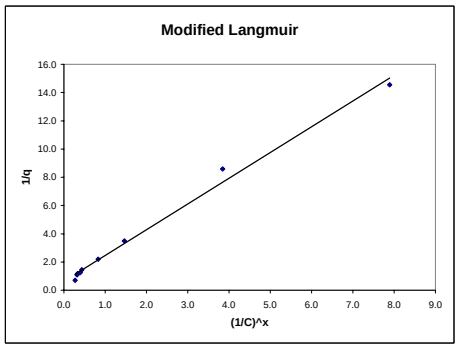

Adsorption Isotherm - DBT in Hexadecane

Sorbent: ACC

Temperature = 50°C

Duration: 24 Hours

Sorbent particle size: 125µ <<250µ

ACC - 125µ

Bulk Solution (DBT + C16)			Conc. Final		Sorbent	Plot data		Linear Plot - Langmuir	
C solution	*weight of Soln*	*n solution*	*C solution*	*n solution*	*weight*	*C solution*	*q*	C	C/q
mmol/L	*g*	*mmol*	*mmol/L*	*mmol*	*g*	*mmol/L*	*mmol/g*		
39.080	5.1456	0.260	18.100	0.12	0.2545	18.100	0.549	18.100	32.984
31.460	5.1063	0.208	14.200	0.09	0.2130	14.200	0.535	14.200	26.528
23.080	5.0632	0.151	4.650	0.03	0.3013	4.650	0.401	4.650	11.606
9.570	5.1324	0.064	1.310	0.01	0.2729	1.310	0.201	1.310	6.519
5.210	4.8213	0.032	0.280	0.0017	0.2679	0.280	0.115	0.280	2.439
2.630	5.0130	0.017	0.200	0.0013	0.1754	0.200	0.090	0.200	2.226
1.450	5.1263	0.010	0.120	0.0008	0.0955	0.120	0.092	0.120	1.299
0.570	4.9345	0.004	0.010	0.0001	0.0957	0.010	0.037	0.010	0.268
								Intercept	2.071
								Slope	1.731
								qm	0.578
								K	0.836
								R²	0.990

Linear Plot - Freundlich	
log (C)	**log (q)**
1.258	-0.261
1.152	-0.271
0.667	-0.397
0.117	-0.697
-0.553	-0.940
-0.699	-1.047
-0.921	-1.035
-2.000	-1.428
K	0.193
n	2.671
R²	0.990

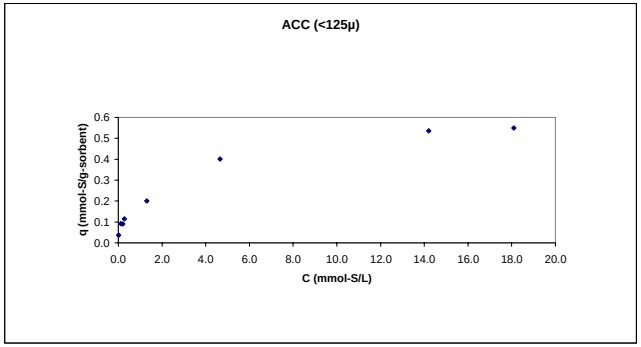

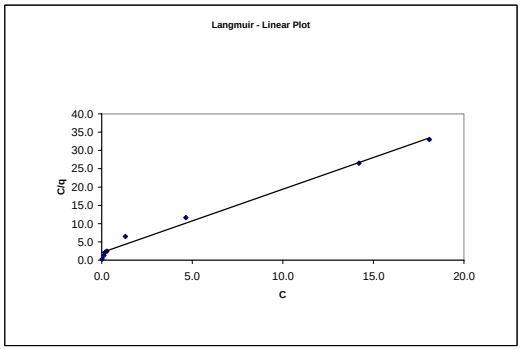

Adsorption Isotherm - DBT in Hexadecane

Sorbent: Ni (2% wt.) on ACC

Temperature = 50°C

Duration: 24 Hours

Sorbent particle size: <125µ

Ni / ACC

Bulk Solution (DBT + C16)			Conc. Final		Sorbent	Plot data		Linear Plot - Langmuir	
C solution	*weight of Soln*	*n solution*	*C solution*	*n solution*	*weight*	*C solution*	*q*	C (mmol/L)	C/q (g/L)
mmol/L	*g*	*mmol*	*mmol/L*	*mmol*	*g*	*mmol/L*	*mmol/g*		
39.080	5.204	0.263	26.52	0.18	0.106	26.520	0.799	26.520	33.185
31.460	5.043	0.205	20.56	0.13	0.097	20.560	0.735	20.560	27.989
23.080	5.001	0.149	13.22	0.09	0.098	13.220	0.650	13.220	20.353
9.570	5.049	0.063	3.34	0.02	0.100	3.340	0.409	3.340	8.174
5.210	5.175	0.035	1.22	0.01	0.095	1.220	0.282	1.220	4.321
2.630	5.239	0.018	0.34	0.00	0.090	0.340	0.173	0.340	1.960
1.450	5.097	0.010	0.19	0.00	0.061	0.190	0.136	0.190	1.400
								Intercept	2.634
								Slope	1.207
								qm	0.828
								K	0.458
								R^2	0.989

Linear Plot - Freundlich	
log (C)	**log (q)**
1.424	-0.097
1.313	-0.134
1.121	-0.187
0.524	-0.389
0.086	-0.549
-0.469	-0.761
-0.721	-0.867
K	0.255
n	2.802
R^2	0.998

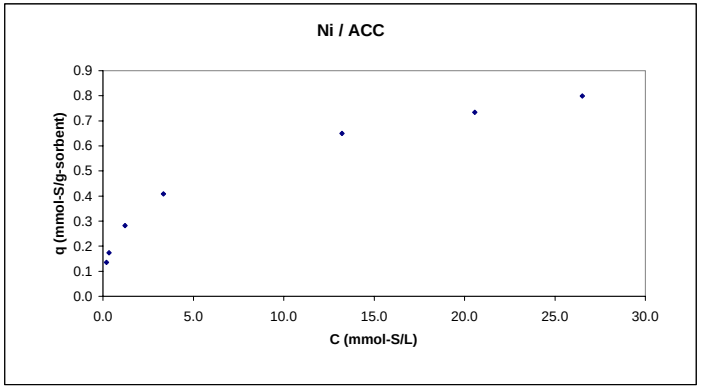

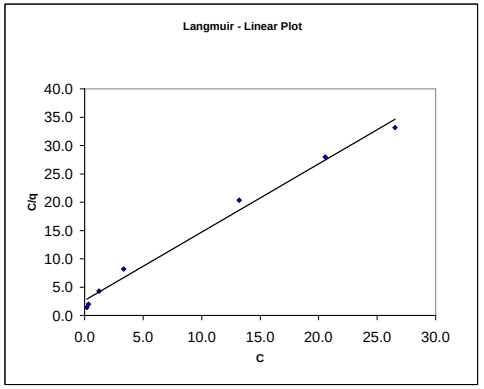

Adsorption Isotherm - DBT in Hexadecane

Sorbent: Ta (2% wt.) on ACC

Temperature = 50°C

Duration: 24 Hours

Sorbent particle size: <125µ

Ta-2 / ACC

Bulk Solution (DBT + C16)		Conc. Final		Sorbent	Sulfur in Solution		Langmuir	
C solution	*weight of Soln*	*C solution*	*n solution*	*weight*	*C (remaining)*	*C (removed)*	*q*	*C/q*
ppm	*g*	*ppm*	*ppm*	*g*	*mmol/L*	*mmol/L*	*mmol/g*	
3096.0	5.102	2355.300	740.70	0.1146	56.895	17.893	1.031	55.209
2145.0	4.615	1549.390	595.61	0.1267	37.427	14.388	0.678	55.209
1914.0	5.006	1388.125	525.88	0.1265	33.532	12.703	0.650	51.559
1143.0	4.622	710.150	432.85	0.1195	17.155	10.456	0.523	32.788
880.9	4.790	655.200	225.70	0.0651	15.827	5.452	0.519	30.498
403.3	4.590	199.080	204.22	0.0825	4.809	4.933	0.355	13.544
200.6	5.149	63.035	137.57	0.0805	1.523	3.323	0.275	5.538
102.3	4.758	12.995	89.31	0.0837	0.314	2.157	0.159	1.979
52.6	4.050	0.965	51.64	0.0937	0.023	1.247	0.070	0.334
							Intercept	7.348
							Slope	1.078
							qm	0.928
							K	0.147
							R^2	0.885

Freundlich	
log (C)	**log (q)**
1.755	0.013
1.573	-0.169
1.525	-0.187
1.234	-0.281
1.199	-0.285
0.682	-0.450
0.183	-0.561
-0.503	-0.800
-1.632	-1.156
K	0.227
n	3.146
R^2	0.987

Modified Langmuir		
$(1/C)^X$	**1/q**	**X**
0.199	0.970	0.400
0.235	1.475	
0.245	1.538	
0.321	1.911	
0.331	1.927	
0.534	2.816	
0.845	3.637	
1.590	6.304	
4.498	14.337	
Intercept	0.913	
Slope	3.035	
qmax	1.096	
K	0.301	
R^2	0.9943	

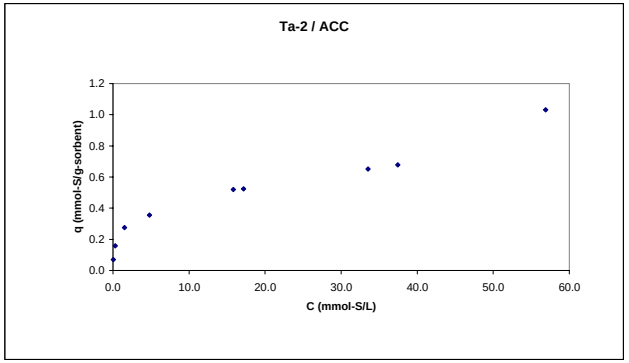

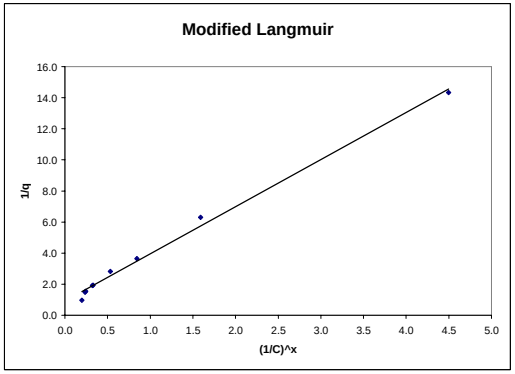

Adsorption Isotherm - DBT in Hexadecane

Sorbent: Ta (10% wt.) on ACC

Temperature = 50°C

Duration: 24 Hours

Sorbent particle size: <125µ

Ta-10 / ACC

Bulk Solution (DBT + C16)		Conc. Final		Sorbent	Sulfur in Solution		Langmuir	
C solution	*weight of Soln*	*C solution*	*n solution*	*weight*	*C (remaining)*	*C (removed)*	*q*	C/q
ppm	*g*	*ppm*	*ppm*	*g*	*mmol/L*	*mmol/L*	*mmol/g*	
3096.0	4.581	2116.90	979.10	0.1332	51.136	23.651	1.052	48.593
2145.0	4.799	1359.12	785.88	0.1666	32.831	18.984	0.707	46.408
1914.0	5.233	1295.06	618.94	0.1449	31.284	14.951	0.699	44.784
1143.0	5.148	722.11	420.89	0.1401	17.443	10.167	0.483	36.094
880.9	4.603	563.32	317.59	0.0998	13.608	7.672	0.458	29.726
403.3	4.416	239.73	163.58	0.0704	5.791	3.951	0.321	18.060
200.6	4.332	35.53	165.08	0.0890	0.858	3.988	0.251	3.417
102.3	4.996	10.93	91.37	0.0704	0.264	2.207	0.203	1.303
52.6	4.787	0.51	52.09	0.0914	0.012	1.258	0.085	0.145
							Intercept	7.879
							Slope	1.029
							qm	0.972
							K	0.131
							R²	0.844

Freundlich	
log (C)	**log (q)**
1.709	0.022
1.516	-0.150
1.495	-0.156
1.242	-0.316
1.134	-0.339
0.763	-0.494
-0.066	-0.600
-0.578	-0.693
-1.909	-1.069
K	0.263
n	3.730
R²	0.947

Modified Langmuir		
$(1/C)^X$	**1/q**	**X**
0.273	0.950	0.330
0.316	1.414	
0.321	1.432	
0.389	2.069	
0.423	2.184	
0.560	3.119	
1.052	3.982	
1.552	4.935	
4.267	11.729	
Intercept	0.928	
Slope	2.563	
qmax	1.078	
K	0.362	
R²	0.9839	

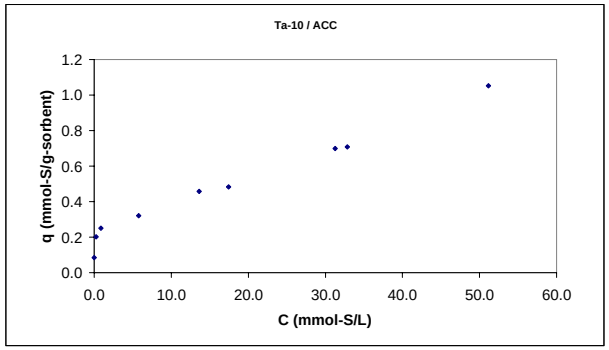

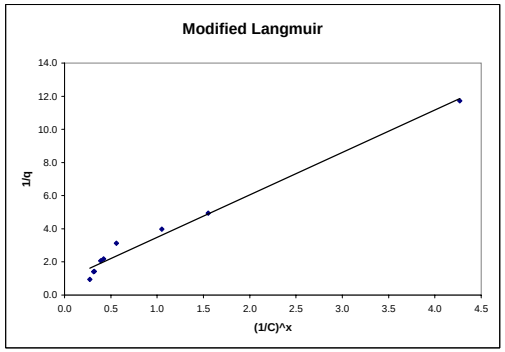

Adsorption Isotherm - DBT in Hexadecane

Sorbent: Ta (5% wt.) on ACC

Temperature = 50°C

Duration: 24 Hours

Sorbent particle size: <125µ

Ta-5 / ACC

Bulk Solution (DBT + C16)		Conc. Final		Sorbent	Sulfur in Solution		Langmuir	
C solution	*weight of Soln*	*C solution*	*n solution*	*weight*	*C (remaining)*	*C (removed)*	*q*	*C/q*
ppm	*g*	*ppm*	*ppm*	*g*	*mmol/L*	*mmol/L*	*mmol/g*	
3096.0	5.312	2263.74	832.26	0.1015	54.683	20.104	1.361	40.175
2145.0	4.992	1445.41	699.60	0.1102	34.916	16.900	0.990	35.256
1914.0	4.753	1216.22	697.78	0.1100	29.379	16.856	0.942	31.182
1143.0	4.533	736.43	406.58	0.0843	17.789	9.821	0.683	26.038
880.9	4.362	532.01	348.90	0.0883	12.851	8.428	0.539	23.860
403.3	4.602	70.75	332.55	0.1116	1.709	8.033	0.429	3.988
200.6	4.773	10.44	190.16	0.0915	0.252	4.594	0.310	0.814
102.3	4.812	0.63	101.68	0.1188	0.015	2.456	0.129	0.117
52.6	4.774	0.13	52.48	0.1044	0.003	1.268	0.075	0.040
							Intercept	4.476
							Slope	0.799
							qm	1.251
							K	0.179
							R^2	0.874

Freundlich	
log (C solution)	*log (q)*
mmol/L	*mmol/g*
1.738	0.134
1.543	-0.004
1.468	-0.026
1.250	-0.165
1.109	-0.269
0.233	-0.368
-0.598	-0.509
-1.821	-0.890
-2.520	-1.125
K	0.373
n	3.792
R^2	0.971

Modified Langmuir		
$(1/C)^X$	1/q	X
0.257	0.735	0.340
0.299	1.010	
0.317	1.061	
0.376	1.464	
0.420	1.857	
0.833	2.334	
1.597	3.226	
4.161	7.770	
7.192	13.336	
Intercept	0.635	
Slope	1.753	
qmax	1.576	
K	0.362	
R^2	0.9961	

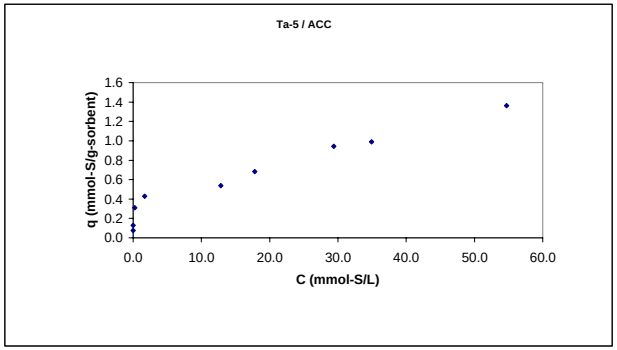

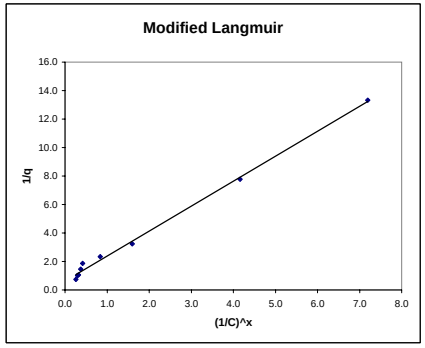

Adsorption Isotherm - 4,6 DMDBT in Hexadecane

Sorbent: ACC

Temperature = 50°C

Duration: 24 Hours

Sorbent particle size: <125µ

ACC

Bulk Solution (4,6 DMDBT + C16)			Conc. Final		Sorbent	Plot data		Langmuir	
C solution	*weight of Soln*	*n solution*	*C solution*	*n solution*	*weight*	*C solution*	*q*	C	C/q
mmol/L	*g*	*mmol*	*mmol/L*	*mmol*	*g*	*mmol/L*	*mmol/g*		
19.51	4.9709	0.125	9.81	0.063	0.1102	9.810	0.566	9.81	17.331
10.53	5.1704	0.070	2.60	0.017	0.1336	2.600	0.397	2.6	6.549
4.96	4.218	0.027	0.16	0.001	0.1750	0.160	0.150	0.16	1.069
2.56	3.2391	0.011	0.22	0.001	0.0564	0.220	0.174	0.22	1.265
1.45	3.6328	0.007	0.02	0.0001	0.0771	0.020	0.087	0.02	0.229
0.54	4.3852	0.003	0.01	0.00006	0.0650	0.010	0.046	0.01	0.216
								Intercept	0.758
								Slope	1.725
								qm	0.580
								K	2.276
								R^2	0.989

Freundlich	
log (C)	**log (q)**
0.99	-0.247
0.41	-0.401
-0.80	-0.825
-0.66	-0.760
-1.70	-1.060
-2.00	-1.335
K	0.277
n	2.911
R^2	0.980

Modified Langmuir		
$(1/C)^X$	**1/q**	**X**
0.254	1.767	0.600
0.564	2.519	
3.003	6.681	
2.481	5.752	
10.456	11.472	
15.849	21.619	
Intercept	2.069	
Slope	1.147	
qmax	0.483	
K	1.804	
R^2	0.9595	

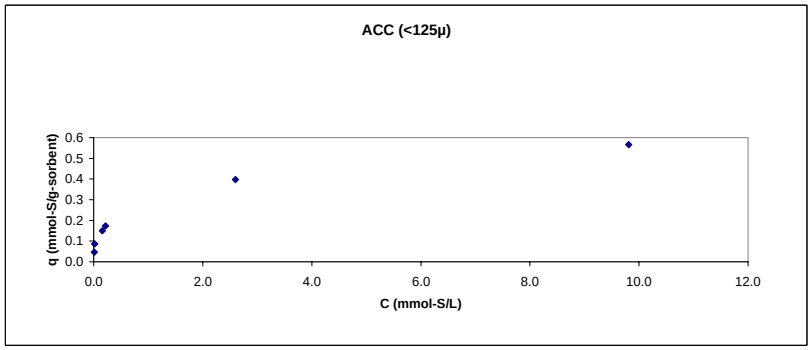

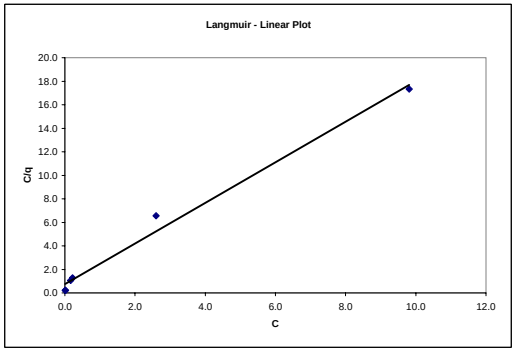

Adsorption Isotherm - 4,6 DMDBT in Hexadecane

Sorbent: Ni (2% wt.) on ACC

Temperature = 50°C

Duration: 24 Hours

Sorbent particle size: <125µ

Ni / ACC (<125µ)

Bulk Solution (4,6 DMDBT + C16)			Conc. Final		Sorbent	Plot data		Langmuir	
C solution	*weight of Soln*	*n solution*	*C solution*	*n solution*	*weight*	*C solution*	*q*	C	C/q
mmol/L	*g*	*mmol*	*mmol/L*	*mmol*	*g*	*mmol/L*	*mmol/g*		
19.51	5.0581	0.128	3.050	0.020	0.2230	3.050	0.483	3.05	6.315
10.53	5.2243	0.071	2.120	0.014	0.1623	2.120	0.350	2.12	6.054
4.96	5.0189	0.032	0.890	0.006	0.1211	0.890	0.218	0.89	4.079
2.56	5.1233	0.017	0.380	0.003	0.1112	0.380	0.130	0.38	2.925
1.45	5.1581	0.010	0.190	0.001	0.1005	0.190	0.084	0.19	2.271
								Intercept	2.428
								Slope	1.433
								qm	0.698
								K	0.590
								R^2	0.931

Freundlich	
log (C)	**log (q)**
0.48	-0.316
0.33	-0.456
-0.05	-0.661
-0.42	-0.886
-0.72	-1.077
K	0.233
n	1.626
R^2	0.998

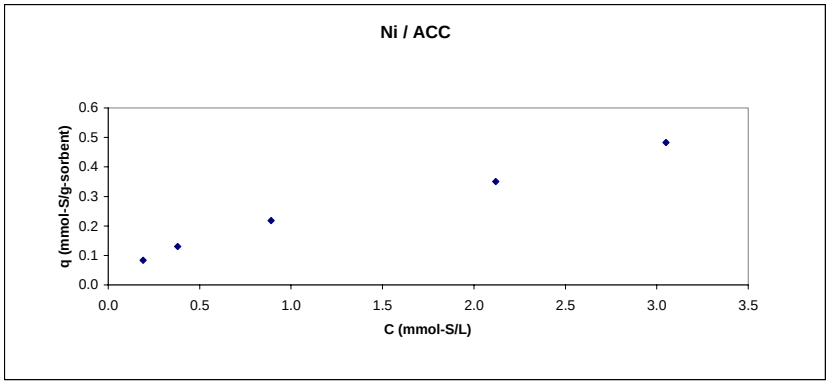

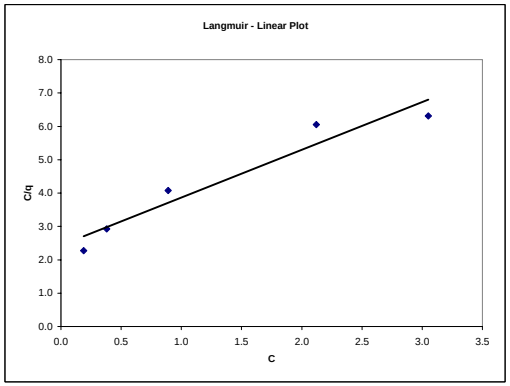

Adsorption Isotherm - 4,6 DMDBT in Hexadecane

Sorbent: Co (2% wt.) on ACC

Temperature = 50°C

Duration: 24 Hours

Sorbent particle size: <125µ

Co /ACC

Bulk Solution (4,6 DMDBT + C16)			Conc. Final		Sorbent	Plot data		Langmuir	
C solution	*weight of Soln*	*n solution*	*C solution*	*n solution*	*weight*	*C solution*	*q*	C	C/q
mmol/L	*g*	*mmol*	*mmol/L*	*mmol*	*g*	*mmol/L*	*mmol/g*		
21.48	5.6133	0.156	12.060	0.088	0.111	12.060	0.619	12.06	19.481
10.21	5.0953	0.067	1.960	0.013	0.163	1.960	0.334	1.96	5.871
4.95	5.1051	0.033	1.280	0.008	0.082	1.280	0.295	1.28	4.336
2.72	5.3495	0.019	0.650	0.004	0.065	0.650	0.221	0.65	2.936
1.34	5.2089	0.009	0.070	0.0005	0.079	0.070	0.108	0.07	0.646
0.64	4.9316	0.004	0.010	0.0001	0.086	0.010	0.047	0.01	0.213
								Intercept	1.531
								Slope	1.516
								qm	0.660
								K	0.990
								R^2	0.978

Freundlich	
log (C)	**log (q)**
1.08	-0.208
0.29	-0.476
0.11	-0.530
-0.19	-0.655
-1.15	-0.965
-2.00	-1.329
K	0.262
n	2.775
R^2	0.997

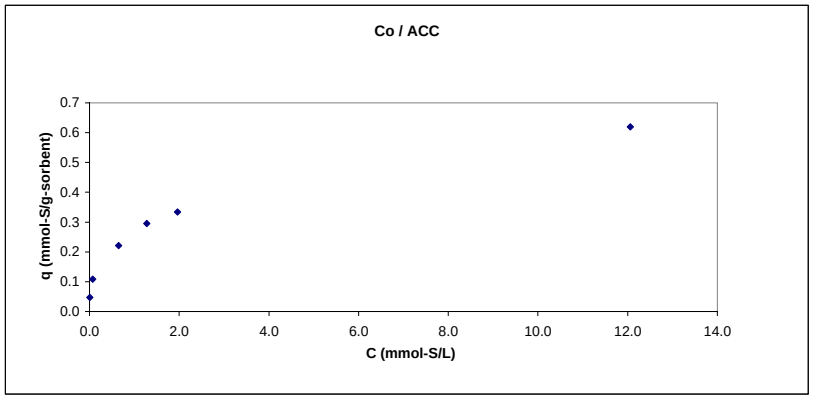

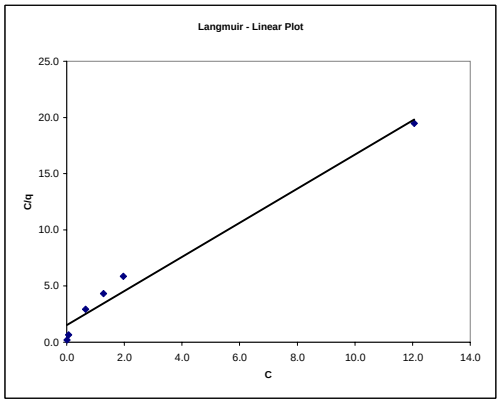

Adsorption Isotherm - 4,6 DMDBT in Hexadecane

Sorbent: ACC

Temperature = 50°C

Duration: 24 Hours

Sorbent particle size: 250µ <<500µ

ACC-500µ

Bulk Solution (4,6 DMDBT + C16)			Conc. Final		Sorbent	Plot data		Langmuir	
C solution	*weight of Soln*	*n solution*	*C solution*	*n solution*	*weight*	*C solution*	*q*	C	C/q
mmol/L	*g*	*mmol*	*mmol/L*	*mmol*	*g*	*mmol/L*	*mmol/g*		
19.51	4.3182	0.109	3.460	0.019	0.252	3.460	0.356	3.46	9.717
10.53	4.4566	0.061	2.700	0.016	0.127	2.700	0.357	2.7	7.572
4.96	4.6556	0.030	0.270	0.002	0.180	0.270	0.157	0.27	1.723
2.56	4.1981	0.014	0.060	0.0003	0.152	0.060	0.090	0.06	0.670
1.45	4.9685	0.009	0.030	0.0002	0.178	0.030	0.051	0.03	0.586
0.54	4.74	0.003	0.010	0.0001	0.204	0.010	0.016	0.01	0.627
								Intercept	0.649
								Slope	2.604
								qm	0.384
								K	4.014
								R^2	0.998

Freundlich	
log (C)	**log (q)**
0.54	-0.448
0.43	-0.448
-0.57	-0.805
-1.22	-1.048
-1.52	-1.291
-2.00	-1.798
K	0.238
n	2.072
R^2	0.932

Modified Langmuir		
$(1/C)^X$	**1/q**	**X**

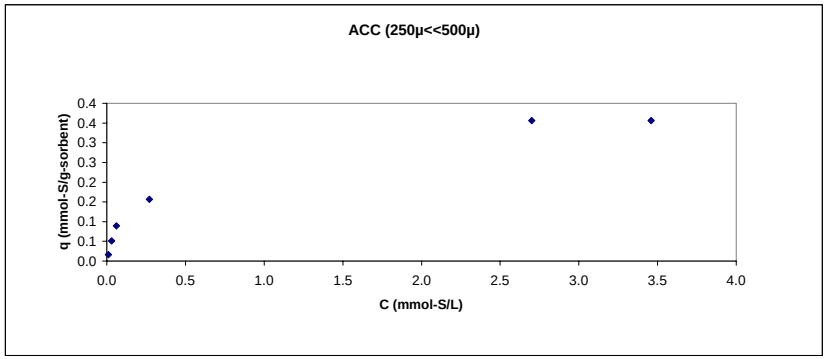

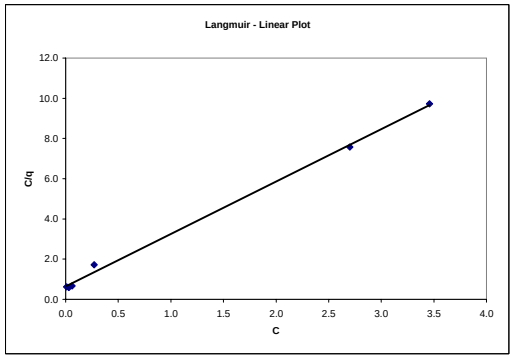

Adsorption Isotherm - 4,6 DMDBT in Hexadecane

Sorbent: Sr (2% wt.) on ACC

Temperature = 50°C

Duration: 24 Hours

Sorbent particle size: <125µ

Sr/ACC

Bulk Solution (4,6 DMDBT + C16)			Conc. Final		Sorbent	Plot data		Langmuir	
C solution	*weight of Soln*	*n solution*	*C solution*	*n solution*	*weight*	*C solution*	*q*	C	C/q
mmol/L	*g*	*mmol*	*mmol/L*	*mmol*	*g*	*mmol/L*	*mmol/g*		
21.48	5.4318	0.151	9.270	0.065	0.149	9.270	0.575	9.27	16.109
10.21	5.1838	0.068	5.100	0.034	0.087	5.100	0.395	5.1	12.918
4.95	5.4814	0.035	1.180	0.008	0.088	1.180	0.304	1.18	3.875
2.72	5.0744	0.018	0.250	0.002	0.101	0.250	0.161	0.25	1.556
1.34	5.3907	0.009	0.040	0.0003	0.104	0.040	0.087	0.04	0.460
0.64	4.7401	0.004	0.020	0.0001	0.111	0.020	0.034	0.02	0.582
								Intercept	1.243
								Slope	1.768
								qm	0.566
								K	1.422
								R^2	0.953

Freundlich	
log (C)	**log (q)**
0.97	-0.240
0.71	-0.404
0.07	-0.516
-0.60	-0.794
-1.40	-1.060
-1.70	-1.464
K	0.243
n	2.467
R^2	0.947

Modified Langmuir		
$(1/C)^X$	**1/q**	**X**

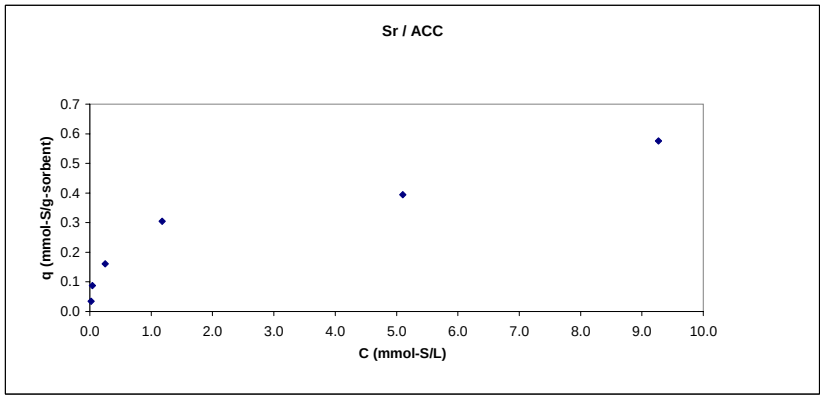

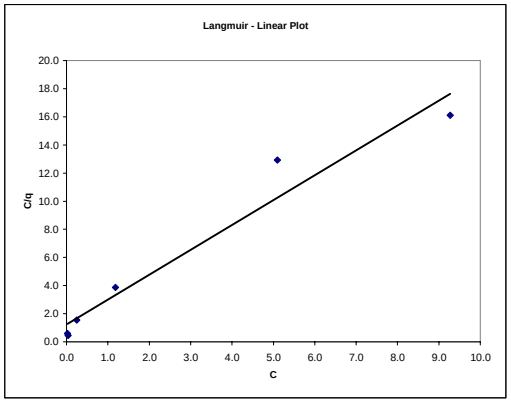

Adsorption Isotherm - 4,6 DMDBT in Hexadecane

Sorbent: Ga (2% wt.) on ACC

Temperature = 50°C

Duration: 24 Hours

Sorbent particle size: <125µ

Ga / ACC

Bulk Solution (4,6 DMDBT + C16)			Conc. Final		Sorbent	Plot data		Langmuir	
C solution	*weight of Soln*	*n solution*	*C solution*	*n solution*	*weight*	*C solution*	*q*	C	C/q
mmol/L	*g*	*mmol*	*mmol/L*	*mmol*	*g*	*mmol/L*	*mmol/g*		
21.48	5.3353	0.148	7.180	0.050	0.182	7.180	0.543	7.18	13.225
10.21	5.1978	0.069	2.710	0.018	0.135	2.710	0.374	2.71	7.244
4.95	5.1484	0.033	0.970	0.006	0.097	0.970	0.274	0.97	3.546
2.72	5.6605	0.020	0.110	0.001	0.148	0.110	0.129	0.11	0.851
1.34	5.1324	0.009	0.030	0.0002	0.128	0.030	0.068	0.03	0.442
0.64	4.352	0.004	0.020	0.0001	0.071	0.020	0.049	0.02	0.406
								Intercept	0.998
								Slope	1.790
								qm	0.559
								K	1.795
								R^2	0.970

Freundlich	
log (C)	**log (q)**
0.86	-0.265
0.43	-0.427
-0.01	-0.563
-0.96	-0.889
-1.52	-1.168
-1.70	-1.308
K	0.263
n	2.549
R^2	0.989

Modified Langmuir		
$(1/C)^X$	**1/q**	**X**

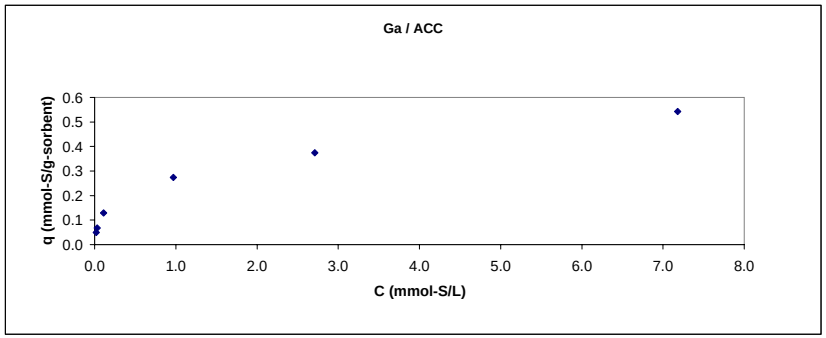

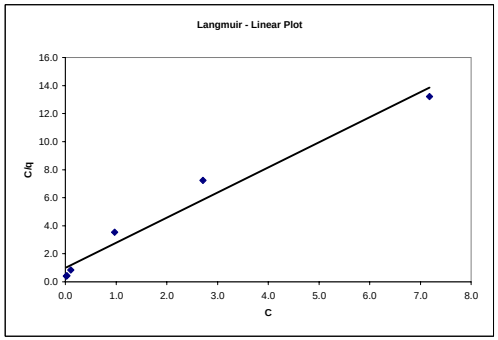

Adsorption Isotherm - 4,6 DMDBT in Hexadecane

Sorbent: Ag (2% wt.) on ACC

Temperature = 50°C

Duration: 24 Hours

Sorbent particle size: <125µ

Ag / ACC

Bulk Solution (4,6 DMDBT + C16)			Conc. Final		Sorbent	Plot data		Langmuir	
C solution	*weight of Soln*	*n solution*	*C solution*	*n solution*	*weight*	*C solution*	*q*	C	C/q
mmol/L	*g*	*mmol*	*mmol/L*	*mmol*	*g*	*mmol/L*	*mmol/g*		
21.48	5.501	0.153	11.060	0.079	0.118	11.060	0.629	11.06	17.585
10.21	5.3876	0.071	3.140	0.022	0.123	3.140	0.402	3.14	7.806
4.95	5.0275	0.032	0.500	0.003	0.132	0.500	0.219	0.5	2.279
2.72	4.9928	0.018	0.150	0.001	0.115	0.150	0.144	0.15	1.042
1.34	5.3139	0.009	0.030	0.0002	0.113	0.030	0.080	0.03	0.375
0.64	5.136	0.004	0.010	0.0001	0.110	0.010	0.038	0.01	0.263
								Intercept	1.060
								Slope	1.544
								qm	0.648
								K	1.457
								R^2	0.977

Freundlich	
log (C)	**log (q)**
1.04	-0.201
0.50	-0.396
-0.30	-0.659
-0.82	-0.842
-1.52	-1.097
-2.00	-1.420
K	0.269
n	2.615
R^2	0.986

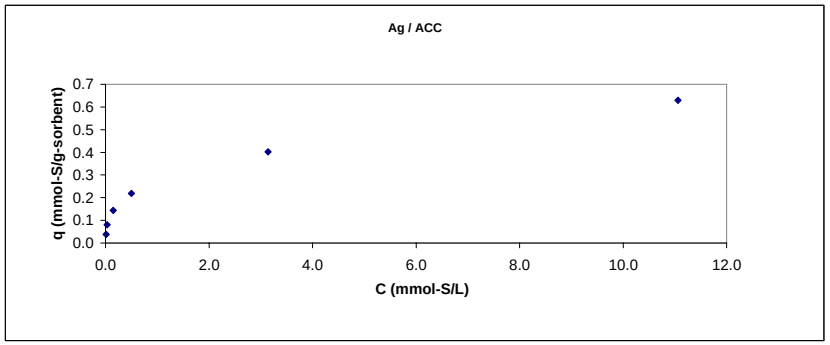

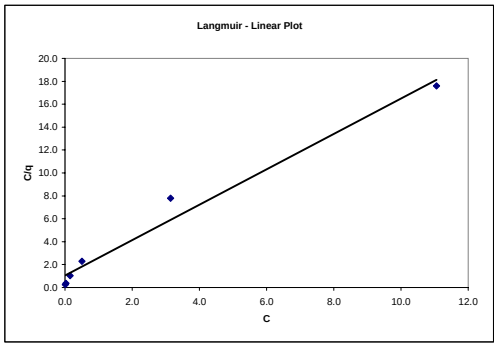

Adsorption Isotherm - 4,6 DMDBT in Hexadecane

Sorbent: Sn (2% wt.) on ACC

Temperature = 50°C

Duration: 24 Hours

Sorbent particle size: <125µ

Sn /ACC

Bulk Solution (4,6 DMDBT + C16)			Conc. Final		Sorbent	Plot data		Langmuir	
C solution	*weight of Soln*	*n solution*	*C solution*	*n solution*	*weight*	*C solution*	*q*	C	C/q
mmol/L	*g*	*mmol*	*mmol/L*	*mmol*	*g*	*mmol/L*	*mmol/g*		
21.48	5.2375	0.146	9.090	0.062	0.139	9.090	0.602	9.09	15.094
10.21	5.0203	0.066	2.760	0.018	0.143	2.760	0.338	2.76	8.157
4.95	5.5603	0.036	1.170	0.008	0.093	1.170	0.294	1.17	3.985
2.72	5.0135	0.018	0.140	0.001	0.117	0.140	0.144	0.14	0.976
1.34	5.1943	0.009	0.060	0.0004	0.094	0.060	0.091	0.06	0.656
0.64	5.0436	0.004	0.010	0.0001	0.086	0.010	0.048	0.01	0.208
								Intercept	1.300
								Slope	1.608
								qm	0.622
								K	1.237
								R^2	0.946

Freundlich	
log (C)	**log (q)**
0.96	-0.220
0.44	-0.471
0.07	-0.532
-0.85	-0.843
-1.22	-1.039
-2.00	-1.318
K	0.263
n	2.761
R^2	0.993

Modified Langmuir		
$(1/C)^X$	**1/q**	**X**

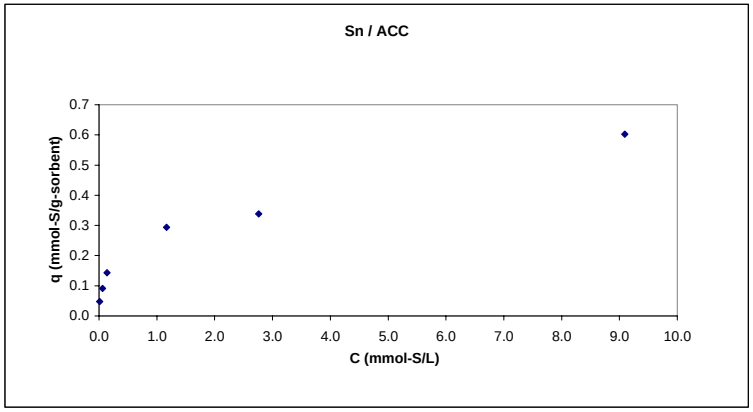

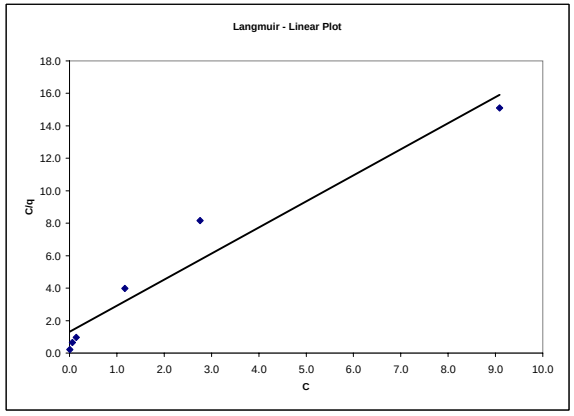

Adsorption Isotherm - 4,6 DMDBT in Hexadecane

Sorbent: Ta (2% wt.) on ACC

Temperature = 50°C

Duration: 24 Hours

Sorbent particle size: <125µ

Ta-2%/ACC

Bulk Solution (4,6 DMDBT + C16)			Conc. Final		Sorbent	Plot data		Langmuir	
C solution	*weight of Soln*	*n solution*	*C solution*	*n solution*	*weight*	*C solution*	*q*	C	C/q
mmol/L	*g*	*mmol*	*mmol/L*	*mmol*	*g*	*mmol/L*	*mmol/g*		
21.48	5.0783	0.141	11.070	0.073	0.0960	11.070	0.712	11.07	15.539
10.21	4.9063	0.065	4.160	0.026	0.0881	4.160	0.436	4.16	9.544
4.95	5.0704	0.032	1.010	0.007	0.0896	1.010	0.288	1.01	3.502
2.72	5.3828	0.019	0.260	0.002	0.1035	0.260	0.166	0.26	1.571
1.34	5.4206	0.009	0.080	0.001	0.0818	0.080	0.108	0.08	0.741
0.64	5.1345	0.004	0.030	0.0002	0.0629	0.030	0.064	0.03	0.466
								Intercept	1.469
								Slope	1.358
								qm	0.737
								K	0.924
								R^2	0.951

Freundlich	
log (C)	**log (q)**
1.04	-0.147
0.62	-0.361
0.00	-0.540
-0.59	-0.781
-1.10	-0.967
-1.52	-1.191
K	0.273
n	2.562
R^2	0.995

Modified Langmuir		
$(1/C)^X$	**1/q**	**X**
0.260	1.404	0.560
0.450	2.294	
0.994	3.467	
2.126	6.042	
4.114	9.258	
7.125	15.524	
Intercept	1.327	
Slope	1.992	
qmax	0.753	
K	0.666	
R^2	0.996	

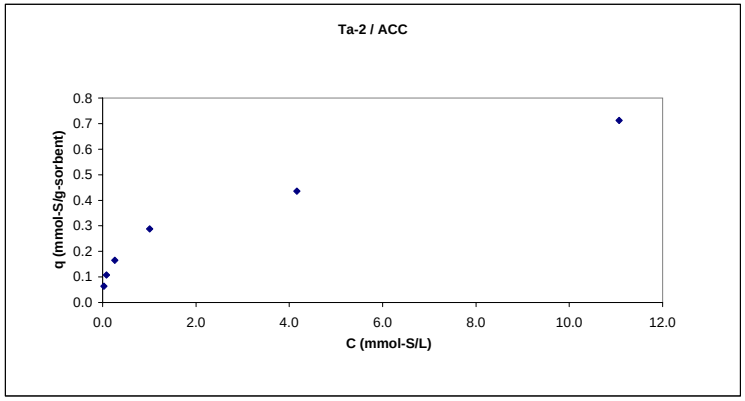

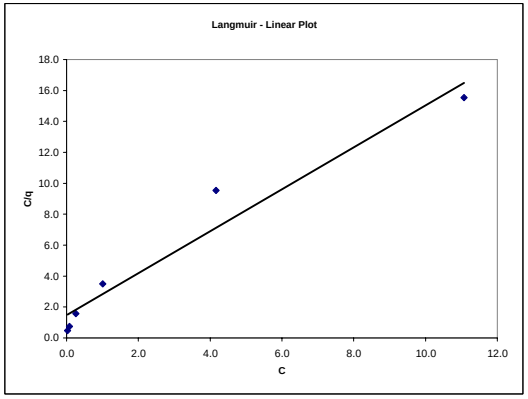

Adsorption Isotherm - 4,6 DMDBT in Hexadecane

Sorbent: Ta (5% wt.) on ACC

Temperature = 50°C

Duration: 24 Hours

Sorbent particle size: <125µ

Ta-5/ACC

Bulk Solution (4,6 DMDBT + C16)		Conc. Final		Sorbent	Sulfur in Solution		Langmuir	
C solution	*weight of Soln*	*C solution*	*n solution*	*weight*	*C (remaining)*	*C (removed)*	*q*	C/q
ppm	*g*	*ppm*	*ppm*	*g*	*mmol/L*	*mmol/L*	*mmol/g*	
801.2	5.4952	347.150	454.050	0.1065	8.386	10.968	0.732	11.454
399.9	4.5726	51.020	348.880	0.1225	1.232	8.428	0.407	3.028
186.1	4.7617	42.150	143.950	0.0554	1.018	3.477	0.387	2.633
104.9	5.0304	20.000	84.900	0.0597	0.483	2.051	0.224	2.161
50.6	4.989	1.110	49.490	0.0812	0.027	1.195	0.095	0.282
25.3	4.9908	0.065	25.235	0.1182	0.002	0.610	0.033	0.047
							Intercept	0.889
							Slope	1.280
							qm	0.781
							K	1.440
							R^2	0.976

Freundlich	
log (C)	**log (q)**
0.92	-0.135
0.09	-0.390
0.01	-0.413
-0.32	-0.651
-1.57	-1.022
-2.80	-1.478
K	0.347
n	2.750
R^2	0.992

Modified Langmuir		
$(1/C)^X$	**1/q**	**X**
0.398	1.366	0.433
0.913	2.457	
0.992	2.586	
1.370	4.473	
4.792	10.524	
16.374	30.033	
Intercept	1.230	
Slope	1.774	
qmax	0.813	
K	0.693	
R^2	0.997	

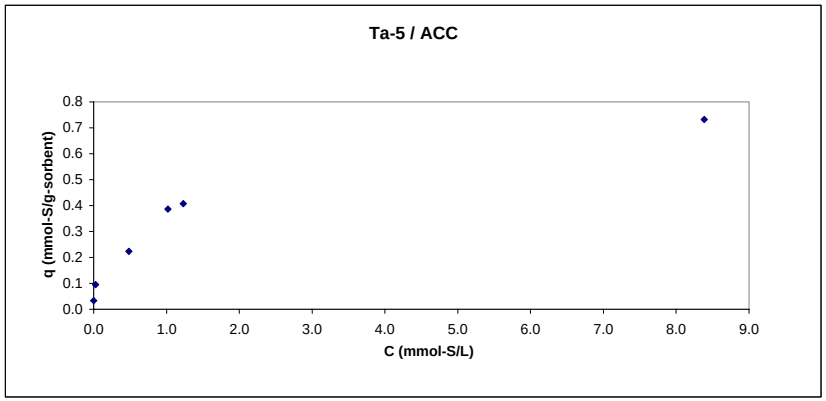

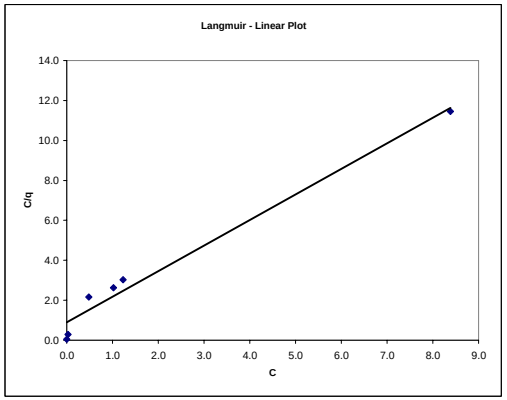

Adsorption Isotherm - 4,6 DMDBT in Hexadecane

Sorbent: Ag (2% wt.) on ACC

Temperature = 50°C

Duration: 24 Hours

Sorbent particle size: <125µ

Ta-10%/ACC

Bulk Solution (4,6 DMDBT + C16)		Conc. Final		Sorbent	Sulfur in Solution		Langmuir	
C solution	*weight of Soln*	*C solution*	*n solution*	*weight*	*C (remaining)*	*C (removed)*	*q*	C/q
ppm	*g*	*ppm*	*ppm*	*g*	*mmol/L*	*mmol/L*	*mmol/g*	
801.2	4.785	497.110	304.090	0.102	12.008	7.346	0.445	26.990
399.9	5.2031	155.070	244.830	0.129	3.746	5.914	0.310	12.092
186.1	5.7563	30.000	156.100	0.122	0.725	3.771	0.230	3.151
104.9	4.5992	8.000	96.900	0.098	0.193	2.341	0.142	1.360
50.6	4.8169	0.780	49.820	0.112	0.019	1.203	0.067	0.281
25.3	5.3904	0.130	25.170	0.189	0.003	0.608	0.022	0.140
							Intercept	1.157
							Slope	2.221
							qm	0.450
							K	1.920
							R^2	0.983

Freundlich	
log (C)	**log (q)**
1.08	-0.352
0.57	-0.509
-0.14	-0.638
-0.71	-0.847
-1.72	-1.173
-2.50	-1.650
K	0.217
n	2.888
R^2	0.968

Modified Langmuir		
$(1/C)^X$	**1/q**	**X**
0.237	2.248	0.580
0.465	3.228	
1.205	4.348	
2.594	7.037	
10.010	14.908	
28.298	44.647	
Intercept	2.187	
Slope	1.478	
qmax	0.457	
K	1.480	
R^2	0.9954	

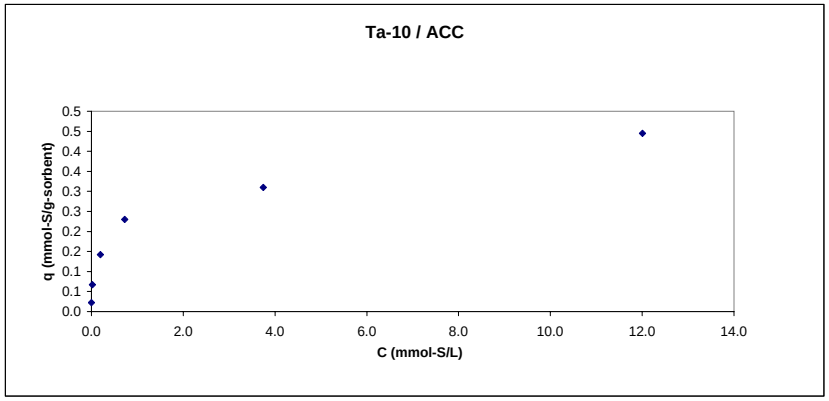

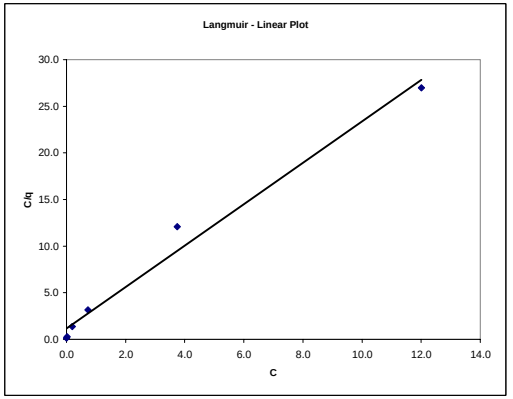

Adsorption Isotherm - 4,6 DMDBT in Hexadecane

Sorbent: ACC

Temperature = 50°C

Duration: 24 Hours

Sorbent particle size: <125µ

ACC

Bulk Solution (4,6 DMDBT + C16)			Conc. Final		Sorbent	Plot data		Langmuir	
C solution	*weight of Soln*	*n solution*	*C solution*	*n solution*	*weight*	*C solution*	*q*	C	C/q
mmol/L	*g*	*mmol*	*mmol/L*	*mmol*	*g*	*mmol/L*	*mmol/g*		
21.48	4.8426	0.135	7.62	0.048	0.158	7.620	0.550	7.62	13.848
10.21	5.4508	0.072	1.69	0.012	0.183	1.690	0.329	1.69	5.134
4.95	5.3719	0.034	0.67	0.005	0.109	0.670	0.273	0.67	2.458
2.72	5.1492	0.018	0.35	0.002	0.084	0.350	0.188	0.35	1.860
1.34	5.4276	0.009	0.01	0.0001	0.129	0.010	0.072	0.01	0.138
0.64	5.0568	0.004	0.01	0.0001	0.101	0.010	0.041	0.01	0.246
								Intercept	0.957
								Slope	1.734
								qm	0.577
								K	1.811
								R^2	0.977

Freundlich	
log (C)	log (q)
0.88	-0.259
0.23	-0.483
-0.17	-0.564
-0.46	-0.725
-2.00	-1.141
-2.00	-1.391
K	0.280
n	2.828
R^2	0.962

Modified Langmuir		
$(1/C)^X$	1/q	X
0.296	1.817	0.600
0.730	3.038	
1.272	3.668	
1.877	5.314	
15.849	13.824	
15.849	24.604	
Intercept	2.319	
Slope	1.069	
qmax	0.431	
K	2.169	
R^2	0.8489	

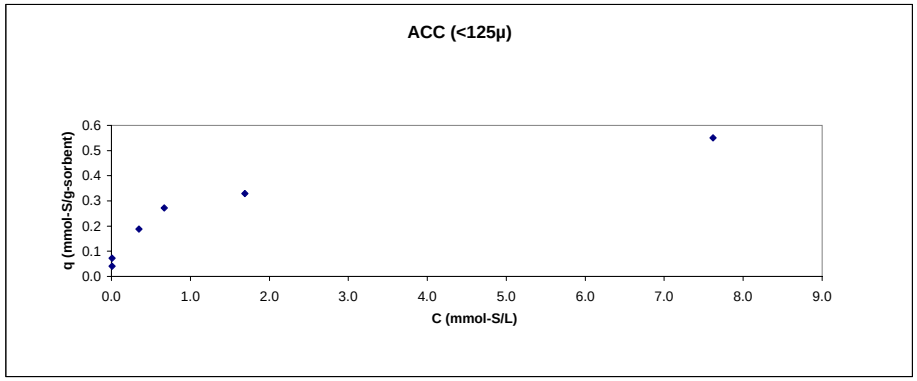

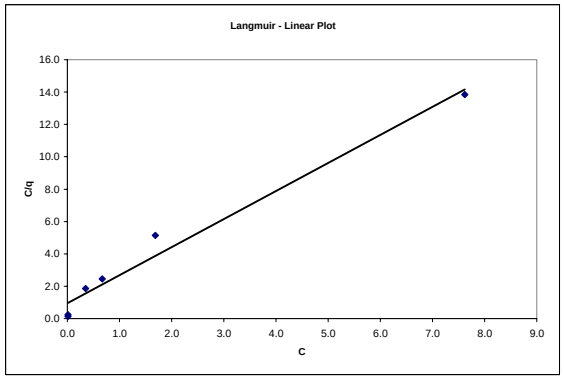

Adsorption Isotherm - 4,6 DMDBT in Hexadecane

Sorbent: Ni (2% wt.) on ACC

Temperature = 50°C

Duration: 24 Hours

Sorbent particle size: <125µ

Ni / ACC (<125µ)

Bulk Solution (4,6 DMDBT + C16)			Conc. Final		Sorbent	Plot data		Langmuir	
C solution	*weight of Soln*	*n solution*	*C solution*	*n solution*	*weight*	*C solution*	*q*	C	C/q
mmol/L	*g*	*mmol*	*mmol/L*	*mmol*	*g*	*mmol/L*	*mmol/g*		
19.51	5.1807	0.131	12.18	0.082	0.079	12.180	0.624	12.18	19.532
10.53	5.5364	0.075	4.47	0.032	0.099	4.470	0.440	4.47	10.165
4.96	5.4834	0.035	2.35	0.017	0.050	2.350	0.367	2.35	6.397
2.56	5.6062	0.019	0.57	0.004	0.067	0.570	0.215	0.57	2.654
1.45	4.0087	0.008	0.04	0.0002	0.089	0.040	0.082	0.04	0.489
								Intercept	1.960
								Slope	1.501
								qm	0.666
								K	0.766
								R^2	0.974

Freundlich	
log (C)	**log (q)**
1.09	-0.205
0.65	-0.357
0.37	-0.435
-0.24	-0.668
-1.40	-1.087
K	0.261
n	2.806
R^2	0.999

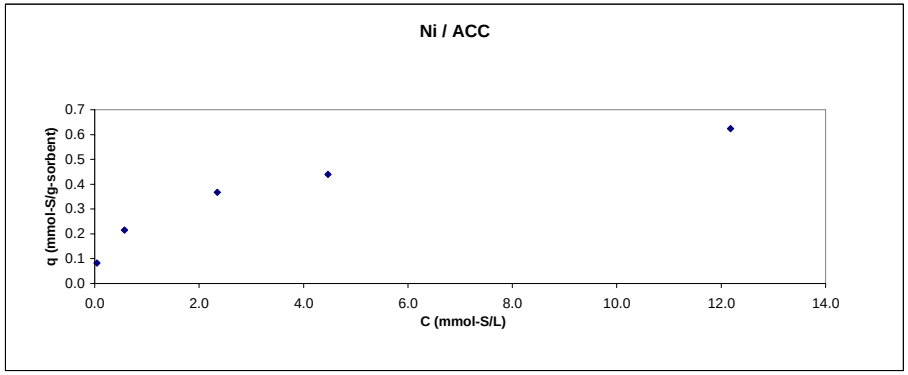

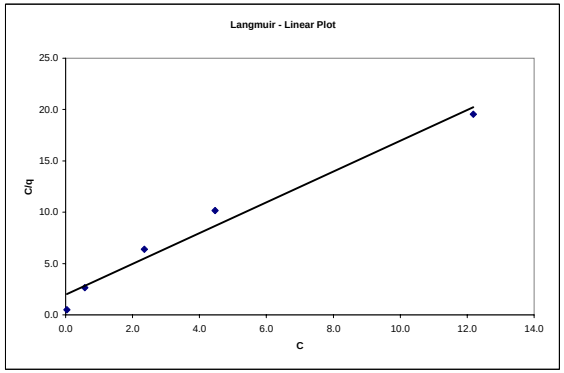

Adsorption Isotherm - 4,6 DMDBT in Hexadecane

Sorbent: Ta (2% wt.) on ACC

Temperature = 50°C

Duration: 24 Hours

Sorbent particle size: <125µ

Ta-2%/ACC

Bulk Solution (4,6 DMDBT + C16)		Conc. Final		Sorbent	Sulfur in Solution		Langmuir	
C solution	*weight of Soln*	*C solution*	*n solution*	*weight*	*C (remaining)*	*C (removed)*	*q*	C/q
ppm	*g*	*ppm*	*ppm*	*g*	*mmol/L*	*mmol/L*	*mmol/g*	
801.2	5.3871	490.22	310.98	0.0684	11.842	7.512	0.765	15.472
399.9	5.3197	189.51	210.40	0.0869	4.578	5.082	0.402	11.374
186.1	5.0118	24.61	161.50	0.1100	0.594	3.901	0.230	2.585
104.9	5.3503	14.28	90.63	0.0816	0.345	2.189	0.186	1.857
50.6	4.892	5.59	45.01	0.0576	0.135	1.087	0.119	1.130
25.3	4.1387	0.39	24.92	0.0697	0.009	0.602	0.046	0.201
							Intercept	1.680
							Slope	1.288
							qm	0.776
							K	0.767
							R^2	0.904

Freundlich	
log (C)	**log (q)**
1.07	-0.116
0.66	-0.395
-0.23	-0.638
-0.46	-0.731
-0.87	-0.923
-2.03	-1.335
K	0.267
n	2.644
R^2	0.990

Modified Langmuir		
$(1/C)^X$	**1/q**	**X**
0.325	1.307	0.46
0.501	2.485	
1.267	4.349	
1.623	5.385	
2.487	8.371	
8.401	21.630	
Intercept	1.277	
Slope	2.456	
qmax	0.783	
K	0.520	
R^2	0.9940	

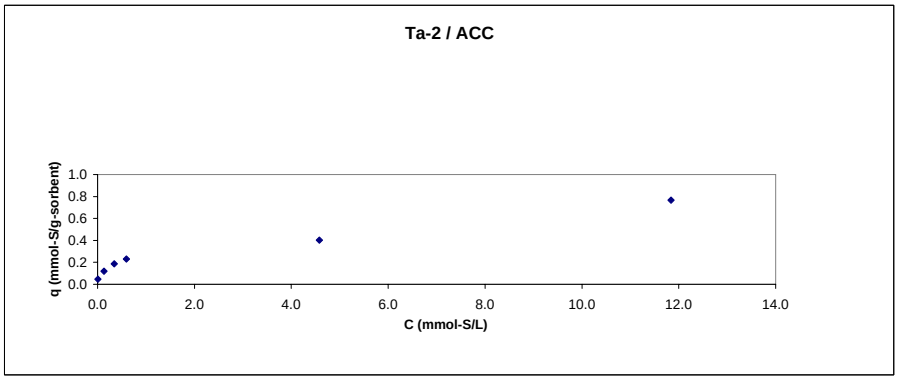

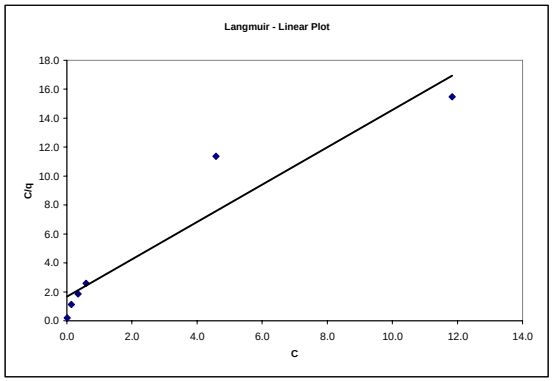

Adsorption Isotherm - 4,6 DMDBT in Hexadecane

Sorbent: Ta (5% wt.) on ACC

Temperature = 50°C

Duration: 24 Hours

Sorbent particle size: <125µ

Ta-5/ACC

Bulk Solution (4,6 DMDBT + C16)			Conc. Final		Sorbent	Plot data		Langmuir	
C solution	*weight of Soln*	*n solution*	*C solution*	*n solution*	*weight*	*C solution*	*q*	C	C/q
mmol/L	*g*	*mmol*	*mmol/L*	*mmol*	*g*	*mmol/L*	*mmol/g*		
21.48	6.824	0.190	13.720	0.121	0.0910	13.720	0.753	13.72	18.225
10.21	6.6157	0.087	6.110	0.052	0.0608	6.110	0.577	6.11	10.587
4.95	5.7778	0.037	1.590	0.012	0.0714	1.590	0.352	1.59	4.520
2.72	6.2297	0.022	0.460	0.004	0.0635	0.460	0.287	0.46	1.604
1.34	7.1261	0.012	0.090	0.001	0.0887	0.090	0.130	0.09	0.693
0.64	6.2019	0.005	0.020	0.0002	0.0797	0.020	0.062	0.02	0.320
								Intercept	1.254
								Slope	1.293
								qm	0.774
								K	1.031
								R^2	0.978

Freundlich	
log (C)	**log (q)**
1.14	-0.123
0.79	-0.239
0.20	-0.454
-0.34	-0.542
-1.05	-0.886
-1.70	-1.205
K	0.305
n	2.695
R^2	0.982

Modified Langmuir		
$(1/C)^X$	**1/q**	**X**
0.219	1.328	0.580
0.350	1.733	
0.764	2.843	
1.569	3.486	
4.041	7.697	
9.669	16.022	
Intercept	1.269	
Slope	1.535	
qmax	0.788	
K	0.827	
R^2	0.9979	

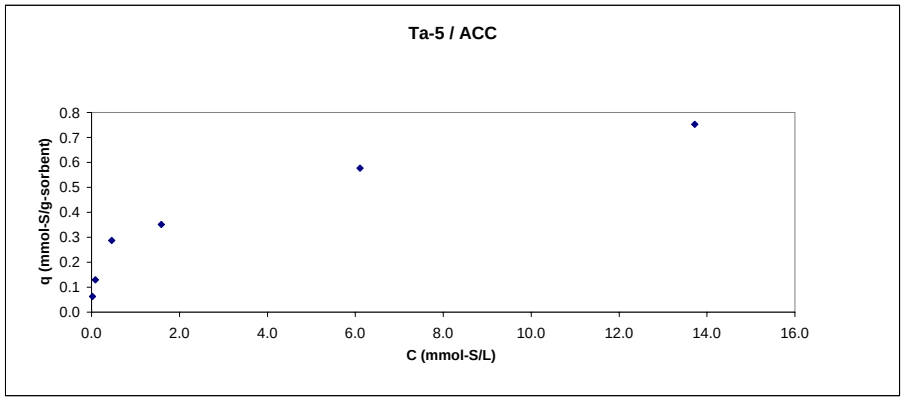

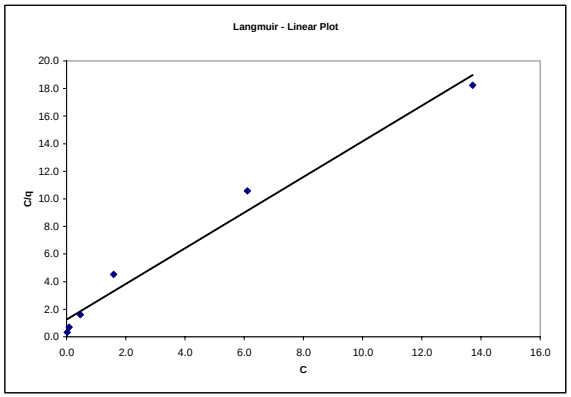

Adsorption Isotherm - 4,6 DMDBT in Hexadecane

Sorbent: Ag (2% wt.) on ACC

Temperature = 50°C

Duration: 24 Hours

Sorbent particle size: <125µ

Ta-10%/ACC

Bulk Solution (4,6 DMDBT + C16)		Conc. Final		Sorbent	Sulfur in Solution		Langmuir	
C solution	*weight of Soln*	*C solution*	*n solution*	*weight*	*C (remaining)*	*C (removed)*	*q*	C/q
ppm	*g*	*ppm*	*ppm*	*g*	*mmol/L*	*mmol/L*	*mmol/g*	
801.2	4.8471	394.00	407.20	0.1377	9.518	9.836	0.448	21.248
399.9	4.6394	171.00	228.90	0.0913	4.131	5.529	0.363	11.364
186.1	4.4673	58.80	127.30	0.0603	1.420	3.075	0.295	4.819
104.9	5.4482	18.60	86.30	0.0851	0.449	2.085	0.173	2.602
50.6	4.3773	1.50	49.10	0.0822	0.036	1.186	0.082	0.443
25.3	4.85	0.49	24.81	0.0766	0.012	0.599	0.049	0.241
							Intercept	1.127
							Slope	2.181
							qm	0.458
							K	1.935
							R^2	0.988

Freundlich	
log (C)	**log (q)**
0.98	-0.349
0.62	-0.440
0.15	-0.531
-0.35	-0.763
-1.44	-1.088
-1.93	-1.309
K	0.230
n	3.021
R^2	0.991

Modified Langmuir		
$(1/C)^X$	**1/q**	**X**
0.303	2.233	0.530
0.472	2.751	
0.830	3.393	
1.528	5.792	
5.803	12.239	
10.500	20.371	
Intercept	2.147	
Slope	1.744	
qmax	0.466	
K	1.231	
R^2	0.9951	

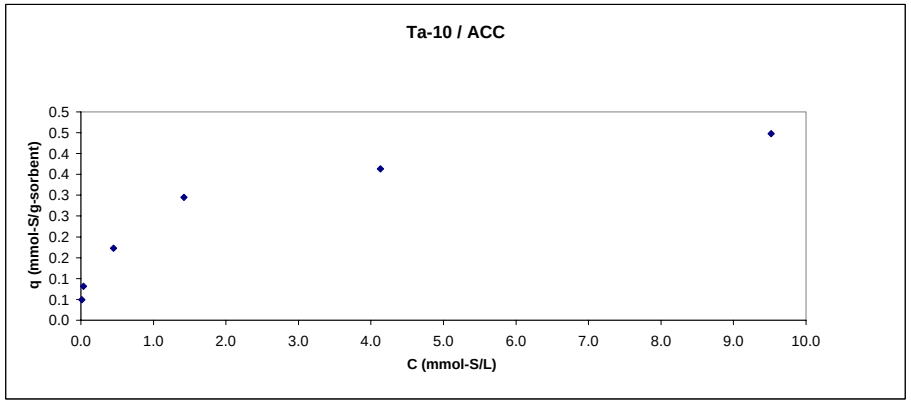

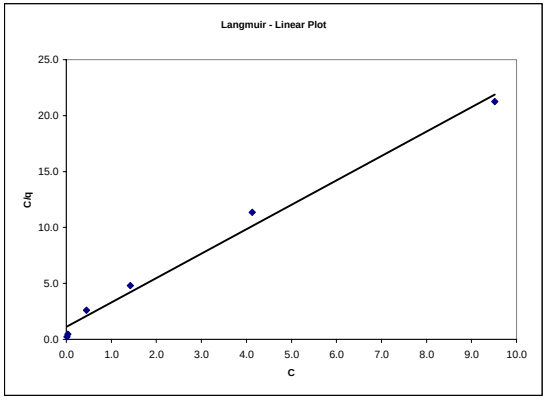

Adsorption Isotherm - 4,6 DMDBT in Hexadecane

Sorbent: ACC s

Temperature = 50°C

Duration: 24 Hours

Sorbent particle size: <125µ

ACC

Bulk Solution (4,6 DMDBT + C16)		Conc. Final		Sorbent	Sulfur in Solution		Langmuir	
C solution	*weight of Soln*	*C solution*	*n solution*	*weight*	*C (remaining)*	*C (removed)*	*q*	C/q
ppm	*g*	*ppm*	*ppm*	*g*	*mmol/L*	*mmol/L*	*mmol/g*	
801.2	4.806	507.82	293.38	0.0775	12.267	7.087	0.569	21.576
399.9	4.965	136.85	263.05	0.1254	3.306	6.354	0.325	10.157
186.1	4.6741	34.11	151.99	0.0961	0.824	3.672	0.231	3.567
104.9	4.6422	5.97	98.93	0.1065	0.144	2.390	0.135	1.070
50.6	4.797	0.50	50.10	0.1273	0.012	1.210	0.059	0.205
25.3	4.8875	0.85	24.45	0.1169	0.021	0.591	0.032	0.643
							Intercept	1.488
							Slope	1.707
							qm	0.586
							K	1.147
							R^2	0.962

Freundlich	
log (C)	**log (q)**
1.09	-0.245
0.52	-0.487
-0.08	-0.636
-0.84	-0.870
-1.92	-1.229
-1.69	-1.496
K	0.227
n	2.665
R^2	0.930

Modified Langmuir		
$(1/C)^X$	**1/q**	**X**
0.222	1.759	0.600
0.488	3.072	
1.123	4.329	
3.196	7.421	
14.151	16.950	
10.293	31.304	
Intercept	3.032	
Slope	1.582	
qmax	0.330	
K	1.916	
R^2	0.6641	

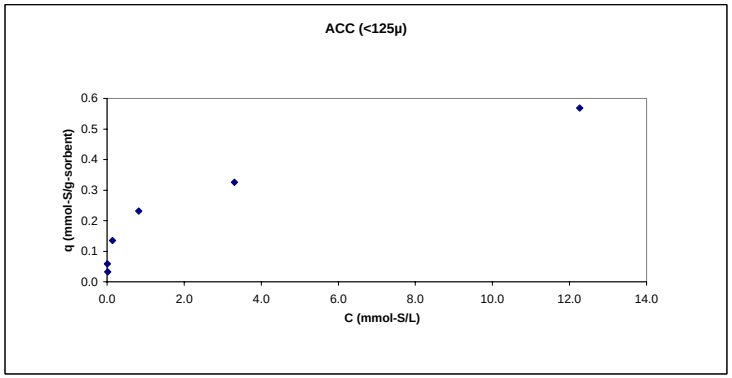

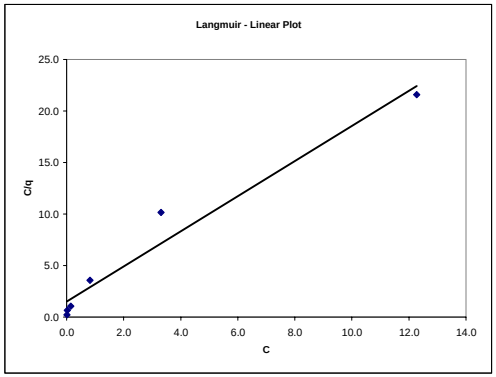

Adsorption Isotherm - 4,6 DMDBT in Hexadecane

Sorbent: Ni (2% wt.) on ACC

Temperature = 50°C

Duration: 24 Hours

Sorbent particle size: <125µ

Ni / ACC (<125µ)

Bulk Solution (4,6 DMDBT + C16)			Conc. Final		Sorbent	Plot data		Langmuir	
C solution	*weight of Soln*	*n solution*	*C solution*	*n solution*	*weight*	*C solution*	*q*	C	C/q
mmol/L	*g*	*mmol*	*mmol/L*	*mmol*	*g*	*mmol/L*	*mmol/g*		
19.51	5.1063	0.129	7.53	0.050	0.1277	7.530	0.620	7.53	12.151
10.53	5.1707	0.070	2.20	0.015	0.1988	2.200	0.280	2.2	7.849
4.96	5.5092	0.035	0.62	0.004	0.1886	0.620	0.164	0.62	3.780
2.56	5.076	0.017	0.10	0.0007	0.1907	0.100	0.085	0.1	1.181
1.45	5.1101	0.010	0.04	0.0003	0.1740	0.040	0.054	0.04	0.747
0.54	5.0199	0.004	0.01	0.0001	0.1662	0.010	0.021	0.01	0.483
0.24	4.9153	0.002	0.01	0.0001	0.1501	0.010	0.010	0.01	1.026
								Intercept	1.598
								Slope	1.525
								qm	0.656
								K	0.955
								R^2	0.888

Freundlich	
log (C)	**log (q)**
0.88	-0.208
0.34	-0.552
-0.21	-0.785
-1.00	-1.072
-1.40	-1.271
-2.00	-1.684
K	0.220
n	2.086
R^2	0.988

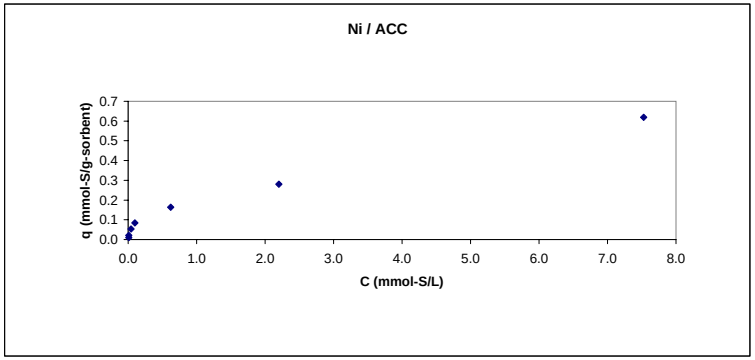

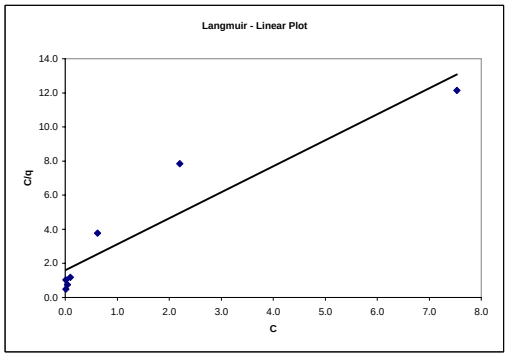

Adsorption Isotherm - 4,6 DMDBT in Hexadecane

Sorbent: Ta (2% wt.) on ACC

Temperature = 50°C

Duration: 24 Hours

Sorbent particle size: <125µ

Ta-2%/ACC

Bulk Solution (4,6 DMDBT + C16)			Conc. Final		Sorbent	Plot data		Langmuir	
C solution	*weight of Soln*	*n solution*	*C solution*	*n solution*	*weight*	*C solution*	*q*	C	C/q
mmol/L	*g*	*mmol*	*mmol/L*	*mmol*	*g*	*mmol/L*	*mmol/g*		
19.51	4.3096	0.109	7.97	0.044	0.0923	7.970	0.697	7.97	11.434
10.53	5.216	0.071	2.95	0.020	0.1398	2.950	0.366	2.95	8.063
4.96	4.6368	0.030	0.50	0.003	0.1303	0.500	0.205	0.5	2.435
2.56	4.4842	0.015	0.14	0.001	0.0862	0.140	0.163	0.14	0.860
1.45	4.7531	0.009	0.04	0.0002	0.0875	0.040	0.099	0.04	0.404
0.54	4.3748	0.003	0.01	0.0001	0.0988	0.010	0.030	0.01	0.329
								Intercept	1.184
								Slope	1.414
								qm	0.707
								K	1.194
								R^2	0.906

Freundlich	
log (C)	**log (q)**
0.90	-0.157
0.47	-0.437
-0.30	-0.688
-0.85	-0.788
-1.40	-1.004
-2.00	-1.518
K	0.285
n	2.411
R^2	0.950

Modified Langmuir		
$(1/C)^X$	**1/q**	**X**
0.234	1.435	0.700
0.469	2.733	
1.625	4.870	
3.960	6.140	
9.518	10.092	
25.119	32.938	
Intercept	1.413	
Slope	1.215	
qmax	0.708	
K	1.162	
R^2	0.9824	

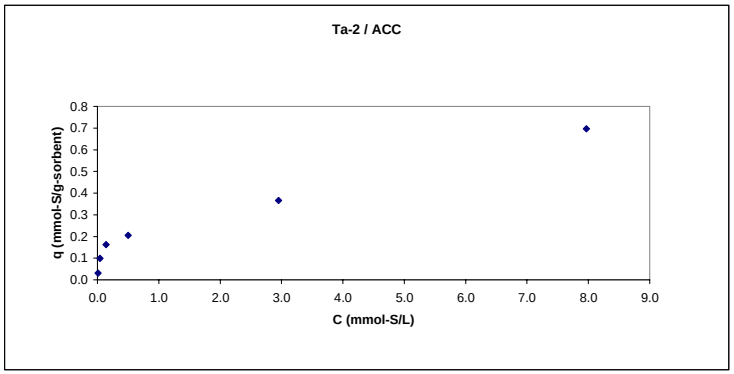

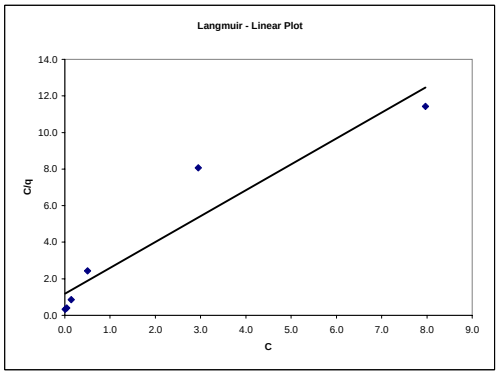

Adsorption Isotherm - 4,6 DMDBT in Hexadecane

Sorbent: Ta (5% wt.) on ACC

Temperature = 50°C

Duration: 24 Hours

Sorbent particle size: <125µ

Ta-5/ACC

Bulk Solution (4,6 DMDBT + C16)			Conc. Final		Sorbent	Plot data		Langmuir	
C solution	*weight of Soln*	*n solution*	*C solution*	*n solution*	*weight*	*C solution*	*q*	C	C/q
mmol/L	*g*	*mmol*	*mmol/L*	*mmol*	*g*	*mmol/L*	*mmol/g*		
21.48	5.7740	0.160	10.33	0.091	0.0879	10.330	0.788	10.33	13.111
10.21	5.1320	0.068	5.03	0.043	0.0502	5.030	0.493	5.03	10.208
4.95	5.0253	0.032	1.22	0.009	0.0769	1.220	0.300	1.22	4.068
2.72	5.0030	0.018	0.37	0.003	0.0596	0.370	0.245	0.37	1.508
1.34	5.4012	0.009	0.06	0.001	0.0763	0.060	0.115	0.06	0.520
0.64	5.6320	0.005	0.02	0.0002	0.0917	0.020	0.049	0.02	0.407
								Intercept	1.387
								Slope	1.263
								qm	0.792
								K	0.910
								R^2	0.924

Freundlich	
log (C)	**log (q)**
1.01	-0.104
0.70	-0.307
0.09	-0.523
-0.43	-0.610
-1.22	-0.938
-1.70	-1.309
K	0.297
n	2.489
R^2	0.969

Modified Langmuir		
$(1/C)^X$	**1/q**	**X**
0.195	1.269	0.700
0.323	2.029	
0.870	3.335	
2.006	4.076	
7.166	8.661	
15.462	20.366	
Intercept	1.475	
Slope	1.187	
qmax	0.678	
K	1.243	
R^2	0.9885	

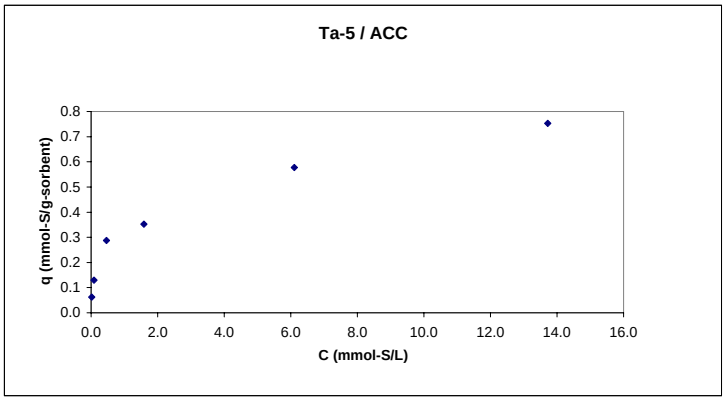

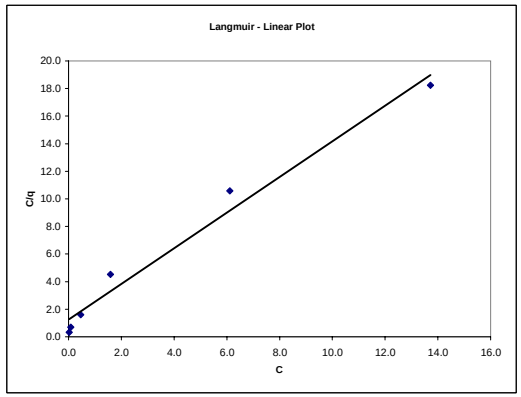

Adsorption Isotherm - 4,6 DMDBT in Hexadecane

Sorbent: Ag (2% wt.) on ACC

Temperature = 50°C

Duration: 24 Hours

Sorbent particle size: <125µ

Ta-10%/ACC

Bulk Solution (4,6 DMDBT + C16)		Conc. Final		Sorbent	Sulfur in Solution		Langmuir	
C solution	*weight of Soln*	*C solution*	*n solution*	*weight*	*C (remaining)*	*C (removed)*	*q*	C/q
ppm	*g*	*ppm*	*ppm*	*g*	*mmol/L*	*mmol/L*	*mmol/g*	
801.2	4.9041	531.48	269.72	0.0815	12.839	6.515	0.507	25.313
399.9	4.6595	137.23	262.68	0.1210	3.315	6.345	0.316	10.487
186.1	4.3858	26.75	159.36	0.1010	0.646	3.849	0.216	2.988
104.9	4.9315	11.92	92.99	0.0872	0.288	2.246	0.164	1.751
50.6	4.8689	1.72	48.88	0.0870	0.042	1.181	0.085	0.486
25.3	4.9862	0.47	24.84	0.1076	0.011	0.600	0.036	0.312
							Intercept	1.414
							Slope	1.917
							qm	0.522
							K	1.356
							R^2	0.978

Freundlich	
log (C)	**log (q)**
1.11	-0.295
0.52	-0.500
-0.19	-0.665
-0.54	-0.784
-1.38	-1.068
-1.95	-1.444
K	0.224
n	2.817
R^2	0.971

Modified Langmuir		
$(1/C)^X$	**1/q**	**X**
0.216	1.972	0.600
0.487	3.164	
1.300	4.624	
2.111	6.085	
6.743	11.698	
14.781	27.805	
Intercept	1.939	
Slope	1.705	
qmax	0.516	
K	1.138	
R^2	0.9910	

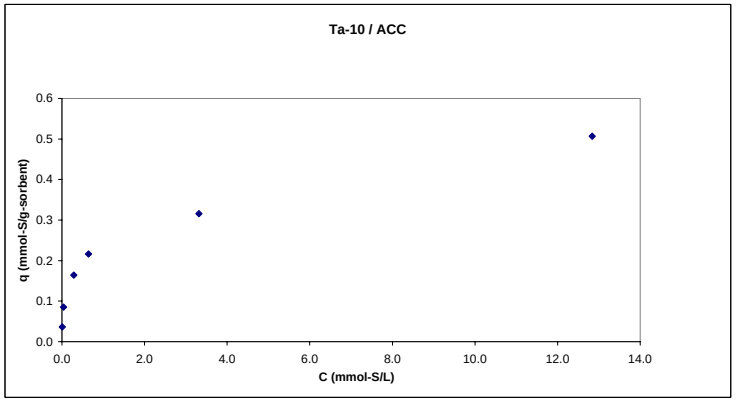

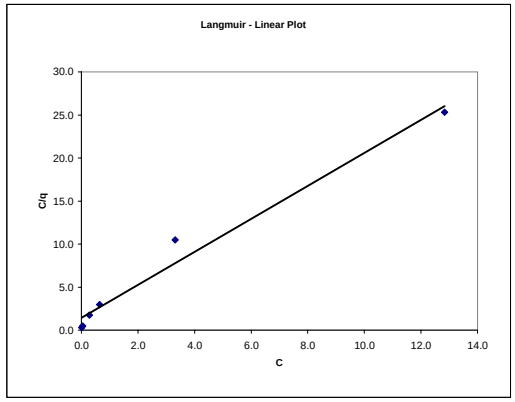

APPENDIX C2 – CALORIMETRY AND BREAKTHROUGH

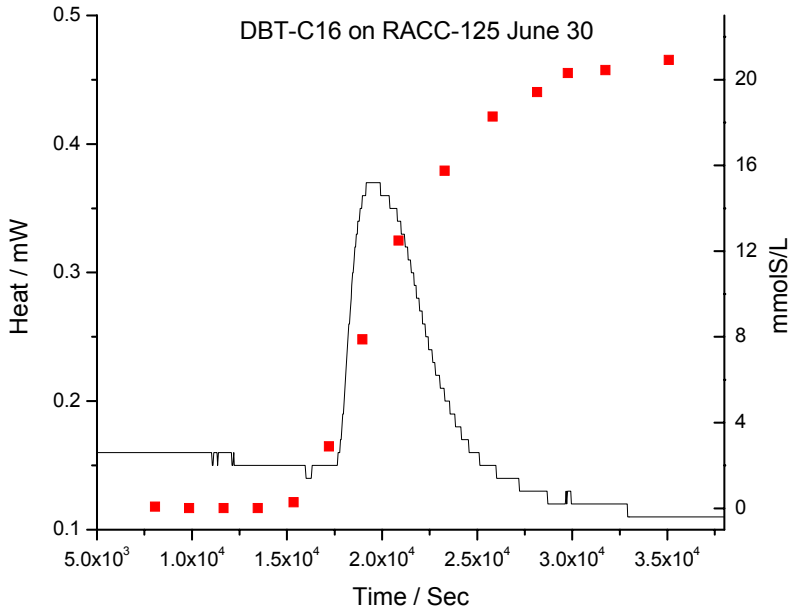

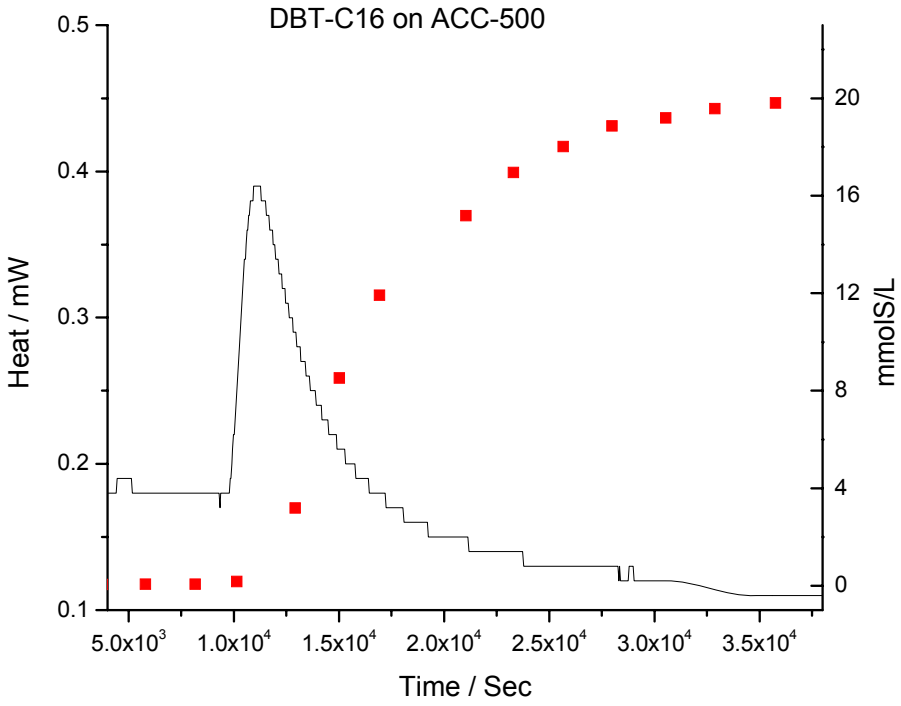

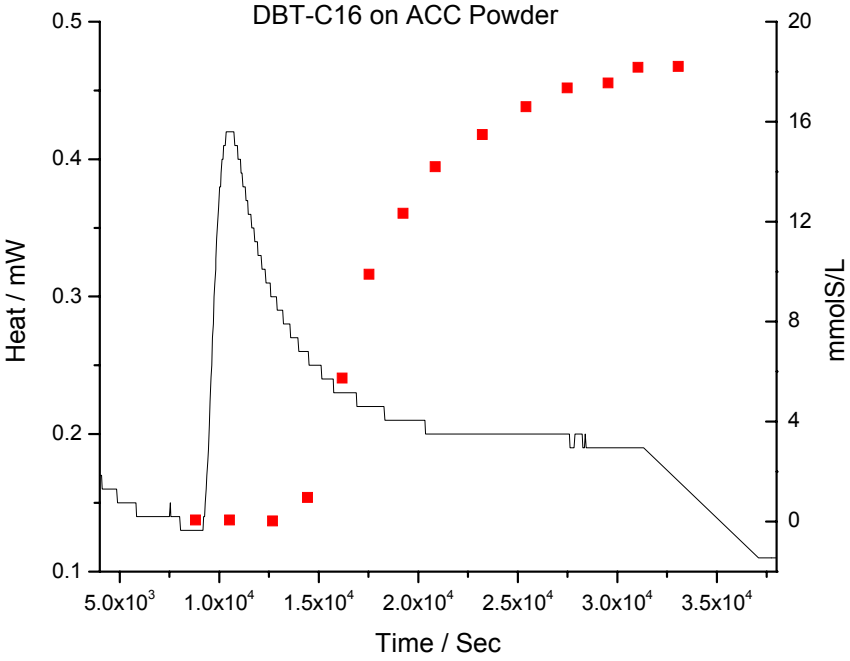
DBT-C16 on ACC Powder
Heat / mW
mmolS/L
Time / Sec
0.5
0.4
0.3
0.2
0.1
20
16
12
8
4
0
5.0x10^3
1.0x10^4
1.5x10^4
2.0x10^4
2.5x10^4
3.0x10^4
3.5x10^4

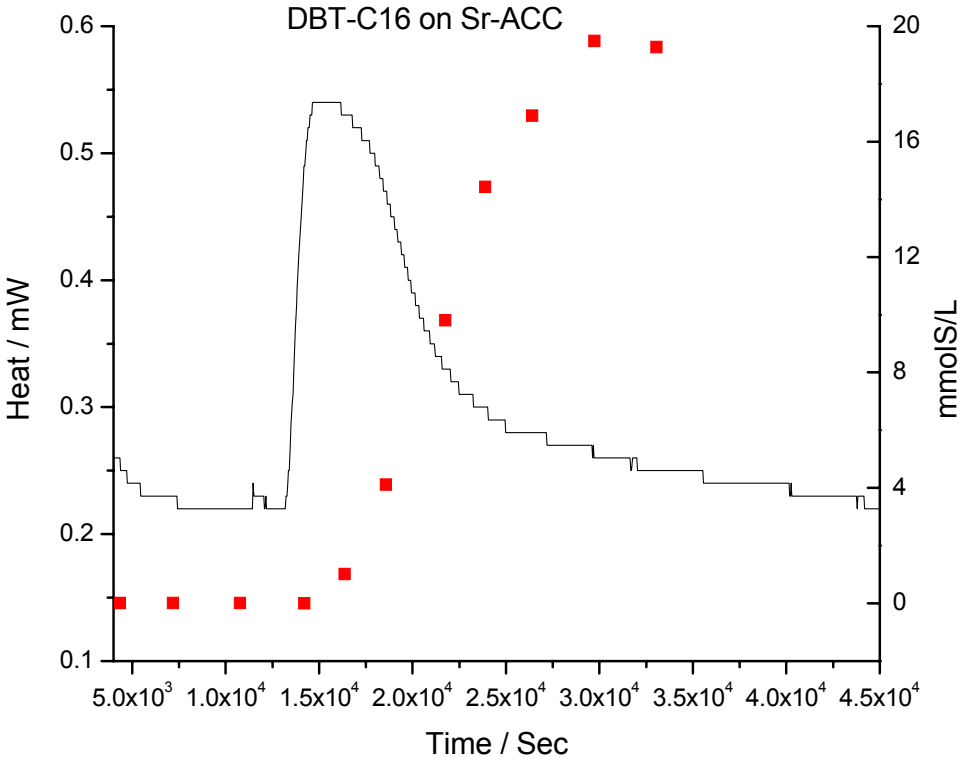
DBT-C16 on Sr-ACC
Heat / mW
mmolS/L
Time / Sec
0.6
0.5
0.4
0.3
0.2
0.1
20
16
12
8
4
0
5.0x10^3
1.0x10^4
1.5x10^4
2.0x10^4
2.5x10^4
3.0x10^4
3.5x10^4
4.0x10^4
4.5x10^4

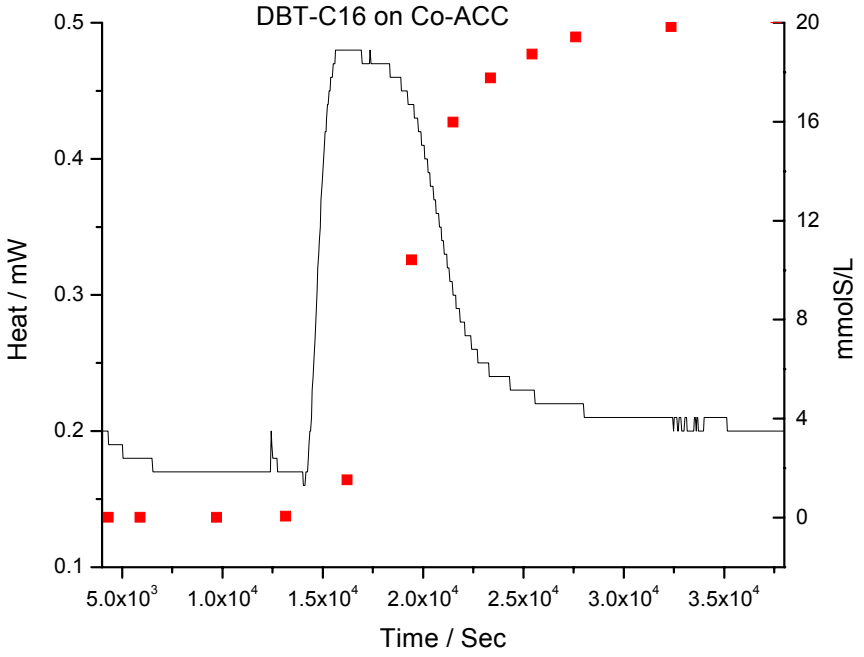
DBT-C16 on Co-ACC
Heat / mW
mmolS/L
Time / Sec
0.5
0.4
0.3
0.2
0.1
20
16
12
8
4
0
5.0x10^3
1.0x10^4
1.5x10^4
2.0x10^4
2.5x10^4
3.0x10^4
3.5x10^4

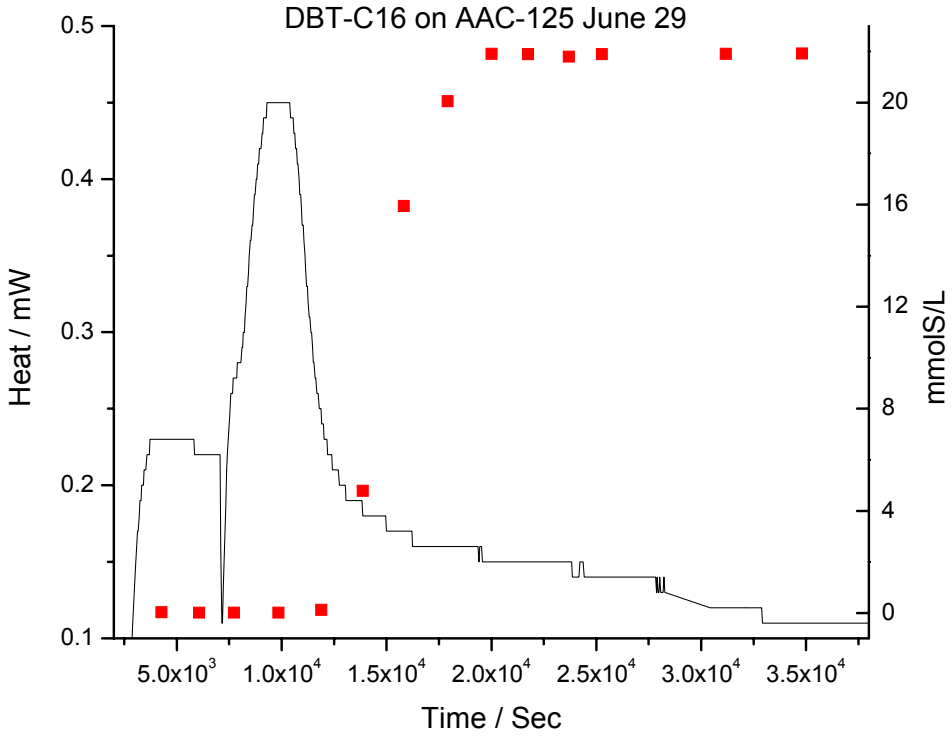
DBT-C16 on AAC-125 June 29
Heat / mW
mmolS/L
Time / Sec
0.5
0.4
0.3
0.2
0.1
20
16
12
8
4
0
5.0x10^3
1.0x10^4
1.5x10^4
2.0x10^4
2.5x10^4
3.0x10^4
3.5x10^4

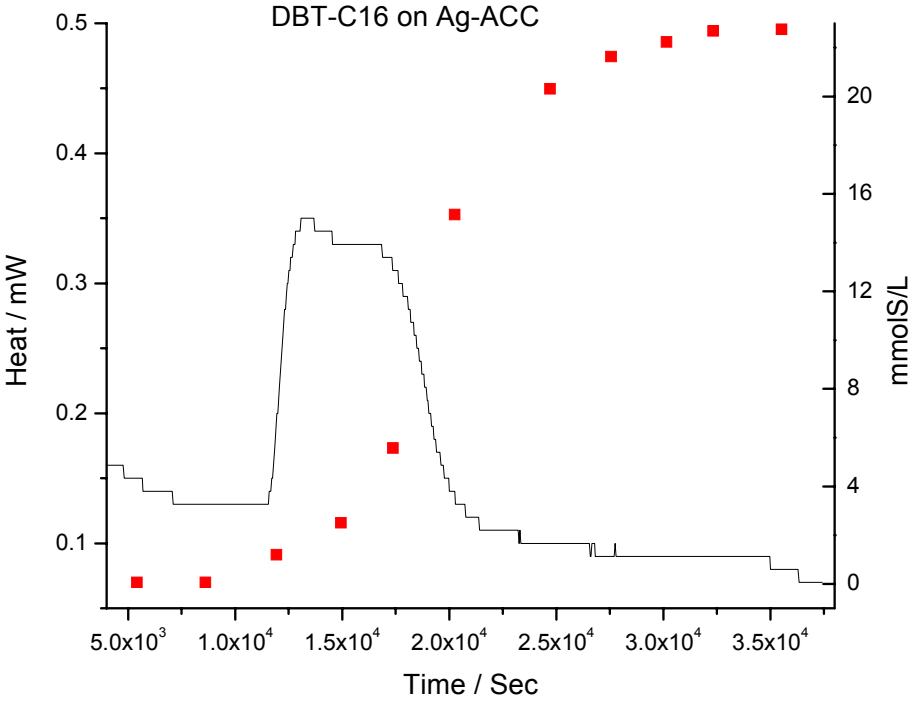
DBT-C16 on Ag-ACC
Heat / mW
mmolS/L
Time / Sec
0.5
0.4
0.3
0.2
0.1
20
16
12
8
4
0
5.0x10^3
1.0x10^4
1.5x10^4
2.0x10^4
2.5x10^4
3.0x10^4
3.5x10^4

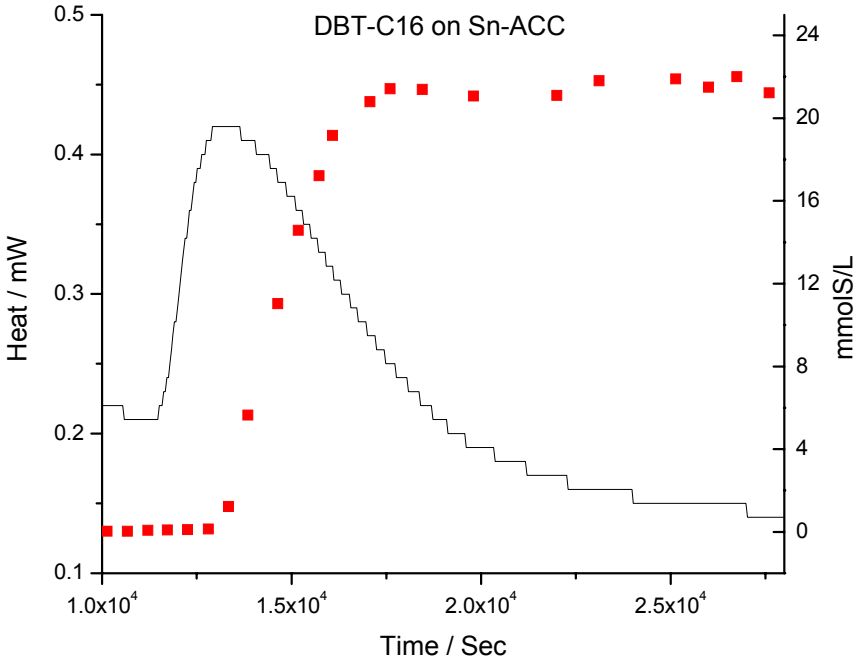
DBT-C16 on Sn-ACC
Heat / mW
mmolS/L
Time / Sec
0.5
0.4
0.3
0.2
0.1
24
20
16
12
8
4
0
1.0x10^4
1.5x10^4
2.0x10^4
2.5x10^4

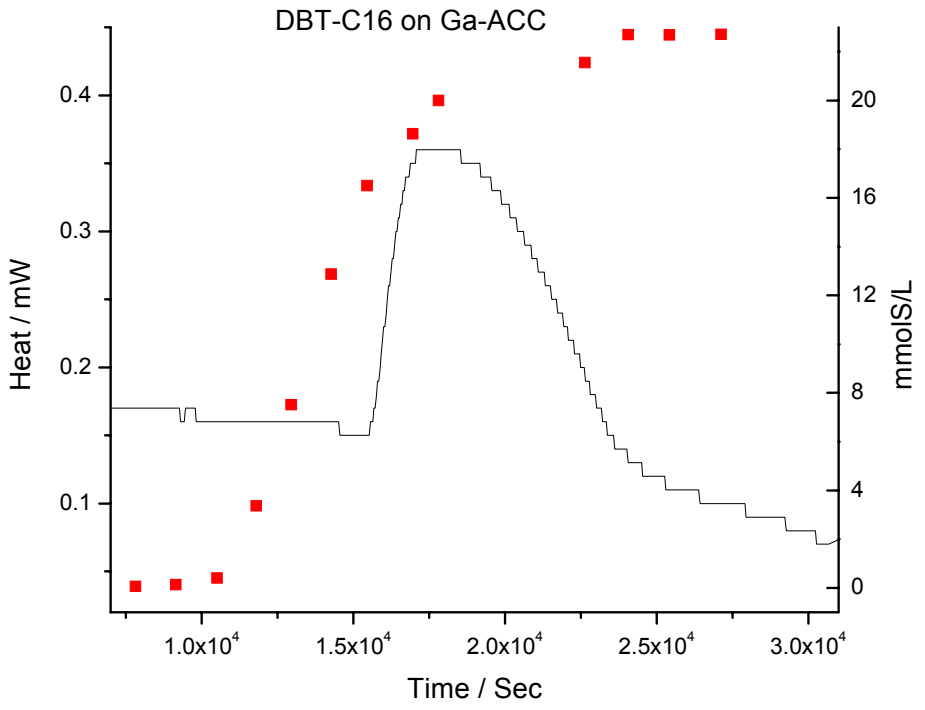
DBT-C16 on Ga-ACC
Heat / mW
mmolS/L
Time / Sec
0.1
0.2
0.3
0.4
0
4
8
12
16
20
1.0x10^4
1.5x10^4
2.0x10^4
2.5x10^4
3.0x10^4

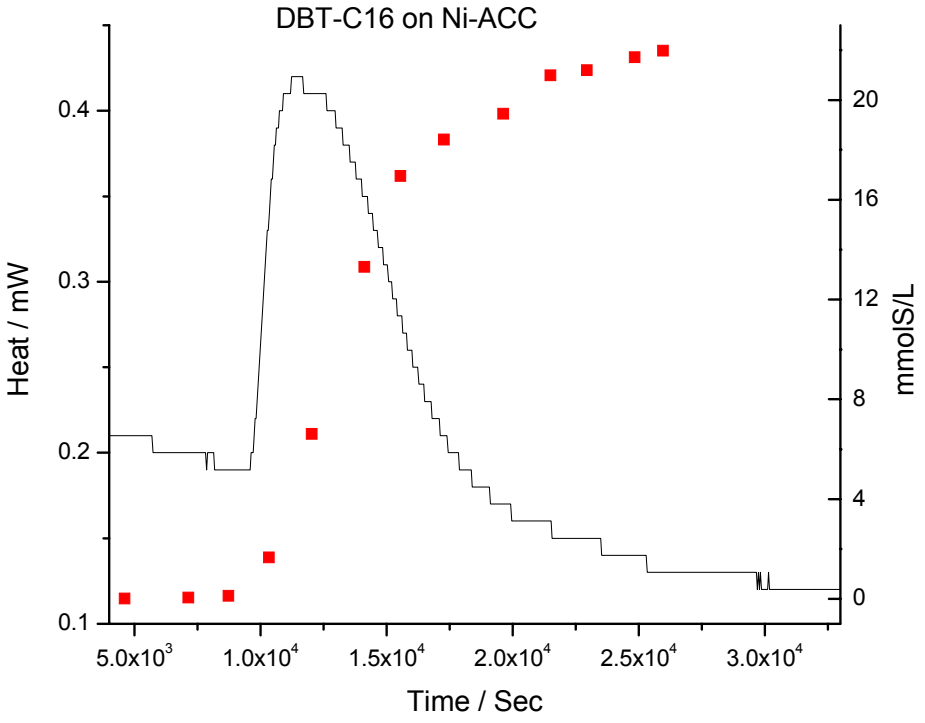
DBT-C16 on Ni-ACC
Heat / mW
mmolS/L
Time / Sec
0.1
0.2
0.3
0.4
0
4
8
12
16
20
5.0x10^3
1.0x10^4
1.5x10^4
2.0x10^4
2.5x10^4
3.0x10^4

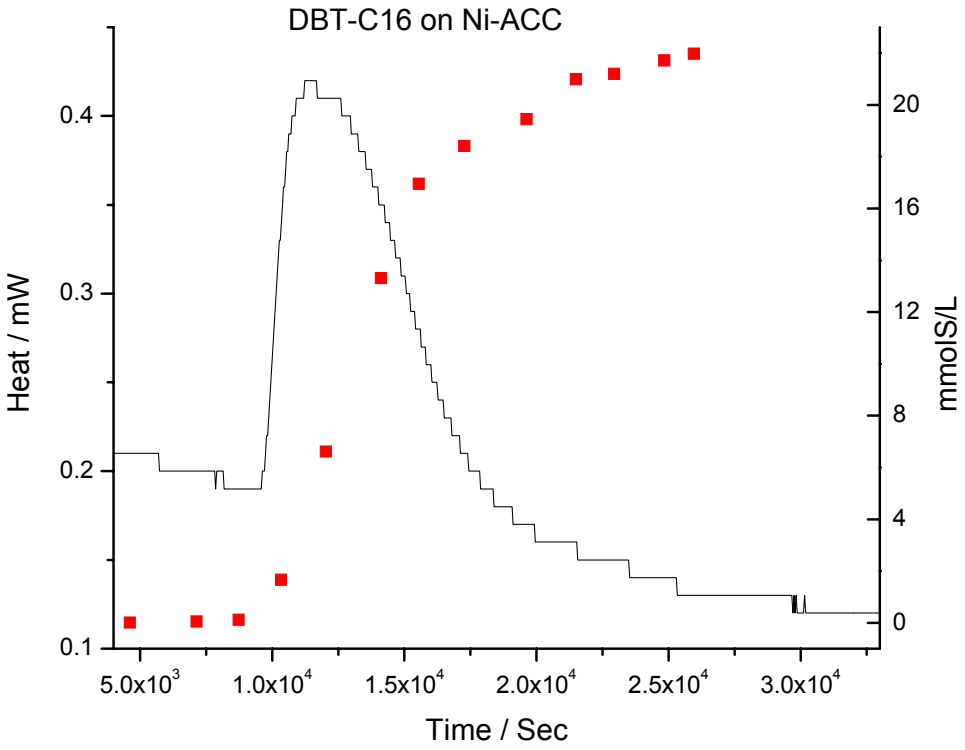
DBT-C16 on Ni-ACC
Heat / mW
mmolS/L
Time / Sec
0.1
0.2
0.3
0.4
0
4
8
12
16
20
5.0x10^3
1.0x10^4
1.5x10^4
2.0x10^4
2.5x10^4
3.0x10^4

APPENDIX C3 – SUPPLEMENTARY DATA – XPS ANALYSIS – FULL SURVEY

FIGURE C4-1 – XPS ANALYSIS FOR ACC – FULL SURVEY

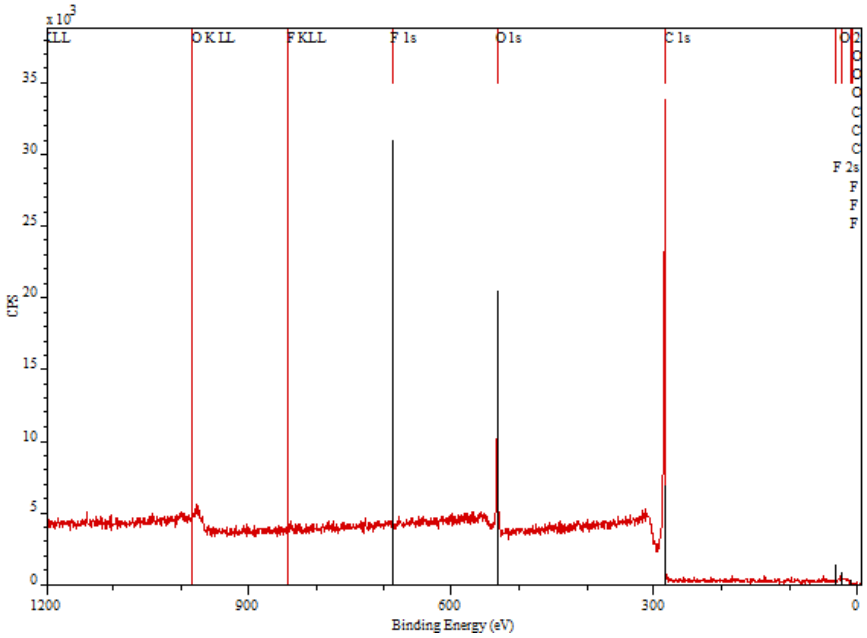

FIGURE C4-2 – XPS ANALYSIS FOR Ta-5/ACC – FULL SURVEY

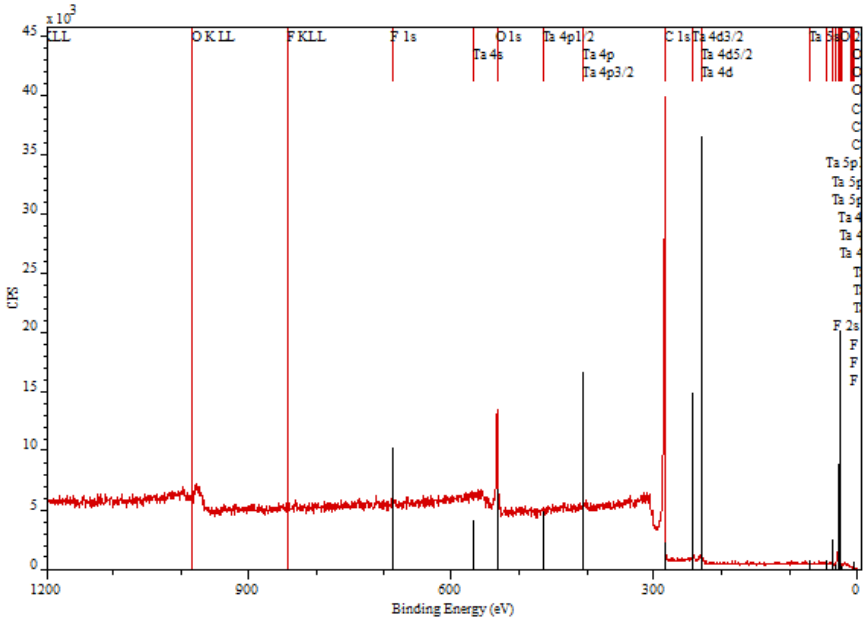

APPENDIX C4 –GC/FID ANALYTICAL METHOD AND CALIBRATION

GC Analytic Methods

1 Liquid Sample Analysis – GC method

The liquid products of adsorption of DBT was analyzed by GC-FID (Varian CP-3800) equipped with a VF-05MS capillary column ($30m \times 0.30mm \times 1.0\mu m$). Ultra high purity helium is used as the carrier gas.

Control method:

Injector: Middle (1177 split/splitless)

Split event table	***Time, min***	***Split state***	***Split ratio***
	Initial	***On***	***55***

Heater: ON; Set point: 250 ; Stabilization time: 0.50 min

Column oven zone:

Temperature program:

Rate, /min	***Step,***		***Time, min***
Initial	***80***		***0.00***
10.0	***250***		***8.00***
		Total time	***25.00***

Column:

Carrier gas	***He***
Length	***15.00 m***
Inside diameter	***320 um***
Constant flow	***Enabled***
Column flow	***6.0 ml/l***
Pressure pulse	***Disabled***

Detectors:

- **Front (FID)**

He makeup flow	H_2 flow	Air flow
28 ml/min	30 ml/min	300 ml/min

FID event table:

Time, min	Range	Auto zero
Initial	12	Yes

Heater: ON; Set point: 300 ℃

1.2 Integration event

Active	Time	Event	On	Value
Yes	0.00	Set peak width		0.1
Yes	0.00	Set threshold		0.1
Yes	0.00	Turn integration	Off	
Yes	2.80	Turn integration	On	

1.3 Example of DBT chromatograph

Fig.C4-4-1 Example of DBT chromatographs at different reaction times under 25^{o}C

Fig.C4-4-2 Change of DBT peak at different reaction times under 25^{o}C

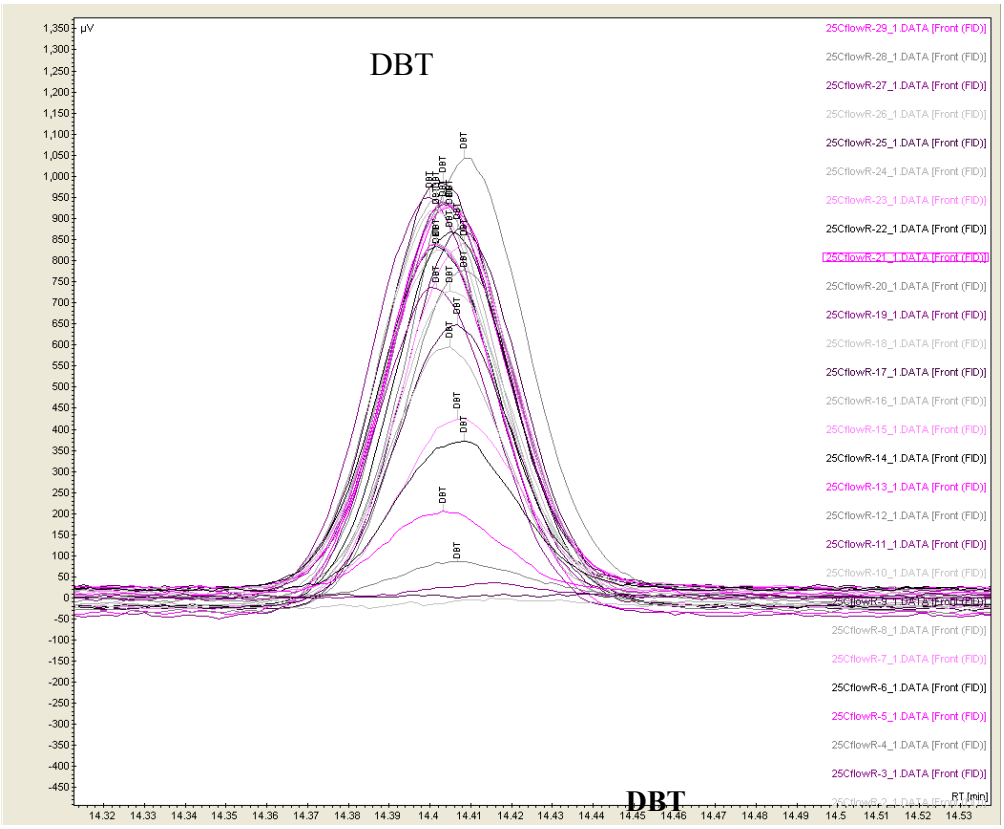

Calibration Method

Method type: External Standard

Response: Area (for FID)

Standard Unit: mmol/L-conc.

Fig. 4-4-3 GC calibration curves of starting reactants, DBT

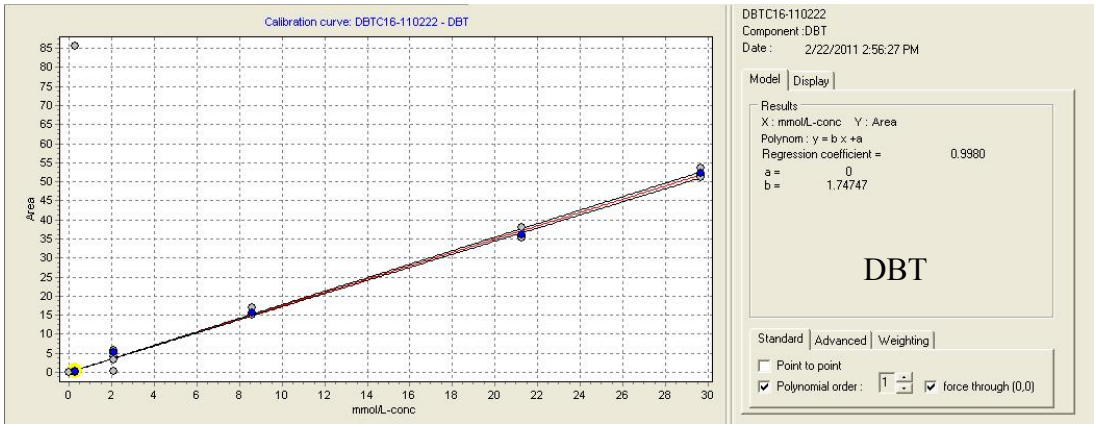

GC Calculation Processes

- **Calculation of product component concentrations in liquid product samples:**

1. Concentration of starting reagents (DBT) in the feedstock:

$$C_j^{inFeed}, ppmw \cdot mol \cdot g^{-1} = \frac{R_j^{inFeed}, ppmw}{MW_R, g \cdot mol^{-1}}$$

2. Concentration of S-adsorption products and starting reagents in liquid product samples:

$C_i, ppmw = \frac{Area^{GC}}{Rf_i}$, Rf: Response factor

$$C_i, ppmw \cdot mol \cdot g^{-1} = \frac{C_i, ppmw}{MW_i, g \cdot mol^{-1}}$$

3. Normalized concentration of the component i based on the composition:

$$C_i, mol\% = \frac{C_i, ppmw \cdot mol \cdot g^{-1}}{\sum_i C_i, ppmw \cdot mol \cdot g^{-1}} \times 100 mol\%$$

- **Conversion of starting reagents:**

$Conv_j = 1 - \sum_{i(i \neq j)} C_i, mol\%$ ---applied in the calculation of conversions of DBT.

Flow Reactor Experiment
Sorbent: ACC (run I)
Run Temperature: 25 °C
Flow rate: 0.1 mL/min
Solution: DBT+C16 Flow
Comment:None in-Situ Activation

Sample ID	Time (min)	Run1	Run2	Average (mmol/L)	Sulfur in outflow (mmol-S.min/L)	Sulfur in Outflow (mmol-S)	Total Sulfur (mmol-S)	Sulfur Removed (mmol-S)	Sorbent Weight (g)	Adsorption Capacity (mmol-S/g-sorbent)	$t^{0.5}$	qe - qt	log(qe - qt)	t/qt
1	20	1.06	1.17	1.115	0	0.000	0.043	0.043	0.1840	0.23	4.47	0.29	-0.53	86.47
2	26	5.15	5.06	5.105	38.9	0.004	0.055	0.051		0.28	5.10	0.25	-0.61	93.01
3	32	7.84	6.44	7.14	115.4	0.012	0.068	0.057		0.31	5.66	0.22	-0.66	104.12
4	38	7.56	7.94	7.75	208.5	0.021	0.081	0.060		0.33	6.16	0.20	-0.70	116.51
5	44	8.14	7.14	7.64	304.7	0.030	0.094	0.063		0.34	6.63	0.18	-0.74	128.18
6	50	8.28	8.61	8.445	405.2	0.041	0.106	0.066		0.36	7.07	0.17	-0.78	139.66
7	56	8.6	9.81	9.205	515.5	0.052	0.119	0.068		0.37	7.48	0.16	-0.80	152.41
8	62	9	8.97	8.985	629.2	0.063	0.132	0.069		0.38	7.87	0.15	-0.82	165.32
9	68	8.74	8.62	8.68	739.6	0.074	0.145	0.071		0.38	8.25	0.14	-0.85	176.89
10	74	8.12	9.56	8.84	849.1	0.085	0.157	0.073		0.39	8.60	0.13	-0.88	187.68
11	80	8.49	9.17	8.83	959.5	0.096	0.170	0.074		0.40	8.94	0.12	-0.92	198.19
12	86	9.28	8.3	8.79	1069.7	0.107	0.183	0.076		0.41	9.27	0.11	-0.95	208.13
13	92	7.02	7.06	7.04	1168.6	0.117	0.196	0.079		0.43	9.59	0.10	-1.02	214.55
14	98	6.9	8.04	7.47	1259.3	0.126	0.209	0.083		0.45	9.90	0.08	-1.12	218.31
15	104	9.2	8.77	8.985	1359.0	0.136	0.221	0.085		0.46	10.20	0.06	-1.21	224.09
16	110	7.05	7.37	7.21	1457.1	0.146	0.234	0.088		0.48	10.49	0.04	-1.35	229.08
17	116	8.1	7.71	7.905	1551.6	0.155	0.247	0.092		0.50	10.77	0.03	-1.57	232.83
18	122	8.5	7.91	8.205	1663.8	0.166	0.260	0.093		0.51	11.05	0.02	-1.73	240.80
19	128	8.17	7.57	7.87	1775.7	0.178	0.272	0.095		0.52	11.31	0.01	-2.00	248.46
20	134	9.95	9.34	9.645	1885.2	0.189	0.285	0.097		0.53	11.58	0.00	-	255.21

Pseudo First Order Kinetics		Pseudo Second Order Kinetics	
qe	0.6	qe	0.66
K_{ad1}	0.0250	K_{ad2}	0.0357
R^2	0.8486	R^2	0.9746
h_1	0.0155	h_2	0.0155

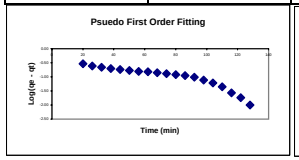

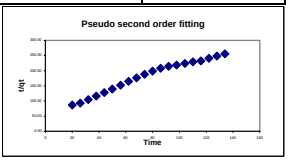

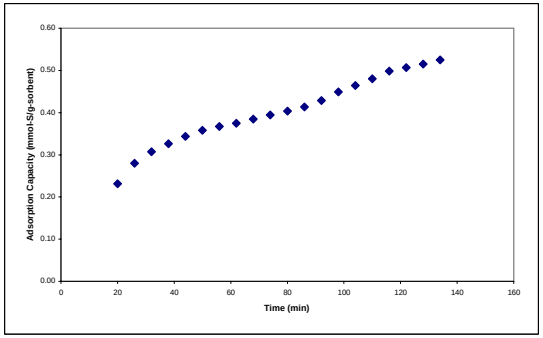

Weber-Morris Intra-Particle Diffusion	
K_{id}	0.03773
C	0.08109

Flow Reactor Experiment
Sorbent: ACC (run II)
Run Temperature: 25 °C
Flow rate: 0.1 mL/min
Solution: DBT+C16 Flow
Comment: in-Situ Activation

Sample #	Time	run1	run2	Average (mmol/L)	Sulfur in outflow (mmol-S.min/L)	Sulfur in Outflow (mmol-S)	Total Sulfur (mmol-S)	Sulfur Removed (mmol-S)	Sorbent Weight (g)	Adsorption Capacity (mmol-S/g-sorbent)	$t^{0.5}$	qe - qt	log(qe - qt)	t/qt
1	20	0.1	0.1	0.1	0	0.000	0.043	0.043		0.16	4.47	0.44	-0.36	125.15
2	26	0.8	0.8	0.8	2.3	0.000	0.055	0.055		0.21	5.10	0.39	-0.41	125.66
3	32	11.1	11.2	11.115	32.0	0.003	0.068	0.065		0.24	5.66	0.35	-0.45	131.33
4	38	15.1	14.9	14.96	97.2	0.010	0.081	0.071		0.27	6.16	0.33	-0.48	142.26
5	44	16.4	16.4	16.42	175.7	0.018	0.094	0.076		0.29	6.63	0.31	-0.51	154.06
6	50	17.2	17.2	17.21	259.8	0.026	0.106	0.080		0.30	7.07	0.30	-0.53	165.58
7	56	18.1	18.1	18.08	348.0	0.035	0.119	0.084		0.32	7.48	0.28	-0.55	176.77
8	62	18.2	18.0	18.08	438.4	0.044	0.132	0.088		0.33	7.87	0.27	-0.57	187.43
9	68	18.4	18.2	18.32	529.4	0.053	0.145	0.092		0.34	8.25	0.25	-0.60	197.36
10	74	18.4	18.3	18.35	621.1	0.062	0.157	0.095		0.36	8.60	0.24	-0.62	206.66
11	80	19.1	18.5	18.775	713.9	0.071	0.170	0.099		0.37	8.94	0.23	-0.64	215.54
12	86	18.9	18.8	18.84	807.9	0.081	0.183	0.102		0.38	9.27	0.21	-0.67	224.08
13	92	18.9	18.8	18.835	902.1	0.090	0.196	0.106		0.40	9.59	0.20	-0.70	232.11
14	98	19.0	18.9	18.985	996.6	0.100	0.209	0.109		0.41	9.90	0.19	-0.72	239.72
15	104	19.1	19.1	19.1	1091.9	0.109	0.221	0.112		0.42	10.20	0.18	-0.75	247.04
16	110	19.1	19.3	19.16	1187.5	0.119	0.234	0.115	0.2663	0.43	10.49	0.16	-0.78	254.03
17	116	20.0	19.4	19.67	1284.6	0.128	0.247	0.118		0.44	10.77	0.15	-0.81	260.97
18	122	19.9	19.4	19.65	1382.9	0.138	0.260	0.121		0.46	11.05	0.14	-0.85	267.82
19	128	19.4	19.5	19.48	1480.7	0.148	0.272	0.124		0.47	11.31	0.13	-0.88	274.24
20	134	19.6	19.5	19.55	1578.3	0.158	0.285	0.127		0.48	11.58	0.12	-0.92	280.31
21	140	19.5	19.6	19.51	1675.9	0.168	0.298	0.130		0.49	11.83	0.11	-0.96	286.12
22	146	19.7	19.5	19.58	1773.7	0.177	0.311	0.133		0.50	12.08	0.10	-1.01	291.67
23	152	19.5	19.8	19.635	1871.7	0.187	0.323	0.136		0.51	12.33	0.09	-1.06	297.06
24	158	19.7	19.8	19.745	1970.1	0.197	0.336	0.139		0.52	12.57	0.08	-1.12	302.30
25	164	19.8	19.6	19.705	2068.8	0.207	0.349	0.142		0.53	12.81	0.06	-1.19	307.37
26	170	19.8	19.8	19.78	2167.5	0.217	0.362	0.145		0.54	13.04	0.05	-1.27	312.25
28	176	19.8	19.9	19.845	2266.5	0.227	0.374	0.148		0.56	13.27	0.04	-1.37	317.01
29	182	19.7	20.0	19.85	2365.8	0.237	0.387	0.151		0.57	13.49	0.03	-1.49	321.64
30	188	19.9	19.7	19.765	2464.8	0.246	0.400	0.154		0.58	13.71	0.02	-1.67	326.04
31	194	19.9	19.9	19.88	2563.9	0.256	0.413	0.156		0.59	13.93	0.01	-1.97	330.31
32	200	19.9	19.8	19.865	2663.3	0.266	0.426	0.159		0.60	14.14	0.00		334.47

Pseudo First Order Kinetics		Pseudo Second Order Kinetics	
qe	0.8	qe	0.83
K_{ad1}	0.0160	K_{ad2}	0.0134
R^2	0.8798	R^2	0.9784
h_1	0.0121	h_2	0.0091

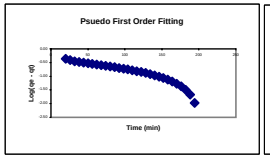

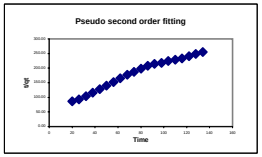

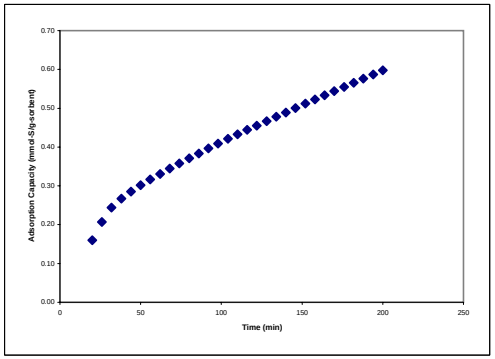

Weber-Morris Intra-Particle Diffusion	
K_{id}	0.04208
C	-0.00439

Flow Reactor Experiment
Sorbent: Ta-5/ACC (run I)
Run Temperature: 25 °C
Flow rate: 0.1 mL/min
Solution: DBT+C16 Flow
Comment: in-Situ Activation

Sample ID	Sample Time (min)	run1	run2	Average (mmol/L)	Sulfur in outflow (mmol-S.min/L)	Sulfur in Outflow (mmol-S)	Total Sulfur (mmol-S)	Sulfur Removed (mmol-S)	Sorbent Weight (g)	Adsorption Capacity (mmol-S/g-sorbent)	$t^{0.5}$	qe - qt	log(qe - qt)	t/qt
1	10	0.05	0.05	0.05	0	0.000	0.021	0.021		0.11	3.16	1.24	0.09	89.86
2	22.5	0.51	0.51	0.51	3.5	0.000	0.048	0.048		0.25	4.74	1.10	0.04	90.52
3	35	1.06	0.94	1	12.9	0.001	0.074	0.073		0.38	5.92	0.97	-0.01	91.45
4	47.5	2.01	2.05	2.03	31.9	0.003	0.101	0.098		0.51	6.89	0.84	-0.08	92.78
5	60	4.33	4.84	4.585	73.2	0.007	0.128	0.120		0.63	7.75	0.72	-0.14	95.32
6	72.5	7.61	7.03	7.32	147.6	0.015	0.154	0.140		0.73	8.51	0.62	-0.21	99.37
7	85	8.99	8.47	8.73	247.9	0.025	0.181	0.156		0.82	9.22	0.54	-0.27	104.13
8	97.5	12.67	13.35	13.01	383.8	0.038	0.207	0.169		0.88	9.87	0.47	-0.33	110.25
9	110	13.81	13.32	13.565	549.9	0.055	0.234	0.179		0.94	10.49	0.42	-0.38	117.45
10	122.5	15.82	15.37	15.595	732.2	0.073	0.261	0.187		0.98	11.07	0.37	-0.43	124.95
11	135	16.2	16.1	16.15	930.6	0.093	0.287	0.194		1.02	11.62	0.34	-0.47	132.91
12	147.5	17.12	16.45	16.785	1136.4	0.114	0.314	0.200		1.05	12.14	0.30	-0.52	140.86
13	160	17.94	16.18	17.06	1347.9	0.135	0.340	0.206		1.08	12.65	0.28	-0.56	148.75
14	172.5	18.73	17.03	17.88	1566.3	0.157	0.367	0.210		1.10	13.13	0.25	-0.60	156.74
15	185	17.82	18.63	18.225	1792.0	0.179	0.394	0.214	0.1912	1.12	13.60	0.23	-0.64	164.94
16	197.5	17.85	17.99	17.92	2017.9	0.202	0.420	0.218		1.14	14.05	0.21	-0.68	172.86
17	210	18.5	17.79	18.145	2243.3	0.224	0.447	0.223		1.16	14.49	0.19	-0.73	180.44
18	222.5	17.14	17.82	17.48	2465.9	0.247	0.473	0.227		1.19	14.92	0.17	-0.78	187.53
19	235	18.76	18.8	18.78	2692.6	0.269	0.500	0.231		1.21	15.33	0.14	-0.84	194.69
20	247.5	21.06	18.62	19.84	2933.9	0.293	0.527	0.233		1.22	15.73	0.13	-0.88	202.89
21	260	19.11	19.36	19.235	3178.2	0.318	0.553	0.235		1.23	16.12	0.12	-0.92	211.16
22	272.5	16.9	19.22	18.06	3411.3	0.341	0.580	0.239		1.25	16.51	0.10	-0.98	218.27
23	285	19.44	17.92	18.68	3640.9	0.364	0.606	0.242		1.27	16.88	0.08	-1.07	224.85
24	297.5	19.77	18.51	19.14	3877.3	0.388	0.633	0.245		1.28	17.25	0.07	-1.16	231.88
25	310	20.48	19.88	20.18	4123.0	0.412	0.660	0.247		1.29	17.61	0.06	-1.23	239.65
26	322.5	18.98	18.04	18.51	4364.8	0.436	0.686	0.250		1.31	17.96	0.05	-1.34	246.90
27	335	19.75	19.46	19.605	4603.0	0.460	0.713	0.253		1.32	18.30	0.03	-1.50	253.65
28	347.5	19.93	20.94	20.435	4853.3	0.485	0.739	0.254		1.33	18.64	0.02	-1.64	261.49
29	360	19.05	19.95	19.5	5102.9	0.510	0.766	0.256		1.34	18.97	0.01	-1.84	269.16
30	372.5	18.59	18.66	18.625	5341.2	0.534	0.793	0.259		1.35	19.30	0.00	-	275.52

Pseudo First Order Kinetics		Pseudo Second Order Kinetics	
qe	1.5	qe	1.79
K_{ad1}	0.0108	K_{ad2}	0.0049
R^2	0.9654	R^2	0.9898
h_1	0.0163	h_2	0.0156

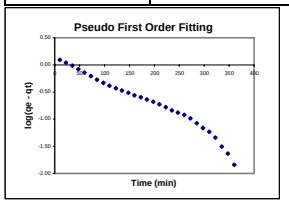

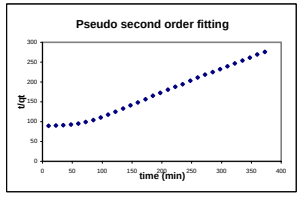

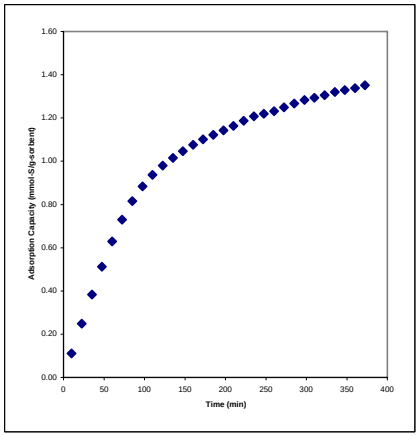

Weber-Morris Intra-Particle Diffusion		C
K_{id2}	0.07246	0.06712

Flow Reactor Experiment
Sorbent: Ta-S/ACC (run II)
Run Temperature: 25 °C
Flow rate: 0.1 mL/min
Solution: DBT+C16 Flow
Comment:in-Situ Activation

Sample #	Time (min)	Run 1	run2	Average (mmol/L)	Sulfur in outflow (mmol-S.min/L)	Sulfur in Outflow (mmol-S)	Total Sulfur (mmol-S)	Sulfur Removed (mmol-S)	Sorbent Weight (g)	Adsorption Capacity (mmol-S/g-sorbent)	$t^{0.5}$	qe - qt	log(qe - qt)	t/qt
1	20	9.84	9.82	9.83	0	0.000	0.043	0.043		0.38	4.47	1.02	0.01	51.98
2	32.5	11.19	11.29	11.24	131.7	0.013	0.069	0.056		0.51	5.70	0.90	-0.04	64.20
3	45	15.52	15.51	15.515	298.9	0.030	0.096	0.066		0.60	6.71	0.81	-0.09	75.57
4	57.5	16.62	16.84	16.73	500.4	0.050	0.122	0.072		0.65	7.58	0.76	-0.12	87.95
5	70	17.46	17.29	17.375	713.6	0.071	0.149	0.078		0.70	8.37	0.71	-0.15	99.78
6	82.5	17.7	17.68	17.69	932.8	0.093	0.176	0.082		0.74	9.08	0.67	-0.18	110.91
7	95	17.43	17.86	17.645	1153.6	0.115	0.202	0.087		0.78	9.75	0.62	-0.20	121.07
8	107.5	18.08	17.92	18	1376.4	0.138	0.229	0.091		0.82	10.37	0.59	-0.23	130.50
9	120	18.37	18.45	18.41	1603.9	0.160	0.255	0.095		0.86	10.95	0.55	-0.26	139.78
10	132.5	18.23	18.49	18.36	1833.8	0.183	0.282	0.099		0.89	11.51	0.52	-0.29	148.68
11	145	18.43	18.56	18.495	2064.1	0.206	0.309	0.102		0.92	12.04	0.49	-0.31	157.03
12	157.5	18.49	18.62	18.555	2295.7	0.230	0.335	0.106		0.95	12.55	0.45	-0.34	165.01
13	170	18.57	18.51	18.54	2527.5	0.253	0.362	0.109		0.99	13.04	0.42	-0.37	172.52
14	182.5	18.89	18.69	18.79	2760.8	0.276	0.388	0.112		1.01	13.51	0.39	-0.40	179.82
15	195	18.8	18.79	18.795	2995.7	0.300	0.415	0.115	0.1106	1.04	13.96	0.37	-0.44	186.96
16	207.5	18.74	18.79	18.765	3230.5	0.323	0.442	0.118		1.07	14.40	0.34	-0.47	193.70
17	220	18.87	18.77	18.82	3465.4	0.347	0.468	0.122		1.10	14.83	0.31	-0.51	200.12
18	232.5	18.87	18.79	18.83	3700.7	0.370	0.495	0.125		1.13	15.25	0.28	-0.55	206.29
19	245	18.8	18.83	18.815	3936.0	0.394	0.521	0.128		1.15	15.65	0.25	-0.59	212.16
20	257.5	18.74	18.83	18.785	4171.0	0.417	0.548	0.131		1.18	16.05	0.23	-0.64	217.70
21	270	18.86	18.91	18.885	4406.4	0.441	0.575	0.134		1.21	16.43	0.20	-0.70	223.06
22	282.5	18.85	18.82	18.835	4642.2	0.464	0.601	0.137		1.24	16.81	0.17	-0.77	228.23
23	295	18.72	18.63	18.675	4876.6	0.488	0.628	0.140		1.27	17.18	0.14	-0.84	232.96
24	307.5	19	18.506667	19	5112.1	0.511	0.654	0.143		1.29	17.54	0.12	-0.94	237.66
25	320	18.6	18.366667	19.2	5350.8	0.535	0.681	0.146		1.32	17.89	0.09	-1.04	242.70
26	332.5	18.53	18.226667	19.4	5592.1	0.559	0.708	0.148		1.34	18.23	0.07	-1.16	247.98
27	345	18.46	18.086667	19.6	5835.8	0.584	0.734	0.151		1.36	18.57	0.05	-1.31	253.50
28	357.5	18.39	17.946667	19.8	6082.1	0.608	0.761	0.152		1.38	18.91	0.03	-1.51	259.29
29	370	18.32	17.806667	19.9	6330.2	0.633	0.787	0.154		1.39	19.24	0.01	-1.84	265.25
30	382.5	18.25	17.666667	20.1	6580.2	0.658	0.814	0.156		1.41	19.56	0.00	-	271.40

Pseudo First Order Kinetics		Pseudo Second Order Kinetics	
qe	1.1	qe	1.73
K_{ad1}	0.0060	K_{ad2}	0.0052
R^2	0.8710	R^2	0.9763
h_1	0.0066	h_2	0.0158

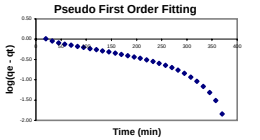

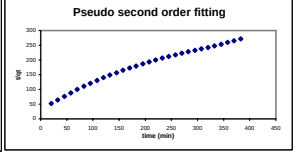

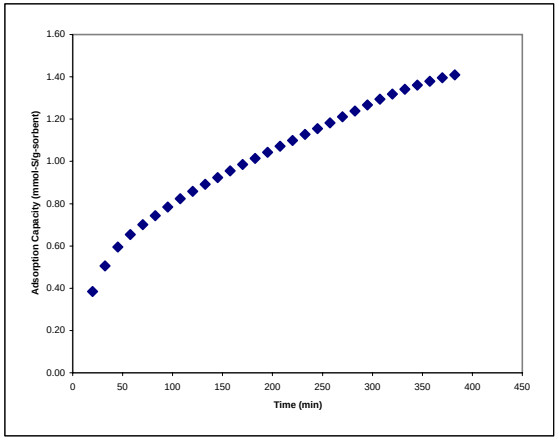

Weber-Morris Intra-Particle Diffusion	
K_{id}	0.06559
C	0.13585

Flow Reactor Experiment
Sorbent: Ta-5/ACC (run III) - Regenerated
Run Temperature: 25 °C
Flow rate: 0.1 mL/min
Solution: DBT+C16 Flow
Comment: in-Situ Activated

Sample ID	Time (min)	run1	run2	Average (mmol/L)	Sulfur in outflow (mmol-S.min/L)	Sulfur in Outflow (mmol-S)	Total Sulfur (mmol-S)	Sulfur Removed (mmol-S)	Sorbent Weight (g)	Adsorption Capacity (mmol-S/g-sorbent)	$t^{0.5}$	qe - qt	log(qe - qt)	t/qt
1	20	5.07	4.73	4.9	0	0.000	0.043	0.043		0.28	4.47	1.07	0.03	71.20
2	32.5	7.84	8.91	8.375	63.8	0.006	0.069	0.063		0.41	5.70	0.94	-0.03	78.43
3	45	11.12	11.24	11.18	159.4	0.016	0.096	0.080		0.53	6.71	0.83	-0.08	85.42
4	57.5	13.94	14.34	14.14	281.6	0.028	0.122	0.094		0.62	7.58	0.73	-0.13	92.48
5	70	16.37	16.28	16.325	426.8	0.043	0.149	0.106		0.70	8.37	0.65	-0.18	99.80
6	82.5	17.22	16.97	17.095	592.7	0.059	0.176	0.116		0.77	9.08	0.59	-0.23	107.49
7	95	18.09	16.95	17.52	771.2	0.077	0.202	0.125		0.83	9.75	0.53	-0.28	115.12
8	107.5	18.35	19.31	18.83	959.9	0.096	0.229	0.133		0.88	10.37	0.48	-0.32	122.69
9	120	18.14	19.36	18.75	1153.0	0.115	0.255	0.140		0.92	10.95	0.43	-0.37	129.82
10	132.5	19.91	19.36	19.635	1351.8	0.135	0.282	0.147		0.97	11.51	0.39	-0.41	136.78
11	145	19.47	19.58	19.525	1562.7	0.156	0.309	0.152		1.01	12.04	0.35	-0.46	144.27
12	157.5	19.8	20.18	19.99	1787.5	0.179	0.335	0.156		1.03	12.55	0.32	-0.49	152.58
13	170	19.86	20.23	20.045	2017.5	0.202	0.362	0.160	0.1515	1.06	13.04	0.30	-0.52	160.99
14	182.5	19.79	20.32	20.055	2245.0	0.225	0.388	0.164		1.08	13.51	0.27	-0.56	168.77
15	195	19.56	20.31	19.935	2471.8	0.247	0.415	0.168		1.11	13.96	0.25	-0.61	176.11
16	207.5	20.38	19.39	19.885	2697.3	0.270	0.442	0.172		1.13	14.40	0.22	-0.65	182.99
17	220	20.58	21.16	20.87	2918.1	0.292	0.468	0.176		1.16	14.83	0.19	-0.72	189.03
18	232.5	19.11	21.03	20.07	3140.2	0.314	0.495	0.181		1.19	15.25	0.16	-0.79	194.93
19	245	19.83	19.94	19.885	3370.4	0.337	0.521	0.184		1.22	15.65	0.14	-0.86	201.42
20	257.5	20.28	19.6	19.94	3602.1	0.360	0.548	0.188		1.24	16.05	0.12	-0.93	207.83
21	270	21.13	20.4	20.765	3830.5	0.383	0.575	0.191		1.26	16.43	0.09	-1.04	213.65
22	282.5	19.17	20.75	19.96	4057.1	0.406	0.601	0.195		1.29	16.81	0.07	-1.18	219.03
23	295	20.77	19.93	20.35	4289.4	0.429	0.628	0.199		1.31	17.18	0.04	-1.36	224.85
24	307.5	20.87	19.85	20.36	4522.6	0.452	0.654	0.202		1.33	17.54	0.02	-1.66	230.57
25	320	20.05	19.5	19.775	4755.5	0.476	0.681	0.205		1.36	17.89	0.00	-	236.08

Pseudo First Order Kinetics		Pseudo Second Order Kinetics	
qe	1.3	qe	1.78
K_{ad1}	0.0094	K_{ad2}	0.0051
R^2	0.9261	R^2	0.9973
h_1	0.0124	h_2	0.0161

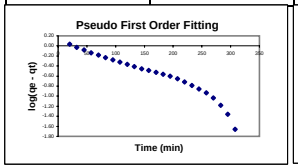

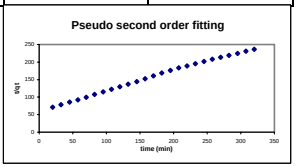

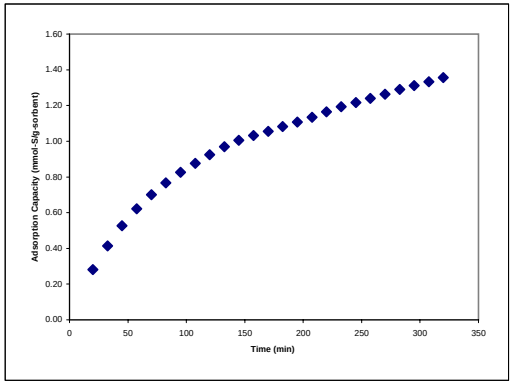

Weber-Morris Intra-Particle Diffusion	
K_{id}	0.07539
C	0.04782

Flow Reactor Experiment
Sorbent: Ta-5/ACC (run I)
Run Temperature: 40 °C
Flow rate: 0.1 mL/min
Solution: DBT+C16 Flow
Comment: in-Situ Activation

Sample ID	Sample Time (min)	Run1	Run2	Average (mmol/L)	Sulfur in outflow (mmol-S.min/L)	Sulfur in Outflow (mmol-S)	Total Sulfur (mmol-S)	Sulfur Removed (mmol-S)	Sorbent Weight (g)	Adsorption Capacity (mmol-S/g-sorbent)	$t^{0.5}$	qe - qt	log(qe - qt)	t/qt
1	25	6.81	6.9	6.855	0	0.000	0.053	0.053		0.38	5.00	0.89	-0.05	66.31
2	37.5	12.24	11.39	11.815	116.7	0.012	0.080	0.068		0.48	6.12	0.78	-0.11	77.67
3	50	14.09	13.95	14.02	278.2	0.028	0.106	0.079		0.56	7.07	0.71	-0.15	89.79
4	62.5	14.61	15.06	14.835	458.5	0.046	0.133	0.087		0.62	7.91	0.64	-0.19	101.20
5	75	15.88	16.49	16.185	652.4	0.065	0.160	0.094		0.67	8.66	0.59	-0.23	112.16
6	87.5	15.95	16.03	15.99	853.5	0.085	0.186	0.101		0.71	9.35	0.55	-0.26	122.44
7	100	16.17	16	16.085	1053.9	0.105	0.213	0.107		0.76	10.00	0.50	-0.30	131.39
8	112.5	15.96	16.37	16.165	1255.5	0.126	0.239	0.114		0.81	10.61	0.46	-0.34	139.45
9	125	17.81	18.13	17.97	1468.8	0.147	0.266	0.119		0.84	11.18	0.42	-0.38	148.10
10	137.5	16.98	17.77	17.375	1689.8	0.169	0.293	0.124		0.88	11.73	0.39	-0.41	156.97
11	150	17.41	17.92	17.665	1908.8	0.191	0.319	0.128		0.91	12.25	0.35	-0.45	164.96
12	162.5	18.43	18.45	18.44	2134.4	0.213	0.346	0.132		0.94	12.75	0.32	-0.49	173.27
13	175	18.73	19.01	18.87	2367.6	0.237	0.372	0.136		0.96	13.23	0.30	-0.52	182.08
14	187.5	20	18.71	19.355	2606.5	0.261	0.399	0.138		0.98	13.69	0.28	-0.55	191.27
15	200	18.84	19.45	19.145	2847.1	0.285	0.426	0.141		1.00	14.14	0.26	-0.58	200.35
16	212.5	18.5	17.73	18.115	3080.0	0.308	0.452	0.144		1.02	14.58	0.24	-0.62	207.98
17	225	19.53	17.8	18.665	3309.9	0.331	0.479	0.148		1.05	15.00	0.21	-0.67	214.84
18	237.5	18.62	18.25	18.435	3541.8	0.354	0.505	0.151	0.1411	1.07	15.41	0.19	-0.72	221.66
19	250	19	18.33	18.665	3773.6	0.377	0.532	0.155		1.10	15.81	0.17	-0.78	228.18
20	262.5	18.37	18.87	18.62	4006.7	0.401	0.559	0.158		1.12	16.20	0.14	-0.84	234.58
21	275	19.83	18.44	19.135	4242.6	0.424	0.585	0.161		1.14	16.58	0.12	-0.91	241.17
22	287.5	19.44	19.08	19.26	4482.6	0.448	0.612	0.163		1.16	16.96	0.10	-0.99	248.12
23	300	19.91	18.93	19.42	4724.3	0.472	0.638	0.166		1.18	17.32	0.09	-1.06	255.13
24	312.5	20.04	19.58	19.81	4969.5	0.497	0.665	0.168		1.19	17.68	0.07	-1.15	262.47
25	325	19.56	20.65	20.105	5219.0	0.522	0.692	0.170		1.20	18.03	0.06	-1.22	270.31
26	337.5	20.59	20.44	20.515	5472.9	0.547	0.718	0.171		1.21	18.37	0.05	-1.29	278.72
27	350	20.57	19.63	20.1	5726.7	0.573	0.745	0.172		1.22	18.71	0.04	-1.37	287.01
28	362.5	20.8	19.12	19.96	5977.1	0.598	0.771	0.174		1.23	19.04	0.03	-1.50	294.58
29	375	20.24	18.97	19.605	6224.4	0.622	0.798	0.176		1.24	19.36	0.02	-1.74	301.50
30	387.5	20.18	20.91	20.545	6475.3	0.648	0.825	0.177		1.25	19.69	0.01	-2.11	308.90
31	400	20.08	20.47	20.275	6730.4	0.673	0.851	0.178		1.26	20.00	0.00	-	316.92
32	412.5	19.06	19.34	19.2	6977.2	0.698	0.878	0.180		1.28	20.31	-0.01	-	323.33
33	425	20.36	20.76	20.56	7225.7	0.723	0.904	0.182		1.29	20.62	-0.03	-	329.92
34	437.5	20.33	20.64	20.485	7482.2	0.748	0.931	0.183		1.29	20.92	-0.03	-	337.87
35	450	19.7	20.14	19.92	7734.7	0.773	0.958	0.184		1.30	21.21	-0.04	-	344.98
36	462.5	19.35	19.21	19.28	7979.7	0.798	0.984	0.186		1.32	21.51	-0.06	-	350.57

Pseudo First Order Kinetics		Pseudo Second Order Kinetics	
qe	1.5	qe	1.56
K_{ad1}	0.0103	K_{ad2}	0.0064
R^2	0.9153	R^2	0.9951
h_1	0.0158	h_2	0.0155

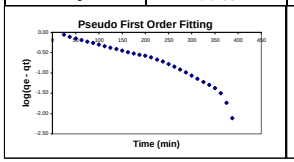

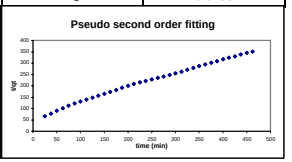

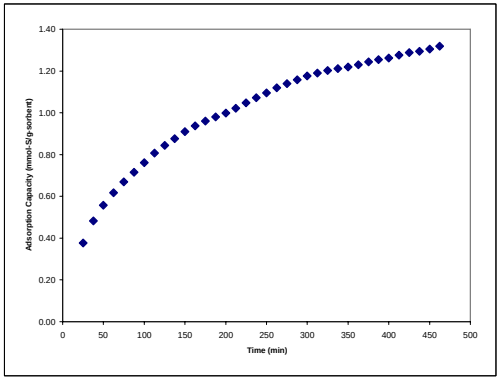

Weber-Morris Intra-Particle Diffusion	
K_{id}	0.05419
C	0.20895

Flow Reactor Experiment
Sorbent: Ta-5/ACC (run II)
Run Temperature: 40 °C
Flow rate: 0.1 mL/min
Solution: DBT+C16 Flow
Comment: in-Situ Activation

Sample #	Time (min)	Run1	Run2	Average (mmol/L)	Sulfur in outflow (mmol-S.min/L)	Sulfur in Outflow (mmol-S)	Total Sulfur (mmol-S)	Sulfur Removed (mmol-S)	Sorbent Weight (g)	Adsorption Capacity (mmol-S/g-sorbent)	$t^{0.5}$	qe - qt	log(qe - qt)	t/qt
1	25	0.1	0.1	0.1	0	0.000	0.053	0.053		0.39	5.00	0.92	-0.04	63.96
2	37.5	0.8	0.8	0.8	116.7	0.012	0.080	0.068		0.50	6.12	0.81	-0.09	74.92
3	50	11.06	11.17	11.115	278.2	0.028	0.106	0.079		0.58	7.07	0.73	-0.14	86.60
4	62.5	15.05	14.87	14.96	458.5	0.046	0.133	0.087		0.64	7.91	0.67	-0.18	97.62
5	75	16.43	16.41	16.42	652.4	0.065	0.160	0.094		0.69	8.66	0.62	-0.21	108.19
6	87.5	17.23	17.19	17.21	853.5	0.085	0.186	0.101		0.74	9.35	0.57	-0.25	118.10
7	100	18.08	18.08	18.08	1053.9	0.105	0.213	0.107		0.79	10.00	0.52	-0.28	126.73
8	112.5	18.17	17.99	18.08	1255.5	0.126	0.239	0.114		0.84	10.61	0.47	-0.33	134.51
9	125	18.41	18.23	18.32	1468.8	0.147	0.266	0.119		0.88	11.18	0.43	-0.36	142.85
10	137.5	18.41	18.29	18.35	1689.8	0.169	0.293	0.124		0.91	11.73	0.40	-0.40	151.40
11	150	19.05	18.5	18.775	1908.8	0.191	0.319	0.128		0.94	12.25	0.37	-0.44	159.12
12	162.5	18.92	18.76	18.84	2134.4	0.213	0.346	0.132		0.97	12.75	0.34	-0.47	167.13
13	175	18.89	18.78	18.835	2367.6	0.237	0.372	0.136		1.00	13.23	0.31	-0.51	175.63
14	187.5	19.04	18.93	18.985	2606.5	0.261	0.399	0.138		1.02	13.69	0.29	-0.53	184.49
15	200	19.07	19.13	19.1	2847.1	0.285	0.426	0.141		1.03	14.14	0.27	-0.56	193.25
16	212.5	19.07	19.25	19.16	3080.0	0.308	0.452	0.144	0.1361	1.06	14.58	0.25	-0.60	200.61
17	225	19.96	19.38	19.67	3309.9	0.331	0.479	0.148		1.09	15.00	0.22	-0.65	207.22
18	237.5	19.86	19.44	19.65	3541.8	0.354	0.505	0.151		1.11	15.41	0.20	-0.70	213.80
19	250	19.44	19.52	19.48	3773.6	0.377	0.532	0.155		1.14	15.81	0.17	-0.76	220.09
20	262.5	19.6	19.5	19.55	4006.7	0.401	0.559	0.158		1.16	16.20	0.15	-0.83	226.27
21	275	19.47	19.55	19.51	4242.6	0.424	0.585	0.161		1.18	16.58	0.13	-0.90	232.63
22	287.5	19.67	19.49	19.58	4482.6	0.448	0.612	0.163		1.20	16.96	0.11	-0.97	239.33
23	300	19.49	19.78	19.635	4724.3	0.472	0.638	0.166		1.22	17.32	0.09	-1.05	246.09
24	312.5	19.67	19.82	19.745	4969.5	0.497	0.665	0.168		1.23	17.68	0.07	-1.13	253.17
25	325	19.79	19.62	19.705	5219.0	0.522	0.692	0.170		1.25	18.03	0.06	-1.21	260.73
26	337.5	19.8	19.76	19.78	5472.9	0.547	0.718	0.171		1.26	18.37	0.05	-1.27	268.84
28	350	19.78	19.91	19.845	5726.7	0.573	0.745	0.172		1.26	18.71	0.04	-1.35	276.84
29	362.5	19.74	19.96	19.85	5977.1	0.598	0.771	0.174		1.28	19.04	0.03	-1.48	284.15
30	375	19.87	19.66	19.765	6224.4	0.622	0.798	0.176		1.29	19.36	0.02	-1.72	290.81
31	387.5	19.89	19.87	19.88	6475.3	0.648	0.825	0.177		1.30	19.69	0.01	-2.10	297.95
32	400	19.94	19.79	19.865	6730.4	0.673	0.851	0.178		1.31	20.00	0.00	-	305.69

Pseudo First Order Kinetics		Pseudo Second Order Kinetics	
qe	1.6	qe	1.61
K_{ad1}	0.0103	K_{ad2}	0.0062
R^2	0.9153	R^2	0.9951
h_1	0.0164	h_2	0.0161

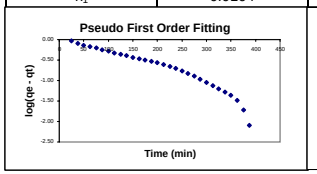

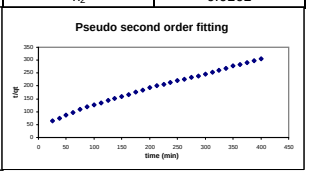

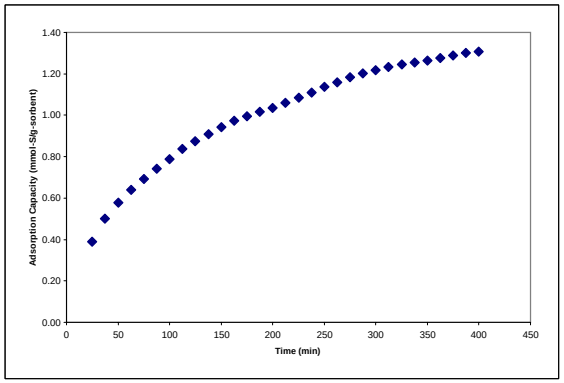

Weber-Morris Intra-Particle Diffusion	
K_{id}	0.05917
C	0.18249

Flow Reactor Experiment
Sorbent: Ta-5/ACC (run I)
Run Temperature: 70 °C
Flow rate: 0.1 mL/min
Solution: DBT+C16 Flow
Comment: in-Situ Activation

Sample ID	Sample Time (min)	run1	run2	Average (mmol/L)	Sulfur in outflow (mmol-S.min/L)	Sulfur in outflow (mmol-S.min/L)	Total Sulfur (mmol-S)	Sulfur Removed (mmol-S)	Sorbent Weight (g)	Adsorption Capacity (mmol-S/g-sorbent)	$t^{0.5}$	qe - qt	log(qe - qt)	t/qt
1	25	7.51	7.37	7.44	0	0.000	0.053	0.053		0.27	5.00	0.52	-0.29	93.80
2	37.5	11.8	11.97	11.89	120.8	0.012	0.080	0.068		0.34	6.12	0.45	-0.35	110.54
3	50	14.17	14.23	14.20	283.8	0.028	0.106	0.078		0.39	7.07	0.39	-0.40	127.93
4	62.5	16.82	16.49	16.66	476.7	0.048	0.133	0.085		0.43	7.91	0.36	-0.45	146.21
5	75	16.87	17.7	17.29	688.8	0.069	0.160	0.091		0.45	8.66	0.33	-0.48	165.03
6	87.5	16.76	17.2	16.98	902.9	0.090	0.186	0.096		0.48	9.35	0.30	-0.52	182.13
7	100	17.81	16.82	17.32	1117.3	0.112	0.213	0.101		0.51	10.00	0.28	-0.55	197.52
8	112.5	17.59	17.84	17.72	1336.2	0.134	0.239	0.106		0.53	10.61	0.26	-0.59	212.32
9	125	17.94	18.02	17.98	1559.3	0.156	0.266	0.110		0.55	11.18	0.23	-0.63	226.72
10	137.5	18.12	17.56	17.84	1783.2	0.178	0.293	0.114		0.57	11.73	0.21	-0.67	240.20
11	150	18.42	18.36	18.39	2009.6	0.201	0.319	0.118		0.59	12.25	0.19	-0.71	253.27
12	162.5	18.23	18.64	18.44	2239.8	0.224	0.346	0.122	0.1996	0.61	12.75	0.17	-0.76	266.31
13	175	18.41	19.62	19.02	2473.8	0.247	0.372	0.125		0.63	13.23	0.16	-0.80	279.47
14	187.5	19.17	18.4	18.79	2710.1	0.271	0.399	0.128		0.64	13.69	0.14	-0.84	292.48
15	200	18.19	19.12	18.66	2944.1	0.294	0.426	0.131		0.66	14.14	0.13	-0.89	304.37
16	212.5	20.27	19.15	19.71	3183.9	0.318	0.452	0.134		0.67	14.58	0.11	-0.94	317.06
17	225	17.66	16.74	17.20	3414.6	0.341	0.479	0.137		0.69	15.00	0.10	-1.01	327.08
18	237.5	17.8	18.5	18.15	3635.5	0.364	0.505	0.142		0.71	15.41	0.07	-1.13	334.28
19	250	18.44	20.06	19.25	3869.3	0.387	0.532	0.145		0.73	15.81	0.06	-1.23	344.06
20	262.5	18.98	18.46	18.72	4106.6	0.411	0.559	0.148		0.74	16.20	0.04	-1.35	354.26
21	275	20.51	18.38	19.45	4345.1	0.435	0.585	0.151		0.75	16.58	0.03	-1.52	364.37
22	287.5	18.57	18.92	18.75	4583.8	0.458	0.612	0.153		0.77	16.96	0.02	-1.78	374.15
23	300	18.8	18.12	18.46	4816.3	0.482	0.638	0.157		0.79	17.32	0.00	-	382.09

Pseudo First Order Kinetics		Pseudo Second Order Kinetics	
qe	0.8	qe	0.96
K_{ad1}	0.0106	K_{ad2}	0.0125
R^2	0.9157	R^2	0.9870
h_1	0.0086	h_2	0.0115

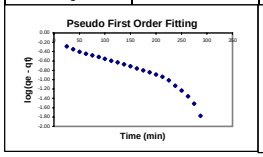

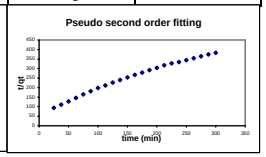

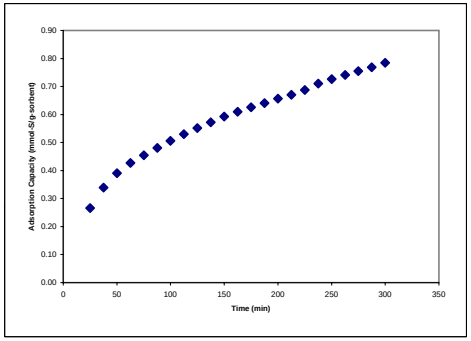

Flow Reactor Experiment
Sorbent: Ta-5/ACC (run II)
Run Temperature: 70 °C
Flow rate: 0.1 mL/min
Solution: DBT+C16 Flow
Comment: in-Situ Activation

Sample ID	Sample Time (min)	run1	run2	Average (mmol/L)	Sulfur in outflow (mmol-S.min/L)	Sulfur in Outflow (mmol-S)	Total Sulfur (mmol-S)	Sulfur Removed (mmol-S)	Sorbent Weight (g)	Adsorption Capacity (mmol-S/g-sorbent)	$t^{0.5}$	qe - qt	log(qe - qt)	t/qt
1	25	3.76	4.03	3.90	0	0.000	0.053	0.053		0.19	5.00	0.57	-0.24	133.14
2	37.5	6.18	6.43	6.31	63.8	0.006	0.080	0.073		0.26	6.12	0.50	-0.30	144.71
3	50	8.71	9.29	9.00	159.5	0.016	0.106	0.090		0.32	7.07	0.44	-0.35	156.62
4	62.5	10.46	10.64	10.55	281.7	0.028	0.133	0.105		0.37	7.91	0.39	-0.41	168.92
5	75	13.22	12.16	12.69	426.9	0.043	0.160	0.117		0.41	8.66	0.35	-0.46	181.77
6	87.5	14.31	13.39	13.85	592.8	0.059	0.186	0.127		0.45	9.35	0.31	-0.50	195.33
7	100	14.16	15.26	14.71	771.3	0.077	0.213	0.136		0.48	10.00	0.28	-0.55	208.84
8	112.5	15.57	15.4	15.49	960.1	0.096	0.239	0.143		0.51	10.61	0.26	-0.59	222.29
9	125	14.63	16.18	15.41	1153.2	0.115	0.266	0.151		0.53	11.18	0.23	-0.64	235.05
10	137.5	16.81	15.99	16.40	1352.0	0.135	0.293	0.157		0.56	11.73	0.21	-0.68	247.52
11	150	17.63	17.07	17.35	1562.9	0.156	0.319	0.163		0.57	12.25	0.19	-0.73	260.90
12	162.5	18.03	16.58	17.31	1779.6	0.178	0.346	0.168		0.59	12.75	0.17	-0.77	274.32
13	175	17.75	19.47	18.61	2004.1	0.200	0.372	0.172	0.2833	0.61	13.23	0.16	-0.81	288.30
14	187.5	18.38	18.01	18.20	2234.1	0.223	0.399	0.176		0.62	13.69	0.14	-0.85	302.57
15	200	18.36	18.05	18.21	2461.7	0.246	0.426	0.179		0.63	14.14	0.13	-0.89	315.83
16	212.5	18.01	18.14	18.08	2688.5	0.269	0.452	0.183		0.65	14.58	0.12	-0.94	328.40
17	225	17.53	18.5	18.02	2914.1	0.291	0.479	0.187		0.66	15.00	0.10	-1.00	340.23
18	237.5	17.83	18.56	18.20	3140.5	0.314	0.505	0.191		0.68	15.41	0.09	-1.06	351.70
19	250	18.19	17.93	18.06	3367.1	0.337	0.532	0.195		0.69	15.81	0.07	-1.14	362.75
20	262.5	18.34	18.14	18.24	3594.0	0.359	0.559	0.199		0.70	16.20	0.06	-1.23	373.41
21	275	18.37	18.81	18.59	3824.2	0.382	0.585	0.203		0.72	16.58	0.05	-1.33	384.28
22	287.5	18.32	18.65	18.49	4055.9	0.406	0.612	0.206		0.73	16.96	0.03	-1.46	395.08
23	300	18.73	17.95	18.34	4286.1	0.429	0.638	0.210		0.74	17.32	0.02	-1.66	405.22
24	312.5	18.77	19.08	18.93	4519.1	0.452	0.665	0.213		0.75	17.68	0.01	-1.99	415.56
25	325	19.72	18.22	18.97	4755.9	0.476	0.692	0.216		0.76	18.03	0.00	-	426.36

Pseudo First Order Kinetics		Pseudo Second Order Kinetics	
qe	0.8	qe	1.00
K_{ad1}	0.0095	K_{ad2}	0.0091
R^2	0.9215	R^2	0.9982
h_1	0.0072	h_2	0.0091

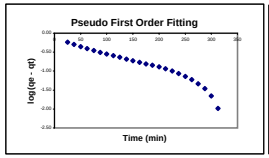

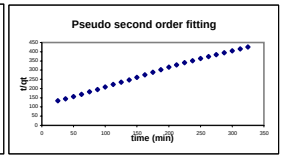

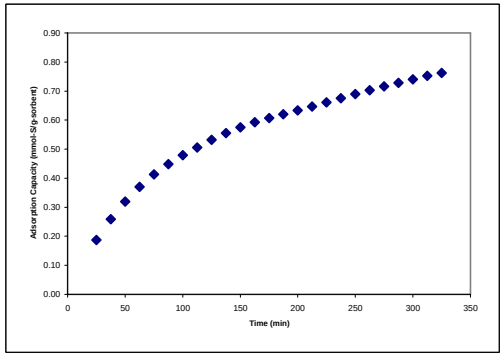

Flow Reactor Experiment
Sorbent: Ta-5/ACC (run I)
Run Temperature: 100 °C
Flow rate: 0.1 mL/min
Solution: DBT+C16 Flow
Comment: in-Situ Activation

Sample ID	Sample Time (min)	run1	run2	Average (mmol/L)	Sulfur in outflow (mmol-S.min/L)	Sulfur in Outflow (mmol-S)	Total Sulfur (mmol-S)	Sulfur Removed (mmol-S)	Sorbent Weight (g)	Adsorption Capacity (mmol-S/g-sorbent)	$t^{0.5}$	qe - qt	log(qe - qt)	t/qt
1	25	0.25	0.35	0.3	0	0.000	0.053	0.053		0.21	5.00	0.57	-0.25	121.63
2	37.5	0.87	0.9	0.885	7.4	0.001	0.080	0.079		0.31	6.12	0.47	-0.33	122.77
3	50	1.81	1.98	1.895	24.8	0.002	0.106	0.104		0.40	7.07	0.37	-0.43	124.53
4	62.5	3.92	3.93	3.925	61.2	0.006	0.133	0.127		0.49	7.91	0.28	-0.55	127.49
5	75	8.84	8.77	8.805	140.7	0.014	0.160	0.146		0.56	8.66	0.21	-0.68	133.39
6	87.5	13.16	14.38	13.77	281.8	0.028	0.186	0.158		0.61	9.35	0.16	-0.79	143.32
7	100	16.84	16.14	16.49	470.9	0.047	0.213	0.166		0.64	10.00	0.13	-0.88	156.20
8	112.5	17.27	18.78	18.025	686.7	0.069	0.239	0.171		0.66	10.61	0.11	-0.95	170.55
9	125	17.1	19.12	18.11	912.5	0.091	0.266	0.175		0.68	11.18	0.10	-1.01	185.14
10	137.5	19.07	18.53	18.8	1143.2	0.114	0.293	0.178		0.69	11.73	0.08	-1.08	199.63
11	150	18.62	20.05	19.335	1381.5	0.138	0.319	0.181		0.70	12.25	0.07	-1.13	214.45
12	162.5	18.92	19.62	19.27	1622.8	0.162	0.346	0.183		0.71	12.75	0.06	-1.19	229.19
13	175	19.27	21.83	20.55	1871.7	0.187	0.372	0.185		0.72	13.23	0.06	-1.24	244.54
14	187.5	19.68	20.13	19.905	2124.5	0.212	0.399	0.187		0.72	13.69	0.05	-1.28	260.17
15	200	22.12	21.92	22.02	2386.6	0.239	0.426	0.187		0.72	14.14	0.05	-1.30	276.92
16	212.5	20.13	20.37	20.25	2650.8	0.265	0.452	0.187	0.2588	0.72	14.58	0.05	-1.30	293.95
17	225	22.79	20.41	21.6	2912.3	0.291	0.479	0.188		0.72	15.00	0.05	-1.32	310.51
18	237.5	21.61	22.56	22.085	3185.3	0.319	0.505	0.187		0.72	15.41	0.05	-1.29	329.00
19	250	19.5	18.89	19.195	3443.3	0.344	0.532	0.188		0.72	15.81	0.05	-1.32	344.84
20	262.5	20.41	21.29	20.85	3693.6	0.369	0.559	0.189		0.73	16.20	0.04	-1.38	359.08
21	275	19.55	19.43	19.49	3945.8	0.395	0.585	0.191		0.74	16.58	0.04	-1.44	373.44
22	287.5	20.34	22.31	21.325	4200.8	0.420	0.612	0.192		0.74	16.96	0.03	-1.49	388.20
23	300	20.04	19.43	19.735	4457.5	0.446	0.638	0.193		0.74	17.32	0.03	-1.54	403.11
24	312.5	20.67	19.9	20.285	4707.6	0.471	0.665	0.194		0.75	17.68	0.02	-1.65	416.48
25	325	20.82	19.78	20.3	4961.3	0.496	0.692	0.195		0.76	18.03	0.02	-1.75	430.40
26	337.5	22.81	21.73	22.27	5227.3	0.523	0.718	0.195		0.76	18.37	0.02	-1.75	446.98
27	350	20.01	21.75	20.88	5497.0	0.550	0.745	0.195		0.75	18.71	0.02	-1.72	464.41
28	362.5	20.12	22.46	21.29	5760.6	0.576	0.771	0.195		0.75	19.04	0.02	-1.74	480.40
29	375	20.34	19.5	19.92	6018.1	0.602	0.798	0.196		0.76	19.36	0.02	-1.82	494.84
30	387.5	18.98	20.13	19.555	6264.8	0.626	0.825	0.198		0.77	19.69	0.01	-2.12	506.36
31	400	20.58	19.13	19.855	6511.2	0.651	0.851	0.200		0.77	20.00	0.00		517.55

Pseudo First Order Kinetics		Pseudo Second Order Kinetics	
qe	0.4	qe	0.86
K_{ad1}	0.0098	K_{ad2}	0.0254
R^2	0.9063	R^2	0.9922
h_1	0.0043	h_2	0.0189

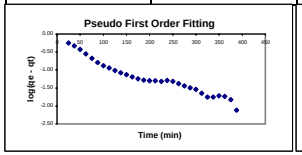

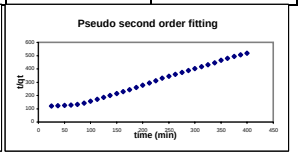

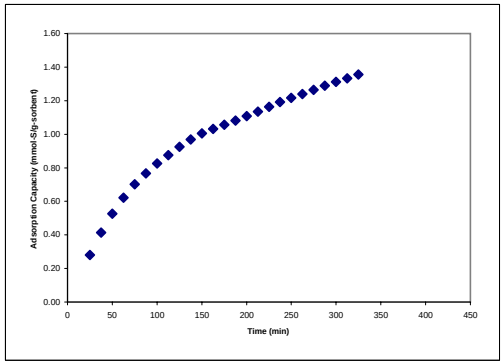

Weber-Morris Intra-Particle Diffusion		C
K_{id1}	0.09060	-0.24104
K_{id2}	0.00967	0.57682

Flow Reactor Experiment
Sorbent: Ta-5/ACC (run II)
Run Temperature: 100 °C
Flow rate: 0.1 mL/min
Solution: DBT+C16 Flow
Comment: in-Situ Activation

Sample ID	Sample Time (min)	run1	run2	Average (mmol/L)	Sulfur in outflow (mmol-S.min/L)	Sulfur in Outflow (mmol-S)	Total Sulfur (mmol-S)	Sulfur Removed (mmol-S)	Sorbent Weight (g)	Adsorption Capacity (mmol-S/g-sorbent)	$t^{0.5}$	qe - qt	log(qe - qt)	t/qt
1	25	0.58	0.65	0.615	0	0.000	0.053	0.053		0.19	5.00	0.60	-0.22	134.60
2	37.5	1.46	1.63	1.545	13.5	0.001	0.080	0.078		0.27	6.12	0.51	-0.29	136.91
3	50	4.26	3.6	3.93	47.7	0.005	0.106	0.102		0.35	7.07	0.43	-0.36	140.92
4	62.5	7.25	6.9	7.075	116.5	0.012	0.133	0.121		0.42	7.91	0.37	-0.44	147.52
5	75	9.92	9.87	9.895	222.6	0.022	0.160	0.137		0.48	8.66	0.31	-0.51	156.41
6	87.5	12.92	12.42	12.67	363.6	0.036	0.186	0.150		0.52	9.35	0.27	-0.58	167.26
7	100	15.32	14.49	14.905	535.9	0.054	0.213	0.159		0.56	10.00	0.23	-0.63	179.91
8	112.5	15.82	15.17	15.495	725.9	0.073	0.239	0.167		0.58	10.61	0.21	-0.69	193.18
9	125	15.43	16.72	16.075	923.3	0.092	0.266	0.174		0.61	11.18	0.18	-0.74	206.16
10	137.5	16.42	16.44	16.43	1126.4	0.113	0.293	0.180		0.63	11.73	0.16	-0.79	218.86
11	150	17.74	21.32	19.53	1351.2	0.135	0.319	0.184		0.64	12.25	0.15	-0.84	233.40
12	162.5	20.23	17.65	18.94	1591.6	0.159	0.346	0.187		0.65	12.75	0.14	-0.86	249.39
13	175	17.71	19.29	18.5	1825.6	0.183	0.372	0.190		0.66	13.23	0.13	-0.90	264.05
14	187.5	18.34	18.2	18.27	2055.4	0.206	0.399	0.193		0.68	13.69	0.11	-0.95	277.62
15	200	18.36	17.9	18.13	2282.9	0.228	0.426	0.197		0.69	14.14	0.10	-1.00	290.35
16	212.5	21.01	19.9	20.455	2524.1	0.252	0.452	0.200		0.70	14.58	0.09	-1.04	304.67
17	225	19.18	19.54	19.36	2772.9	0.277	0.479	0.201		0.70	15.00	0.09	-1.07	319.85
18	237.5	18.99	17.9	18.445	3009.2	0.301	0.505	0.204	0.2864	0.71	15.41	0.08	-1.12	332.71
19	250	19.49	18.39	18.94	3242.8	0.324	0.532	0.208		0.73	15.81	0.06	-1.20	344.77
20	262.5	20.31	18.76	19.535	3483.3	0.348	0.559	0.210		0.73	16.20	0.05	-1.26	357.62
21	275	21.76	21.51	21.635	3740.6	0.374	0.585	0.211		0.74	16.58	0.05	-1.29	373.11
22	287.5	20.43	19.84	20.135	4001.7	0.400	0.612	0.212		0.74	16.96	0.05	-1.30	389.16
23	300	21.27	19.66	20.465	4255.4	0.426	0.638	0.213		0.74	17.32	0.05	-1.34	403.75
24	312.5	20.28	20.58	20.43	4511.0	0.451	0.665	0.214		0.75	17.68	0.04	-1.37	418.53
25	325	19.98	19.87	19.925	4763.3	0.476	0.692	0.215		0.75	18.03	0.04	-1.43	432.49
26	337.5	19.93	19.67	19.8	5011.5	0.501	0.718	0.217		0.76	18.37	0.03	-1.51	445.46
27	350	19.84	19.82	19.83	5259.2	0.526	0.745	0.219		0.76	18.71	0.02	-1.60	458.09
28	362.5	18.35	21.84	20.095	5508.8	0.551	0.771	0.220		0.77	19.04	0.02	-1.72	470.91
29	375	18.4	18.58	18.49	5749.9	0.575	0.798	0.223		0.78	19.36	0.01	-1.98	481.73
30	387.5	19.97	20.92	20.445	5993.3	0.599	0.825	0.225		0.79	19.69	0.00	-2.60	492.78
31	400	21.83	20.08	20.955	6252.0	0.625	0.851	0.226		0.79	20.00	0.00	-	507.05
32	412.5	19.28	20.03	19.655	6505.8	0.651	0.878	0.227		0.79	20.31	0.00	-	520.10
33	425	19.2	21.2	20.2	6754.9	0.675	0.904	0.229		0.80	20.62	-0.01	-	531.90
34	437.5	18.43	19.17	18.8	6998.7	0.700	0.931	0.231		0.81	20.92	-0.02	-	542.28
35	450	17.74	18.53	18.135	7229.5	0.723	0.958	0.235		0.82	21.21	-0.03	-	549.42

Pseudo First Order Kinetics		Pseudo Second Order Kinetics	
qe	0.8	qe	0.95
K_{ad1}	0.0105	K_{ad2}	0.0136
R^2	0.9103	R^2	0.9973
h_1	0.0080	h_2	0.0121

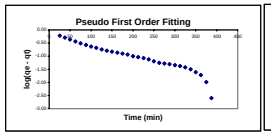

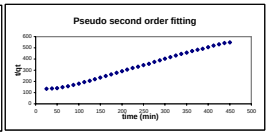

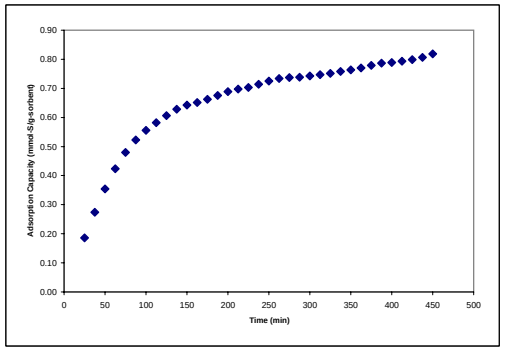

Weber-Morris Intra-Particle Diffusion		C
K_{id1}	0.07565	-0.18535
K_{id2}	0.01968	0.40053